Gas-Liquid Precipitation of Water Dissolved Heavy Metal Ions Using Hydrogen Sulfide Gas

by

Mousa Al-Tarazi

Gas-Liquid Precipitation of Water Dissolved Heavy Metal Ions Using Hydrogen Sulfide Gas

Promotion committee:

Prof.dr.ir. L. van Wijngaarden, voorzitter	Universiteit Twente
Prof. dr. ir. G.F. Versteeg, promotor	Universiteit Twente
Dr. ir. A.B.M. Heesink, assistent-promotor	Universiteit Twente
Dr. ir. J.L. Huisman, referent	Paques, the Netherlands
Prof. dr. ir. J.A.M. Kuipers	Universiteit Twente
Prof.dr.ir. M.M.C.G. Warmoeskerken	Universiteit Twente
Prof.dr. naif Darwish	Jordan University of Science and Technology
Prof.dr.ir. H.J. Heeres	Rijksuniversiteit Groningen

This research was financially supported by EET.

Al-Tarazi M.Y.M.

Gas-Liquid Precipitation of Water Dissolved Heavy Metal Ions Using Hydrogen Sulfide Gas
Thesis, University of Twente, the Netherlands

ISBN 90-365-2035-5

Print: PrintPartner Ipskamp, P.O. Box. 333, 7500 AH Enschede, the Netherlands, www.ppi.nl

GAS-LIQUID PRECIPITATION OF WATER DISSOLVED HEAVY METAL IONS USING HYDROGEN SULFIDE GAS

PROEFSCHRIFT

ter verkrijging van
de graad van doctor aan de Universiteit Twente,
op gezag van de rector magnificus,
prof.dr. F.A. van Vught,
volgens besluit van het College voor Promoties
in het openbaar te verdedigen
op donderdag 25 maart 2004 om 13.15 uur

door

Mousa Yahya Mohammad Al-Tarazi
geboren op 21 August 1972
te Irbid (Jordan)

Dit proefschrift is goedgekeurd door de promotor,

Prof. dr. ir. G.F. Versteeg

en de assistent-promotor,

Dr. ir. Bert Heesink

To my parents and my wife

Contents

Gas-Liquid Precipitation of Water Dissolved Heavy Metal Ions Using Hydrogen Sulfide Gas

Introduction

0. Introduction

The intensification of industrial activity during recent years is greatly contributing to an increasing dispersion of toxic compounds in natural environments, mainly in aquatic systems [1]. In most cases it is possible to reduce dramatically the level of toxic substances through the use of conventional technologies, although the associated costs of these processes are mostly high, When these substances are associated with metallic ions these technologies are fairly inefficient and the non-degradable nature of these elements means that supplementary methods must be used to satisfy environmental discharge patterns and legislations.

Often in industries diluted streams of sulphuric acid, contaminated with metals have to be treated, for example in zinc production and batteries recycling [2,3]. Currently these streams are neutralized using lime or other alkaline components. This results in the precipitation of sulphates as gypsum and metals as metal hydroxides, respectively, which have to be landfilled. In addition to having negative environmental impacts, these treatment processes also have high operating costs and metals removal is relatively low. In the light of increasing pressure from environmental protection organizations as well as governments landfilling is getting more and more expensive as special depots being introduced to avoid any leading of metals to groundwater.

The company Paques Bio systems of the Netherlands have developed the so-called Thiopaq® process for the simultaneous removal of sulfate and heavy metal ions from electrowinning effluent. This process involves biological reduction of sulfate towards sulfide that subsequently reacts with the present metal ions to form metal sulfide precipitate. This process does not demand the addition of large amounts of chemicals and produces much less waste making it more attractive than the conventional methods of lime addition.

This process has been used at the Pasminco zinc refinery (in Budel, the Netherlands) since 1992 for the treatment of 300 m^3/h of contaminated groundwater to remove sulphate and zinc. The installation was extended in 1998 to treat 400 m^3/h of groundwater and sulphate containing process waters. In the second half of 1999 a second full scale installation using hydrogen as electron donor was started up to convert 500 kg/h SO_4 to ZnS.

Though these units work satisfactory, the separation of the fine metal sulfide precipitation sometimes is difficult. It would be convenient if coarser particles were produced. Furthermore the biosludge that is produced during the sulfate mixes with the metal sulfide thereby increasing the amount of solid waste. This work aims at finding solutions for these difficulties. Before describing the contents of this thesis in more detail, first more background information is given on zinc production and environmental aspects.

0.1 Zinc Production Process

Zinc is produced from zinc ore (mainly ZnS) by electrolytically or pyrometallurgically. In electrolytic production (electrowinning), the zinc product does not need to be refined. Whereas zinc produced by pyrometallurgy contains 0.7–3% Pb, up to 0.2% Fe, up to 0.3% Cd, and sometimes small amounts of As, depending on composition of the ore. Zinc to be used to produce pressure-casting alloys should have a purity of 99.99–99.995%, where as a purity of 98.5–99.95% is needed for galvanizing processes. Hence, in pyrometallurgical processes distillation is applied to obtained commercial zinc grades.

In electrowinning, zinc is deposited electrolytically from aqueous solutions or molten salts. However, only aqueous electrolytes (i.e., solutions of zinc sulphate in dilute sulphuric acid) have so far been used in industry. The electrolytic production (electrowinning) of zinc from such solutions has undergone unparalleled growth in recent decades. Approximately 80 % of the total world production comes from this process today, although a number of problems still need to be solved, principally in the preparation of pure electrolyte solutions. The electrolytic process consists of the following steps: Roasting, Leaching, Liquor purification, Electrolysis and Melting and Casting. See Figure 1.

The current operation at the Pasminco zinc plant in Budel involves a conventional roast-leach-electrowinning process. The amongst others sulphate and zinc containing wastewater from electrowinning section is treated biologically, followed by the precipitation and dewatering of the separated ZnS and biosludge which can be recycled to the process feed. The biological conversion of SO_4^{2-} to S^{2-} is carried out in the bioreactor using methanol or hydrogen as an electron donor. The excess of S^{2-} in the bioreactor effluent is converted to elemental sulphur, which can be used for e.g. the production of sulphuric acid. A schematic diagram of the process sequence is presented in Figure 1.

Numerous methods have been proposed in literature of physical and chemical methods for the removal of heavy metals, such as sulphide and hydroxide precipitation, solvent extraction, ion exchange, adsorption and reverse osmosis. Whilst usually very effective, such techniques generally require large capital, reagent and/or energy costs. Under the right economic circumstances there remains therefore, a niche, for alternatives technologies, of which biosorption is now a well recognized contender [4]. Below all applied methods are described.

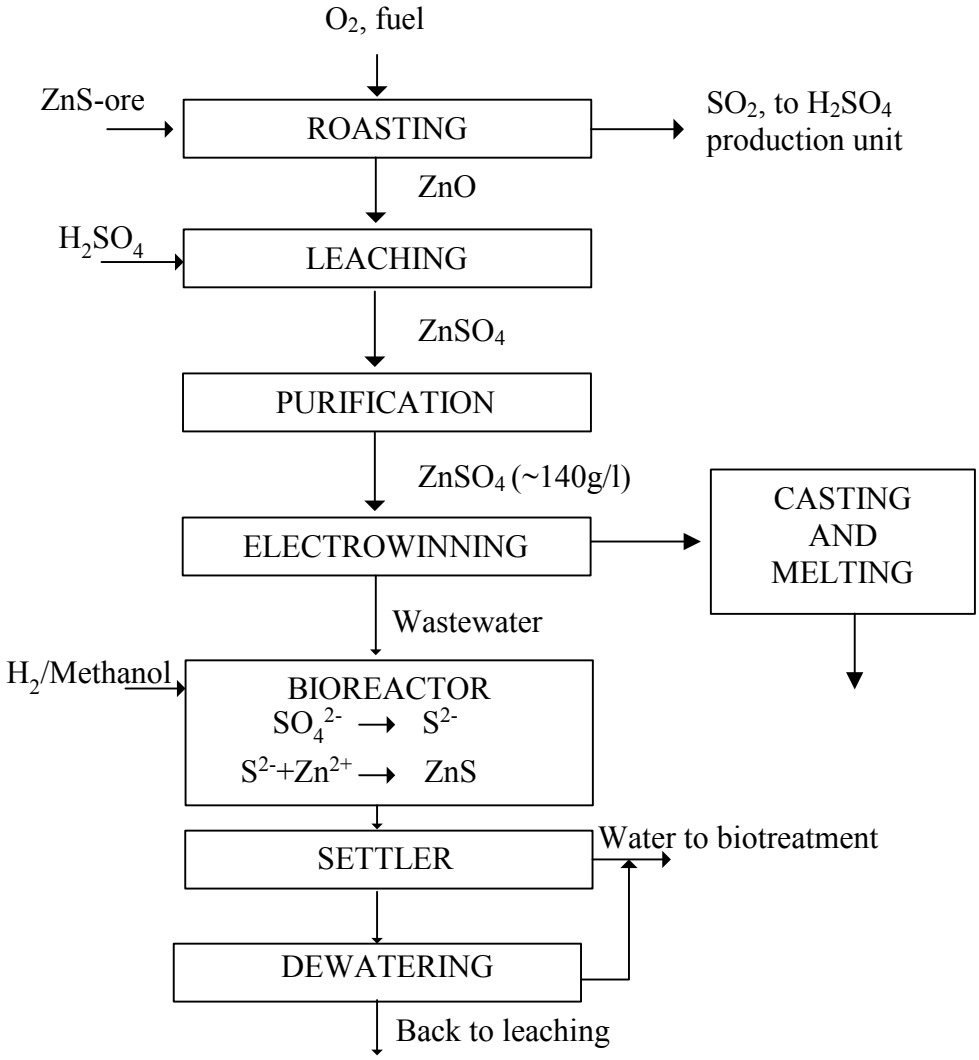

Figure 1: *Schematic sequence of the current plant Pasminco Budel Zinc*

0.2 Metal Removal Methods

0.2.1 Hydroxide (lime) Precipitation

The conventional processes for the treatment of acidic, metal loaded effluents from industry, including acid mine drainage, involve neutralisation by the addition of alkaline chemicals such as limestone, lime, sodium hydroxide, sodium carbonate or magnesia [5]. This is followed by precipitation-settling of the metal hydroxides followed by thickening or filtration of the sludge. Most of the zinc electroplating industries in the United States and all in Brazil, for example, treat their effluents by precipitation [6]. This method, from a technical point of view, presents several limitations, such as incomplete precipitation, chemical instability of the precipitates, limed effluent treatment and formation of large volumes of difficult to filter sludge. The operating costs of this process are high while

sulphate and metals removals are relatively low (1500 mg/l for sulphate and 0.5 – 5 ppm for the metals). In addition, all valuable metals are lost in the sludge [7].

0.2.2 Sulphide Precipitation

Sulphide precipitation (with Na_2S, NaHS or CaS) is an effective process for the treatment of industrial waste containing highly toxic heavy metals. The attractive features of the sulphide precipitation process are the attainment of a high degree of metal removal over a broad pH range, effective precipitation of certain metals even at very low pH levels and fast reaction. The removal of heavy metals from wastewater with sulphide precipitation processes has consequently gained considerable importance in the last few decades. Unfortunately, sulphide precipitation has a tendency to form toxic H_2S at low pH values.

The separation of precipitates from liquid is difficult, owing to the formation of loose spongy form flocks. Conventional thickeners and filters that are used extensively for separating the precipitate product are expensive and slow. In addition, the large units of dewatering equipment require excessive space [8].

Combination of lime and sulphide precipitation could precipitate all the heavy metals completely. It could overcome the disadvantages of incomplete precipitation by lime alone and hydrogen formation by sulphide alone.

0.2.3 Carrier Magnetic Separation For Precipitates/Liquid Separation

Carrier magnetic separation is a method that is proposed to improve the precipitate separation performance [8]. It is combined with lime or sulfide precipitation and involves the addition of small amounts of magnetite. The sharp increase in magnetic response shown by a particle containing even small amounts (less than 1%) of a material such as magnetite arises because of the much greater magnetic susceptibility of ferromagnetic or ferrimagnetic materials compared with paramagnetic minerals, such as siderite. It has been calculated that a volumetric concentration of only 0.01 – 0.1 % of magnetite is required to render the non-magnetic materials sufficiently magnetic, so that they can be recovered by conventional high-intensity magnetic separation.

Carrier magnetic separation could be used for fast, effective separation of precipitates and liquid, without involving time-consuming, ineffective sedimentation and filtration steps.

0.2.4 Adsorption on Ion Exchange Resin

Simpson and Laurie (1999) developed an ion exchange resin that can be used for the recovery of zinc from industrial waste liquor [9]. Lewatit OC-1026 resin was found to have good zinc selectivity, whilst the chelating resins Purolite S-930, Metalfix Chelamine and Metalfix Chelosolve showed greater selectivity for the major contaminant ions, Cu,

Cd and Pb. These resins however, showed some loss in activity after a small number of repeated cycles.

0.2.5 Solvent Extraction

Schneider et al. (2001) studied the recovery of zinc from industrial waste liquors. A model solution containing zinc and copper ions was prepared from the corresponding metal chloride salts and used in tests [3]. It is stated that solvent extraction probably offers the best selectivity, and zinc selective reagents have been developed. However, the costs of installing a plant for large-scale solvent extraction and subsequent recovery of the solvent are relatively high.

0.2.6 Flotation

The removal of metal ions by flotation has been proposed by several researchers through various methods and techniques but not many industrial applications have been reported [6]. The main methods are precipitate flotation (as hydroxides, other insoluble salts or complexes with surfactants), adsorbing colloid flotation and adsorbing particulate flotation. The latter is a variant of the adsorbing colloid flotation process, which instead of colloids employs particulates as carrier and sorption material for the metal ion. The carrier can be a mineral particle, a polymeric resin, activated coal or a by-product sharing good sorption properties, high surface area and amenability for flotation. Using mineral particles, the flotation process resembles the metal "activation" process, a very well known technique utilized in the mineral-processing field. The removal of Zn, Cu and Ni ions, from diluted solutions, by the adsorptive particulate flotation (APF) process, was studied on laboratory scale. Zeolite (Chabazite) fines, in small concentrations, were used as the particulate sorption for the metal ions and dissolved air flotation was employed for the solid/liquid separation of the loaded "carrier" [6]. Results showed almost complete removal (>98%) of the heavy metal ions using $Fe(OH)_3$ precipitates to "aggregate" the carrier (coprecipitation). The process efficiency depended on solution and interfacial chemistry and aggregation effectiveness. A feed stream containing 2 ppm of Ni, Cu and Zn respectively was cleaned to 0.05 ppm for all metals.

0.2.7 Biosorption

The ability of biomass to concentrate heavy metals, acting as a biological resin, is becoming a useful means of treating industrial solutions contaminated with heavy metals [1]. The potential of living or non-living microorganisms to accumulate heavy metal ions is well documented, and there are now several systems in operation tackling low concentration metal contamination. The process, generally called biosorption, is easily handled in conventional fixed-bed reactors. This type of reactor has a very simple

operational mode, with low cost, in comparison to sophisticated treatment techniques. Therefore biosorption could be used as a complementary technology to treat effluents contaminated with heavy metals.

0.2.8 Adsorption on Nonliving Biomass

The general advantage of dead organisms are that they need no sustenance from the contaminated stream to be treated, however, they are obviously non-regenerative, and cannot metabolize any polluting organic residues [4].

Heavy metal ions readily adsorb onto the nonliving biomass of many aquaphytes [3]. Further, in many cases the metal ions can be readily desorbed from the biomass by use of a suitable eluting agent. It has been shown in certain cases, at least, that the biomass can be subjected to a number of loading and elution cycles without the biomass losing its adsorption capacity.

0.2.9 Adsorption on Biofilm Covered Granular Activated Carbon

A comprehensive biofilm of living bacteria bound together in an excreted polysaccharide matrix and attached to granular activated carbon, enhances both rate and quantity of metal uptake from contaminated solutions [4]. Electron micrographs illustrate an open film that provides a high surface area for biosorption of metal ions such as cadmium, copper, zinc and nickel. Studies have provided data on both equilibrium loadings (mg metal/g adsorbent) and adsorption rate coefficients. This data indicated the superior performance of the biofilm. This system, employing granular activated carbon as a biofilm support, has been demonstrated to both entrap metals and also adsorb other contaminants, including an organic residue (atrazine). With this system the advantages of metal removal can be combined with that of for inorganic salts and organic residues, which could in turn be metabolized by microorganisms colonizing the surface.

0.2.10 Biological alkaline precipitation

Van Hille et al. (1999) describe a process that utilizes alkalinity generated by the algae *Spirulina sp.* in a continuous system to precipitate heavy metals [5]. The design of the system separates the algal component from the metal containing stream to overcome metal toxicity. The primary treatment process consistently remove over 99% of the iron and between 80 and 95% of the zinc and lead. The running costs of the proposed process are claimed to be low, as the salinity and nutrient requirements for the algal culture could be provided by using tannery effluent or a combination of saline water and sewage. This would have the additional benefit of treating simultaneous either a tannery or sewage effluent as part of an integrated process.

0.2.11 Biomagnetic Separation Process

The biomagnetic separation process was developed to overcome difficulties in precipitation of heavy metal sulphide [10]. It consists of passing water contaminated with heavy metals together with $FeSO_4$ and suitable nutrients into an anaerobic bioreactor containing sulphate-reducing bacteria (SRB). The metals are precipitated as metal sulphide onto the surface of the SRB. Precipitated iron makes the SRB sufficiently magnetic. The produced precipitated complex can be removed by using a high gradient magnetic separator (HGMS). If the SRB are only weakly magnetic, a separator which employs both high magnetic fields and high magnetic field gradients is necessary for complete separation. Immobilization of metal ions from solution by the SRB has shown that heavy metal sulphide is removed from solution to residual levels less than 1 ppb. Further each bacterium can take on a considerable amount of material; in many cases the weight can be 3 to 4 times the wet weight of the bacterium. The process suffers from low strength and inconsistency in magnetic properties of the microorganisms and the used adsorbent product. Improvements have been made in this field, but work is still continuing.

0.2.12 Biological Sulphide Precipitation (Sulphate/Sulphur Reducing Bacteria)

Sulphate/Sulphur reducing bacteria have the capacity to reduce sulphate to sulphide [11]. The produced sulphide ions react with the dissolved metals, such as copper, iron and zinc, producing insoluble precipitates. Metals such as copper and zinc can be precipitated separately into saleable products. The system acidity is reduced by the sulphate reduction and by the carbon metabolism of the bacteria. Biological sulphide precipitation can be implemented in two possible flow schemes:

- *Sulphur Reduction*, in which the elemental sulphur is reduced to produce the sulphide ions. The bioreactor is operated independently of the metal precipitation stage. The bioreactor size is, therefore, usually smaller than a sulphate reduction bioreactor. However, no alkalinity is produced by the reduction of sulphur and it is needed to be adjusted externally. The wastewater stream does not pass the bioreactor and thus the sulphate that exists in the wastewater stream is not reduced. The bioreactor is fed either with hydrogen or with an organic electron donor such as methanol. The produced sulfide can be contacted to the wastewater in a precipitator (see Figure 2).

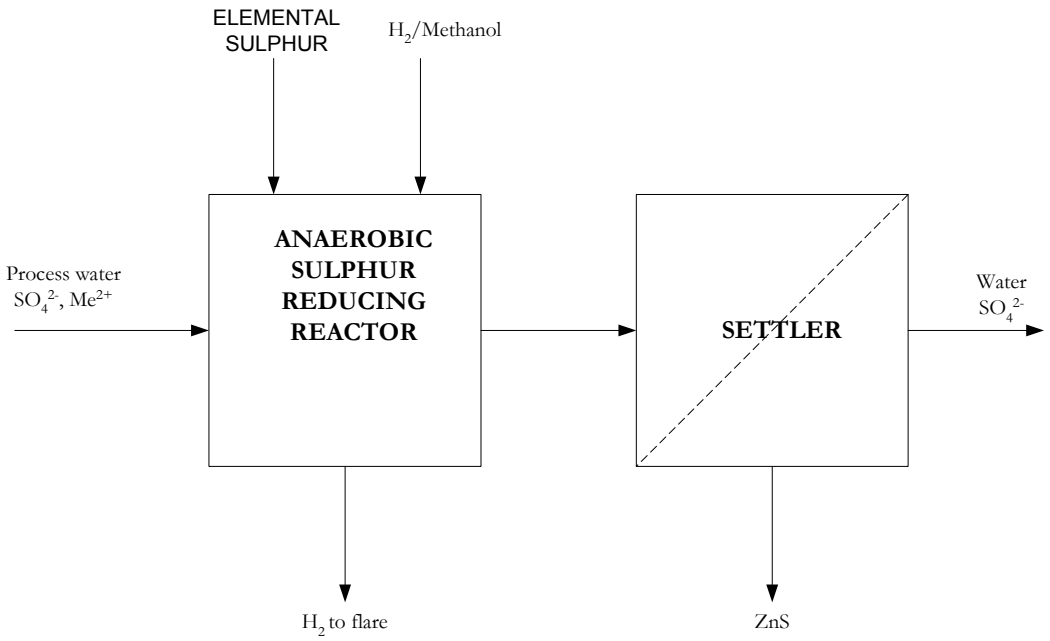

Figure 2: *Schematic diagram for precipitation of metal ions using sulphur reducing bacteria*

- *Sulphate Reduction*, in which the wastewater is passed through a bioreactor to reduce the contained sulphate and to produce the sulphide ions. Sulfide ions will then precipitate the exist metals in the stream. In this case, therefore, the biological and metal precipitation stages are fully integrated. Hydrogen can be provided by steam reforming of natural gas. Biogenic alkalinity is produced by the sulphate reduction reaction.

An electron donor is necessary for the sulphate/sulphur reduction process. Hydrogen provides an efficient electron donor for large-scale applications and can be supplied by electrolysis, steam reforming of natural gas or LPG, cracking of methanol or from a partial oxidation burner [11]. For small-scale applications, ethanol or an organic waste stream can be used as electron donor [7].

For some applications the biologically produced sulphide has to be more concentrated before it can be used. This can be accomplished by membrane separation or by using (selective) absorption and stripping techniques. Excess sulfide can be converted to a value-added co-product, such as NaHS or elemental sulphur for industrial recycle. Bacteria have certain specific environmental requirements that must be fulfilled: an anaerobic environment with redox potential lower than – 100 mV and a pH higher than 5.5. Both factors can limit the acid mine drainage treatment when the medium conditions have to be fixed. In any case, in contrast to this fact, biological activity in wetlands and lake sediments receiving acid mine drainage has been observed, due to the presence of active sulphate reducing bacteria populations even at pH around 3.

0.2.13 H_2S Contactor and Metal Precipitation

The biogenic sulphide ions produced by the anaerobic reduction of SO_4^{2-}, can be used for the precipitation of metals in solution inside the sulphate reduction reactor or in a separate vessel (see Figure 3) [11]. The latter can be performed by contacting H_2S containing recycle gas (H_2S-CO_2-CH_4-H_2) with process water to precipitate dissolved metal ions. Coagulants such as $FeCl_3$ be added at this stage to ensure rapid precipitation of the metal sulphides. This system provides more control over the separate functions of ZnS precipitation and sulphate reduction. It also prevents the interference of metal precipitation with the bioreactor, e.g. the poisoning of the bacteria by the metals.

This thesis is mainly concerned with this promising process which is involving gas liquid mass transfer accompanied by precipitation. Not much is known yet about the interactions between all relevant parameters and about their influence on product quality.

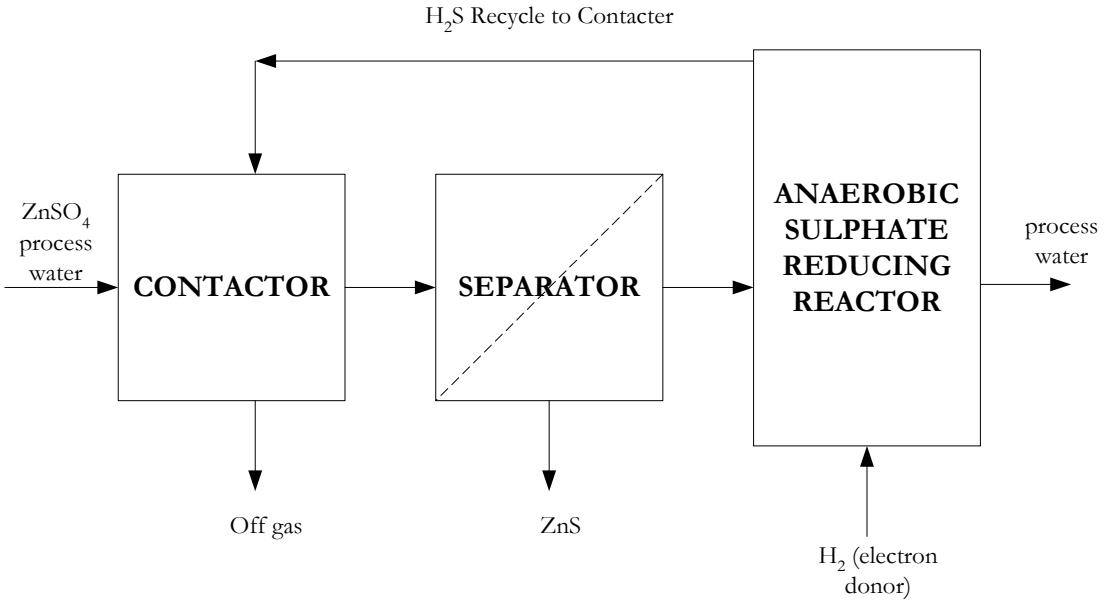

Figure 3: *Sulfate reduction process with separation between precipitation and biological sulfate removal*

Other Features Of Biological Sulfide Precipitation

Other toxic heavy metals such as cadmium, arsenic, antimony, lead, nickel and cobalt can also be precipitated as sulphides. Metals such as nickel can also be recovered selectively as a byproduct if present in sufficient concentration. It might in some cases be necessary to treat the liquid discharge from the ZnS separation further in a lime plant for final neutralization and precipitation of iron and aluminum. This configuration still presents savings in lime and a reduction in both volume and toxicity of the lime plant sludge, thereby reducing long-term liability of sludge storage and maintenance. In some cases, however, effluent can be discharged without further treatment.

In general, biological sulphide precipitation includes the following advantages [7]:

- Lower costs per ton sulfide produced;
- Removal of metals up to concentrations of 1-100ppb;
- More efficient recovery of valuable metals, Pb, Cu, Zn and Co;
- Better selectivity forwards heavy metals;
- Out-performs alkaline treatment due to the lower solubilities of metal sulphides as opposed to hydroxides
- Minimize sludge disposal
- The process also qualifies for SO_x and CO_2 emission credits [11].

0.3 This Thesis

Precipitation of solids promoted by gas-liquid reactions is applied for production of fine chemicals, in biotechnology, in heavy metal removal (this work) and in gas cleaning [12]. Despite the importance of gas-liquid precipitation no extensive studies have been carried out until recently. The physical characteristics of the produced particles are of great significance for downstream processing and/or technical applications and are determined by process conditions and formation kinetics. Mass transfer, hydrodynamics, chemical reaction, nucleation, crystals growth, agglomeration, disruption and ripening are all important. During the induction period of crystallization, mass transfer and chemical reaction generate supersaturation. Nucleation and subsequent crystal growth will proceed at rates that depend on the level of supersaturation delivered. When crystal formation is fast compared to the dispersion of the reaction product, significant non-uniformities may occur throughout the solution and mixing effects thus become important. Secondary nucleation may also occur due to particle breakage or attrition. Crystals will grow due to molecular or ionic growth at the crystal surface or due to agglomeration. Small crystals may dissolve whereas the resulting solute attaches to larger crystals (Ostwald ripening) or get enclosed inside agglomerates oozes out, sweating.

It is extremely difficult to predict a priori how all these phenomena interact and affect the size distribution of the produced crystals. To get better insight in this matter a mathematical model in chapter 1 of this thesis will be prepared. This model includes both mass transfer and kinetics and makes use of Higbie's penetration theory to describe the phenomena at the gas-liquid interface [14]. Arbitrary power low kinetics are applied in the first instance due to lack of data for the fast nucleation and growth of metals sulfide crystals. In chapter 2 and 3 the kinetics of CuS and ZnS precipitation are examined using a so-called Mixed Suspension Mixed product removal (MSMPR) reactor. Though some information were obtained with regard to e.g. agglomeration behavior, intrinsic kinetics of the fast precipitation reactions could hardly be obtained as mixing phenomena seemed

to influence the experimental results to large extent. Therefore an alternative technique was developed to measure nucleation and crystal growth kinetics more precisely. This technique involves the use of a laminar jet reactor and is described in chapter 4 Test were carried out with CuS precipitation and indeed much more reliable kinetic data could be acquired.

The choice of a reactor is of substantial importance for the precipitation process under concern. Gas-liquid mass transfer phenomena determine the level of solute supersaturation and its spatial distribution in the liquid phase, whereas hydrodynamics will influence. Agglomeration and subsequent ageing processes are likely to be affected by flow dynamics such as motion of the suspension of solids and the fluid shear stress distribution. Figure 4 shows some common gas-liquid contactors and table 1 summarized their characteristics

Table 1: *Characteristic data of equipment for gas absorption with chemical reaction in aqueous systems [13]*

Type of gas-liquid contactor	Specific surface, a (m^{-1})	Volume fraction liquid phase (1-ε)	*Sh*= $k_L d/D_A$	Al
Spray column	60	0.05	10-25	2-10
Plate column	150	0.15	200-600	40-100
Packed column	100	0.08	10-100	10-100
Wetted wall column	50	0.05	10-50	10-50
Bubble column	20	0.98	400-1000	$4000\text{-}10^4$
Agitated bubble	200	0.90	100-500	150-800

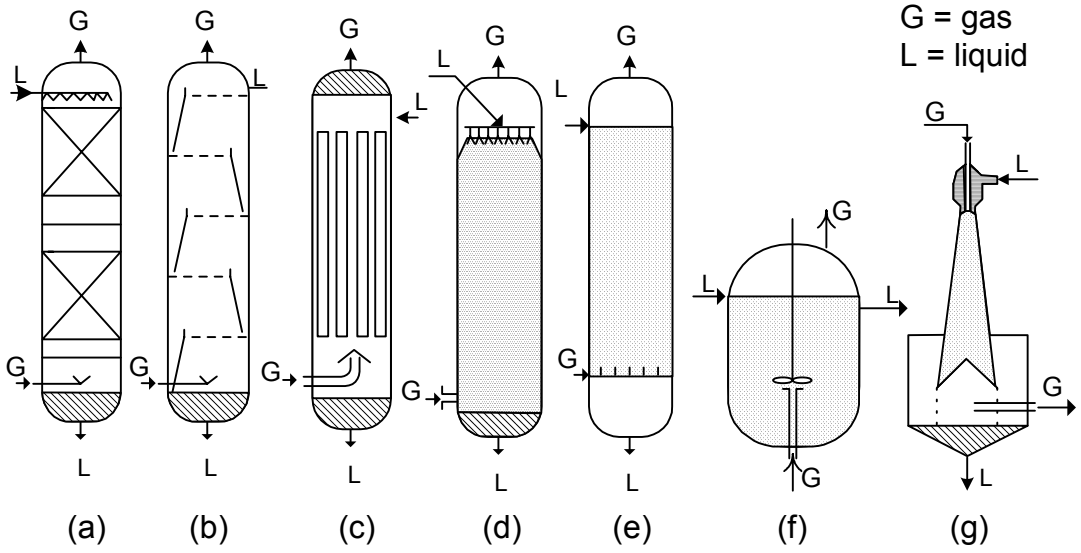

Figure 4: *Some common types of gas-liquid reactors. (a)-packed column, (b) tray column, (c) falling film reactor, (d) spray column, (e) bubble column, (f)agitated tank reactor, (g) venturi reactor [13]*

In chapter 5 a study is presented into the precipitation of ZnS and CuS in a bubble column contactor. The influence of mass transfer on product quality was examined. The effects of inlet gas concentration, superficial gas velocity, pressure and initial metal concentration were investigated.

The effect of reactor geometry and mass transfer coefficient on crystal morphology is studied in Chapter 6. Metal sulfide samples from different reactors and produced at different conditions are compared by examining them using SEM and TEM photo's.

References

1. Costa A. C. A, L. M. S. Mesquita, J. Tornovsky. "Batch and continuous heavy metals biosorption by a brown seaweed from a zinc-producing plant", Minerals Engineering, Volume 9, No. 8, pp 811 – 824, 1996.
2. Reuter M. A, S. Sudholter, J. Kruger, S. Koller. "Synthesis of processes for the production of environmentally clean zinc", Minerals Engineering, Volume 8, No. 1/2, pp 201 – 219, 1995.
3. Schneider I. A. H, J. Rubio, R. W. Smith. "Biosorption of metals onto plant biomass: exchange adsorption or surface precipitation?", Int. J. of Min. Pro, Volume 62, pp 111 – 120, 2001.
4. Scott J. A, A. M. Karanjkar, D. L. Rowe. "Biofilm covered granular activated carbon for decontamination of streams containing heavy metals and organic chemicals", Minerals Engineering, Volume 8, No. 1/2, pp. 221 – 230, 1995.
5. Van Hille R. P, G. H. Boshoff, P. D. Rose, J. R. Duncan. "A continuous process for the biological treatment of heavy metal contaminated acid mine water", Resources, Conservation and Recycling, Volume 27, pp 157 – 167, 1999.
6. Rubio J, F. Tessele. "Removal of heavy metal ions by adsorptive particulate flotation", Minerals Engineering, Volume 10, No. 7, pp 671 – 679, 1997.
7. Buisman C. J. N, S. H. J. Vellinga, G. H. R. Janssen, and H. Dijkman. "Biological Sulphide Production for Metal recovery", Affiliated by PAQUES Bio Systems B.V., Netherlands, TMS Congress 1999, Fundamentals of Lead and Zinc Extraction and Recycling, 1999.
8. Feng, D, C. Aldrich, H. Tan. "Treatment of Acid Mine Water by Use of Heavy Metal Precipitation and Ion Exchange", Minerals Engineering, Volume 13, No. 6, pp 623 – 642, 2000.
9. Simpson C, S. H. Laurie. "Ion exchange studies on zinc-rich waste liquors", Hydrometallurgy, Volume 51, pp 335 – 344, 1999.

10. Watson J. H. P, D. C. Ellwood, C. J. Duggleby. "A chemostat with magnetic feedback for the growth of sulphate reducing bacteria and its application to the removal and recovery of heavy metals from solution", Minerals Engineering, Volume 9, No. 9, pp 973 – 983, 1996.

11. PAQUES B.V. The Netherlands, www.paques.nl .

12. Shun Wachi and Alan Jones. "Mass Transfer With Chemical Reaction and Precipitation", Che. Eng. Sci. Vol. 46, No. 4, pp 1027-1033, 1991.

13. Westererp K. R, W. P. M. van Swaaij and A. A. C. M. Beernackers. *Chemical reactor Design and Operation*. Johon Wiley &Sons Ltd. Chichester, (1995).

14. Higbie R. "The Rate of Absorption of pure Gas into a Still Liquid During Short Periods of Exposure". Trans. AICHE, Vol. 31, p 365, 1935.

Chapter 1

Precipitation of Metal Sulfides Using Gaseous Hydrogen Sulfide: Mathematical Modeling

Abstract

A mathematical model has been developed that describes the precipitation of metal sulfides in an aqueous solution containing two different heavy metal ions. The aqueous solution is assumed to consist of a well-mixed bulk and an interfacial area that is contacted with hydrogen sulfide gas. The model makes use of Higbie's penetration model to calculate the transfer rate of gaseous hydrogen sulfide through this interface. The conditions that have been used in the simulations resemble those of industrial wastewater from a zinc factory. The model predicts the rate of H_2S absorption, the size distribution of the metal sulfide crystals and the selectivity of the precipitation.

Higher precipitation rates are predicted at higher pH values and higher H_2S concentrations. In all cases considered, the rate of precipitation is fully controlled by mass transfer of H_2S, higher H_2S concentrations and higher specific surface areas yielding higher precipitation rates. The size of the obtained crystals is predicted to increase with H_2S concentration, but to decrease with specific surface area and liquid side mass transfer. These results illustrate the importance of the reactor selection, layout and operating conditions on the process of gas-liquid precipitation.

1.1 Introduction

Crystallization involves the transformation of an amorphous solid, a liquid, or a gas into the crystalline state [1]. As with any chemical process, a certain driving force is needed to accomplish this task; in crystallization this driving force is delivered by supersaturation. Supersaturation can be achieved by cooling the solution, evaporating the solvent, adding an inert substance that reduces the solubility (drowning-out) or by reaction. Precipitation, or reactive crystallization, involves the reaction of two or more reactants to form a sparingly soluble product, which then becomes supersaturated and, as a result, crystallizes.

Precipitation of solids promoted by gas-liquid reactions takes place in many industrial processes [2]. Despite the importance of this principle (in this chapter further referred to as "gas-liquid precipitation") no extensive studies have been dedicated to it until recently. The size distribution of the solid particles is fully determined by precipitation conditions, which may vary quite significant from the gas-liquid interface to the liquid bulk. This size distribution is of great importance for separation and down stream processing of the particles. A good understanding of the relevant phenomena is therefore of utmost interest.

Gas-liquid precipitation is applied for the synthesis of many chemicals such as ammonium phosphate, ammonium sulphate, barium carbonate, calcium carbonate, calcium fluoride, gypsum (calcium sulphate), goethite, sodium bicarbonate, strontium carbonate and terephthalic acid [3]. In addition gas-liquid precipitation can be applied in gas cleaning, heavy metal removal and in biotechnology [4]. This paper deals with the simultaneous precipitation of two heavy metal ions by gaseous H_2S and the modeling thereof.

The process of gas-liquid precipitation generally involves mass transfer, chemical reaction, supersaturation, nucleation, molecular growth, agglomeration, disruption and ripening. During the so-called induction period mass transfer and chemical reaction cause the generation of supersaturation. Nucleation and subsequent crystal growth then follow at a rate that depends on the delivered level of supersaturation. The size of solids formed upon nucleation will increase by molecular or ionic growth at the crystal surface as well as by agglomeration. Small crystals may also dissolve while the resulting solute is transported to the larger crystals, which are thermodynamically more stable and will grow (Ostwald ripening). All mentioned phenomena occur simultaneously and are inter-related, making gas-liquid precipitation a rather complex process. By precisely describing each phenomenon and combining the obtained sub-models in a comprehensive overall model, a tool is obtained that can be used to predict the particle size distribution of the obtained particles as a function of reactor layout and operating conditions.

The selection and layout of the gas-liquid contactor is of substantial importance for the product quality as well as for production efficiency. Compare for example a spray tower with a bubble column: mass transfer and mixing phenomena are completely different in these contactors and the size distributions of the produced particles in both contactors are likely to differ substantially. Each stage of particle formation is affected by the way of gas-liquid contacting. Gas-liquid mass transfer phenomena determine the level of solute supersaturation and its spatial distribution in the liquid phase. Agglomeration and subsequent ageing processes are likely to be affected by flow dynamics, motion of the suspended solids and by fluid shear stress distribution as well.

Thus during precipitation of dissolved species with gaseous compounds, mass transfer often controls overall precipitation behavior and product characteristics [5]. Nevertheless, its effect has not yet been studied extensively, even though small differences in concentrations at micro-level may highly influence the size of the obtained crystals due to the high sensitivity of nucleation kinetics and crystal growth towards the level of supersaturation.

1.2 Previous work

Wachi et al. (1991) modeled the gas-liquid precipitation of calcium carbonate using gaseous CO_2 [2]. Gas-liquid mass transfer, chemical reaction and crystallization, were analyzed making use of the film theory to describe gas-liquid mass transfer coupled with chemical reaction. Mass and population balances were used to calculate the obtained particle size distribution. They solved the resulting equations for a stirred cell reactor, operated in semi-batch mode. They calculated that the spatial distribution of supersaturation due to the mass transfer resistance has an effect on the resulting crystal size distribution: according to model prediction larger particles are formed under conditions of fast mass transfer while small particles of uniform size are produced when mass transfer is slow.

Narayan S. Tavare (1991) reviewed the techniques employed for the evaluation of experimental data from batch crystallizers [9]. They presented a number of useful general techniques to extract crystallization kinetics and to assess crystallizer performance.

Jones et al (1992) studied the effect of liquid mixing on primary crystal size during the precipitation of calcium carbonate in a stirred cell [7]. They used the film model to describe gas-liquid mass transfer coupled with chemical reaction and a dynamic population balance to describe crystal growth. Experimentally they found that small crystals of approx. 1 *micron* are formed in the vicinity of the gas-liquid interface during the early stages of batch precipitation. The primary crystals were found to grow reaching

a diameter of approximately 6 *microns* in the bulk. This mean crystal size was found to increase with increasing agitation rate, which is consistent with their model predictions.

Wachi and Jones (1992) studied the influence of agglomeration on the gas-liquid precipitation of calcium carbonate [10]. They described the effects of agglomeration using two extra terms in the population balance (birth and death). Their model predicts the evolution of particle size distribution in time. They found that the formation of agglomerated precipitates could be modeled in terms of overall particle size and the number of primary crystals within a particle.

Hostomsky and Jones (1995) modeled the precipitation of calcium carbonate crystals in a semibatch stirred cell using Higbie's penetration model to describe gas-liquid mass transfer [6]. They studied the effect of mass transfer on the rate of precipitation using thermodynamic and kinetic data from literature. They found that the nucleation rate in the region close to the gas-liquid interface will increase with decreasing mass transfer rates; at very low mass transfer rates (i.e. long contact times), however nucleation rates become inhibited by the depletion of Ca^{2+} ions. They also found that at low mass transfer rates, nucleation predominantly proceeds in the interfacial region rather than in the bulk solution. They predicted that the nucleation rate, particle number density and mean particle size show a maximum at a position away from the gas-liquid interface.

Wachi and Jones (1995) reviewed gas-liquid precipitation with particular focus on how to control the physical form of the product [3]. They also examined the secondary processes of particle agglomeration and particle disruption and the effects of reactor fluid dynamics.

Al-Rashed and Jones (1999) performed a CFD analysis to predict the effect of mixing during batch-wise gas-liquid precipitation [8]. They developed a 2 D flow simulation model and compared their CFD-based predictions with the results of the applied film and penetration models for the calcium carbonate system. They observed that the CFD based predictions reveal crystal size distributions in between those predicted by the film model and those predicted by the penetration model, thereby highlighting the role of hydrodynamics in the precipitation process.

All models yet available consider the precipitation of just one metal ion whereas most models assume the bulk to be non-reactive.

1.3 Present Model

In this work a mass transfer accompanied by reactions model has been developed that describes the precipitation of metal sulfides in an aqueous solution containing two different heavy metal ions (Cu^{2+} and Zn^{2+} are taken as example) that is continuously contacted with hydrogen sulfide gas in e.g. a stirred cell (Figure 1). This mathematical model is able to predict the effects of operation and process conditions and reactor layout

on the rate of precipitation and the size distribution of the produced particles. It is able to describe the combined effect of two different precipitates and therefore it can predict also selectivities. The model makes use of Higbie's penetration model to calculate the transfer of gaseous hydrogen sulfide to the aqueous liquid. Besides the liquid side mass transfer resistance also the gas side resistance is taken into account because of the expected high reaction rates. Mass balances for all species and the overall electroneutrality demand are used to calculate concentration profiles. Required equilibrium and kinetic data were taken from literature. The model includes nucleation and crystal growth in the interfacial area as well as in the bulk. Both gas and liquid bulk are assumed to be ideally mixed and the H_2S concentration in the gas bulk is assumed not to change in time. Besides the two heavy metal ions, sulfate ions are assumed to be present in the liquid. In this way the composition of a typical wastewater stream as frequently encountered in metal production plants is resembled.

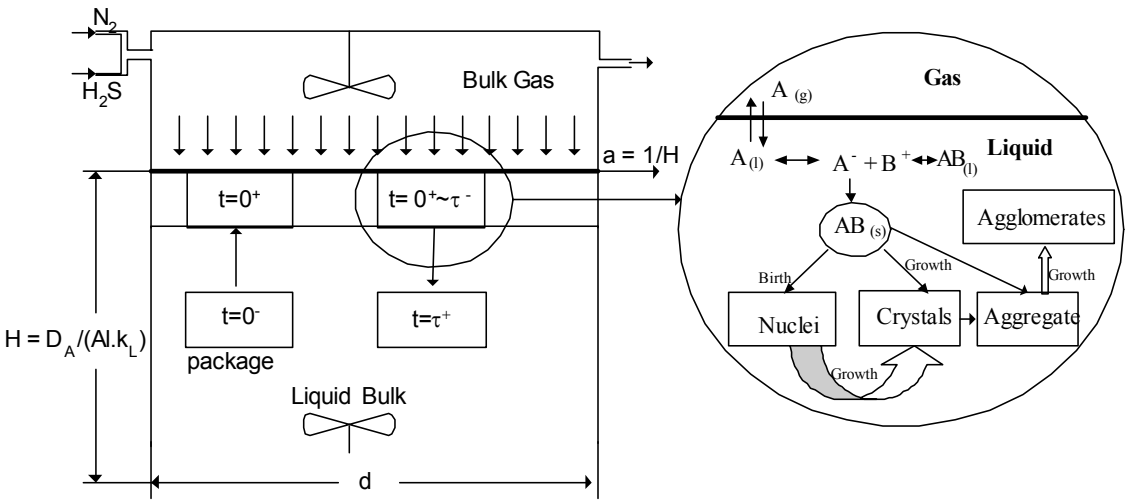

Figure 1: *Schematic diagram of the gas-liquid contactor applied in the model. Formation of aggregates and agglomerates is not included in the present model.*

The chemistry of the mixed ions system can be described by the following equations:

$$H_2S_{(g)} \longleftrightarrow H_2S_{(l)} \tag{A}$$

$$H_2S_{(l)} \xleftrightarrow{k_1,\frac{k_1}{k_{eq1}}} HS^- + H^+ \tag{B}$$

$$HS^- \xleftrightarrow{k_2,\frac{k_2}{k_{eq2}}} S^{2-} + H^+ \tag{C}$$

$$Me_1^{2+} + S^{2-} \xrightarrow{k_3} Me_1S \tag{D}$$

$$Me_2^{2+} + S^{2-} \xrightarrow{k_4} Me_2S \tag{E}$$

$$H^+ + OH^- \quad \xleftrightarrow{k_5, k_5 kw} \quad H_2O \tag{F}$$

$$HSO_4^- \quad \xleftrightarrow{k_6, \frac{k_6}{ks}} \quad SO_4^{2-} + H^+ \tag{G}$$

"Reaction" (A) occurs only at the gas-liquid interface. The concentration of dissolved H_2S at the gas liquid interface is calculated by an iterative procedure involving the gas side mass transfer rate and Henry's law. The reversible reactions (B), (C), (F) and (G) are very fast and are assumed to be at equilibrium. However, for numerical reasons kinetic constants are used (having very high values; see Table 1). The consumption rates are calculated according:

$$r_{H_2S} = k_1 c_{H_2S} - \frac{k_1}{k_{eq_1}} c_{HS^-} c_{H^+} \tag{1}$$

$$r_{HS^-} = k_2 c_{HS^-} - \frac{k_2}{k_{eq_2}} c_{S^{2-}} c_{H^+} - k_1 c_{H_2S_{(l)}} + \frac{k_1}{k_{eq_1}} c_{HS^-} c_{H^+} \tag{2}$$

$$r_{S^{2-}} = -k_2 c_{HS^-} + \frac{k_2}{k_{eq_2}} c_{S^{2-}} c_{H^+} + r_{Me_1S} + r_{Me_2S} \tag{3}$$

$$r_{Me_1^{2+}} = -r_{Me_1S} \tag{4}$$

$$r_{Me_2^{2+}} = -r_{Me_2S} \tag{5}$$

$$\begin{aligned} r_{H^+} = {} & -k_1 c_{H_2S_{l)}} + \frac{k_1}{k_{eq_1}} c_{HS^-} c_{H^+} - k_2 c_{HS^-} + \frac{k_2}{k_{eq_2}} c_{S^{2-}} c_{H^+} + k_5 c_{H^+} c_{OH^-} \\ & - k_6 c_{HSO_4^-} + \frac{k_6}{k_{eq_3}} c_{SO_4^{2-}} c_{H^+} - k_5 kw \end{aligned} \tag{6}$$

$$r_{OH^-} = k_5 c_{H^+} c_{OH^-} - k_5 kw \tag{7}$$

$$r_{HSO_4^-} = k_6 c_{HSO_4^-} - \frac{k_6}{k_{eq_3}} c_{H^+} c_{SO_4^{2-}} \tag{8}$$

$$r_{SO_4^{2-}} = -k_6 c_{HSO_4^-} + \frac{k_6}{k_{eq_3}} c_{H^+} c_{SO_4^{2-}} \tag{9}$$

$$-r_{Me_1S} = G_1' + B_1' - \sqrt{k_{sp_1}} \tag{10}$$

$$-r_{Me_2S} = G_2' + B_2' - \sqrt{k_{sp_2}} \tag{11}$$

According to Higbie's penetration model [11], stagnant packages of solution arise from the bulk, move to the gas-liquid interface, remain there for a certain period of time

(contact time τ) and are then swept back to the bulk. The concentration profiles of all individual species in the liquid package can be calculated as a function of time using the following equations (mass balances):

$$\frac{\partial c_{H_2S_{(l)}}}{\partial t} = D_{H_2S_{(l)}} \frac{\partial^2 c_{H_2S_{(l)}}}{\partial x^2} - r_{H_2S} \tag{12}$$

$$\frac{\partial c_{HS^-}}{\partial t} = D_{HS^-} \frac{\partial^2 c_{HS^-}}{\partial x^2} - z_{HS^-} D_{HS^-} \frac{F}{RT} \frac{\partial (\phi c_{HS^-})}{\partial x} - r_{HS^-} \tag{13}$$

$$\frac{\partial c_{S^{2-}}}{\partial t} = D_{S^{2-}} \frac{\partial^2 c_{S^{2-}}}{\partial x^2} - z_{S^{2-}} D_{S^{2-}} \frac{F}{RT} \frac{\partial (\phi c_{S^{2-}})}{\partial x} - r_{S^{2-}} \tag{14}$$

$$\frac{\partial c_{Me_1^{2+}}}{\partial t} = D_{Me_1^{2+}} \frac{\partial^2 c_{Me_1^{2+}}}{\partial x^2} - z_{Me_1^{2+}} D_{Me_1^{2+}} \frac{F}{RT} \frac{\partial (\phi c_{Me_1^{2+}})}{\partial x} - r_{Me_1^{2+}} \tag{15}$$

$$\frac{\partial c_{Me_2^{2+}}}{\partial t} = D_{Me_2^{2+}} \frac{\partial^2 c_{Me_2^{2+}}}{\partial x^2} - z_{Me_2^{2+}} D_{Me_2^{2+}} \frac{F}{RT} \frac{\partial (\phi c_{Me_2^{2+}})}{\partial x} - r_{Me_2^{2+}} \tag{16}$$

$$\frac{\partial c_{H^+}}{\partial t} = D_{H^+} \frac{\partial^2 c_{H^+}}{\partial x^2} - z_{H^+} D_{H^+} \frac{F}{RT} \frac{\partial (\phi c_{H^+})}{\partial x} - r_{H^+} \tag{17}$$

$$\frac{\partial c_{OH^-}}{\partial t} = D_{OH^-} \frac{\partial^2 c_{OH^-}}{\partial x^2} - z_{OH^-} D_{OH^-} \frac{F}{RT} \frac{\partial (\phi c_{OH^-})}{\partial x} - r_{OH^-} \tag{18}$$

$$\frac{\partial c_{HSO_4^-}}{\partial t} = D_{HSO_4^-} \frac{\partial^2 c_{HSO_4^-}}{\partial x^2} - z_{HSO_4^-} D_{HSO_4^-} \frac{F}{RT} \frac{\partial (\phi c_{HSO_4^-})}{\partial x} - r_{HSO_4^-} \tag{19}$$

$$\frac{\partial c_{SO_4^{2-}}}{\partial t} = D_{SO_4^{2-}} \frac{\partial^2 c_{SO_4^{2-}}}{\partial x^2} - z_{SO_4^{2-}} D_{SO_4^{2-}} \frac{F}{RT} \frac{\partial (\phi c_{SO_4^{2-}})}{\partial x} - r_{SO_4^{2-}} \tag{20}$$

The mass balances of Me_1S and Me_2S are not needed since the rate of crystal growth and nucleation are expressed as separate functions of super-saturation and population balances are used (see below).

The electrostatic potential gradient (ϕ) can be calculated by the use of the Nernst-Einstein [12] equation assuming dynamic electroneutrality:

$$\phi(x,t) = \frac{RT}{F} \frac{\sum_{i=1}^{NC} z_i D_i \frac{\partial c_i}{\partial x}}{\sum_{i=1}^{NC} z_i^2 D_i c_i} \tag{21}$$

Assuming no agglomeration or attrition (death and secondary nucleation) the crystal size distribution follows from the population balance proposed by Randolph [13]

$$\frac{\partial n_1}{\partial t} + G_1\left(\frac{\partial n_1}{\partial L}\right) = D_{p_1}\frac{\partial^2 n_1}{\partial x^2} \tag{22}$$

$$\frac{\partial n_2}{\partial t} + G_2\left(\frac{\partial n_2}{\partial L}\right) = D_{p_2}\frac{\partial^2 n_2}{\partial x^2} \tag{23}$$

Diffusion of particles is mainly due to random motion of these particles. Incorporating of this term is important since the packages are assumed to be stagnant (Higbie's penetration model). Migration of particles within a package will influence the growth rate as well as the mean particle size distribution within that package. For sufficiently small particles, the diffusivity of the crystals within the liquid film may be described by the Stokes-Einstein equation [14]:

$$\mathrm{D_p} = \frac{k_b T}{6\pi\eta r} \tag{24}$$

The rate of nucleation (J_n), the linear growth rate (G) and the molar growth rate (G′) are given by:

$$G = k_g\left[\frac{\sqrt{c_{Me^{2+}}c_{S^{2-}}}}{c^*_{MeS}} - 1\right]^g \tag{25}$$

$$J_n = k_n\left[\frac{\sqrt{c_{Me^{2+}}c_{S^{2-}}}}{c^*_{MeS}} - 1\right]^n \tag{26}$$

$$B' = \alpha\rho J_n L_o^3 \tag{27}$$

$$G' = \sum_{i=1}^{\infty}\{\beta\rho n(z, L_i^2)GL_i^2(L_i - L_{i-1})\} \tag{28}$$

$$c^*_{MeS} = \sqrt{k_{sp}} \tag{29}$$

The initial and boundary conditions for the above equations are:

$$c_i(t=0) = c_i^{bulk} \tag{30}$$

$$n(x,L,t=0) = n(L)_{bulk} \tag{31}$$

To derive the appropriate boundary conditions near the gas-liquid interface; mass balances over a control volume of thickness Δx should be used for all species involved:

$$\frac{\partial}{\partial t}\int_0^{\Delta x} c_{H_2S}\,dx = J_{H_2S} + D_{HS^-}\frac{\partial c_{H_2S}}{\partial x} - \int_0^{\Delta x} r_{H_2S}\,dx \tag{32-a}$$

$$\frac{\partial}{\partial t}\int_0^{\Delta x} c_{HS^-}\,dx = D_{HS^-}\frac{\partial c_{HS^-}}{\partial x} - z_{HS^-}D_{HS^-}\frac{F}{RT}\phi c_{HS^-} - \int_0^{\Delta x} r_{HS^-}\,dx \tag{32-b}$$

$$\frac{\partial}{\partial t}\int_0^{\Delta x} c_{S^{2-}}\,dx = D_{S^{2-}}\frac{\partial c_{S^{2-}}}{\partial x} - z_{S^{2-}}D_{S^{2-}}\frac{F}{RT}\phi c_{S^{2-}} - \int_0^{\Delta x} r_{S^{2-}}\,dx \tag{32-c}$$

$$\frac{\partial}{\partial t}\int_0^{\Delta x} c_{H^+}\,dx = D_{H^+}\frac{\partial c_{H^+}}{\partial x} - z_{H^+}D_{H^+}\frac{F}{RT}\phi c_{H^+} - \int_0^{\Delta x} r_{H^+}\,dx \tag{32-d}$$

$$\frac{\partial}{\partial t}\int_0^{\Delta x} c_{HO^-}\,dx = D_{HO^-}\frac{\partial c_{HO^-}}{\partial x} - z_{HO^-}D_{HO^-}\frac{F}{RT}\phi c_{HO^-} - \int_0^{\Delta x} r_{HO^-}\,dx \tag{32-e}$$

$$\frac{\partial}{\partial t}\int_0^{\Delta x} c_{HSO_4^-}\,dx = D_{HSO_4^-}\frac{\partial c_{HSO_4^-}}{\partial x} - z_{HSO_4^-}D_{HSO_4^-}\frac{F}{RT}\phi c_{HSO_4^-} - \int_0^{\Delta x} r_{HSO_4^-}\,dx \tag{32-f}$$

$$\frac{\partial}{\partial t}\int_0^{\Delta x} c_{SO_4^{2-}}\,dx = D_{SO_4^{2-}}\frac{\partial c_{SO_4^{2-}}}{\partial x} - z_{SO_4^{2-}}D_{SO_4^{2-}}\frac{F}{RT}\phi c_{SO_4^{2-}} - \int_0^{\Delta x} r_{SO_4^{2-}}\,dx \tag{32-g}$$

$$\frac{\partial}{\partial t}\int_0^{\Delta x} c_{Me_1^{2+}}\,dx = D_{Me_1^{2+}}\frac{\partial c_{Me_1^{2+}}}{\partial x} - z_{Me_1^{2+}}D_{Me_1^{2+}}\frac{F}{RT}\phi c_{Me_1^{2+}} - \int_0^{\Delta x} r_{Me_1^{2+}}\,dx \tag{32-h}$$

$$\frac{\partial}{\partial t}\int_0^{\Delta x} c_{Me_2^{2+}}\,dx = D_{Me_2^{2+}}\frac{\partial c_{Me_2^{2+}}}{\partial x} - z_{Me_2^{2+}}D_{Me_2^{2+}}\frac{F}{RT}\phi c_{Me_2^{2+}} - \int_0^{\Delta x} r_{Me_2^{2+}}\,dx \tag{32-i}$$

For an instantaneous reaction the reaction rate becomes infinite and therefore integration is not possible. In such cases elimination of the rate terms in the above equations can be achieved by adding or subtracting those mass balances that are linked by the accumulation terms. By doing so, the accumulation terms vanish while the time derivatives of all concentrations are assumed to remain bounded. Accordingly, the following boundary conditions are obtained:

$$J_{H_2S} + \begin{bmatrix} D_{HS^-}\dfrac{\partial c_{H_2S}}{\partial x} + D_{HS^-}\dfrac{\partial c_{HS^-}}{\partial x} - z_{HS^-}D_{HS^-}\dfrac{F}{RT}\phi c_{HS^-} + D_{S^{2-}}\dfrac{\partial c_{S^{2-}}}{\partial x} \\ - z_{S^{2-}}D_{S^{2-}}\dfrac{F}{RT}\phi c_{S^{2-}} - D_{Me_1^{2+}}\dfrac{\partial c_{Me_1^{2+}}}{\partial x} + z_{Me_1^{2+}}D_{Me_1^{2+}}\dfrac{F}{RT}\phi c_{Me_1^{2+}} \\ - D_{Me_2^{2+}}\dfrac{\partial c_{Me_2^{2+}}}{\partial x} + z_{Me_2^{2+}}D_{Me_2^{2+}}\dfrac{F}{RT}\phi c_{Me_2^{2+}} \end{bmatrix} = 0 \tag{33-a}$$

$$2J_{H_2S} + \left[\begin{array}{l} D_{H^+}\dfrac{\partial c_{H^+}}{\partial x} - z_{H^+}D_{H^+}\dfrac{F}{RT}\phi c_{H^+} - D_{HO^-}\dfrac{\partial c_{HO^-}}{\partial x} + z_{HO^-}D_{HO^-} \\ \dfrac{F}{RT}\phi c_{HO^-} + D_{HSO_4^-}\dfrac{\partial c_{HSO_4^-}}{\partial x} - z_{HSO_4^-}D_{HSO_4^-}\dfrac{F}{RT}\phi c_{HSO_4^-} \\ + D_{HS^-}\dfrac{\partial c_{HS^-}}{\partial x} - z_{HS^-}D_{HS^-}\dfrac{F}{RT}\phi c_{HS^-} + 2D_{HS^-}\dfrac{\partial c_{H_2S}}{\partial x} \end{array}\right]_{x=0} = 0 \qquad \text{(33-b)}$$

$$\left[\begin{array}{l} D_{HSO_4^-}\dfrac{\partial c_{HSO_4^-}}{\partial x} - z_{HSO_4^-}D_{HSO_4^-}\dfrac{F}{RT}\phi c_{HSO_4^-} + D_{SO_4^{2-}}\dfrac{\partial c_{SO_4^{2-}}}{\partial x} \\ - z_{SO_4^{2-}}D_{SO_4^{2-}}\dfrac{F}{RT}\phi c_{SO_4^{2-}} \end{array}\right]_{x=0} = 0 \qquad \text{(33-c)}$$

This elimination process gives three independent equations (33-a, b, c). To achieve the complete boundary conditions the following six equations expressing that chemical equilibria are accomplished are also needed:

$$k_{eq_1}c_{H_2S} - c_{HS^-}c_{H^+} = 0 \qquad \text{(33-d)}$$

$$k_{eq_2}c_{HS^-} - c_{H^+}c_{S^{2-}} = 0 \qquad \text{(33-e)}$$

$$k_{sp_1} - c_{S^{2-}}c_{Me_1^{2+}} = 0 \qquad \text{(33-f)}$$

$$k_{sp_2} - c_{S^{2-}}c_{Me_2^{2+}} = 0 \qquad \text{(33-g)}$$

$$kw - c_{H^+}c_{OH^-} = 0 \qquad \text{(33-h)}$$

$$k_{eq_3}c_{HSO_4^-} - c_{H^+}c_{SO_4^{2-}} = 0 \qquad \text{(33-i)}$$

However, the use of far more simplified boundary conditions will give similar results [5]. Therefore, in order to reduce the calculation time and to improve numerical stability; commonly the following simplified boundary conditions were used:

$$-D_{H_2S}\frac{\partial c_{H_2S}}{\partial x}_{x=0} = k_{m,g}\left(c^{bulk}_{H_2S_{(g)}} - \frac{c^{i}_{H_2S_{(L)}}}{m}\right) \qquad \textit{for } H_2S \qquad (34)$$

and for the other components:

$$z_i D_i \frac{F}{RT}(\phi c_i)\Big|_{x=0} - D_i\frac{\partial c_i(t)}{\partial x}_{x=0} = 0 \quad \textit{for ionic components} \qquad (35)$$

$$\frac{\partial c\ (t)}{\partial x}_{x=0} = 0 \quad \textit{for neutral non-volatile components} \qquad (36)$$

$$c_i(t)_{x=z_o} = c_i^{bulk}(t) \qquad (37)$$

The thickness of the package is calculated using the film model for the species with the highest diffusivity, i.e. hydrogen ions. For safety reasons this thickness is multiplied by two to make sure that the condition of "infinite" package thickness is obliged.

$$z_o = 2\frac{D_{H^+}}{k_{m,l}} \tag{38}$$

$$\left(\frac{\partial n}{\partial x}\right)_{x=0} = 0 \tag{39}$$

$$\frac{dn(x, L_0, t)}{dt} = J_n G \text{ , where } L_0 \text{ is the critical size of a nucleus} \tag{40}$$

The equations describing the concentration profiles in the package are coupled with the equations that describe the time dependent concentrations and particle size distribution in the well-mixed bulk by means of the time varying boundary conditions and initial conditions:

$$\frac{\partial c_i^{bulk}}{\partial t} = -r_i \tag{41}$$

$$\frac{\partial n_k}{\partial t} + G_k\left(\frac{\partial n_k}{\partial L}\right) = 0 \qquad \text{where k can be } Me_1 \text{ or } Me_2 \tag{42}$$

The initial concentrations of all species in a package and liquid bulk as well as the initial particle size distribution are updated after each penetration time by mixing the concentrations and particle size distribution in the bulk with the average concentrations and particle size distribution in the returning packages in a weighed manner (Figure 2 illustrates the applied algorithm):

$$c_i^{bulk}(t=\tau) = \frac{Al-1}{Al} c_i^{bulk}(t=\tau^-) + \frac{1}{Al}\sum_{k=0}^{n} c_i^{package}(x_k, \tau^-)(x_{k+1} - x_k) \tag{43}$$

where Al is the Hinterland ratio (volume of packages/total volume of liquid).

In this manner it is ensure that the calculated concentrations and particle size distributions are averaged over both bulk and film layer respectively.

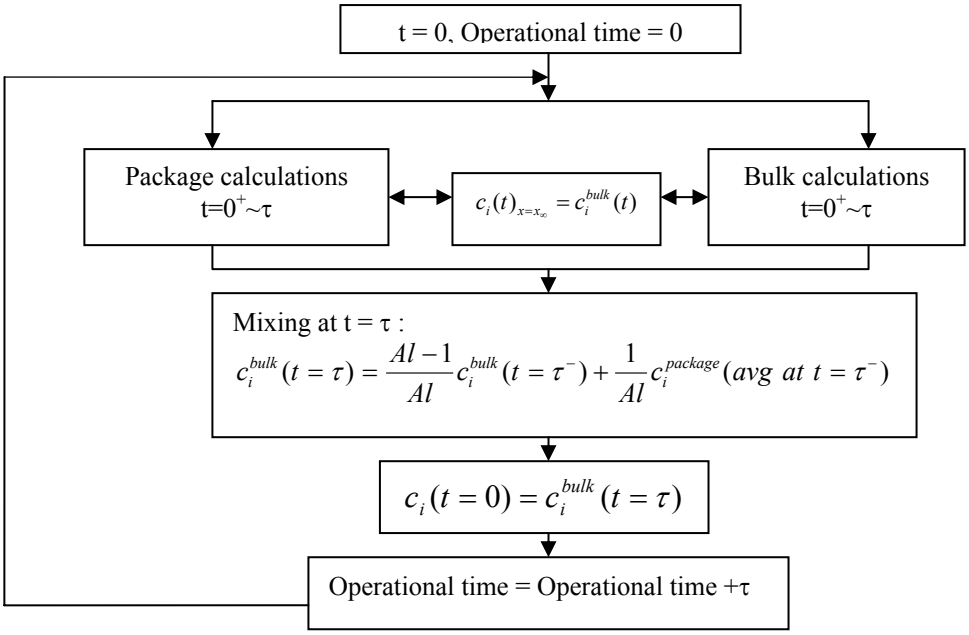

Figure 2: *Algorithm for calculation of bulk concentrations; same routine is used for particle size distribution.*

The time derivative and the second partial derivatives of the above model equations are discretised using the scheme proposed by Baker and Oliphant [15]. The convection term (electroneutrality term) is discretised using the first order upwind scheme. In this model the boundary conditions at the liquid bulk side of the package are up-dated every time step by recalculation of the bulk concentrations while making use of equations (41) and (42).

The model has been applied to simulate the simultaneous precipitation of copper and zinc ions with H_2S. Most data necessary to solve the model has been taken from literature; see Table 1

Table 1: *List of numerical values for the constants used in the model (1 =Cu, 2=Zn).*

Parameters	Value		Source
k_{sp_1}	6.3×10^{-30}	mol^2/m^6	[16]
k_{sp2}	1.6×10^{-18}	mol^2/m^6	[16]
ρ_1	41650.0	mol/m^3	[16]
ρ_2	45420.0	mol/m^3	[16]
L_{01}	5.6655×10^{-7}	m	[1]
L_{02}	5.392×10^{-7}	m	[1]
g_1	1.3	-	[17]
g_2	1.5	-	[17]

n_1	3.0	-	[17]
n_2	4.2	-	[17]
k_{n_1}	$1.1\text{x}10^{-23}$	m/s	[17]
k_{n_2}	$1.3\text{x}10^{-13}$		[17]
k_{g_1}	$2.06\text{x}10^{-20}$	m/s	[17]
k_{g_2}	$1.96\text{x}10^{-14}$	m/s	[17]
α	$\pi/6$	-	For spherical particles
β	π	-	For spherical particles
$D_{H_2S(l)}$	$1.92\text{x}10^{-9}$	m^2/s	[18]
$D_{H_2S(g)}$	$2.366\text{x}10^{-4}$	m^2/s	[18]
D_{HS^-}	$1.731\text{x}10^{-9}$	m^2/s	[18]
$D_{S^{2-}}$	$1.03\text{x}10^{-9}$	m^2/s	[19]
$D_{Me_1^{2+}}$	$0.703\text{x}10^{-9}$	m^2/s	[18]
$D_{Me_2^{2+}}$	$0.714\text{x}10^{-9}$	m^2/s	[17]
D_{H^+}	$9.311\text{x}10^{-9}$	m^2/s	[18]
D_{OH^-}	$5.273\text{x}10^{-9}$	m^2/s	[18]
$D_{HSO_4^-}$	$1.331\text{x}10^{-9}$	m^2/s	[18]
$D_{SO_4^{2-}}$	$1.065\text{x}10^{-9}$	m^2/s	[18]
$m(c_L^i / c_g^i)$	3.1773	-	[18]
k_1	$1\text{x}10^5$	1/s	Assumed
k_2	$3\text{x}10^{11}$	m^3/mol.s	Assumed
k_3	$5\text{x}10^{12}$	m^3/mol.s	Assumed
k_4	$3\text{x}10^{12}$	m^3/mol.s	Assumed
k_5	$2.2\text{x}10^{15}$	m^3/mol.s	Assumed
k_6	$1\text{x}10^2$	1/s	Assumed
$k_{m,g}$	$1.0\text{x}10^{-2}$	m/s	Assumed
$k_{eq}(HSO_4^- / SO_4^{2-})$	10.233	mol/m^3	[18]
$k_{eq}(H_2S / HS^-)$	$1.07152\text{x}10^{-4}$	mol/m^3	[18]
$k_{eq}(HS^- / S^{2-})$	$1.259\text{x}10^{-10}$	mol/m^3	[18]
k_W	$1\text{x}10^{-8}$	mol^2/m^6	[18]

1.4 Results and Discussion

The model was used to predict the effects of mass transfer coefficient, specific gas-liquid area, pH, metal concentration and H_2S gas concentration on the simultaneous precipitation of copper and zinc. A semi-batch reactor with a liquid volume of 0.001 m^3

was simulated (see Figure1). The specific gas-liquid surface area of this reactor amounts to 0.785 m^2/m^3 (when operated as a stirred cell with a smooth horizontal interface). The standard simulation involves a temperature of 298 K, a pressure of 1 bar, a gas side mass transfer coefficient ($k_{m,g}$) of $1x10^{-2}$ m/s (in case of gas mixtures), a H_2S concentration of 10 vol %, a liquid side mass transfer coefficient ($k_{m,l}$) of $5x10^{-4}$ m/s, an initial Cu^{2+} concentration of 6 mole/m^3, an initial Zn^{2+} concentration of 6 mole/m^3 and an initial pH of 5 (before adding any $CuSO_4$ or Zn SO_4).

The calculated concentration profile of H_2S inside a fresh package (not containing any precipitate yet) as a function of time is shown in Figure 3-a for the standard case defined above. At the beginning the concentration profile is very steep due to the precipitation reaction near the interface and due to the fact that the package initially is completely free of H_2S. When time increases, the H_2S concentration near the interface increases while the metal concentration near the surface decreases resulting in lower reaction rates and consequently lower H_2S fluxes. The concentration of S^{2-} in the package is 2 orders of magnitude smaller than the values calculated for H_2S absorption in clear water due to the consumption of S^{2-} in the reaction with Cu^{2+} and Zn^{2+} (see also figure 3-b). Typical concentration profiles of H_2S, HS^-, S^{2-}, Cu^{2+} and Zn^{2+} at the end of the penetration time are shown in Figure 3-b.

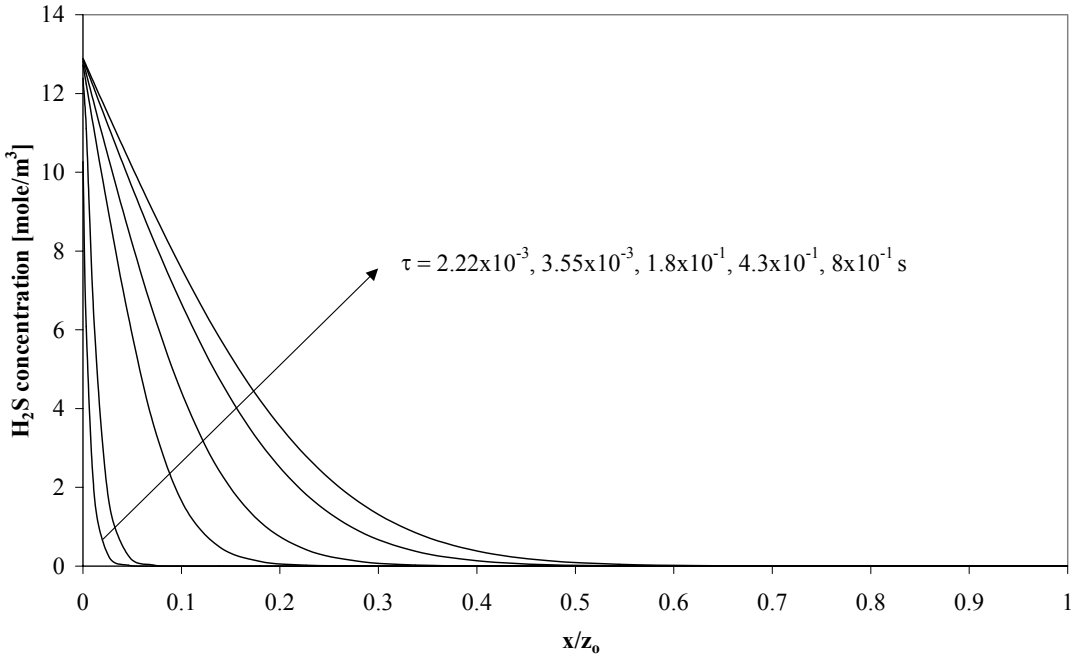

Figure 3-a: *Concentrations profiles for H_2S gas [mole/m^3] in the liquid package during the penetration time. Conditions: [H_2S]=10 vol%, $[Cu^{2+}]_{initial}$ = 6mol/m^3, $[Zn^{2+}]_{initial}$= 6mol/m^3,initial pH = 5, volume of liquid =1 l, a=0.785 m^2/m^3, $k_{m,l}=5x10^{-5}$ m/s, $k_{m,g}=1x10^{-2}$ m/s, T=298 K, P=1 bar.*

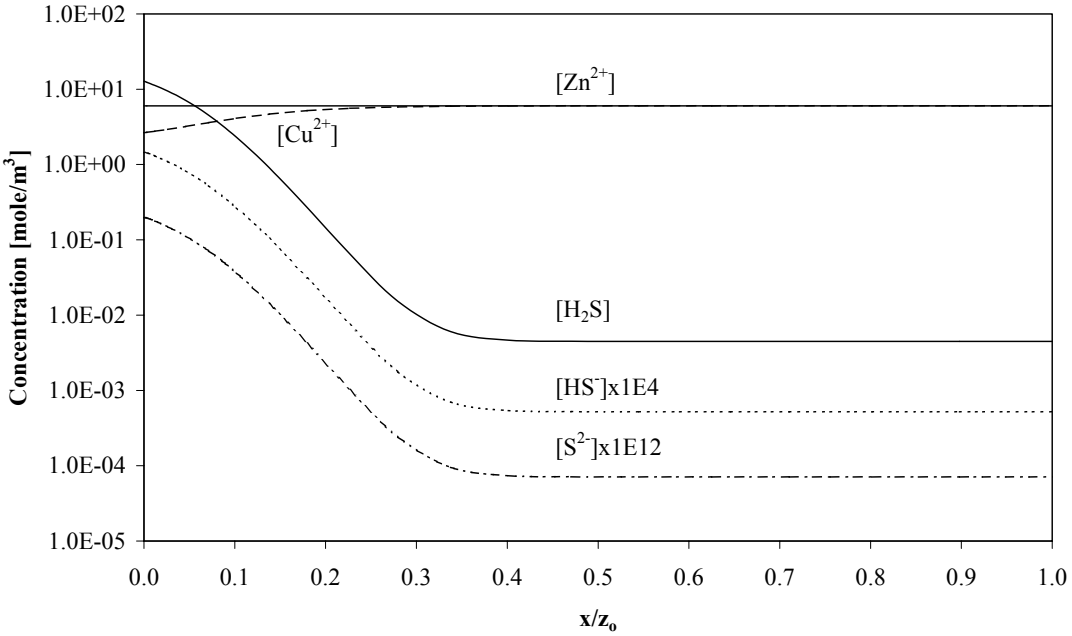

Figure 3-b: Typical *concentrations profile for H_2S, HS^-, S^{2-}, Me_1^{2+} and Me_2^{2+} [mole/m^3] in the liquid package after the penetration time. Conditions: [H_2S]=10 vol%, $[Cu^{2+}]_{initial}$ = 6mol/m^3, $[Zn^{2+}]_{initial}$= 6mol/m^3,initial pH = 5, volume of liquid =1 l, a=0.785 m^2/m^3, $k_{m,l}$=5x10^{-5} m/s, $k_{m,g}$=1x10^{-2} m/s, T=298 K, P=1 bar.*

Figure 4 compares the H_2S fluxes with and without the presence of metals. From the fact that the initial fluxes with and without the presence of metals are about equal, one may conclude that no chemical enhancement of H_2S absorption is observed for the process conditions applied. This is due to the fact that the bulk concentrations of Cu^{2+} and Zn^{2+} are much lower than the concentration of H_2S at the liquid side of the interface, resulting in very low values of the infinite enhancement factor ($E_{a,\infty}$) which for the penetration model is define by [20]:

$$E_{a,\infty} = 1 + \frac{c_{Me}^{bulk}}{c_{H_2S}^{i}} \left(\frac{D_{Me}}{D_{H_2S}} \right)^{0.5} \tag{43}$$

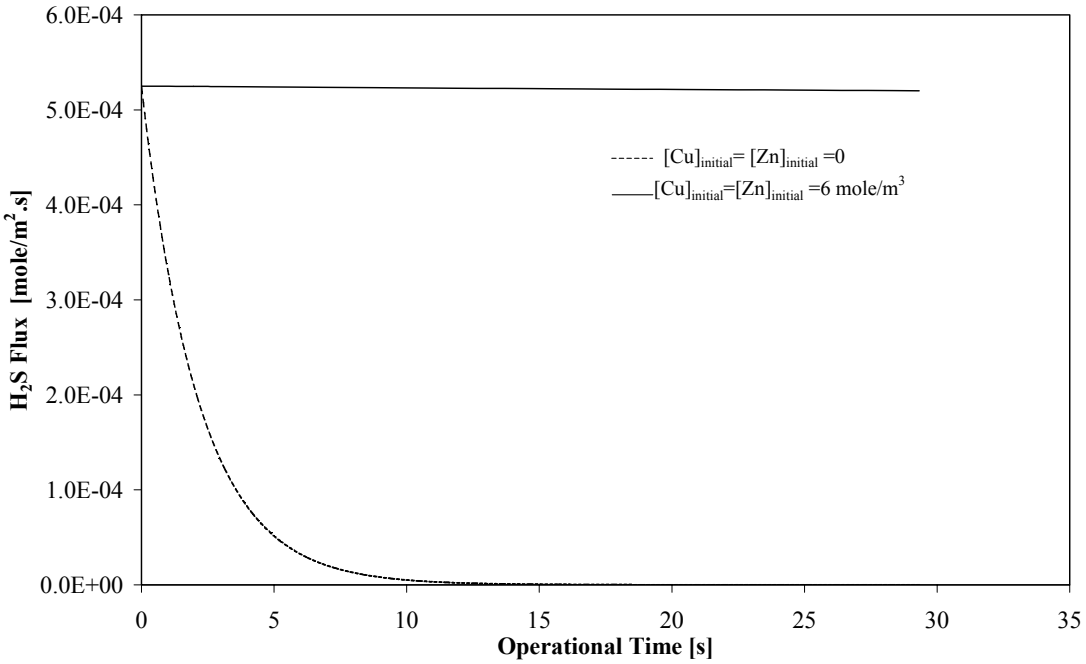

Figure 4: *Effect of the presence of precipitating metal ions on the flux of H_2S. Conditions: $[H_2S]$=10 vol%, $[Cu^{2+}]_{initial}$ = 6mol/m^3, $[Zn^{2+}]_{initial}$= 6mol/m^3,initial pH= 5, volume of liquid =1 l, a=0.785 m^2/m^3, $k_{m,l}$=5x10^{-5} m/s, $k_{m,g}$=1x10^{-2} m/s, T=298 K, P=1 bar.*

Figures 5-a and 5-b show the effects of initial pH and initial zinc concentration on the H_2S flux respectively. A decrease in the initial pH leads to much lower H_2S fluxes. A decrease in initial zinc concentration only has a small effect on the flux (Figure 5-b); apparently most H_2S initially is reacting with Cu^{2+} to form CuS, which is less soluble than ZnS.

Figure 6 shows the effect of H_2S concentration on the decrease in copper and zinc concentrations with time in the bulk. Increasing the gas concentration will increase slightly the rate of metal depletion in the solution. The flux slightly decreases with time due to the decrease in metal concentration and the decrease in pH that tends to push the equilibrium towards H_2S rather than S^{2-} resulting in a lower driving force for mass transfer and lower precipitation rates. From the differences between the disappearance rates of Zn^{2+} and Cu^{2+} one may again conclude that CuS precipitates faster than ZnS, illustrating the possibilities for selective metal removal.

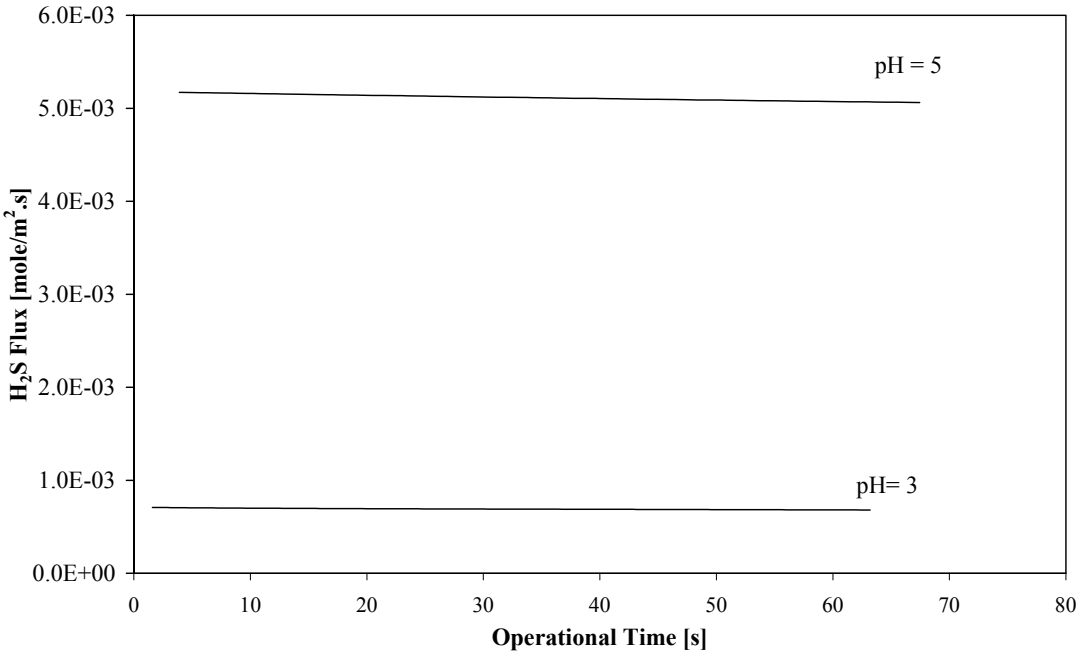

Figure 5-a: *Effect of initial pH on the H_2S flux. Conditions: $[H_2S]$=100 vol%, $[Cu^{2+}]_{initial}$ = 6mol/m^3, $[Zn^{2+}]_{initial}$= 6mol/m^3, volume of liquid =1 l, a=0.785 m^2/m^3, $k_{m,l}$=7.2x10^{-5} m/s, T=298 K, P=1 bar.*

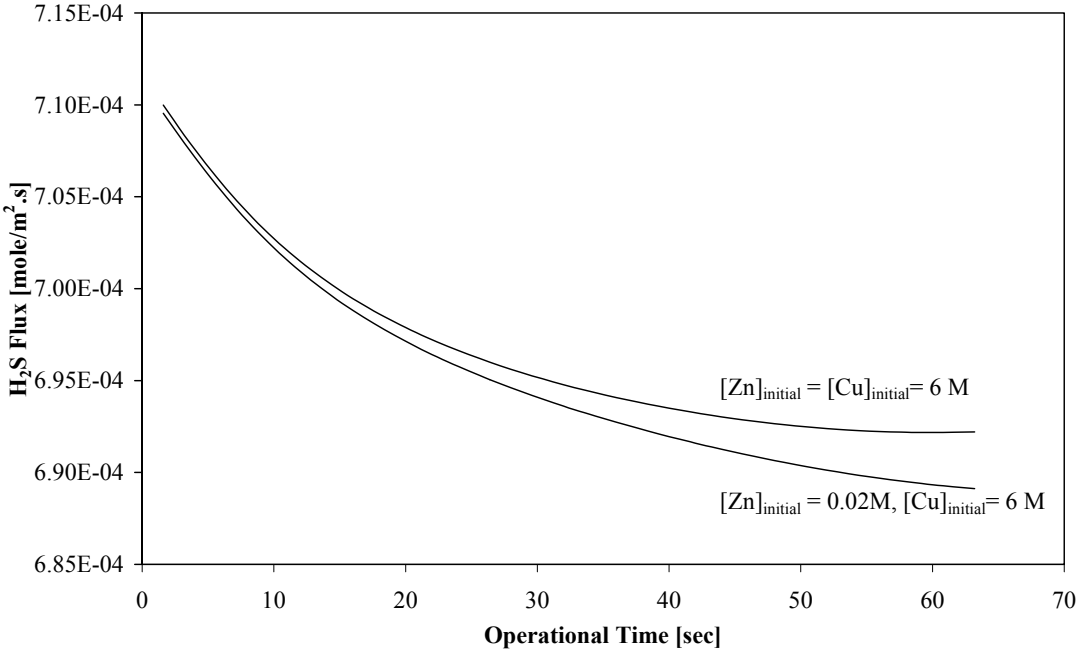

Figure 5-b: *Effect of Zn^{2+} initial concentration on the H_2S flux. Conditions: $[H_2S]$=10 vol%, $[Cu^{2+}]_{initial}$ = 6mol/m^3, initial pH = 5, volume of liquid=1 l, a=0.785 m^2/m^3, $k_{m,l}$=7.2x10^{-5} m/s, $k_{m,g}$=1x10^{-2} m/s, T=298K, P=1bar.*

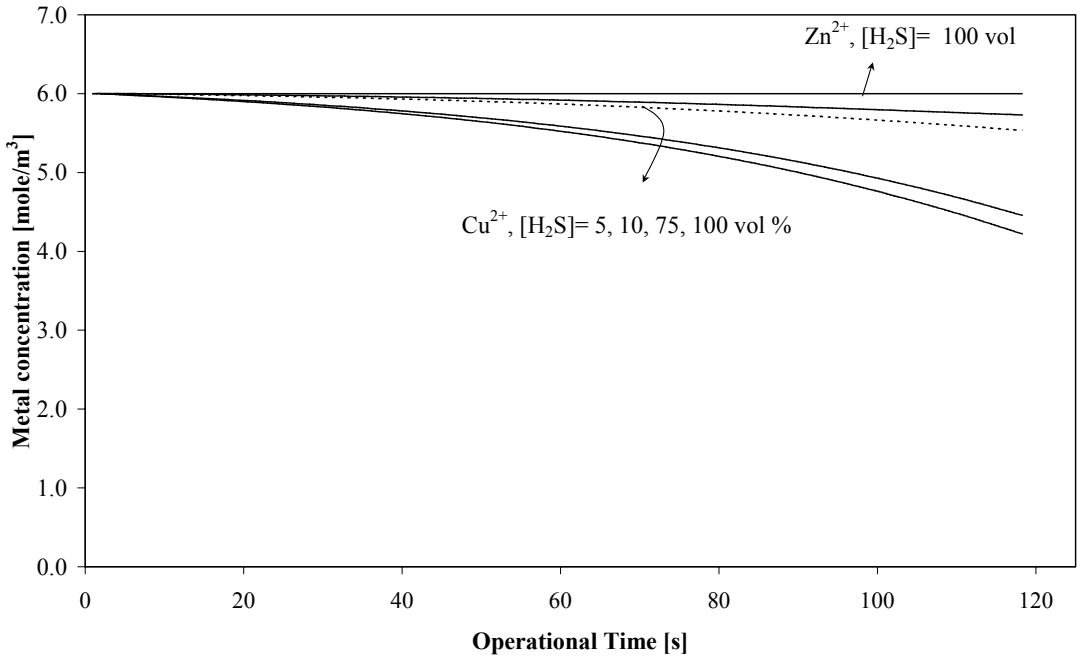

Figure 6: *Effect of H_2S concentration on the concentrations of Cu^{2+} and Zn^{2+} in the liquid bulk. Conditions: $[Cu^{2+}]_{initial}$ = 6mol/m^3 (lower 4 lines), $[Zn^{2+}]_{initial}$= 6mol/m^3 (upper line),initial pH = 5, volume of liquid =1 l, a=0.785 m^2/m^3, $k_{m,l}$=5x10^{-5} m/s, $k_{m,g}$=1x10^{-2} m/s(in case of gas mixtures), T=298 K, P=1 bar.*

The effect of H_2S concentration on the Sauter diameter (d_s) of the CuS precipitate is shown in Figure 7. Increasing the H_2S concentration in the gas phase apparently leads to an increase in average diameter: the H_2S flux increases while the concentration of S^{2-} remains almost constant due to the fast precipitation reactions (around the equilibrium concentration) which leads to an increase of metal depletion, a decrease in supersaturation and consequently lower nucleation rates and bigger diameters of the fewer particles.

The effects of the Hinterland ratio [$Al = k_{m,l}/(a.D)$] on copper depletion and average particle diameter are demonstrated in Figures 8 and 9. A decrease in Hinterland ratio (or an increase in specific gas liquid surface area) leads to faster Cu-depletion as precipitation is fully controlled by the rate of mass transfer. On the other hand the formed particles become smaller because of higher average supersaturation values and consequently higher nucleation rates. So, increasing the contact area will accelerate the removal rate of the metal ions but at the same time yield smaller particles as more particles are formed and crystal growth is less.

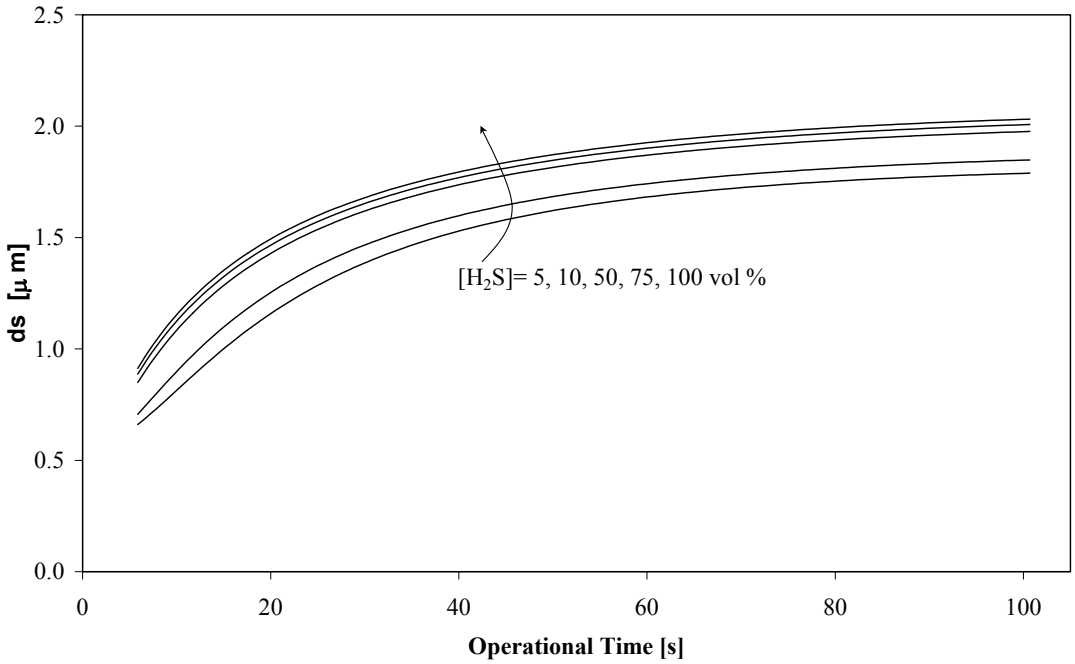

Figure 7: *Effect of H_2S concentration on Sauter diameter of CuS-precipitate in the reactor. Conditions: $[Cu^{2+}]_{initial}$ = 6 mol/m^3, $[Zn^{2+}]_{initial}$= 6 mol/m^3, initial pH = 5, volume of liquid =1 l, a=0.785 m^2/m^3, $k_{m,l}$=5x10^{-5} m/s, $k_{m,g}$=1x10^{-2} m/s(in case of gas mixtures), T=298 K, P=1 bar.*

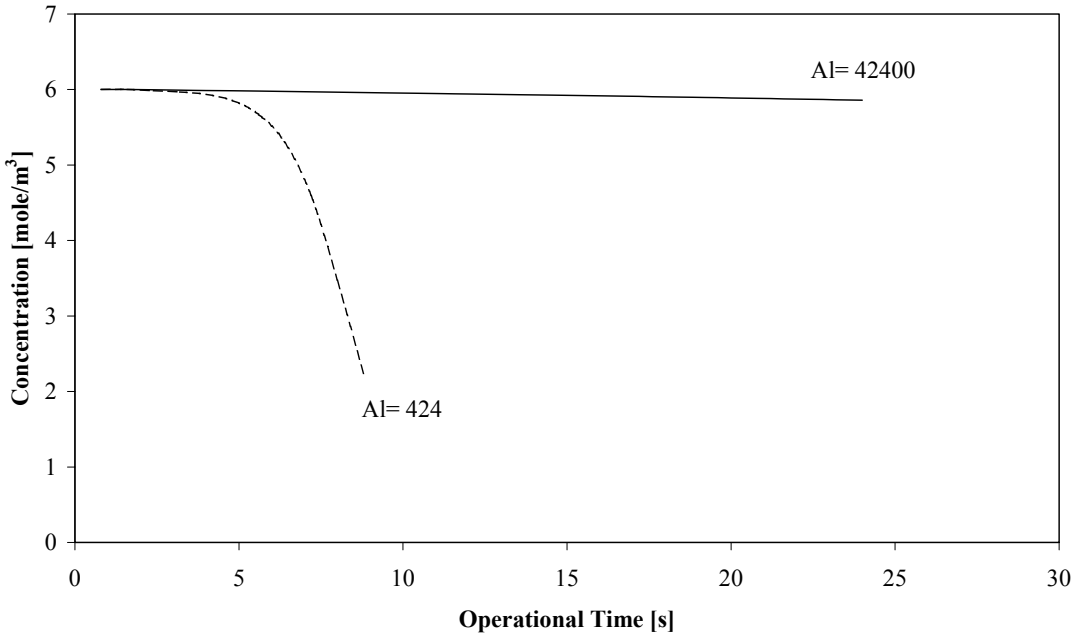

Figure 8: *Effect of Hinterland ratio on Cu^{2+} concentration depletion in the liquid bulk. Conditions: $[H_2S]$=10 vol%, $[Cu^{2+}]_{initial}$ = 6 mol/m^3, $[Zn^{2+}]_{initial}$= 6 mol/m^3, initial pH = 5, volume of liquid =1 l, $k_{m,l}$=5x10^{-5} m/s, $k_{m,g}$=1x10^{-2} m/s, T=298 K, P=1 bar.*

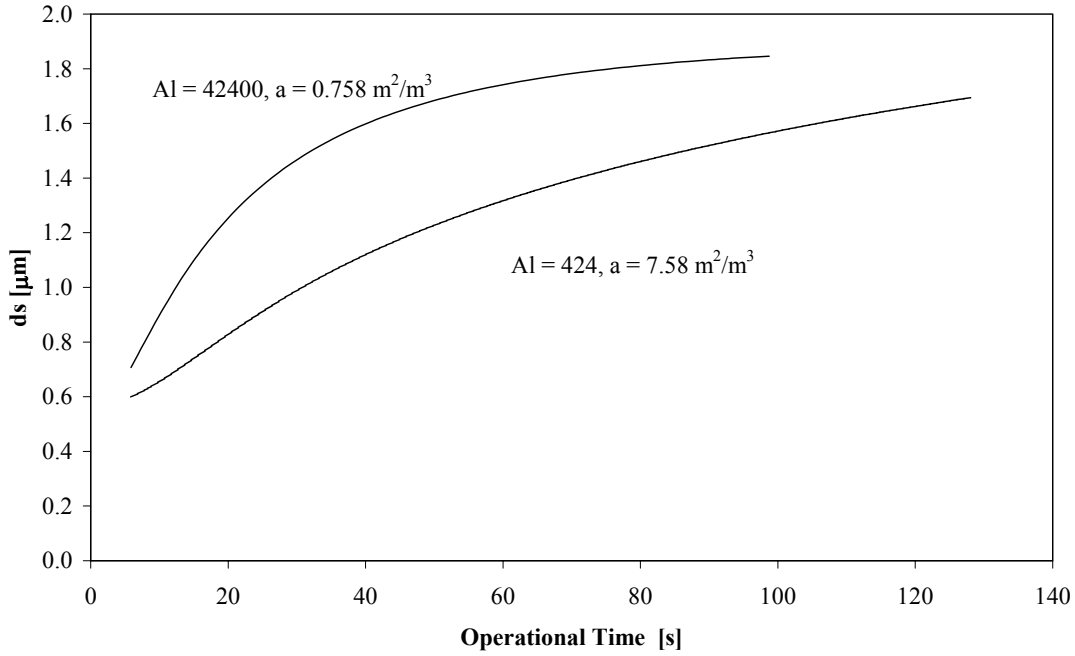

Figure 9: *Effect of Hinterland ratio on Sauter diameter of CuS precipitate in reactor. Conditions: [H_2S]=10 vol%, [Cu^{2+}]$_{initial}$ = 6 mol/m^3, [Zn^{2+}]$_{initial}$= 6 mol/m^3,initial pH = 5, volume of liquid =1 l, $k_{m,l}$=5x10^{-5} m/s, $k_{m,g}$=1x10^{-2} m/s, T=298 K, P=1 bar.*

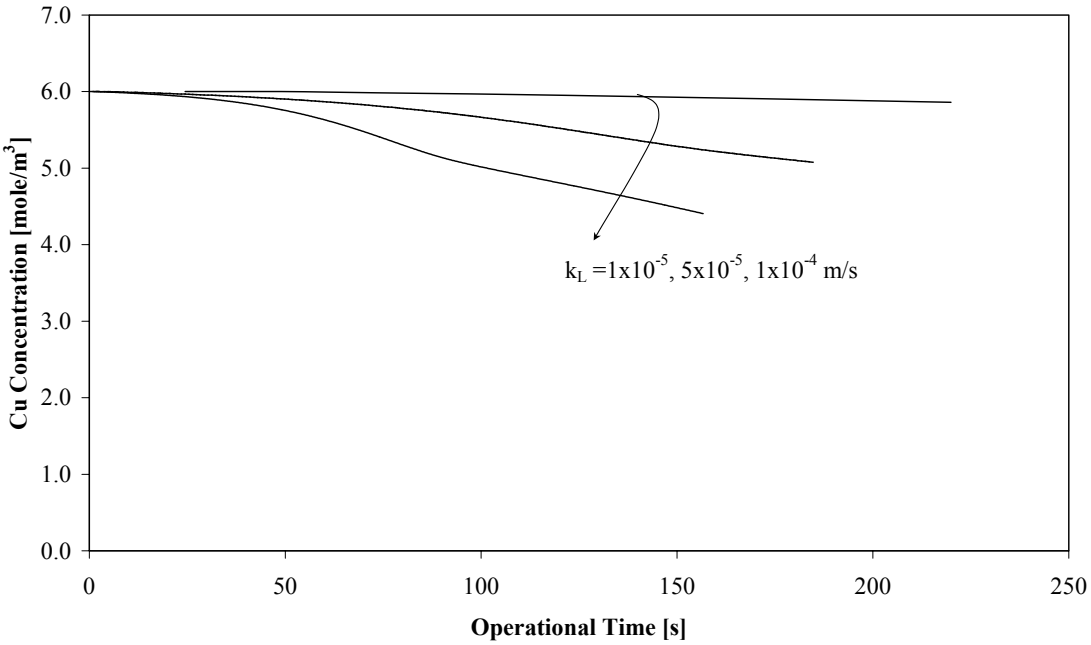

Figure 10: *Effect of mass transfer coefficient on Cu^{2+} depletion in the liquid bulk. Conditions: [H_2S]=10 vol%, [Cu^{2+}]$_{initial}$ = 6 mol/m^3, [Zn^{2+}]$_{initial}$= 6 mol/m^3 , initial pH = 5, volume of liquid =1 l, a=0.785 m^2/m^3, $k_{m,g}$=1x10^{-2} m/s, T=298 K, P=1 bar.*

The effect of the mass transfer coefficient on copper depletion and average particle diameter is shown in Figures 10 and 11 respectively. As to be expected increasing $k_{m,l}$ values yield higher rates of precipitation. On the other hand the average particle diameter

obtained after longer operation times is increasing with decreasing $k_{m,l}$ values (Figure 11). A decreasing $k_{m,l}$-value corresponds to a higher contact time τ and hence lower average supersaturation values due to depletion of the metal ions present in the package. Lower supersaturation values are favorable for crystal growth as growth is less sensitive to supersaturation than nucleation (compare value of n=3 in eqn (26) with g =1.3 in eqn (25)). This result is in agreement with the findings of Wachi et al [2]. At shorter operational times things may seem a bit confusing. At lower $k_{m,l}$-values it takes more time for the crystals to enter the bulk (for example at $k_{m,L}= 1x10^{-5}$, $\tau= 24.192$ s, at $k_{m,L}= 5x10^{-5}$, $\tau= 0.968$ s, at $k_{m,L}=1x10^{-4}$, $\tau= 0.242$ s). The first calculation results are therefore obtained after longer operation times.

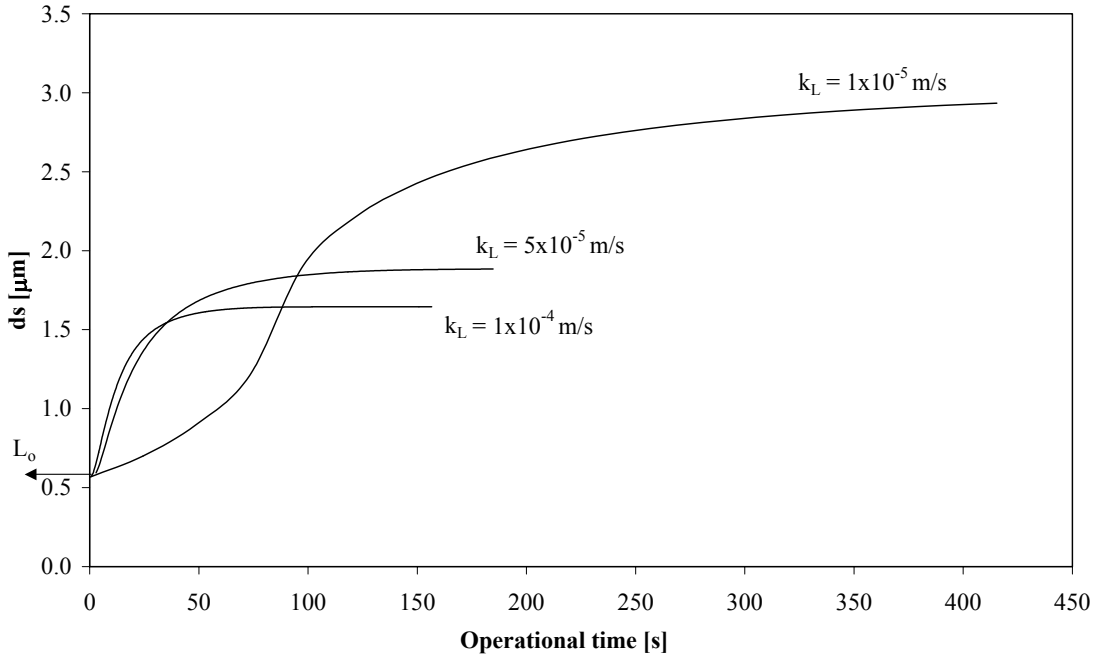

Figure 11: *Effect of mass transfer coefficient on the Sauter diameter of CuS precipitate in reactor. Conditions: [H_2S]= 10 vol%, [Cu^{2+}]$_{initial}$ = 6 mol/m^3, [Zn^{2+}]$_{initial}$= 6 mol/m^3, initial pH = 5, volume of liquid =1 l, a=0.785 m^2/m^3, $k_{m,g}$=1x10^{-2} m/s, T=298 K, P=1 bar.*

Finally, the model predicts selective precipitation of Copper as shown by Figure 12. The difference in the solubilities of CuS and ZnS obviously is so large that all S^{2-} initially reacts with Cu^{2+}. Only after all Cu^{2+} has been consumed Zn^{2+} starts to precipitate.

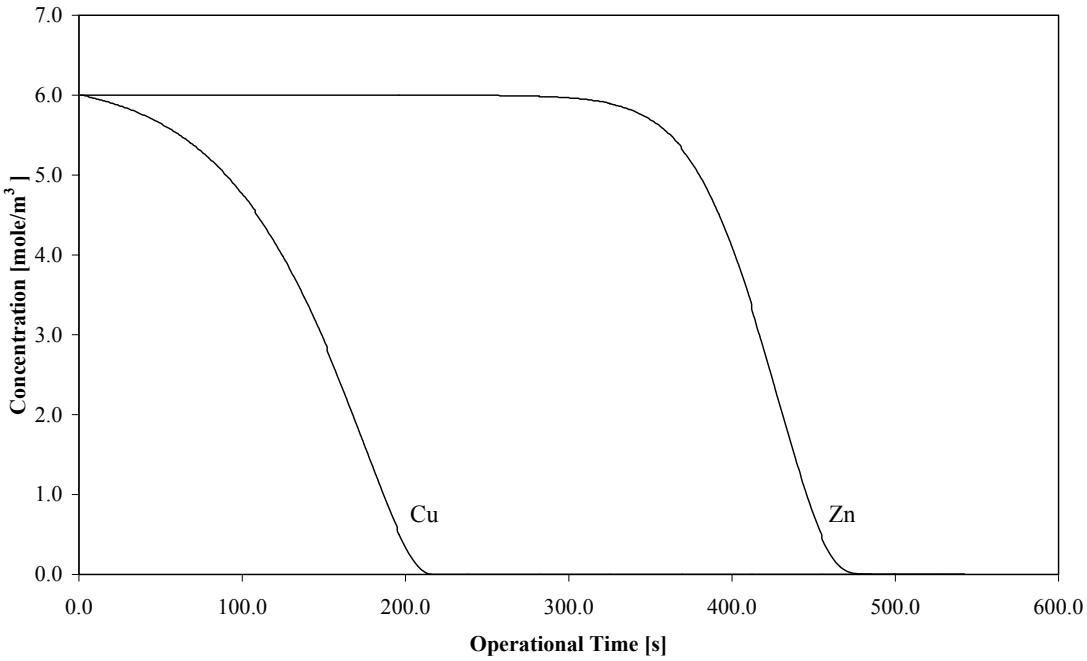

Figure 12: *Concentration of Cu^{2+} and Zn^{2+} in the bulk liquid as a function of operation time. Conditions: $[H_2S]$=10 vol%, $[Cu^{2+}]_{initial}$ = 6 mol/m^3, $[Zn^{2+}]_{initial}$= 6 mol/m^3, initial pH = 5, volume of liquid =1 l, a=0.785 m^2/m^3, $k_{m,l}$=5x10^{-5} m/s, $k_{m,g}$=1x10^{-2} m/s, T=298 K, P=1 bar.*

1.5 Conclusions

A mathematical model has been developed to simulate the simultaneous precipitation of two heavy metal ions with H_2S-gas. The model predicts higher precipitation rates for higher pH values and higher H_2S concentrations. Furthermore selective precipitation of the least soluble metal can be observed in cases where the solubilities of the two metal sulfides differ much. The rate of precipitation is fully controlled by mass transfer of the H_2S, higher H_2S concentrations and higher specific surface areas therefore yielding higher precipitation rates. Chemical enhancement of H_2S transfer has not been found at the realistic metal concentrations applied on the model. The size of the obtained crystals is predicted to increase with H_2S concentration, but to decrease with specific surface area and liquid side mass transfer rates. These results illustrate the importance of reactor layout and operating conditions on the process gas-liquid precipitation. Based on the model predictions, to obtained bigger crystals reactor needs to have low mass transfer coefficient and low interfacial area for example spray column.

Acknowledgments

This project was supported with a grant of the Dutch Program EET (Economy, Ecology, Technology) a joint initiative of the Ministries of Economic Affairs, Education, Culture and Sciences, and of Housing, Spatial Planning and Environment. This program is

coordinated by the EET Program Office, a partnership of Senter and Novem. Hans Kuipers and Martin Van Sint Annaland are acknowledged for their help in the mathematical field.

List of symbols

a	Specific surface area [m^2/m^3]
Al	Hinterkland ratio [-]
B′	Mass nucleation rate [$mole/m^3.s$]
c_i^*	Equilibrium concentration of species (i) [$mole/m^3$]
c_i^{bulk}	Concentration of species (i) in the liquid bulk [$mole/m^3$]
c_i	Concentration of species (i) in the package [$mole/m^3$]
[Cu]	Concentration of copper ions [$mole/m^3$]
D_i	Diffusion coefficient of species (i) [m^2/s]
d_s	Sauter diameter [m]
$E_{a,\infty}$	Infinite enhancement factor [-]
F	Faraday constant [C/mole]
(g)	Gas (subscript)
G	Linear growth rate [m/s]
G′	Mass growth rate [$mole/m^3.s$]
g	Exponent of growth rate [-]
H	Height of the liquid in the reactor [m]
$[H_2S]$	H_2S concentration [$mole/m^3$]
k	Reaction rate constant [SI unit]
k_{eq}	Equilibrium constant [SI unit]
k_b	Constant in eqn 24, 1.38×10^{-21}
k_g	Growth rate constant [m/s]
$k_{m,g}$	Gas side mass transfer coefficient [m/s]
k_n	Nucleation rate constant [$\#/m^4.s$]
k_{sp}	Solubility product constant[$mole^2/m^6$]
k_w	Ionic product of water [$mole^2/m^6$]
(l)	Liquid (subscript)
L_0	Critical nucleus diameter [m]
L	Particle diameter [m]
J_n	Rate of nucleation [$\#/m^4.s$]
m	Distribution coefficient [-]
n_i	Particle size density of species (i) [$\#/m^3.m$]
n	Exponent of nucleation [-]

p	Particle
i	Interfacial (subscript)
r	Radius of particle
R	Universal gas constant [Pa.m3/mole.K]
r_i	Rate of consumption of species (i) [mole/m^3.s]
t	Time [s]
T	Temperature [K]
x	Distance (depth of the package) [m]
z	Ionic valency [-]
z_0	Package thickness [m]
[Zn]	Zinc ions concentration [mole/m^3]

Greek

ϕ	Electrostatic potential gradient [V/m]
α	Volume to length shape factor [-]
β	Surface to length shape factor [-]
η	Viscosity of the solution [Pa.m/s]
ρ	Crystal density [mole/m^3]
τ	Contact time [s]

References

1. Mersmann A., Crystallization Technology Handbook. Marcell Dekker, New York Basel (1995).
2. Wachi Shun and Alan Jones. Mass Transfer With Chemical Reaction and Precipitation. Chem. Eng. Sci. Vol. 46, No. 4, pp 1027-1033, 1991.
3. Wachi Shun and Alan Jones. Aspect of Gas –Liquid Reaction Systems with Precipitate Particle Formation. Reviews in Chemical Engineering, Vol. 11, No. 11, pp 1-51, 1995.
4. Paques, www.paques.nl
5. Versteeg, G.F, J. A. M. Kuipers, F.P. H. Beckum and W. P. M. Van Swaaij. Mass Transfer with Complex Reversible Chemical Reactions-I. Single Reversible Chemical Reaction. Chem. Eng. Sci. Vol. 44, No. 10, pp 2295-2310, 1989.
6. Hostomsky J. and Jones A. G. A Penetration Model of Gas- Liquid Reactive Precipitation of Calcium Carbonate Crystals. Trans. ICHEME, Vol. 73, Part A, pp 241-245, April 1995.

7. Jones, A.G, J. Hostomsky and Zhou Li. On the Effect of Liquid Mixing rate on primary Crystal Size During the Gas-Liquid Precipitation of Calcium Carbonate. Che. Eng. Sci, Vol. 47, No. 13/14, pp 3817-3824, 1992.
8. Mohsen H. Al- Rahed and Alan G. Jones. CFD Modeling of Gas-Liquid Reactive Precipitation. Che. Eng. Sci, Vol. 54, pp 4779-4784, 1999.
9. Narayan S. Tavare. Batch Crystallizers. Reviews in Chemical Engineering, Vol. 7, No. 3-4, pp 213-352, 1991.
10. Wachi Shun and Jones A.G. Dynamic Modeling of Particle Size Distribution and Degree of Agglomeration During Precipitation. Chem. Eng. Sci, Vol. 47, No. 12, pp 3145-3148, 1992.
11. Higbie R. The Rate of Absorption of Pure Gas into a Still Liquid During Short Periods of Exposure. Trans. AICHE, Vol. 31, p 365, 1935.
12. Newman, J.S. Electrochemical Systems, Prentice Hall Inc. Englewood Cliffs N.J. (1973)
13. Randolph, A.D. and Larson, M.A. Theory of Particulate Processes, 2nd ed. Academic Press, New York (1988).
14. Sutherland, W. A Dynamical Theory of Diffusion for Non-electrolytes and the Molecular Mass of Albumin. Phil. Mag. Vol. 9, pp 781-785,1905.
15. Baker, G. A. and T. A. Oliphant. An implicit, numerical method for solving the two-dimensional heat equation. Quart. Appl. Math, 17, pp 361-373, 1960.
16. Dean, John A. Lange's Handbook of Chemistry, Fourteenth edition, McGraw-Hill, New York (1992).
17. Mousa Al-Tarazi, A. Bert M. Heesink and Geert F. Versteeg. Precipitation kinetics of ZnS and CuS in MSMPR, to be published.
18. Horvath A.L. Handbook of Aqueous electrolytes solution physical properties, estimation and correlation methods, John Wiley & Sons, New York (1985).
19. David R. Lide. Handbook of chemistry and physics, 75th edition, CRC, London (1994).
20. Westerterp K. R. W.P.M. Swaaij and A.A.C.M. Beenackers. Chemical reactor design and operation. John Wiley & Sons, New York, (1987).

Chapter 2

Crystallization Kinetics of CuS Precipitation; An Experimental Study Using the Mixed-Suspension-Mixed-Product Removal (MSMPR) Method

Abstract

The precipitation kinetics of copper sulfide were studied using a lab scale mixed-suspension-mixed-product removal (MSMPR) precipitation reactor. The vessel was operated at different feed concentrations, molar ratios, stirrer speeds, pH-values and residence times. Primary nucleation and volume average crystal growth rates as well as agglomeration kernel were determined. Relationships were found between the rates of the different crystallization steps on the one hand and supersaturation, stirrer speeds, pH-values Cu^{2+} to S^{2-} ratio on the other. These show that larger crystals will be obtained at high supersaturation, moderate stirrer speeds, small residence times, a pH-value of around 5 and high Cu^{2+} to S^{2-} ratios. One should realize though that the applied MSMPR method is not the most optimal technique for examining fast precipitation reactions. The crystallization rate may be much higher than (local) mixing rates making it impossible to measure the intrinsic kinetics of the different crystallization steps.

2.1 Introduction

The characteristics of a crystal product with regard to filterability, flowability, drying, caking and tabletting behavior is mainly determined by crystal size distribution, morphology, degree of agglomeration and purity [1]. In order to predict product quality it is therefore necessary to know the kinetics of nucleation and crystal growth and their dependency on (local) concentrations i.e. supersaturation. During the precipitation of sparingly soluble solids, agglomeration competes with molecular ionic crystal growth at the solid-liquid interface [2]. Knowledge of agglomeration behavior is therefore also required. The resulting size distribution, shape, internal surface area, structure and voidage of the particles determine ultimate the product quality.

Before precipitation can start, a solution must be supersaturated. This can be realized by various methods such as reactive precipitation or changing temperature in order to diminish solubility. Precipitation mainly involves two stages: 1) nucleation and 2) growth. Other processes like aggregation, agglomeration, disruptation and Ostwald ripening may also occur. Numerous models have been developed in order to describe each elementary step. However, the different steps that take place simultaneously and are interconnected and therefore the description of the complete process is rather complicated.

The company Paques of the Netherlands (www.paques.com) has developed a new process to precipitate heavy metal in industrial wastewater. The process consists of two steps. The first step involves a bio-reactor where sulfate is reduced to sulfide. The second step is the precipitator where part of the effluent of the bio-reactor is mixed with the heavy metal ions containing stream. Although this process has been implemented on a large scale, lack of kinetic data of the precipitation reactions prevents full control of the process.

Reliable kinetic data are of the utmost importance for the successful modeling and scale-up of precipitation processes. Crystallization kinetics (including primary nucleation rates, growth rates and agglomeration kernel) are usually measured using the Mixed-Suspension-Mixed-Products Removal (MSMPR) crystallizer technique [3]. This technique permits the simultaneous determination of nucleation and growth kinetics by measuring the particle size distributions (PSD) as a function of average residence time. When precipitating sparingly soluble solids, secondary processes such as agglomeration may also play an important role in determining the product quality (PSD). It is quite difficult to measure the kinetics of agglomeration separately and to distinguish between this agglomeration and the crystal growth [4]. However, MSMPR experiments can also be used to predict the agglomeration kernel. This kernel can be obtained from the population balances in volume coordinate while assuming size independent agglomeration behavior.

2.2 Previous work

Narayan and Patwardhan (1992) studied the agglomeration of copper sulfate pentahydrate, nickel ammonium sulfate, potassium sulfate and soy protein in an MSMPR crystallizer. They determined nucleation rates, crystal growth rates and agglomeration kernels [5]. They measured product crystal size distributions and transformed these into crystal volume coordinates. They used two methods; i.e. moments analysis and an optimization procedure for parameter characterization.

Alan Jones et al. (1996) developed a model for particle formation during agglomerative crystal precipitation [6]. In their work, the kinetics of processes which determine the formation of both primary particles and crystal agglomerates are briefly reviewed together with established simulation techniques for analyzing and predicting primary and secondary particle size distributions and studies of agglomerative precipitation.

Zuoliag and Palosaari (1997) developed a model to analyze nucleation and growth in a non-ideal MSMPR crystallizer [7]. Their model takes the effects of mixing intensity and product removal location on particle size distribution into account.

Leubner (1998) has developed a new crystal nucleation theory for the continuous precipitation of silver halides [8]. His model was developed based on a dynamic balance between nucleation and growth. This model is applicable for non-seeded systems with diffusion controlled nucleation and growth. The proposed model can predict particle size distribution from average crystal size, residence time, solubility, feed concentrations and temperature. Also the model can predict the maximum growth rate, the ratio of nucleation to growth rates, the ratio of average to critical crystal size and the size of nasent nuclei. Experimental results show good agreement with model predictions.

Jones and Zauner (2000) studied the precipitation kinetics of calcium oxalate in an MSMPR reactor [9]. They operated their reactor at 37^{o}C at different residence times, feed concentrations, stirrer speeds and feed positions. A new procedure to determine the kinetic parameters for nucleation, growth, agglomeration and particle disruption was introduced. They concluded that crystal growth proceeds along a surface-integration controlled mechanism with a second order dependence on absolute supersaturation. Nucleation rates were found to be dependent on power input and feed position, and it was concluded that these rate depend on the hydrodynamics conditions. Agglomeration rates were found to exhibit a maximum with increasing power input. They observed that at higher stirrer speeds the number of agglomerates is decreased due to breakage of these agglomerates by the stirrer.

Jones et al (2001) developed a model to describe agglomerative crystal precipitation based on the Monte Carlo simulation technique [3]. The processes of nucleation, crystal growth and aggregation are first simulated to obtain the particle size distribution (PSD)

for continuous mixed-suspension, mixed-product-removal (MSMPR) aggregative precipitation. An extension is then made to account for particle disruption by considering two alternative particle size reduction mechanisms-one enforcing particle splitting into two parts of equal volume and the other accounting for micro attrition. A comparison is made of predicted and experimental determined PSD's for both calcium oxalate and calcium carbonate precipitation. This comparison showed reasonable agreement.

2.3 Present Work

This work discusses the determination of crystallization kinetics of copper sulfide in a lab-scale MSMPR reactor. The effects of supersaturation, pH, molar ratio and stirrer speed on the rates of nucleation, growth and agglomeration kernel were studied.

2.4 Theory

To predict crystallizer performance, three different conventional balances need to be regarded, i.e. mass balances, energy balances and population balances. Mass and energy balances are based upon (local) operating conditions that determine convection rates, diffusion rates, kinetics and mass and heat transfer. Population balances are needed to derive particle size distribution (product quality). To be able to make use of the population balances the rates of nucleation, growth and particle aggregation must first be quantified [10]. In general, the population balance for any crystallizer can be represented as shown in Figure 1.

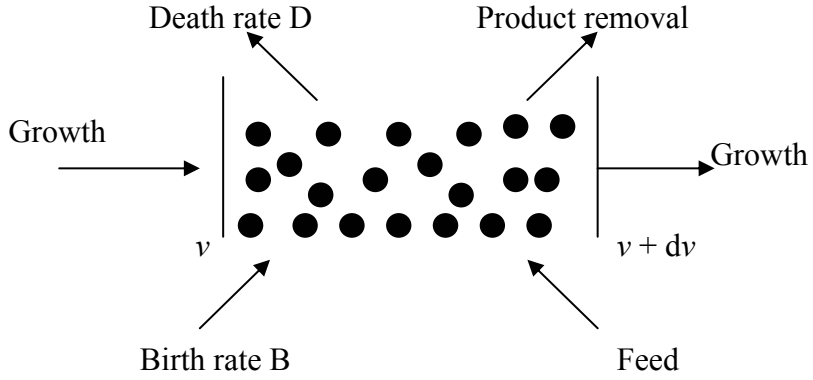

Figure 1: *Change in the number of crystals per unit volume in the crystal size range between L and L+dL*

The general equation for the population balance of a crystallizer having volume V is given by:

$$\frac{\partial n}{\partial t} + \frac{\partial (G_v n)}{\partial v} + n\frac{\partial V}{V \partial t} + D - B + \sum_k \frac{\dot{V}_k \cdot n_k}{V} = 0 \qquad (1)$$

Where n is the number density and the expression $\partial(G_v n)/\partial v$ describes the accumulation of crystals due to growth. The term $n\partial V/V\partial t$ takes changes in crystal volume (e.g. due to evaporation of solvent) into account. The parameters D and B represent the death and birth rates, which arise from agglomeration, attrition and breakage. Finally, the term $(\sum_k \dot{V}_i n_i / V)$ represents particle accumulation due to flows entering and leaving the crystallizer. The above equation is difficult to solve since the B and D terms in general cannot be formulated as these two terms depend on (local) system hydrodynamics which are mostly difficult to determine. However, a laboratory scale reactor with good mixing characteristics, containing particles smaller than 10 microns and operated at low supersaturation will hardly show any agglomeration or attrition [10, 11]. Moreover, intensive mixing leads to growth of all crystals at the same speed whereas no crystals will dissolve.

Crystal growth happens when the solutes present in the supersaturated solution reach the surface of a particle, leading to an increase in crystal size [10, 11]. Crystal growth can be seen as a succession of events namely: i) transport of reactive species through the solution, ii) adsorption on the crystal/surface interface, iii) surface diffusion and iv) surface reaction and incorporation of the product into the crystal lattice. The growth rate can be controlled by transport of ions through the solution (caused by convection and diffusion), by various processes at the crystal surface, or by a combination of these two. For sparingly soluble salts three different mechanisms are proposed that may control linear crystal growth rate, i.e. i) ion transport (g =1 in eqn 2a), ii) surface spiral growth (g=2 in eqn 2a), and iii) surface polynucleation (eqn 2b). The rate constant can be related to the mass transfer coefficient of ions diffusing from the bulk solution to the crystal surface and/or the diffusion rate of the ions at the crystal surface.

$$G_L = k_g \left[S-1\right]^g \qquad \textit{Where } S = \sqrt{\frac{[A][B]}{k_{sp}}} \tag{2a}$$

$$G_L = k_g S^{7/6} \left[S-1\right]^{2/3} (\ln S)^{1/6} \exp(-k_{sp}/(\ln S)) \tag{2b}$$

As for nucleation, several thermodynamic models are available that link the rate of nucleation to supersaturation. Theoretically, homogeneous nuclei are formed which are unstable in the mother liquor. It is assumed that such nuclei have the same properties as the macroscopic crystals that grow from them. The primary nucleation rate can then be derived from the difference between the free enthalpies of the crystal and the solution. This leads to the following expression [11]:

$$\frac{B_o}{D_{AB}(N_A c_c)^{5/3}} = 0.965\left(\frac{c^*}{c_c}\right)^{7/3} S^{7/3}\sqrt{f\ln\frac{c_c}{c^*}}\exp\left[-1.19f\left(\ln\frac{c_c}{c^*}\right)^3\left(\frac{1}{\nu\ln S}\right)^2\right] \quad (3)$$

where B_o is the primary nucleation rate (nuclei/m^{3}s).

The above formula is based on several assumptions. In some cases, especially at high supersaturation, a deviation of 200% can occur [12]. In order to minimise the deviation and to establish a more stable numerical routine for mathematical modelling, a simple power law formula is usually preferred [3, 5, 11 and 13]:

$$B_o = k_n\left[S-1\right]^{nb} \quad (4)$$

Using the above fitting formula will enable us to include the influences of different variables, which cannot be accounted for in a fundamental way.

In precipitation reaction crystallization, small particles are normally formed that cluster together forming agglomerates or aggregates. Interparticle collisions may result in permanent attachment if the particles are small enough for the Van der Waals forces to exceed collision forces, a condition generally obtained for particles smaller than 1 micron. Unlike nucleation and crystal growth, agglomeration does not occur in all crystallization process. Its appearance depends on the crystallizing system in terms of physicochemistral properties and crystallization conditions. Three types of aggregation/agglomeration can be distinguished [10]:

1. If the cohesion forces are weak, agglomeration is called flocculation.
2. If the fusing crystals become strongly bonded due to joint growth, the process is called agglomeration.
3. For intermediary processes and for processes also taking place without joint crystal growth, one speaks of aggregation.

Key parameters that affect agglomeration are:

1. Hydrodynamics (mixing, local turbulence, etc.)
2. The nature of the solvent (viscosity, density, etc.)
3. The size and habit of the crystals, which have a strong effect on the impact of a collision and the contact time. It appears that for reaction crystallization leading to small particles, agglomeration will be important.
4. The population density of the crystals, which has an important influence on the collision frequency.
5. Supersaturation which determines the rates of nucleation, crystal growth and agglomeration.

6. The cohesion forces between solvent, impurities and crystals.

Agglomeration during crystallization has been poorly studied because it is very difficult to distinguish it from crystal growth and to measure the number and size of the monocrystals in a particle/agglomerate.

The processes of nucleation, growth and agglomeration interact in a crystallizer and all contribute to the particle size distribution (PSD) of the products [11]. Kinetic data needed for crystallizer design purposes can be obtained with a laboratory scale mixed-suspension, mixed-product removal (MSMPR) crystallizer. The setup used for this study is shown in Figure 2.

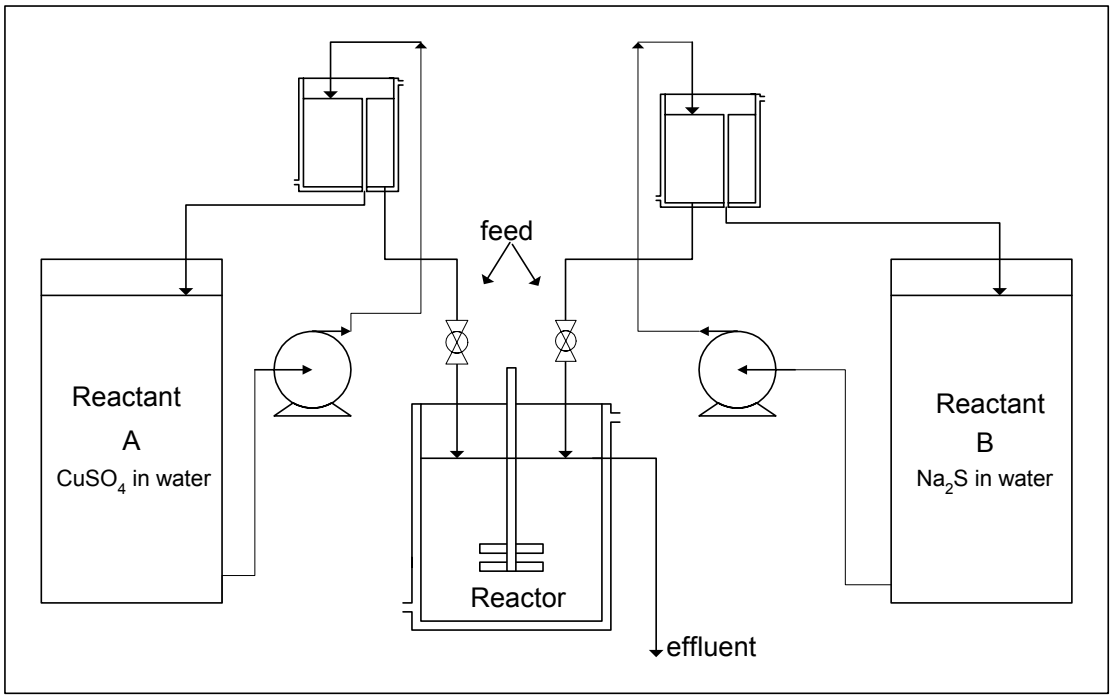

Figure 2: *Applied laboratory scale MSMPR crystallizer.*

It is assumed that all crystals have the same shape and do not break down due to attrition, that the reactor volume is constant, that there are no crystals in the feed, that steady state operation is established and that crystals do not dissolve. It is further assumed that the particles are small so that the growth is independent of particle size [5] and that the residence time of the solution and the crystals is equal. Although many assumptions are made, in practice most of them are actually complied with MSMPR measurements. We then arrive at the following equation describing the population balance:

$$G_v \frac{dn}{dv} + \frac{n}{\tau} = B - D \tag{5}$$

G_v represents the volume average growth rate (m^3/s) and n the crystal population density expressed as a function of crystal volume ($\#/m^3.m^3$). *B* and *D* represent the empirical birth and death functions over a volume range of *v*. Agglomeration of two particles having volumes *u* and *v* - *u* leading to the formation of a particle with volume *v*, can be represented by the following birth and death functions [5]:

$$B = \frac{1}{2}\int_0^v \beta(u, v-u)n(u,t)n(v-u)du \tag{6}$$

$$D = n(v)\int_0^\infty \beta(u,v)n(u)du \tag{7}$$

The agglomeration kernel $\beta(u, v-u)$ is a measure of the frequency of collisions between particles of volumes *u* and *v* – *u* that yield a particle of volume *v*. The factor ½ in equation (6) prevents that such collisions are counted twice.

Transformation of the population balance using the moments technique for the first three moments (μ_j) yields:

$$\mu_j = \int_0^\infty n(v)v^j dv \qquad\qquad j = 0, 1, 2, 3,..,m \tag{8}$$

Assuming the agglomeration kernel to be independent on particle size, the population balance (equation 5) can be rewritten in moments notation using equations (6) and (7) as follows:

$$-B_o + \frac{\mu_o}{\tau} = -\frac{1}{2}\beta_o\mu_o^2 \tag{9}$$

$$\frac{\mu_1}{\tau} = G_v\mu_o \tag{10}$$

$$\frac{\mu_2}{\tau} = 2G_v\mu_1 + \beta_o\mu_1^2 \tag{11}$$

The rates of nucleation, crystal growth and agglomeration kernel observed in a series of experiments can be correlated by empirical kinetic relations [5]:

$$G_v = k_g(S-1)^g \tag{12}$$

$$B_o = K_R G_v^i \varphi_T^j \tag{13}$$

$$\beta_o = k_\beta G_v^h B_o^p \tau^q \tag{14}$$

These equations were used to derive kinetic data from the MSMPR experiments. In these experiments reactants A and B were continuously added to the reactor in an equimolar ratio. When steady state operation was established a sample of the effluent was taken for analysis. The sample was then analyzed using Laser Doppler Diffraction to determine the average particle size (L_{50}), the average surface area (a_T) and the solids hold up (φ_T) as well as the particle number density as a function of particle size. On the basis of these measurements the rates of nucleation, growth and agglomeration kernel were calculated at different supersaturations. This was done by performing experiments at different feed concentrations. Making use of equations (9) to (11), a set of (G_v, B_o and β_o)-data was obtained at different supersaturations. After plotting the values for G_v, B_o and β_o as a function of supersaturation, one can make use of any fitting software to calculate the values of k_g, g, K_R, i, j, k_β, h, p and q in equations (12), (13) and (14) [5].

In this work the crystallization kinetics of copper sulfide have been examined using a laboratory scale MSMPR crystallizer.

2.5 Experimental Procedure

In order to investigate precipitation kinetics and to determine the parameters influencing crystallization kinetics, experiments have been carried out using the MSMPR method at different feed concentrations, stirrer speeds, residence times and molar ratios.

The experimental setup (see Figure 2) consisted of a gastight reactor out of glass and equipped with a multi speed disk & blade mixer and four baffles. The reactor had a volume of 750 ml and a diameter of 11 cm and was connected to a pressure indicator and a thermometer. A jacket around the reactor enabled temperature control. Two peristaltic feed pumps and one withdrawing suction pump were used to adjust the flows of the feed streams and the effluent stream respectively. The liquid hold up was kept constant by using an overflow system by which the liquid level could be controlled. The reactor was thermostated by either cooling or heating water. All experiments were carried out at ambient temperature (i.e. 20^{o}C). The sulfide concentration in the crystallizer as well as the pH were measured online using stationary electrodes. The feed streams (i.e. solutions of copper sulfate and sodium sulfide) were introduced into the crystallizer via stainless steel tubes. Because copper sulfide is hydrophobic and exhibits a tendency to agglomerate, small amounts of detergent (X100) were added to the samples to inhibit this effect. The reactor was operated under nitrogen and at a constant overpressure of 0.1 atm to prevent the oxidation of sulfide ions by air/oxygen. Even at high stirring speeds bubble formation was avoided and the contact between gas and liquid always was minimal. The particle size distribution of the produced crystals was measured within 10 minutes after

sampling using Dynamics Light Scattering (DLS), whereas the copper concentration in the feed and the effluent was measured by Atomic Absorption Spectrophotometer (AAS).

To ensure that steady state was reached when sampling, the pH and the copper ions concentration were monitored continuously using ion selective electrodes. It was observed that steady state was always achieved after 12-14 average residence times. After achieving steady state, 500 ml of effluent was collected for analysis. X-ray diffraction (Microtrac X100, size range 0.45 -1000 microns) and a Zeta-sizer (Zetasizer 5000, size range 1-5000 nm) were used to determine particle size distribution. AAS was used to measure the concentration of free copper ions in the effluent. The sample was filtered, dried and weighed to check the copper balance. Solids hold up was calculated from the mass balance of the copper ions. Particle volume density was calculated from the solids hold up and the particle size distribution using the following formula:

$$n_i = \varphi_T \frac{v\%}{\rho_s (v_p)_i ((v_p)_i - (v_p)_{i-1})} \qquad \textit{where i represent the class number} \qquad (15)$$

2.6 Results and Discussion

In order to investigate the crystallization kinetics of copper sulfide several experiments were conducted at different feed concentrations (supersaturations), stirrer speeds, residence times, feed molar ratios and pH-values. Supersaturation was calculated on basis of the feed concentrations of both copper and sulphide ions while using equation (16)

$$S = \sqrt{\frac{[Cu^{2+}][S^{2-}]}{k_{sp}}} \qquad (16)$$

The effect of relative supersaturation on the volume average growth rate of the produced particles is shown in Figure 3. Relative supersaturation was varied over a wide range (from $3.2x10^{14}$ to $3.5x10^{16}$) while keeping the molar ratio at 1. The volume average growth rate (G_v) was found to vary from $2.1x10^{-25}$ to $1.25x10^{-19}$ m^3/s. The obtained growth rates are comparable with growth rates found in literature for other systems e.g. potassium sulphate. A linear fit delivers:

$$G_v = 3.87x10^{-36}(S-1) \qquad (17)$$

The growth rate constant (k_g) is $3.87x10^{-36}$ m^3/s for the applied conditions.

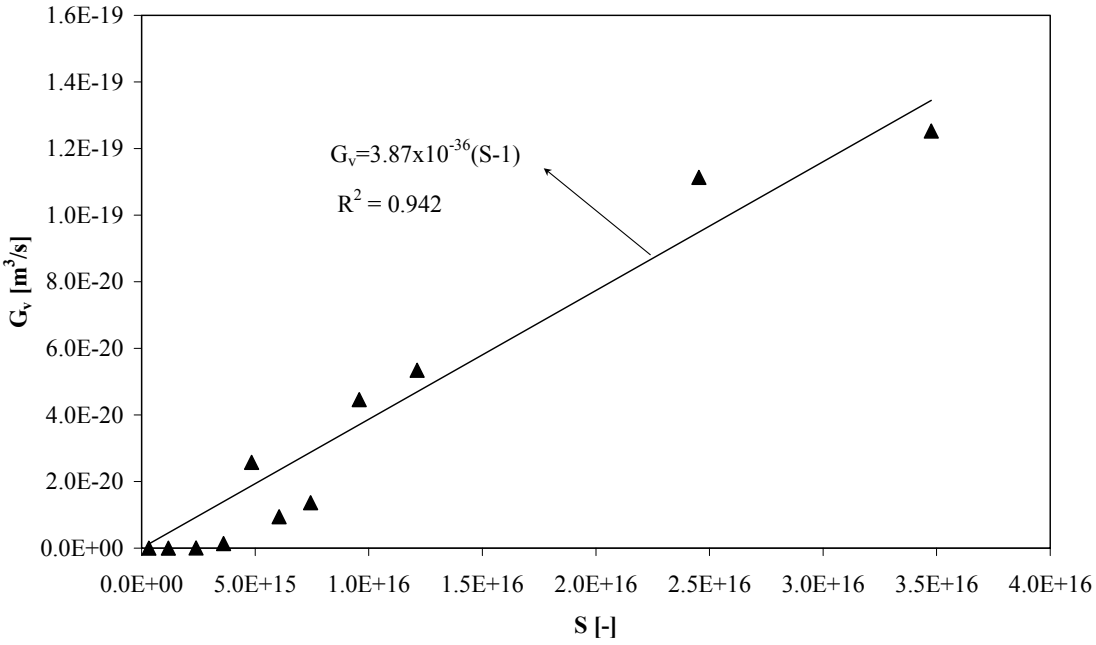

Figure 3: *Linear plot of volume average growth rate vs. relative supersaturation (S): the solid line represents the fitting equation. RPM = 710, molar feed ratio Cu^{2+}:S^{2-} = 1:1, pH = 5.9, residence time = 157 s*

Although the fit is reasonable over the whole range of supersaturation one can observe two regions indicating that the growth rate may be influenced by particle size. The reaction between copper ions and sulphide ions was found to be instantaneous but only at supersaturations higher than $1x10^{16}$ 100% conversion was achieved whereas at lower supersaturation a conversion of typically 60% was found. This might be due to the formation of complexes such as $Cu(HS)_2$ which tends to form at relatively low pH-values. The average size of the produced particles was varying from 190 nm at low relative supersaturation ($3.2x10^{14}$-$5x10^{15}$) to 10 microns at higher relative supersaturations. The obtained average particle size is expressed as a function of supersaturation by equation (18). The volume average growth rate can be rewritten in terms of linear growth rate yielding equation (19). By substituting equation (18) into equation (19) one may conclude that the linear growth is surface integration rate limited (see equations 20 and 2a) [13].

$$d_s = \kappa(S\text{-}1)^{-0.48} \tag{18}$$

$$G_v = \frac{\pi}{2} d_s^2 G_L \tag{19}$$

$$G_L = \frac{2}{\pi\kappa^2} k_g (S-1)^{1.96} \tag{20}$$

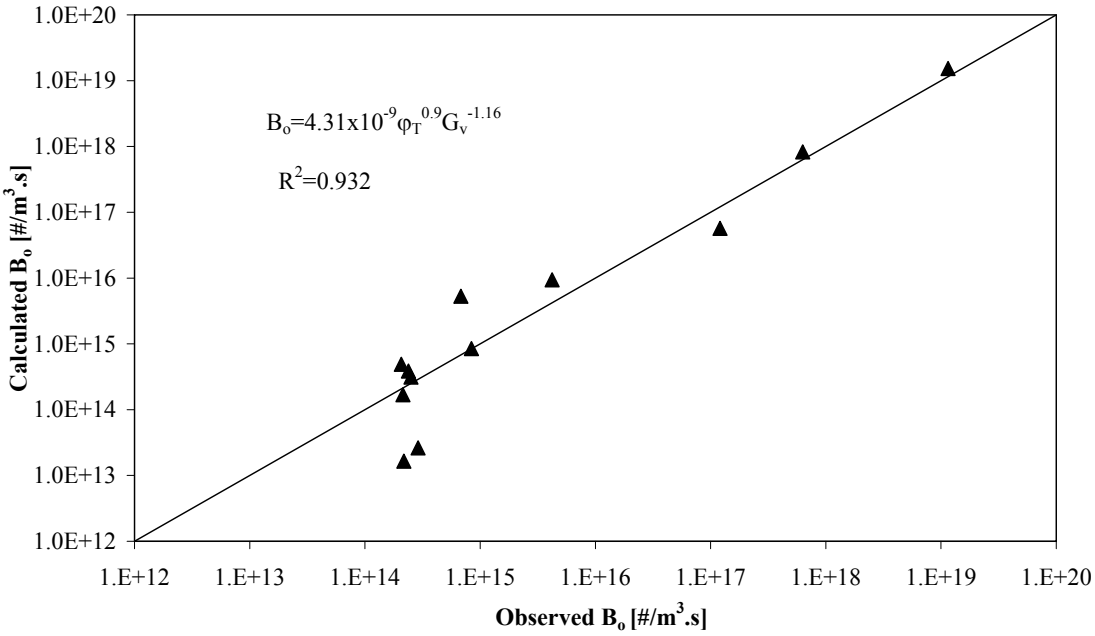

Figure 4: *Calculated rate using the proposed fitting equation vs. observed primary nucleation rate; RPM = 710, molar feed ratio Cu^{2+}: S^{2-} = 1:1, pH = 5.9, residence time = 157 s, $[Cu^{2+}]_{inlet}= [S^{2-}]_{inlet}= 8x10^{-3}\sim8x10^{-2}$ mol/m^3*

In order to arrive at function of the form of equation (13) the observed primary nucleation rates have been expressed as a function of volume average growth rate and solids hold up using a fitting correlation. The Newton method for multi-dimension optimization was used to calculate the best-fit coefficients of equation (13):

$$B_o = 4.31x10^{-9}\varphi_T^{0.9}G_v^{-1.16} \tag{21}$$

Figure 4 shows the values calculated with this correlation versus the experimentally observed values. An increase of the volume average growth rate corresponds to a decrease in nucleation rate as to be expected. However increasing the solids holdup yields a proportional increase in primary nucleation rate. Substituting the effects of supersaturation on volume growth rate [$G_v=3.86x10^{-36}$ *(S-1)*] and observed solids hold up [$\varphi_T = 2.3x10^{-16}$ *(S-1)*] delivers the relationship between supersaturation and primary nucleation rate:

$$B_o = 4.36x10^{18}(S-1)^{-0.26} \tag{22}$$

This relation shows that an increase in supersaturation has a slight negative effect on the primary nucleation rate. This rather surprising phenomenon was also noticed by Tavare and Patwardhan [5] for potassium sulphate. It can be explained by the fact that the agglomeration rate also increases with supersaturation (see lateron), thereby suppressing the primary nucleation rate and enhancing the observed average growth rate.

Agglomerates that grow as one particle grow faster than a single small particle and hence primary nucleation becomes less apparent [13].

The agglomeration kernel was also calculated from the experimental results using equation (11). The experimental results were again fitted by means of nonlinear regression to identify the relationship between agglomeration kernel on the one the hand and primary nucleation rate and volume average growth rate on the other (as expressed by equation (14)). See Figure 5. Although the fit is certainly not perfect it can be concluded that an increase of the primary nucleation rate and/or the average volume growth rate corresponds with an increase in agglomeration kernel as to be expected [10]:

$$\beta_o = 8.32x10^{-7} B_o^{0.89} G_v^{1.25} \tag{23}$$

As residence time was not varied the factor τ^q (from equation 14) has been included in the value of k_β (=8.32x10^{-7}) in equation (22). Based on theory, collisions of bigger particles (occurring at higher G_v- values) are more successful in producing agglomerates. Also an increase in particle concentration will raise agglomeration kernel due to an increase in collision frequency.

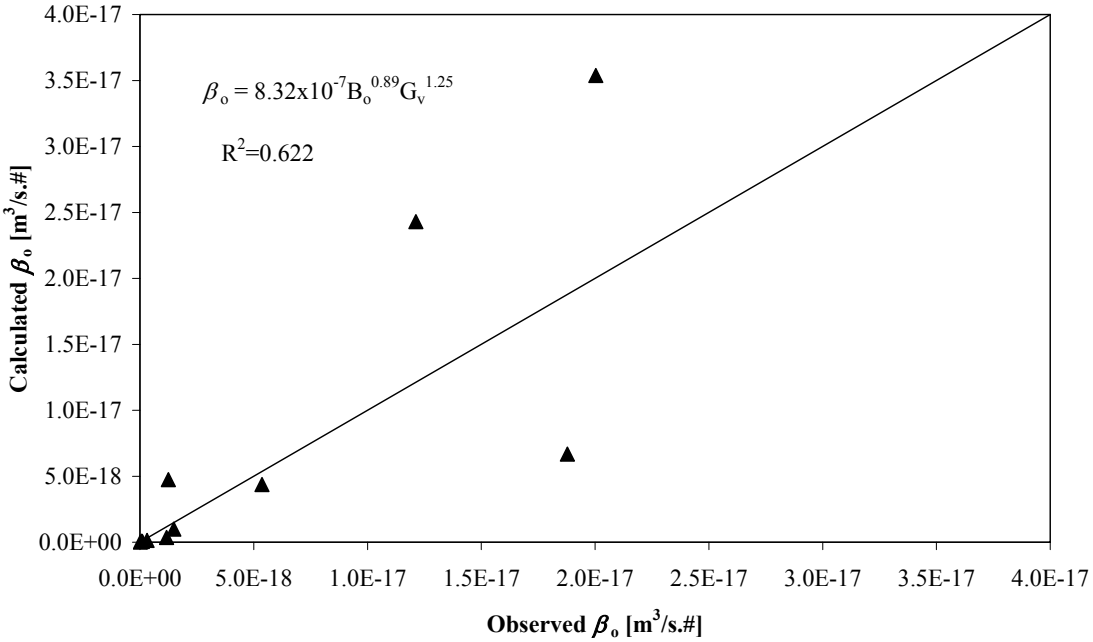

Figure 5: *Calculated agglomeration kernel using the proposed fitting equation vs. observed kernel. RPM = 710, molar feed ratio Cu^{2+}:S^{2-} = 1:1, pH=5.9, residence time = 157 s, $[Cu^{2+}]_{inlet}$= $[S^{2-}]_{inlet}$=8x10^{-3}~8x10^{-2} mol/m^3*

The effect of the stirrer speed on the volume average growth rate of the CuS crystals is demonstrated in Figure 6. As it can be seen by increasing the stirrer speed until 1200 RPM the observed growth rate increased, however, a further increase in stirrer speed will

cause the observed growth rate to decrease again. In theory increasing the stirrer speed would result in a decrease in local supersaturation, which would indeed make the conditions more favorable for crystal growth than primary nucleation. However, this observation seems to be in conflict with the above-mentioned experimental findings regarding the sensitivities of G_v and B_o to S. It is more likely that agglomeration plays a role here. By increasing the stirrer speed the collision frequency will increase and therefore leading to more agglomerates. Further increase of the stirrer speed also causes more disruption of the agglomerated particles resulting in a reduction in observed particle size and G_v.

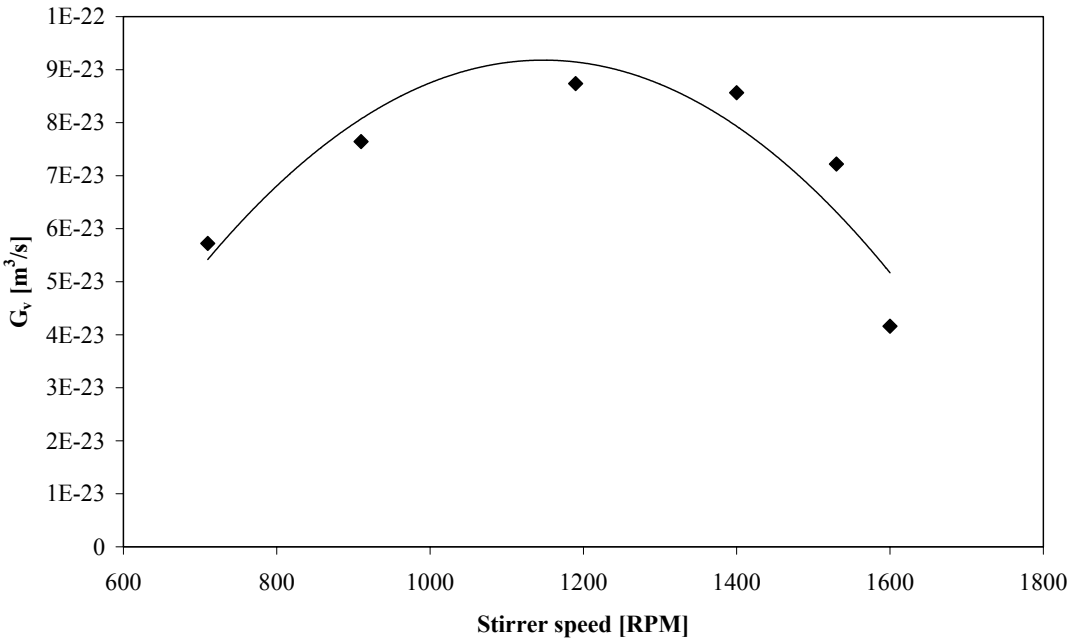

Figure 6: *Effect of stirrer speed on volume average growth rate. Molar feed ratio Cu^{2+}:S^{2-} = 1:1, pH = 5.9, residence time = 157 s, $[Cu^{2+}]_{inlet}=[S^{2-}]_{inlet}= 8x10^{-3}$ mol/m^3*

Figures 7 and 8 show the effect of stirrer speed on the primary nucleation rate and agglomeration kernel respectively. For both, upon increasing stirrer speed, first a decrease is observed (until 1000-1200 RPM) and afterwards an increase. As mentioned earlier increasing the stirrer speed will first increase the growth rate but after 1200 RPM disruption of the particles will become more favorable and hence more particles will be present. An increase in the number of particles will increase the collision frequency resulting in higher β_o-values as well as higher apparent primary nucleation rates (B_o).

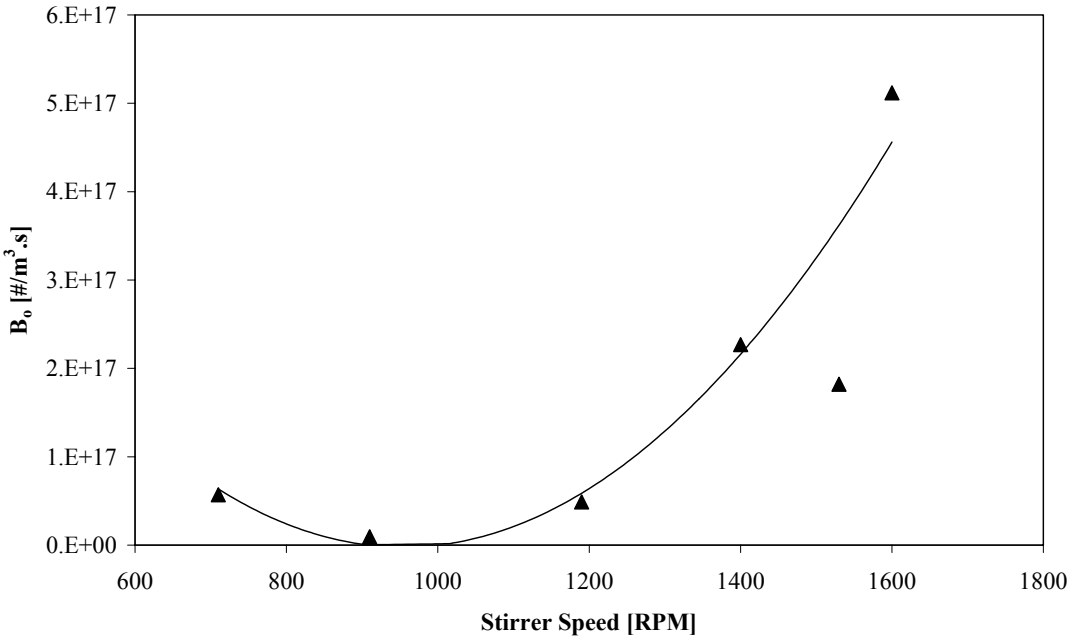

Figure 7: *Effect of stirrer speed on primary nucleation rate. Conditions: molar feed ratio Cu^{2+}:S^{2-} = 1:1, pH = 5.9, residence time = 157 s, $[Cu^{2+}]_{inlet}=[S^{2-}]_{inlet}= 8x10^{-3}$ mol/m³*

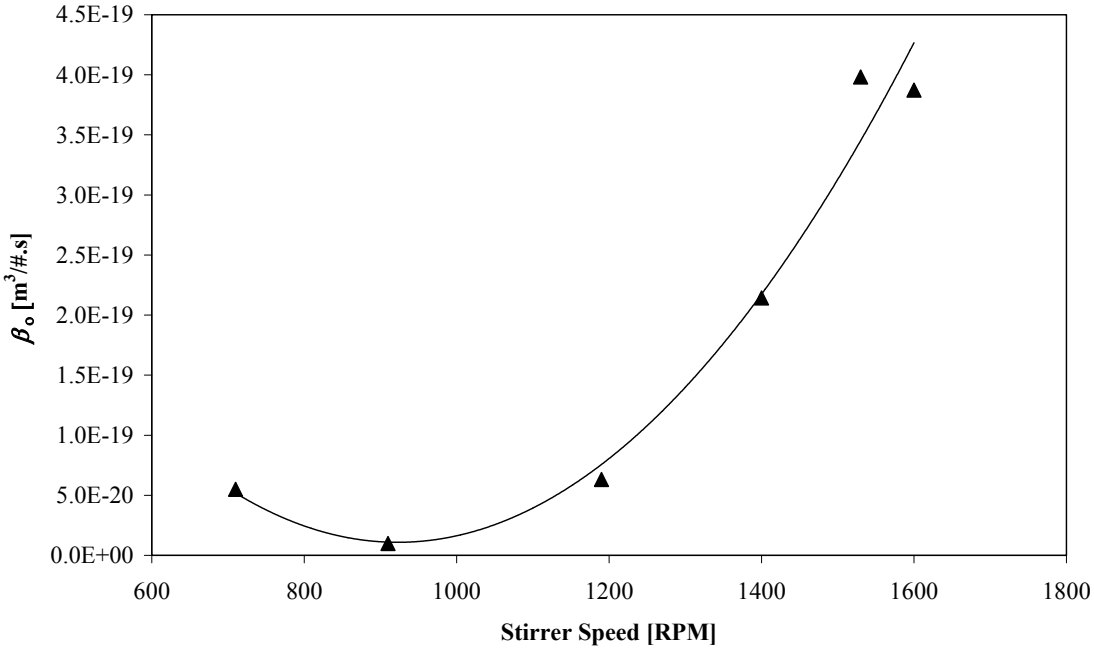

Figure 8: *Effect of stirrer speed on agglomeration kernel. Conditions: molar feed ratio Cu^{2+}:S^{2-} = 1:1, pH = 5.9, residence time = 157 s, $[Cu^{2+}]_{inlet}=[S^{2-}]_{inlet}= 8x10^{-3}$ mol/m³*

Figures 9, 10 and 11 show the effect of residence time on volume average growth rate, primary nucleation rate and agglomeration kernel respectively. Residence time was changed by adjusting the liquid feed flowrate while keeping all other conditions constant.

An increase in residence time results in a sharp decrease in volume average growth rate. Also the primary nucleation rate and the agglomeration kernel were found to decrease with residence time. Increasing the residence time by decreasing the feed flowrate while keeping the stirrer speed constant, will lead to lower local supersaturation values at the feed points resulting in lower (local) volume average growth rates. On the other hand increasing the residence time of the particles inside the reactor will raise the number of particle collisions resulting in more agglomeration. The net effect, however, is negative as the agglomeration kernel decreases with increasing residence time in the reactor.

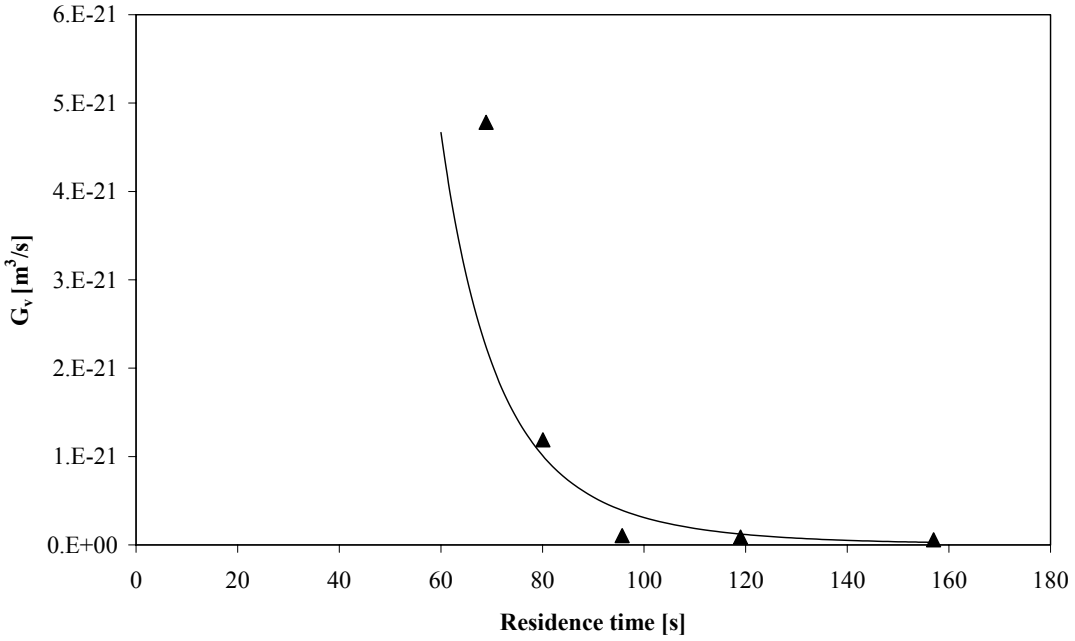

Figure 9: *Effect of residence time on volume average growth rate. Molar feed ratio Cu^{2+}:S^{2-} = 1:1, RPM = 710, pH = 5.9, $[Cu^{2+}]_{inlet}=[S^{2-}]_{inlet}= 8x10^{-3}$ mol/m^3*

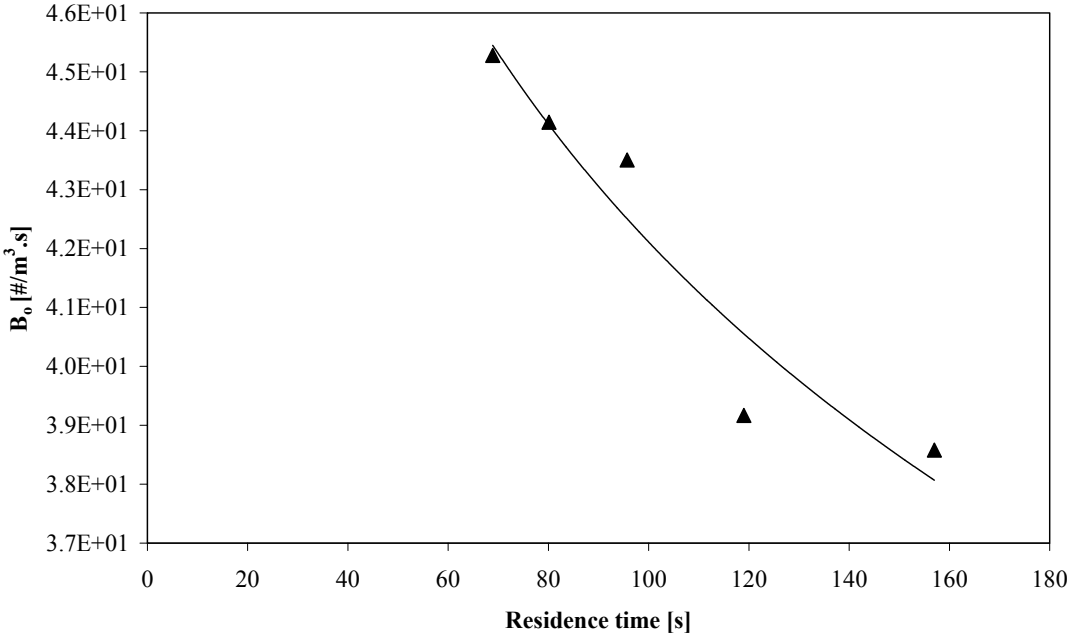

Figure 10: *Effect of residence time on primary nucleation rate. Molar feed ratio Cu^{2+}:S^{2-} = 1:1, RPM = 710, pH = 5.9, $[Cu^{2+}]_{inlet}=[S^{2-}]_{inlet}$= 8x10^{-3} mol/m^3*

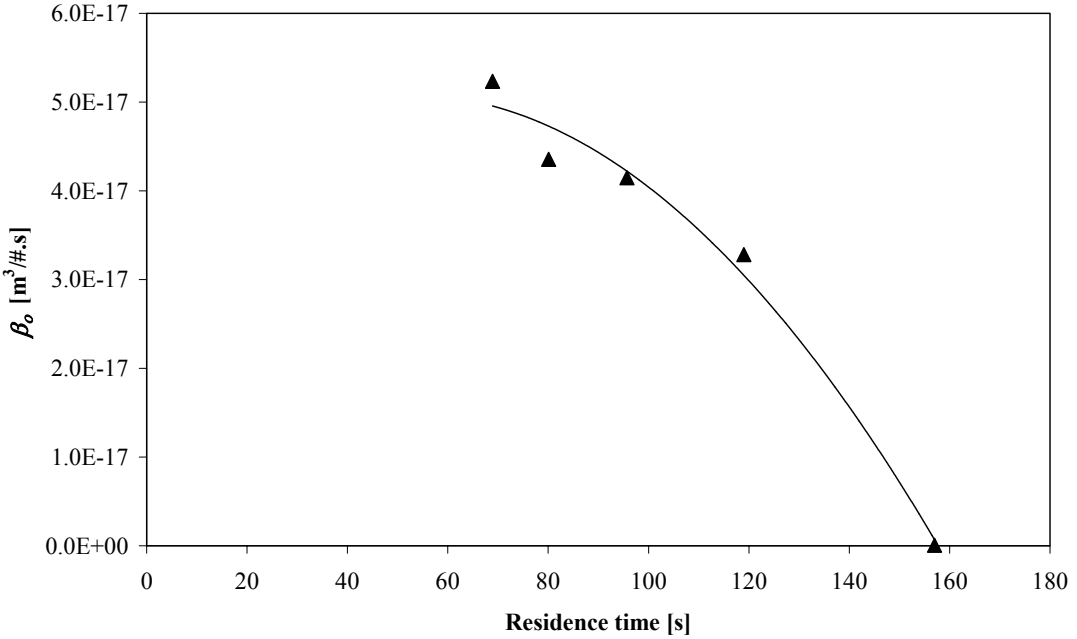

Figure 11: *Effect of residence time on agglomeration kernel. Molar feed ratio Cu^{2+}:S^{2-} = 1:1, RPM = 710, pH = 5.9, $[Cu^{2+}]_{inlet}=[S^{2-}]_{inlet}$= 8x10^{-3} mol/m^3*

Figures 12, 13 and 14 show the effect of molar feed ratio (Cu^{2+}:S^{2-}) on the volume average growth rate, primary nucleation rate and agglomeration kernel respectively. The ratio has been adjusted by changing the feed concentrations of Cu^{2+} or S^{2-} while keeping all other parameters constant. Copper conversion was around 60% when the Cu^{2+} to S^{2-} ratio was higher than unity. Increasing the Cu^{2+} to S^{2-} ratio was found to increase the volume average growth rate and agglomeration kernel. The primary nucleation rate was

found to decrease though. No large effects were found at Cu^{2+} to S^{2-} ratios higher than 2. This can be explained by the fact that at small Cu^{2+}:S^{2-} ratios (realized by increasing the S^{2-} concentration in the feed) polysulfides were observed. These inhibit the growth of particles and consequently increase the rate of primary nucleation due to their surface active properties.

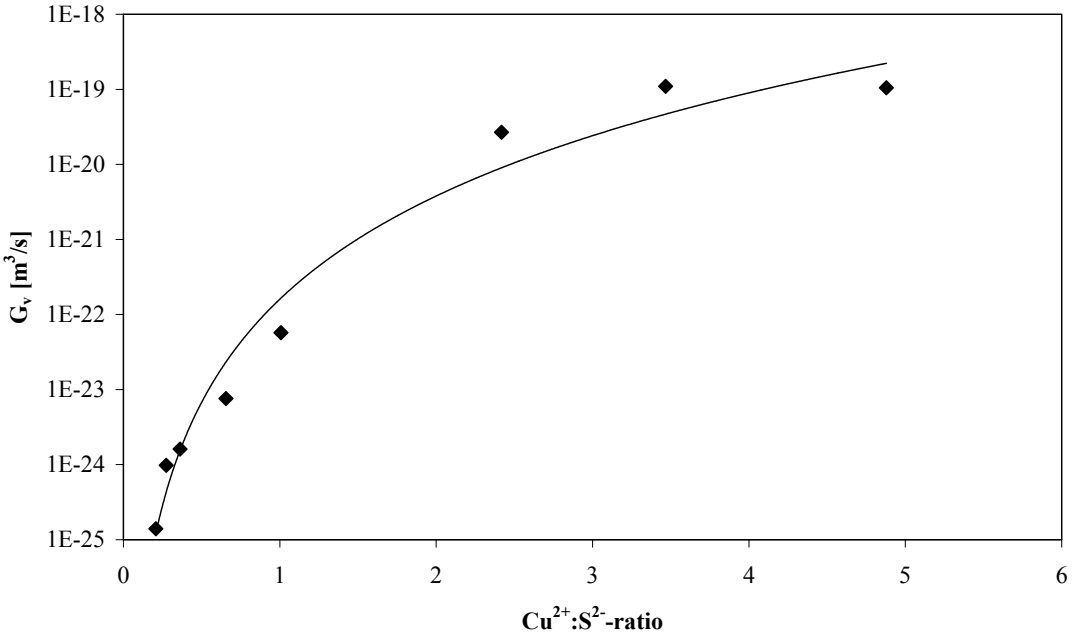

Figure 12: *Effect of molar feed ratio on the volume average growth rate. Conditions: RPM = 710, pH = 5.9,residence time = 157 s, $[Cu^{2+}]_{inlet}$ = 8x10^{-3}~3x10^{-2} mol/m^3, $[S^{2-}]_{inlet}$ = 8x10^{-3}~3x10^{-2} mol/m^3*

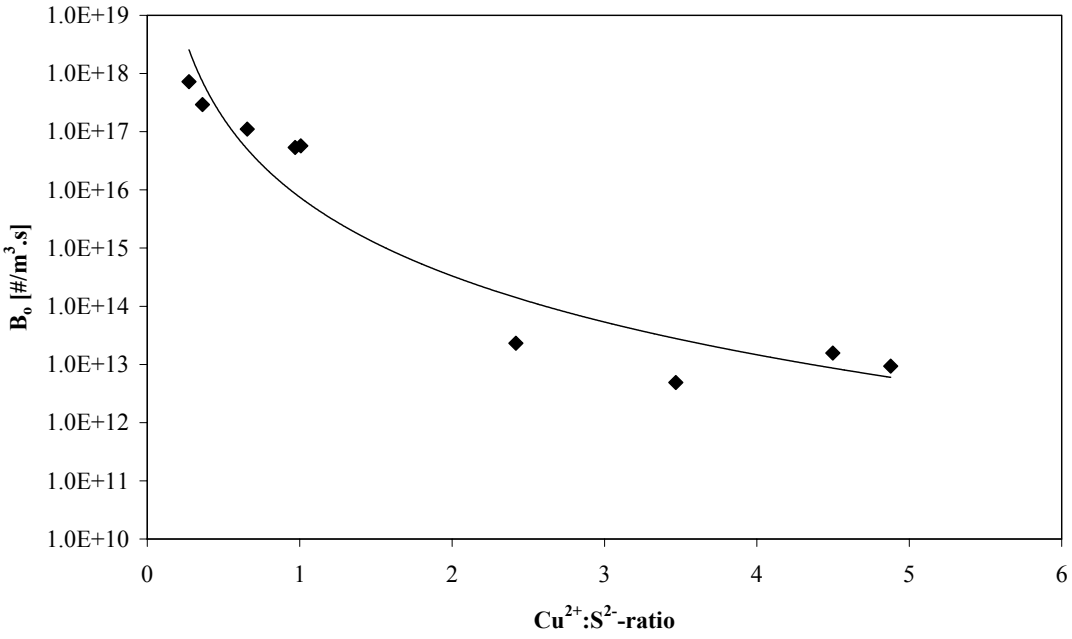

Figure 13: *Effect of molar feed ratio on the primary nucleation rate. Conditions: RPM = 710, pH = 5.9,residence time = 157 s, $[Cu^{2+}]_{inlet}$ = 8x10^{-3}~3x10^{-2} mol/m^3, $[S^{2-}]_{inlet}$= 8x10^{-3}~3x10^{-2} mol/m^3*

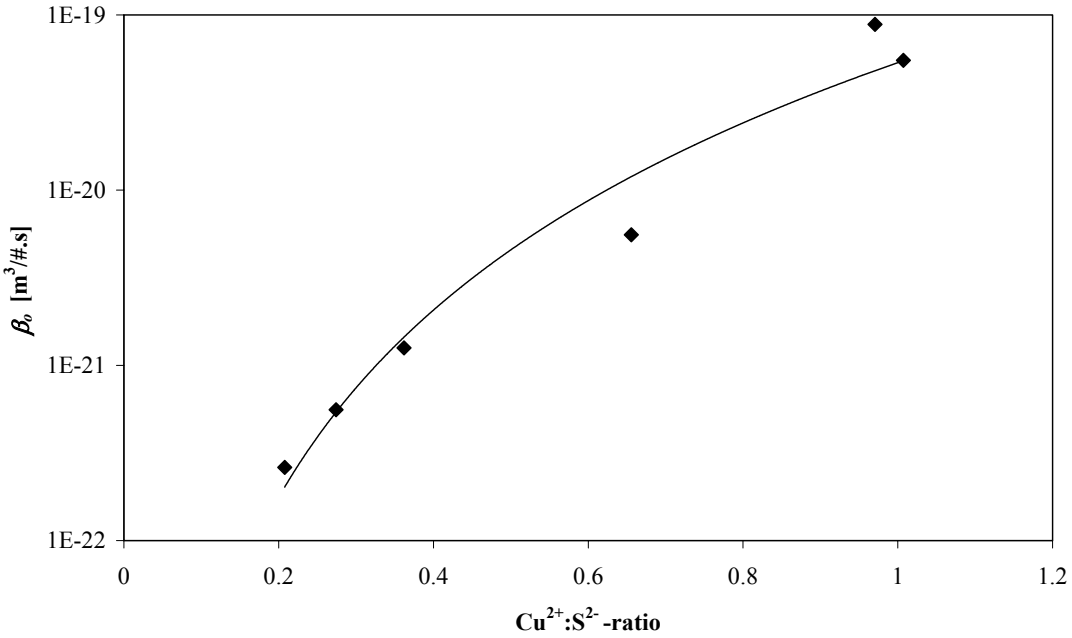

Figure 14: *Effect of molar feed ratio on agglomeration kernel. Conditions: RPM = 710, pH = 5.9, residence time = 157 s, $[Cu^{2+}]_{inlet}$ = 8x10^{-3}~3x10^{-2} mol/m^3, $[S^{2-}]_{inlet}$= 8x10^{-3} ~3x10^{-2} mol/m^3*

Figures 15, 16 and 17 show the effect of pH on volume average growth rate, primary nucleation rate and agglomeration kernel respectively. The pH was adjusted by adding sulfuric acid to the Cu^{2+} feed stream. In all experiments 60~70% conversion of Cu^{2+} was observed. Increasing the pH up to a value of about 5 increases the volume average growth rate and agglomeration kernel whereas it decreases the primary nucleation rate. One can thus conclude that a pH-value of around 5 is optimum when large crystals are to be produced. This can be due to the growing tendency of hydrophobic CuS to escape from water as the pH is decreased. The low conversion of Cu^{2+} is probably due to the formation of complexes such as $Cu(HS)_2$ which forms at low pH-values. With regard to agglomeration two regions can be distinguished, one above pH=5 where no influence of pH is observed and one below pH=5 where an increase of agglomeration kernel is observed with pH. This can again be caused by the hydrophobic properties of CuS or by other agglomeration mechanisms such as Brownian motion or size dependent agglomeration behavior which has not been accounted for in the analysis of the experimental data. In general the particle size was observed to increase with pH, for example at pH=2.2 the average particle size was found to be 62 nm whereas this value was 2287 nm at pH= 4.7.

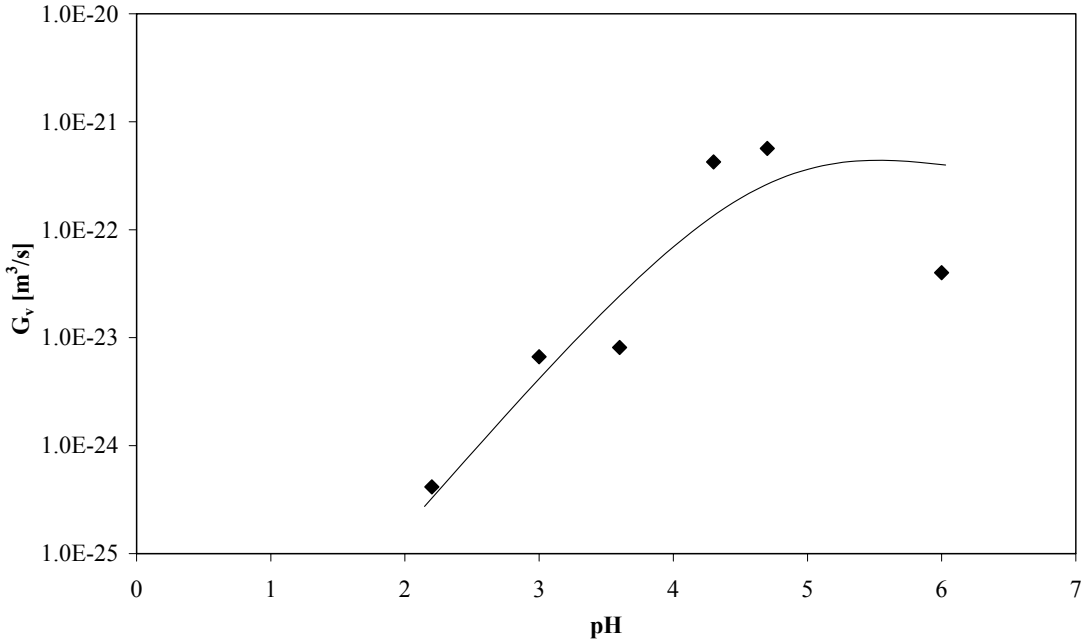

Figure 15: *Effect of pH on volume average growth rate. Conditions: molar feed ratio Cu^{2+}:S^{2-} = 1:1, RPM = 710, $[Cu^{2+}]_{inlet}=[S^{2-}]_{inlet}$= 6x10^{-3} mol/$m^3$, residence time 157 s*

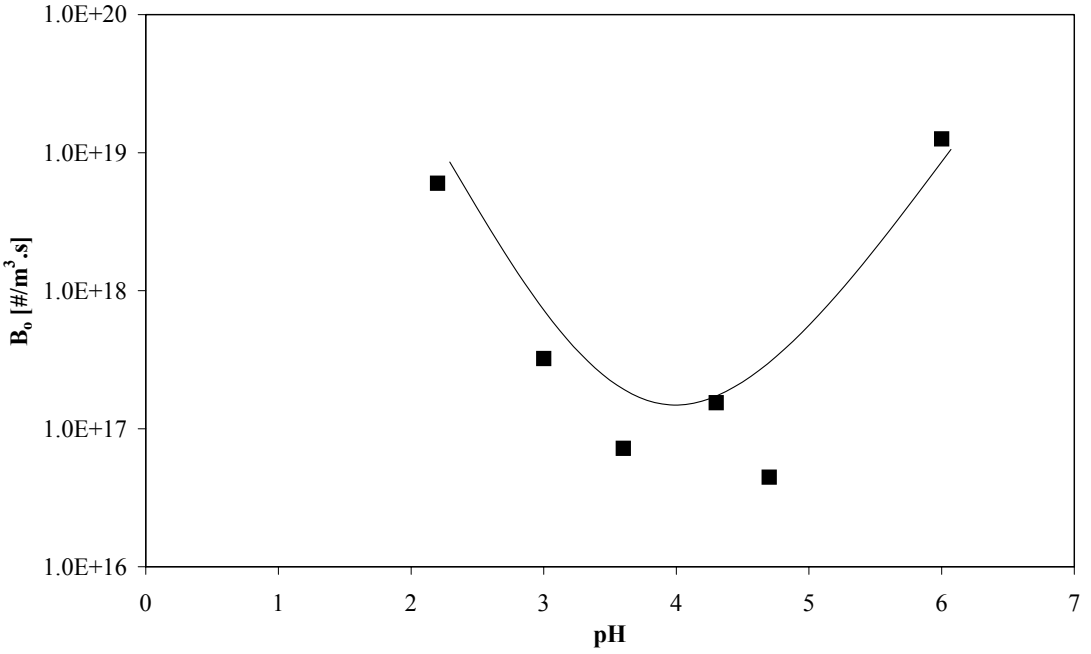

Figure 16: *Effect of pH primary nucleation rate. Conditions: molar feed ratio Cu^{2+}:S^{2-} = 1:1, RPM = 710, $[Cu^{2+}]$inlet=$[S^{2-}]_{inlet}$= 6x10^{-3} mol/m^3, residence time 157 s*

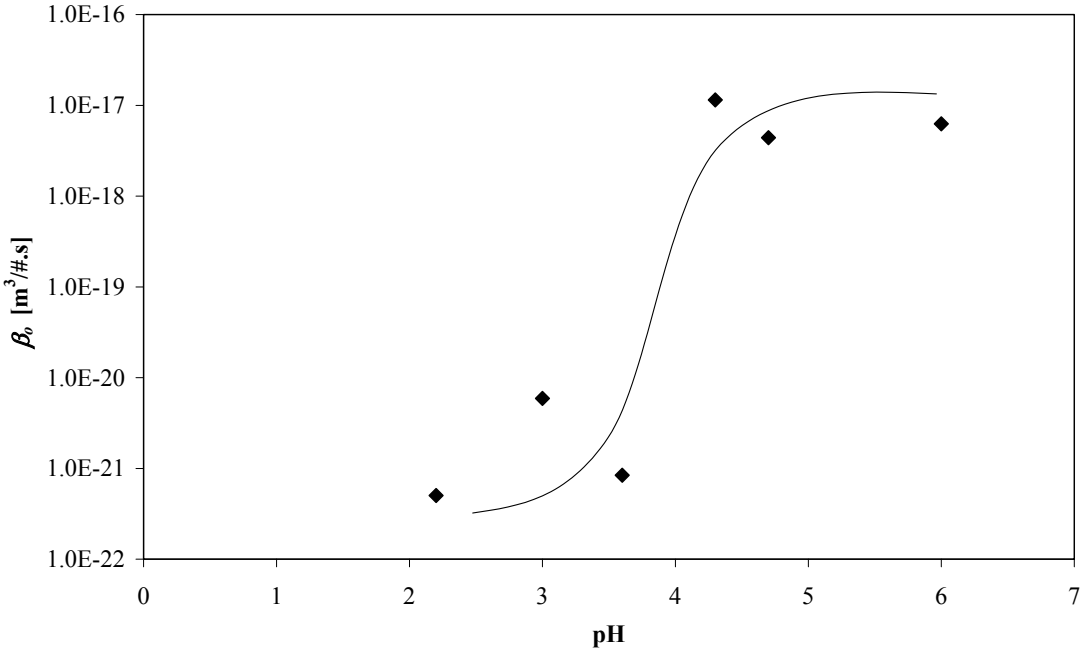

Figure 17: *Effect of pH on agglomeration kernel. Conditions: molar feed ratio Cu^{2+}:S^{2-} = 1:1, RPM = 710, $[Cu^{2+}]_{inlet}=[S^{2-}]_{inlet}= 6x10^{-3}$ mol/m^3, residence time 157 s*

2.7 Conclusions

The size distribution of particles produced in a crystallizer depends on the kinetics of nucleation and crystal growth. In a precipitation process where solids are formed with an extremely low solubility it is also strongly influenced by agglomeration. This work was concerned with the characterization of crystallization kinetics (primary nucleation, crystal growth and agglomeration) of CuS using an MSMPR crystalliser (see Table 1). Crystallization kinetics of CuS were found to depend on supersaturation, stirrer speed, pH, molar feed ratio and residence time. An increase in supersaturation leads to a proportional increase in volume average crystal growth and agglomeration kernel whereas the rate of primary nucleation is hardly affected. Stirrer speed, pH and molar ratio were found to show optima with regard to particle size. However, one should bear in mind that these results were highly influenced by unknown mixing phenomena. Using the obtained kinetic data for design or scale up purposes can therefore be dangerous. Only when the hydrodynamic conditions are precisely known, intrinsic kinetic data can be obtained. The results could be used though for similar reactor types than the one applied in this work.

Table 1: *CuS crystallization kinetic.*

Growth	$G_v = 3.87x10^{-36}(S-1)$
Primary nucleation	$B_o = 4.31x10^{-9}\varphi_T^{0.9}G_v^{-1.16}$
Agglomeration kernel	$\beta_o = 8.32x10^{-7}B_o^{0.89}G_v^{1.25}$

Acknowledgment

This project was supported with a grant of the Dutch Programme EET (Economy, Ecology, Technology) a joint initiative of the Ministries of Economic Affairs, Education, Culture and Sciences, and of Housing, Spatial Planning and Environment. This program is coordinated by the EET Program Office, a partnership of Senter and Novem.

List of symbols

a_T	Specific surface area of the produced particles [m^2/m^3]
B	Secondary nucleation rate [$\#/m^3.m^3.s$]
B_o	Primary nucleation rate [$\#/m^3.s$]
c*	Equilibrium molar concentration [mol/m^3]
c_c	Crystal molar density [mol/m^3]
D	Death rate [$\#/m^3.m^3.s$]
D_{AB}	Diffusion coefficient of A in B [m^2/s]
d_s	Sauter average particle size [m]
f	Correction factor between 0.9 and 0.5 in eqn 3 [-]
g	Supersaturation exponent in the growth rate correlation [-]
G_L	Linear average crystal growth rate [m/s]
G_v	Volume average crystal growth rate [m^3/s]
h	Exponent of growth rate in the agglomeration kernel correlation [-]
i	Exponent of growth rate in the primary nucleation correlation [-]
j	Exponent of solid holdup in the primary nucleation correlation [-]
k_β	Rate coefficient for agglomeration kernel [$m^3/\#.s$]
k_g	Growth rate constant [m/s]
k_n	Nucleation rate constant [$\#/m^3.s$]
K_R	Relative nucleation rate constant [$\#/m^3.s$]
k_{sp}	Solubility constant [mol^2/m^6]
L_{50}	Average particle size [m]
n	Crystal volume population density [$\#/m^3.m^3$]
N_A	Avocado number [#/mol]
n_b	Supersaturation exponent in the primary nucleation rate correlation [-]
p	Exponent of nucleation rate in agglomeration correlation [-]
q	Exponent of mean residence time in agglomeration correlation [-]
S	Relative supersaturation [-]
t	Time [s]
V	Volume of reactor [m^3]
v	Volume [m^3]

	v_p	Volume of particle [m^3]
	$\dot{V}$	Volumetric flowrate [m^3/s]
Greek		
	σ	Absolute relative supersaturation [-]
	φ_T	Solid holdup [kg/m^3]
	β	Agglomeration kernel in volume coordinates [m^3/#.s]
	β_o	Size independent agglomeration kernel in volume coordinate [m^3/#.s]
	μ_j	Moment of j
	τ	Residence time [s]
	ρ_s	Density of solids [mol/m^3]
	κ	Constant in equation (17) [m]
	ν	Stoichiometric ratio [-]

References:

1. Herman J.M. Kramer, Sean K. Bermingham and Gerda M. van Rosmalen. "Design of industrial crystallisers for a given product quality". Journal of crystal growth, Vol. 198/199, pp 729-737, 1999.
2. Jones A.G, Hostomsky J and Shun Wachi."Modelling and analysis of particle formation during agglomeration crystal precipitation processes". Chem. Eng. Comm. Vol. 146, pp 105-130 1996.
3. Jones A.G. Falope G. O. and R. Zauner, "On modelling continuous agglomerative crystal precipitation via Monte Carlo simulation". Chem. Eng. Sci. Vol. 56, pp 2567-2574, 2001.
4. Hatakka H, Oinas P. Reunanen J. and Palosaari S. "The effect of supersaturation on agglomeration". Chem. Eng. Comm. Vol. 146, pp 76-78 1996.
5. Narayan S. Tavare and Anand V. Patwardhan. "Agglomeration in continuous MSMPR crystallizer". AIChE J. Vol. 38, No.3, pp 377-384, 1992.
6. Alan G. Jones, Jiri Hostomsky and Shun Wachi. "Modelling and analysis of particle formation during agglomerative crystal precipitation processes". Chem. Eng. Comm. Vol.146, pp 105-130, 1996.
7. Zuoliang SHA and Seppo Palosaari, "a model of crystallization in an imperfect suspension crystallizer. Acta Polytech". Scand, Chem Technol. Ser 244, pp 79-81,1997.
8. Ingo H. Leubner. "A new crystal nucleation theory for continuous precipitation of silver halides". J. Imaging Sci & Tec. Vol. 42, no. 4, pp 355-364, 1998.

9. Alan G. Jones and Rudolf Zauner, “Determination of nucleation, growth, agglomeration and disruption kinetics from experimental precipitation data: the calcium oxalate system”. Chem. Eng. Sci. Vol. 55, pp 4219-4232, 2000.
10. Mersmann A. Crystallization technology handbook. New York, (1995).
11. Mullin J. W. Crystallization, third edition, plant tree, London-UK, (1992).
12. Mersmann A. ”Calculation of interfacial tension”. J. of crystal growth, vol. 102, pp 841-847, 1990.
13. Hounslow M. J, A.S. Bramley, R. Newman, W.R. Paterson and C. Pogessi. “The role of solution composition on aggregation during precipitation”, Trans IchemE, Vol. 75, Part A, pp119-124, 1997.

Chapter 3

Crystallization Kinetics of ZnS Precipitation; An Experimental Study Using the Mixed-Suspension-Mixed-Product-Removal (MSMPR) Method

Abstract

The precipitation kinetics of zinc sulfide were studied using a lab scale mixed-suspension-mixed-product-removal (MSMPR) precipitation reactor. The vessel was operated at different feed concentrations, molar ratios, stirrer speeds, pH-values, feed injection positions and residence times. Primary nucleation and volume average crystal growth rates as well as agglomeration kernel were determined. Relationships were found between the rates of the different crystallization steps on the one hand and supersaturation, stirrer speeds, pH-values, Zn^{2+} to S^{2-} ratio, feed positions on the other. These show that larger crystals are obtained at high supersaturation, moderate stirrer speeds, small residence times, a pH-value of around 5 and high Zn^{2+} to S^{2-} ratios. One should realize though that the applied MSMPR method is not the most optimal technique for examining fast precipitation reactions.

3.1 Introduction

The characteristics of a crystal product with regard to filterability, flowability, drying, caking and tabletting behavior is mainly determined by crystal size distribution, morphology, degree of agglomeration and purity [1]. Many chemical processes, such as the synthesis of catalysts, pigments and pharmaceutical products, offshore oil drilling, and water treatment, involve precipitation in one or more key steps of the overall operation. Precipitation is a very complex process, since it is influenced by several interacting phenomena, and for this reason it has attracted much attention. Precipitation occurs through several steps, namely nucleation, crystal growth, and eventually aggregation and breakup. During the precipitation of sparingly soluble solids, agglomeration competes with molecular ionic crystal growth at the solid-liquid interface [2]. Knowledge of agglomeration behavior is therefore also required.

Before precipitation can start, a solution must be supersaturated. This can be realized by various methods such as reactive precipitation or changing temperature in order to diminish solubility. Precipitation mainly involves two stages: 1) nucleation and 2) growth. Other processes like aggregation, agglomeration, disruptation and Ostwald ripening may also occur. Numerous models have been developed in order to describe each elementary step. However, the different steps that take place simultaneously and are interconnected and therefore the description of the complete process is rather complicated.

Reliable kinetic data are of the utmost importance for the successful modeling and scale-up of precipitation processes. Crystallization kinetics (including primary nucleation rates, growth rates and agglomeration kernel) are usually measured using the Mixed-Suspension-Mixed-Products Removal (MSMPR) crystallizer technique [3]. This technique permits the simultaneous determination of nucleation and growth kinetics by measuring particle size distribution (PSD) as a function of average residence time. When precipitating sparingly soluble solids, secondary processes such as agglomeration may also play an important role in determining the product quality. It is quite difficult to distinguish between agglomeration and the crystal growth kinetics [4]. However, MSMPR experiments can also be used to predict agglomeration kernel. This kernel can be obtained from the population balances in volume coordinates while assuming size independent agglomeration behavior.

3.2 Previous work

The size distribution, shape, internal surface area, structure and voidage of crystal particles determine ultimate product quality. Since the precipitation process is fast, mixing at various scales plays a crucial role in determining the final crystal size

distribution, and crystal morphology. Several precipitation reactions have been used for investigation of the interaction between precipitation kinetics and mixing, e.g. those forming calcium carbonate, barium sulfate, calcium oxalate, yttrium oxalate.

Narayan and Patwardhan (1992) studied the agglomeration of copper sulfate pentahydrate, nickel ammonium sulfate, potassium sulfate and soy protein in an MSMPR crystallizer. They determined nucleation rates, crystal growth rates and agglomeration kernels [5]. They measured product crystal size distributions and transformed these into crystal volume coordinates. They used two methods; i.e. moments analysis and an optimization procedure for parameter characterization.

Alan Jones et al. (1996) developed a model for particle formation during agglomerative crystal precipitation [6]. In their work, the kinetics of processes which determine the formation of both primary particles and crystal agglomerates are briefly reviewed together with established simulation techniques for analyzing and predicting primary and secondary particle size distributions and studies of agglomerative precipitation.

Zuoliang and Palosaari (1997) developed a model to analyze nucleation and growth in a non-ideal MSMPR crystallizer [7]. Their model takes the effects of mixing intensity and product removal location on particle size distribution into account.

Leubner (1998) has developed a new crystal nucleation theory for the continuous precipitation of silver halides [8]. His model was developed based on a dynamic balance between nucleation and growth. This model is applicable for non-seeded systems with diffusion controlled nucleation and growth. The proposed model can predict particle size distribution from average crystal size, residence time, solubility, feed concentrations and temperature. Also the model can predict the maximum growth rate, the ratio of nucleation to growth rates, the ratio of average to critical crystal size and the size of nasent nuclei. Experimental results show good agreement with model predictions.

Jones and Zauner (2000) studied the precipitation kinetics of calcium oxalate in an MSMPR reactor [9]. They operated their reactor at 37^{o}C at different residence times, feed concentrations, stirrer speeds and feed positions. A new procedure to determine the kinetic parameters for nucleation, growth, agglomeration and particle disruption was introduced. They concluded that crystal growth proceeds along a surface-integration controlled mechanism with a second order dependence on absolute supersaturation. Nucleation rates were found to be dependent on power input and feed position, and it was concluded that these rates depend on the hydrodynamics conditions. Agglomeration rates were found to exhibit a maximum with increasing power input. They observed that at higher stirrer speeds the number of agglomerates is decreased due to breakage of these agglomerates by the stirrer.

Jones et al (2001) developed a model to describe agglomerative crystal precipitation based on the Monte Carlo simulation technique [3]. The processes of nucleation, crystal growth and aggregation are first simulated to obtain the particle size distribution (PSD) for continuous mixed-suspension, mixed-product-removal (MSMPR) aggregative precipitation. An extension is then made to account for particle disruption by considering two alternative particle size reduction mechanisms-one enforcing particle splitting into two parts of equal volume and the other accounting for micro attrition. A comparison is made of predicted and experimental determined PSD's for both calcium oxalate and calcium carbonate precipitation. This comparison showed reasonable agreement.

Al-Tarazi et al (2003) studied the precipitation kinetics of copper sulfide using a lab scale MSMPR precipitation reactor [10]. They operated the vessel at different feed concentrations, molar ratios, stirrer speeds, pH-values and residence times. In their work, they determined the primary nucleation and volume average crystal growth rates as well as agglomeration kernel. They found that larger crystals are obtained at high supersaturation, moderate stirrer speeds, small residence times, a pH-value of around 5 and high Cu^{2+} to S^{2-} ratios.

3.3 Present Work

This work comprises an experimental study to determine the crystallization kinetics of zinc sulfide using a lab-scale MSMPR reactor. The effects of supersaturation, pH, molar ratio, feed positions and stirrer speed on the rates of nucleation, growth and agglomeration kernel are studied.

3.4 Theory

To predict crystallizer performance, mass balances, energy balances and population balances need to be solved. Mass and energy balances are based upon (local) operating conditions that determine convection rates, diffusion rates, kinetics and mass and heat transfer. Population balances are needed to derive the size distribution of the produced particles (product quality). To be able to use population balances, the rates of nucleation, growth and particle aggregation must first be quantified [11]. In general, the population balance for any crystallizer can be represented as shown in Figure 1.

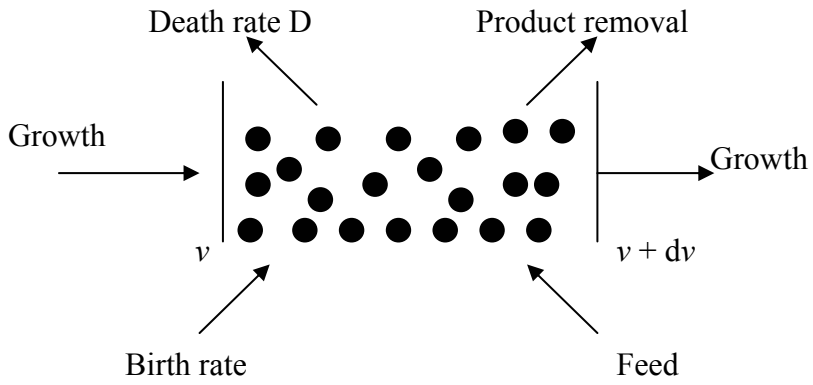

Figure 1: *Change in the number of crystals per unit volume in the crystal size range between L and L+dL*

The population balance expressed in terms of particle number density *n(v, t)* and based on volumetric coordinates is given by:

$$\frac{\partial n}{\partial t} + \frac{\partial (G_v n)}{\partial v} + n\frac{\partial V}{V \partial t} + D - B + \sum_k \frac{\dot{V}_k \cdot n_k}{V} = 0 \qquad (1)$$

Where n is the number density and the expression $\partial(G_v n)/\partial v$ describes the accumulation of crystals due to growth. The term $n\partial V / V\partial t$ takes changes in crystal volume (e.g. due to evaporation of solvent) into account. The parameters D and B respectively represent the rates of death and birth, due to agglomeration, attrition and breakage. Finally, the term $(\sum_k \dot{V}_i n_i / V)$ represents particle accumulation due to flows entering and leaving the crystallizer. The above equation is difficult to solve since the B and D terms cannot be defined a priori as these two terms depend on (local) system hydrodynamics which are mostly difficult to determine. However, a laboratory scale reactor with good mixing characteristics, containing particles smaller than 10 microns and operated at low supersaturation will generally hardly show any agglomeration or attrition [10]. Moreover, intensive mixing leads to growth of all crystals at the same speed whereas no crystals will dissolve.

Crystal growth happens when the solutes present in the supersaturated solution attach to the surface of a particle, leading to an increase in crystal size [10,11]. Crystal growth can be seen as a succession of events namely: i) transport of reactive species through the solution, ii) adsorption on the crystal/surface interface, iii) surface diffusion and iv) surface reaction and incorporation of the product into the crystal lattice. The growth rate can be controlled by transport of ions through the solution (caused by convection and diffusion), by various processes at the crystal surface, or by a combination of these two. For sparingly soluble salts three different mechanisms are proposed that may control

linear crystal growth rate, i.e. i) ion transport (g =1 in eqn 2a), ii) surface spiral growth (g=2 in eqn 2a), and iii) surface polynucleation (eqn 2b). The rate constant can be related to the mass transfer coefficient of ions diffusing from the bulk solution to the crystal surface and/or the diffusion rate of the ions at the crystal surface.

$$G_L = k_g \left[S-1\right]^g \qquad Where\ S = \sqrt{\frac{[A][B]}{k_{sp}}} \tag{2a}$$

$$G_L = k_g S^{7/6} \left[S-1\right]^{2/3} (\ln S)^{1/6} \exp(-k_{sp}/(\ln S)) \tag{2b}$$

As for nucleation, several thermodynamic models are available that link the rate of nucleation to supersaturation. Theoretically, homogeneous nuclei are formed which are unstable in the mother liquor. It is assumed that such nuclei have the same properties as the macroscopic crystals that grow from them. The primary nucleation rate can then be derived from the difference between the free enthalpies of the crystal and the solution. This leads to the following expression [12]:

$$\frac{B_o}{D_{AB}(N_A c_c)^{5/3}} = 0.965 \left(\frac{c^*}{c_c}\right)^{7/3} S^{7/3} \sqrt{f \ln \frac{c_c}{c^*}} \exp\left[-1.19 f \left(\ln \frac{c_c}{c^*}\right)^3 \left(\frac{1}{\nu \ln S}\right)^2\right] \tag{3}$$

where B_o is the primary nucleation rate (nuclei/m^{3}s). This formula is based on several assumptions. In some cases, especially at high supersaturation, a deviation of 200% can occur [13]. In order to minimise the deviation and to establish a more stable numerical routine for mathematical modelling, a simple power law formula is usually preferred [3, 5, 11, 13]:

$$B_o = k_n \left[S-1\right]^{nb} \tag{4}$$

In precipitation reaction crystallization, small particles are normally formed that cluster together forming agglomerates or aggregates when supersaturation is high. Interparticle collisions may result in permanent attachment if the particles are small enough for the Van der Waals forces to exceed collision forces, a condition generally obeyed by particles smaller than 1 micron. Unlike nucleation and crystal growth, agglomeration does not occur in all crystallization processes. Its appearance depends on the crystallizing system in terms of physicochemistral properties and crystallization conditions. Three types of aggregation/agglomeration can be distinguished [11]:

1. If the cohesion forces are weak, agglomeration is called flocculation.
2. If the fusing crystals become strongly bonded due to joint growth, the process is called agglomeration.

3. For intermediary processes and for processes also taking place without joint crystal growth, one speaks of aggregation.

Key parameters that affect agglomeration are:

1. Hydrodynamics (mixing, local turbulence, etc.)
2. The nature of the solvent (viscosity, density, etc.)
3. The size and habit of the crystals, which have a strong effect on the impact of a collision and the contact time. It appears that for reaction crystallization leading to small particles, agglomeration will be important.
4. The population density of the crystals, which has an important influence on the collision frequency.
5. Supersaturation which determines the rates of nucleation, crystal growth and agglomeration.
6. The cohesion forces between solvent, impurities and crystals.

Agglomeration during crystallization has been poorly studied because it is very difficult to distinguish it from crystal growth and to measure the number and size of the monocrystals in a particle/agglomerate.

The processes of nucleation, growth and agglomeration interact in a crystallizer and all contribute to the particle size distribution (PSD) of the products [12]. Kinetic data needed for crystallizer design purposes can be obtained with a laboratory scale mixed-suspension, mixed-product removal (MSMPR) crystallizer. The setup used for this study is shown in Figure 2.

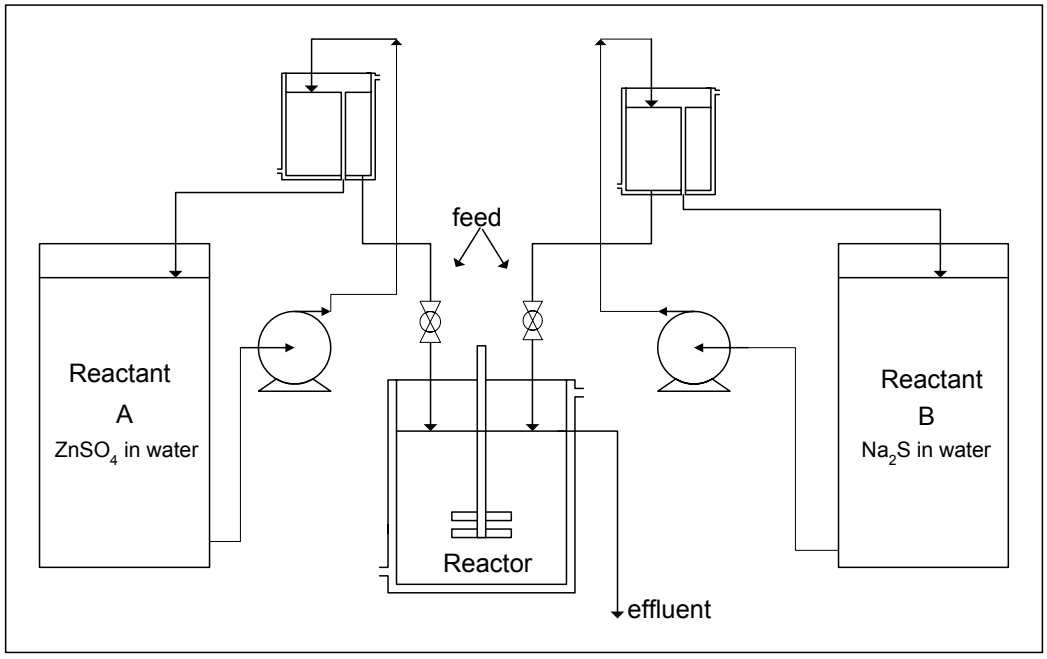

Figure 2: *Applied laboratory scale MSMPR crystallizer.*

It is assumed that all crystals have the same shape and do not break down due to attrition, that the reactor volume is constant, that there are no crystals in the feed, that steady state operation is established and that crystals do not redissolve. It is further assumed that the particles are so small that the growth is independent of the particle size [5] and that the residence time of the solution and the crystals is equal. We then arrive at the following equation describing the population balance:

$$G_v \frac{dn}{dv} + \frac{n}{\tau} = B - D \tag{5}$$

G_v represents the volume average growth rate (m^3/s) and n the crystal population density expressed as a function of crystal volume ($\#/m^3.m^3$). *B* and *D* represent the empirical birth and death functions over a volume range of *v*. Birth and death due to agglomeration of two particles having volumes *u* and *v* - *u* leading to the formation of a particle with volume *v*, are given by the following functions [5]:

$$B = \frac{1}{2}\int_0^v \beta(u, v-u)n(u,t)n(v-u)du \tag{6}$$

$$D = n(v)\int_0^\infty \beta(u,v)n(u)du \tag{7}$$

The agglomeration kernel $\beta(u, v-u)$ is a measure of the frequency of collisions between particles of volumes *u* and *v* – *u* that yield a particle of volume *v*. The factor ½ in equation (6) prevents that such collisions are counted twice. The agglomeration kernel can be described assuming size-independent, Brownian motion, gravitational settling, shear, particle inertia or empirical Thomson's kernel as mechanism [15]. Depending on the chosen mechanism equations (6) and (7) can be integrated and incorporated in the population balance.

Moment μ_j is defined as follows:

$$\mu_j = \int_0^\infty n(v)v^j dv \qquad\qquad j = 0, 1, 2, 3,..,m \tag{8}$$

Assuming the agglomeration kernel to be independent on particle size, the population balance (equation 5) can be rewritten in moments notation using equations (6) and (7):

$$-B_o + \frac{\mu_o}{\tau} = -\frac{1}{2}\beta_o \mu_o^2 \tag{9}$$

$$\frac{\mu_1}{\tau} = G_v \mu_o \tag{10}$$

$$\frac{\mu_2}{\tau} = 2G_v \mu_1 + \beta_o \mu_1^2 \tag{11}$$

The rates of nucleation, crystal growth and agglomeration kernel observed in a series of experiments can be correlated by empirical kinetic relations [5]:

$$G_v = k_g (S-1)^g \tag{12}$$

$$B_o = K_R G_v^i \varphi_T^j \tag{13}$$

$$\beta_o = k_\beta G_v^h B_o^p \tau^q \tag{14}$$

3.5 Derivation of Kinetic Data from MSMPR-Experiments

Equations (9 to 14) are used to derive kinetic data from the MSMPR experiments. In these experiments reactants A and B are continuously added to the reactor. When steady state operation is established a sample of the effluent is taken for analysis. The sample is then analyzed using e.g. Laser Doppler Diffraction to determine the average particle size (L_{50}), the average surface area (a_T) and the solids hold up (φ_T) as well as the particle number density as a function of particle size. On the basis of these measurements the rates of nucleation, growth and agglomeration kernel are calculated at different supersaturations. Making use of equations (9) to (11), a set of (G_v, B_o and β_o)-data is obtained at different supersaturations. After plotting the values of G_v, B_o and β_o as a function of supersaturation, one can make use of any fitting software to calculate the values of k_g, g, K_R, i, j, k_β, h, p and q in equations (12), (13) and (14) [5].

In this work the crystallization kinetics of zinc sulfide has been examined using a laboratory scale MSMPR crystallizer.

3.6 Experimental Procedure

In order to investigate precipitation kinetics and to determine the parameters influencing crystallization kinetics, experiments have been carried out using the MSMPR method at different feed concentrations, stirrer speeds, residence times, feed positions and molar ratios.

The experimental setup (see Figure 2) consisted of a gastight reactor out of glass that was equipped with a multi speed disk & blade mixer and four baffles. The reactor had a volume of 750 ml and a diameter of 11 cm and was connected to a pressure indicator and a thermometer. A jacket around the reactor enabled temperature control. Two peristaltic feed pumps and one withdrawing suction pump were used to adjust the flows of the feed streams and the effluent stream respectively. The liquid hold up was kept constant by using an overflow system by which the liquid level could be controlled. The reactor was thermostated by either cooling or heating water. All experiments were carried out at ambient temperature (i.e. 20^{o}C). The sulfide concentration in the crystallizer as well as the pH were measured online using ion selective electrodes. The feed streams (i.e. solutions of zinc sulfate and sodium sulfide) were introduced into the crystallizer via stainless steel tubes that could be positioned at different locations inside the reactor. Because zinc sulfide exhibits a tendency to agglomerate, small amounts of detergent (X100) were added to the samples to inhibit the agglomeration of the crystals. The reactor was operated under nitrogen and at a constant overpressure of 0.1 atm to prevent the oxidation of sulfide ions by air/oxygen. Even at high stirring speeds bubble formation was avoided and the contact between gas and liquid was always minimal to minimize possible oxidation of produced ZnS crystals, the formation of poly-sulfide and H_2S stripping. The particle size distribution of the produced crystals was measured within 10 minutes after sampling.

To ensure that steady state was reached when sampling, the pH was continuously monitored. It was observed that steady state was always achieved after 12-14 average residence times. After achieving steady state, 500 ml of effluent was collected for analysis. X-ray diffraction (Microtrac X100, size range 0.45 -1000 microns) and a Zeta-sizer (Zetasizer 5000, size range 1-5000 nm) were used to determine particle size distribution. Atomic absorption spectroscopy (AAS) was used to measure the concentration of free zinc ions in the effluent. The sample was filtered, dried and weighed to check the zinc balance. Solids hold up was calculated from the mass balance of the zinc ions. Particle volume density was calculated from the solids hold up and the particle size distribution using the following formula:

$$n_i = \varphi_T \frac{v\%}{\rho_s (v_p)_i ((v_p)_i - (v_p)_{i-1})} \quad \textit{where i represents the class number} \tag{15}$$

3.7 Results and Discussion

In order to investigate the crystallization kinetics of zinc sulfide several experiments were conducted at different feed concentrations (supersaturations), stirrer speeds, residence

times, feed molar ratios, feeds positions and pH-values. Supersaturation was calculated on basis of the feed concentrations of both zinc and sulphide ions while using equation (16)

$$S = \sqrt{\frac{[Zn^{2+}][S^{2-}]}{k_{sp}}} \tag{16}$$

The effect of relative supersaturation on the volume average growth rate of the produced particles is shown in Figure 3. Relative supersaturation was varied over a wide range (from $1x10^8$ to $5x10^{10}$) while keeping the molar ratio at 1. The volume average growth rate (G_v) was found to vary from $5x10^{-19}$ to $9x10^{-18}$ m^3/s. In general the growth rate of ZnS is higher than that earlier obtained for CuS (G_v = $1x10^{-20}$ to $1.2x10^{-19}$) [10]. A logarithmic fit delivers:

$$G_v = 9.77x10^{-23}(S-1)^{0.47} \tag{17}$$

the growth rate constant (k_g) being $9.77x10^{-23}$ m^3/s for the applied conditions.

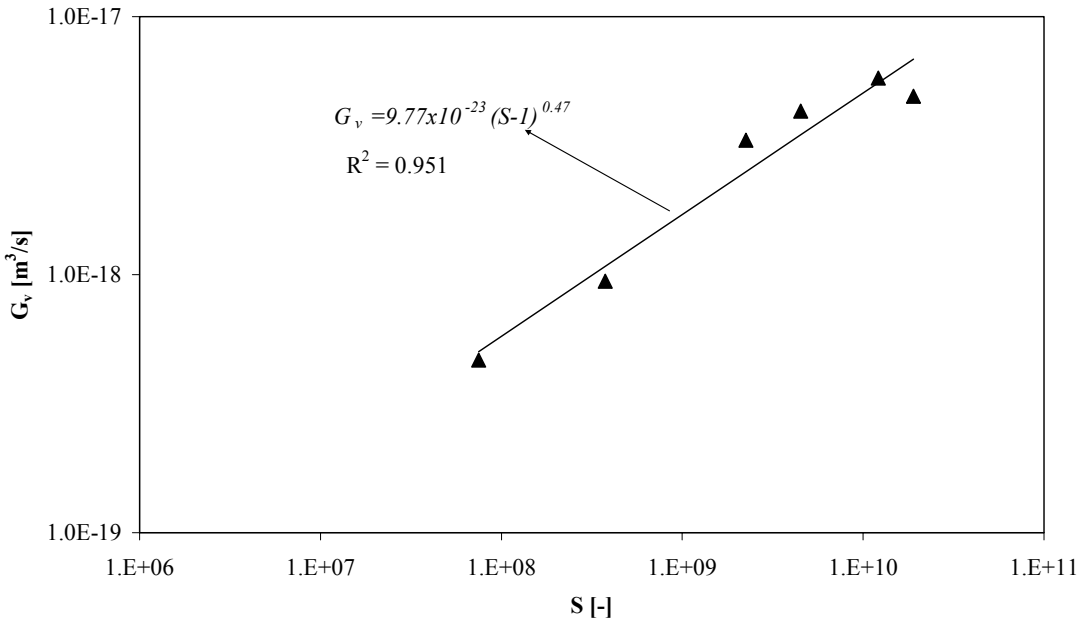

Figure 3: *Logarithmic plot of volume average growth rate vs. relative supersaturation (S): the solid line represents the fitting equation. RPM = 720, molar feed ratio Zn^{2+}:S^{2-} = 1:1, pH = 5.6, residence time = 157 s*

The reaction between zinc ions and sulphide ions was found to be very fast, but only at supersaturations higher than $1.9x10^{10}$ 100% conversion was achieved whereas at lower supersaturation a conversion of typically 75% was found. The average size of the produced particles was varying from 1 micron at low relative supersaturation ($7.5x10^7$) to 9.1 microns at higher relative supersaturations. The obtained average particle size is

expressed as a function of supersaturation by equation (18). The volume average growth rate can be rewritten in terms of linear growth rate yielding equation (19). By substituting equation (18) into equation (19) one may conclude that linear growth proceeds through the mechanism of polynucleation (see equations 20 and 2b).

$$d_s = 1.44x10^{-8}(S-1)^{0.345} \tag{18}$$

$$G_v = \frac{\pi}{2} d_s^2 G_L \tag{19}$$

$$G_L = 2.98x10^{7}(S-1)^{-0.3} \tag{20}$$

The linear growth rate (equation 20) apparently decreases with supersaturation. This is probably due to the assumption of independent size growth, which is not necessarily valid.

In order to arrive at a function of the form of equation (13) the observed primary nucleation rate has been expressed as a function of volume average growth rate and solids hold up using a fitting correlation. The Newton method for multi-dimension optimization was used to calculate the best-fit coefficients for equation (13):

$$B_o = 1.66x10^{-18} G_v^{-1.76} \varphi_T^{1.6} \tag{21}$$

Figure 4 shows the values calculated with this correlation versus the experimentally observed values. An increase of the volume average growth rate corresponds to a decrease in nucleation rate as to be expected. However increasing the solids holdup yields a more than proportional increase in primary nucleation rate which may be related to higher agglomeration rates at higher solids hold up. Substituting the observed effects of supersaturation on volume growth rate [$G_v = 9.77x10^{-23}(S-1)^{0.47}$] and solids hold up [$\varphi_T = 1.2x10^{-7}(S-1)$] delivers the relationship between supersaturation and primary nucleation rate:

$$B_o = 9.31x10^{9}(S-1)^{0.77} \tag{22}$$

This relation shows that an increase in supersaturation corresponds with an increase in primary nucleation rate. In theory, the primary nucleation rate is expected to be highly dependent on supersaturation (the exponent in equation (22) is expected to be in between 5 and 15 [11, 12]). This result can be explained by the fact that the rate of agglomeration also increases with supersaturation, thereby suppressing the primary nucleation rate and enhancing the observed average volume growth rate. Agglomerates grow faster than a single small particle and hence primary nucleation becomes less apparent [14].

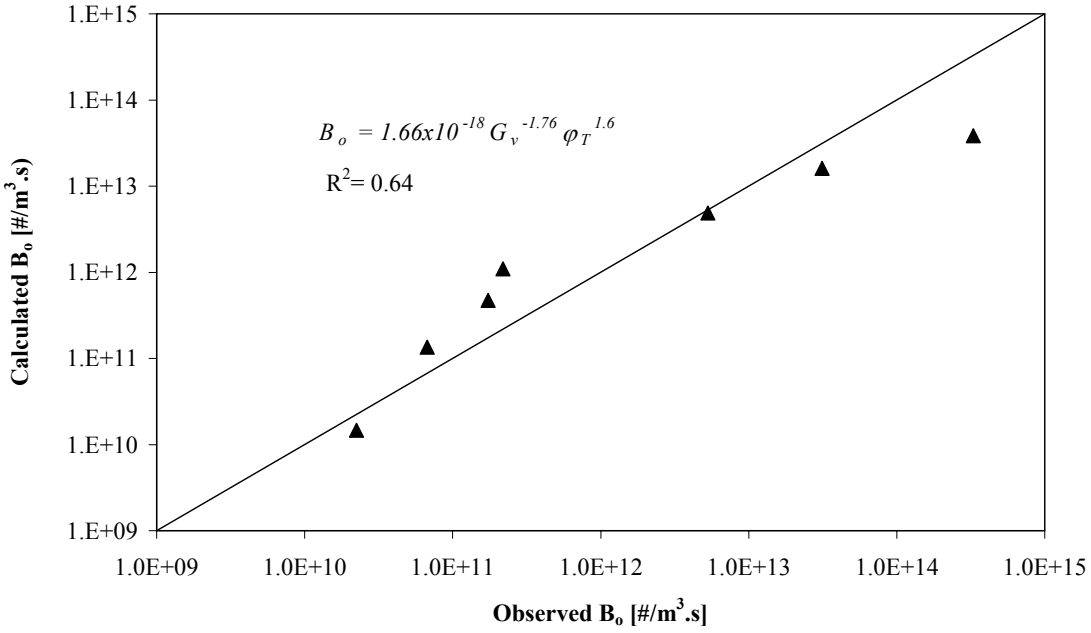

Figure 4: *Calculated rate using the proposed fitting equation vs observed primary nucleation rate; RPM = 720, molar feed ratio Zn^{2+}: S^{2-} = 1:1, pH = 5.6, residence time = 157 s, $[Zn^{2+}]_{inlet} = [S^{2-}]_{inlet} = 8.9x10^{-2} \sim 2.8x10^{1}$ mol/m^3*

Agglomeration kernel was also calculated from the experimental results using equation (11). The experimental results were fitted by means of nonlinear regression to identify the relationship between agglomeration kernel on the one hand and primary nucleation rate and volume average growth rate on the other (as expressed by equation (14)). See Figure 5. Although the fit is certainly not perfect we can conclude that an increase of the primary nucleation rate and a decrease of the average volume growth rate correspond with an increase in agglomeration kernel as to be expected [11]:

$$\beta_o = 2.27x10^{-44} B_o^{0.3} G_v^{-1.47} \qquad (23)$$

As residence time was not varied the factor τ^g (in equation 14) has been included in the value of k_β (=2.268x10^{-44} m$^{6.5}$/#$^{1.3}$.s$^{-0.3}$) in equation (22). An increase in the primary nucleation rate increases the agglomeration kernel while an increase in the volume average growth rate decreases the agglomeration kernel. In general, increasing supersaturation corresponds with a decrease in agglomeration kernel (β_o=5.6x10^{-9}(S-1)$^{-0.5}$). Collisions of bigger particles (occurring at higher G_v- values) are more successful in producing agglomerates. Also an increase in particle concentration will raise agglomeration kernel due to an increase in collision frequency.

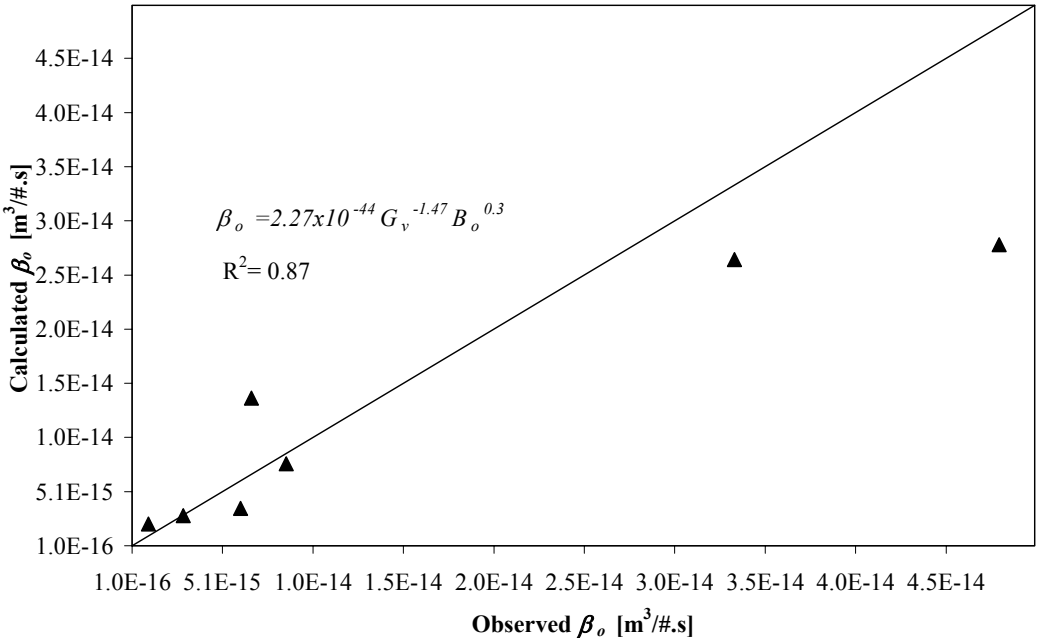

Figure 5: *Calculated agglomeration kernel using the proposed fitting equation vs. observed kernel. RPM = 720, molar feed ratio Zn^{2+}:S^{2-} = 1:1, pH = 5.6, residence time = 157 s, $[Zn^{2+}]_{inlet}$= $[S^{2-}]_{inlet}$= 8.9x10^{-2}~2.8x10^{1} mol/m^3*

The effect of stirrer speed on the volume average growth rate of the ZnS crystals is demonstrated in Figure 6. As can be seen increasing the stirrer speed increases the observed growth rate. Increasing the stirrer speed results in a decrease in local supersaturation near the feed points, which would indeed make the conditions more favorable for crystal growth than for primary nucleation. By increasing the stirrer speed the collision frequency will increase leading to more agglomerates. A further increase of the stirrer speed is expected to cause more disruption of the agglomerated particles resulting in a reduction in particle size and G_v. However, we did not observe this in the range of the stirred speeds applied in this work.

Figures 7 and 8 show the effects of stirrer speed on primary nucleation rate and agglomeration kernel respectively. For both a decrease is observed as stirrer speed is increased. As mentioned earlier, increasing the stirrer speed will result in lower local supersaturation values and hence yield a decrease in primary nucleation rate. As the rate of volume average crystal growth is increasing while the primary nucleation rate is decreasing, agglomeration kernel will lower as stirrer speed is increased. A decrease in the number of particles will decrease the collision frequency resulting in lower β_o-values.

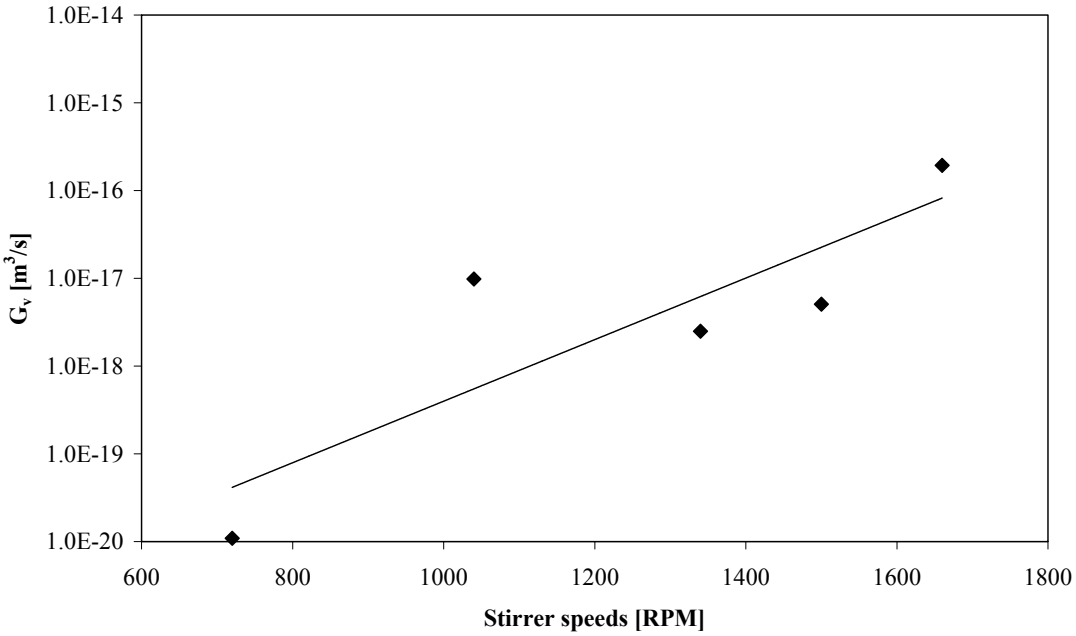

Figure 6: *Effect of stirrer speed on volume average growth rate. Molar feed ratio Zn^{2+}:S^{2-} = 1:1, pH = 5.6, residence time = 157 s, $[Zn^{2+}]_{inlet}=[S^{2-}]_{inlet}=8.9$ mol/m^3*

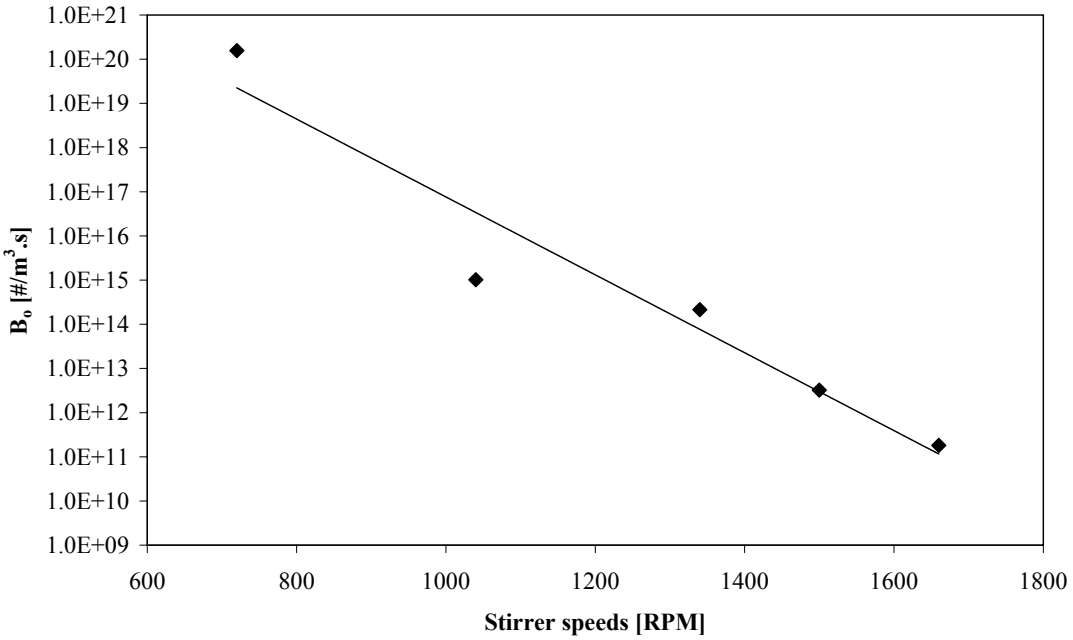

Figure 7: *Effect of stirrer speed on primary nucleation rate. Molar feed ratio Zn^{2+}:S^{2-} = 1:1, pH = 5.6, residence time = 157 s, $[Zn^{2+}]_{inlet}=[S^{2-}]_{inlet}=8.9$ mol/m^3*

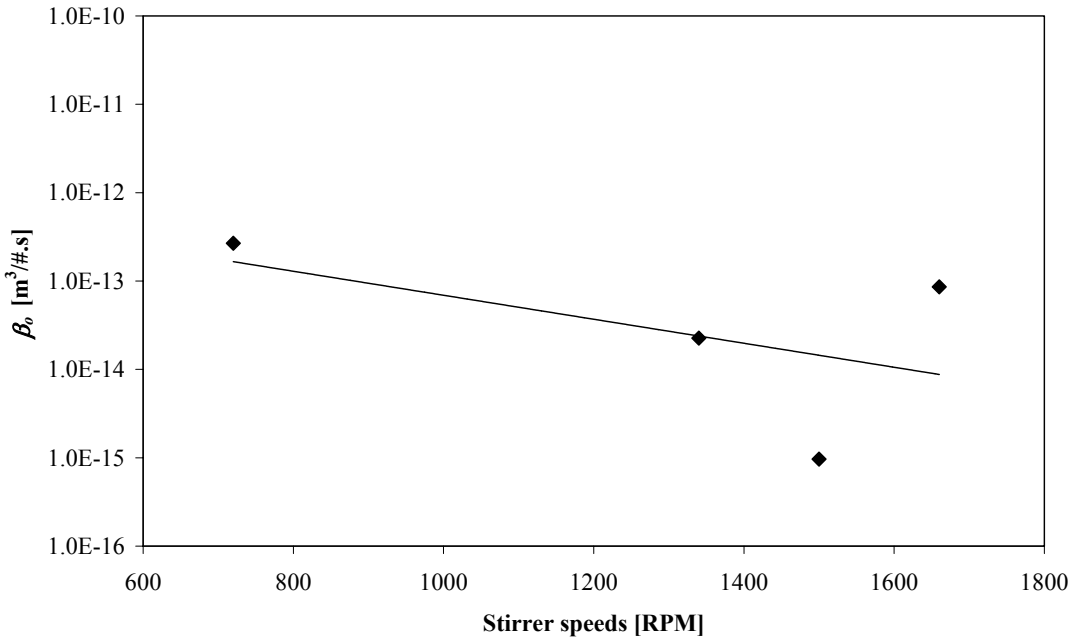

Figure 8: *Effect of stirrer speed on agglomeration kernel; Molar feed ratio Zn^{2+}:S^{2-} = 1:1, pH = 5.6, residence time = 157 s, $[Zn^{2+}]_{inlet}=[S^{2-}]_{inlet}$= 8.9 mol/m^3*

Figures 9, 10 and 11 show the effects of residence time on volume average growth rate, primary nucleation rate and agglomeration kernel respectively. Residence time was changed by adjusting the feed flowrates while keeping all other conditions constant. An increase in residence time results in an exponential increase in volume average growth rate. The primary nucleation rate and the agglomeration kernel were found to decrease with residence time. Increasing the residence time by decreasing the feed flowrate (while keeping the stirrer speed constant) will lead to lower local supersaturation values at the feed points. As the rate of crystal growth is less dependent on supersaturation than that of primary nucleation, new formed ZnS-molecules will increasingly tend to attach to existing crystals instead of forming new nuclei as residence time is increased. This results in a drop in number of particles. On the other hand increasing the residence time of the particles inside the reactor will raise the number of particle collisions resulting in more agglomeration. The net effect, however appears to be negative as the agglomeration kernel decreases with increasing residence time in the reactor.

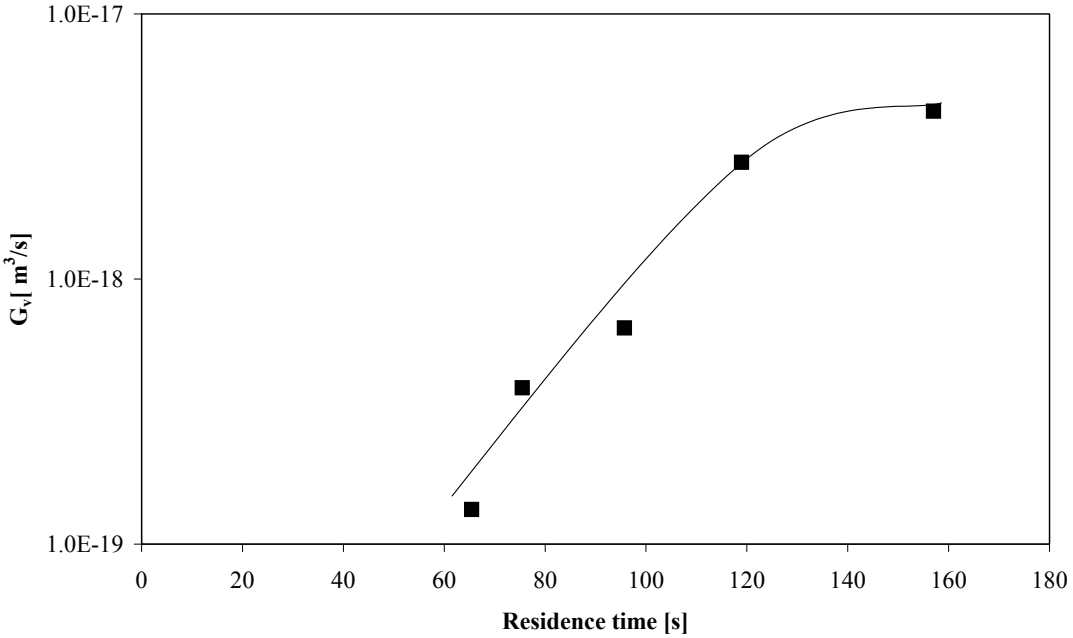

Figure 9: *Effect of residence time on volume average growth rate. Molar feed ratio Zn^{2+}:S^{2-} = 1:1, RPM = 720, pH = 5.6, $[Zn^{2+}]_{inlet}$=$[S^{2-}]_{inlet}$= 8.9 mol/m^3*

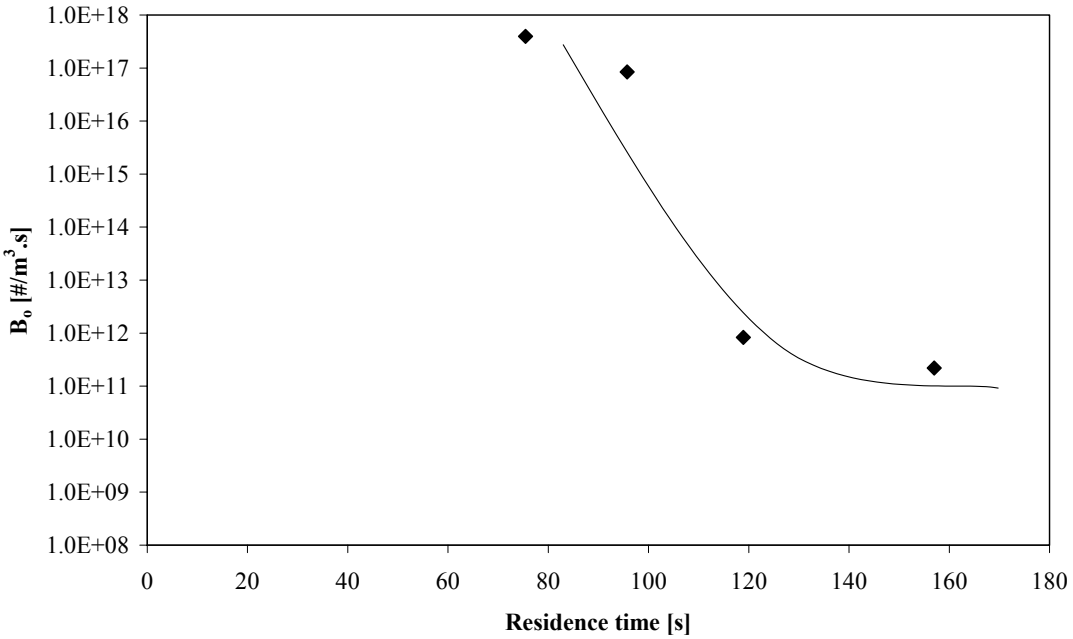

Figure 10: *Effect of residence time on primary nucleation rate. Molar feed ratio Zn^{2+}:S^{2-} = 1:1, RPM = 720, pH = 5.6, $[Zn^{2+}]_{inlet}$=$[S^{2-}]_{inlet}$= 8.9 mol/m^3*

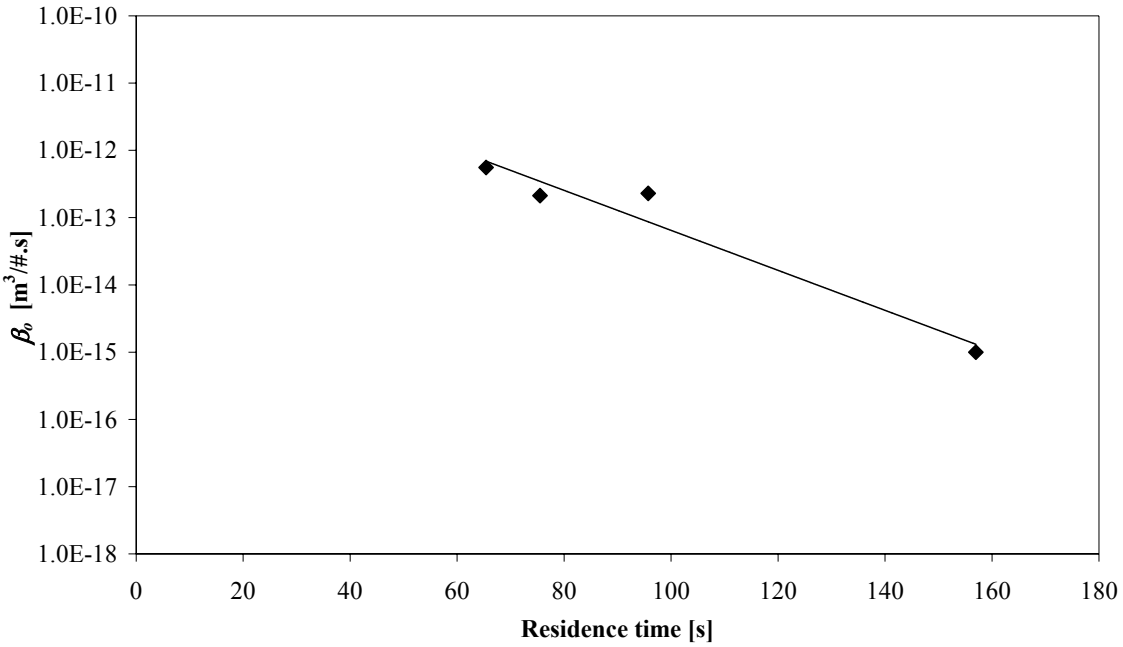

Figure 11: *Effect of residence time on agglomeration kernel. Molar feed ratio Zn^{2+}:S^{2-} = 1:1, RPM = 720, pH = 5.6, $[Zn^{2+}]_{inlet}=[S^{2-}]_{inlet}$= 8.9 mol/m^3*

Figures 12, 13 and 14 show the effects of molar feed ratio (Zn^{2+}:S^{2-}) on the volume average growth rate, primary nucleation rate and agglomeration kernel respectively. The ratio has been adjusted by changing the feed concentrations of Zn^{2+} or S^{2-} while keeping all other parameters constant. Zinc conversion was around 56% when the Zn^{2+} to S^{2-} ratio was higher than unity (instead of typically 75% at a ratio of 1). Increasing the Zn^{2+} to S^{2-} ratio was found to increase the volume average growth rate and agglomeration kernel while decreasing the primary nucleation rate. No large effects were found at Zn^{2+} to S^{2-} ratios higher than 2. This can be explained by the fact that at small Zn^{2+}:S^{2-} ratios (realized by increasing the S^{2-} concentration) polysulfides were observed. These consume the sulfides ions and hence decrease supersaturation. The decrease in supersaturation will decrease the primary nucleation rate and encourage the growth rate.

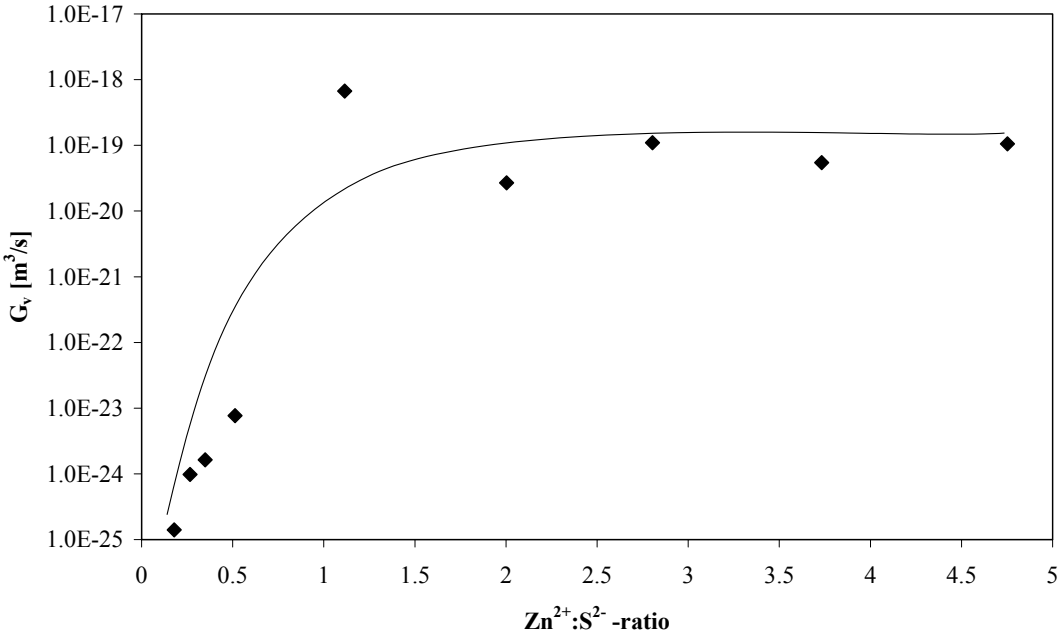

Figure 12: *Effect of molar feed ratio on the volume average growth rate. RPM = 720, pH =5.6, residence time = 157 s, $[Zn^{2+}]_{inlet}$ =2.6~14.3 mol/m^3, $[S^{2-}]_{inlet}$= 3 ~ 15 mol/m^3*

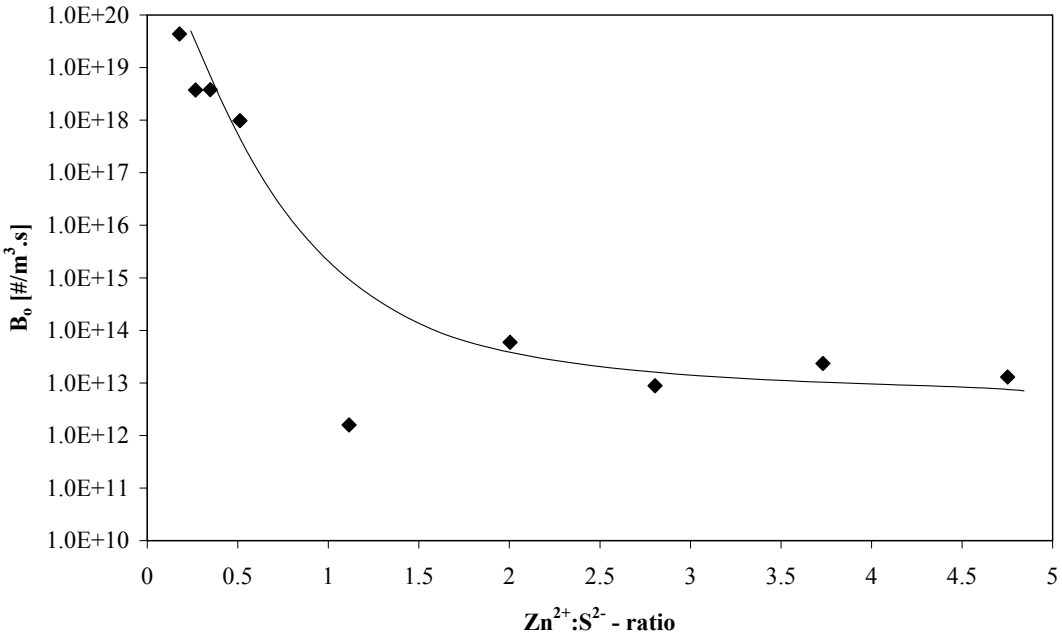

Figure 13: *Effect of molar feed ratio on the primary nucleation rate. RPM = 720, pH = 5.6, residence time = 157 s, $[Zn^{2+}]_{inlet}$ = 2.6~14.3 mol/m^3, $[S^{2-}]_{inlet}$= 3 ~ 15 mol/m^3*

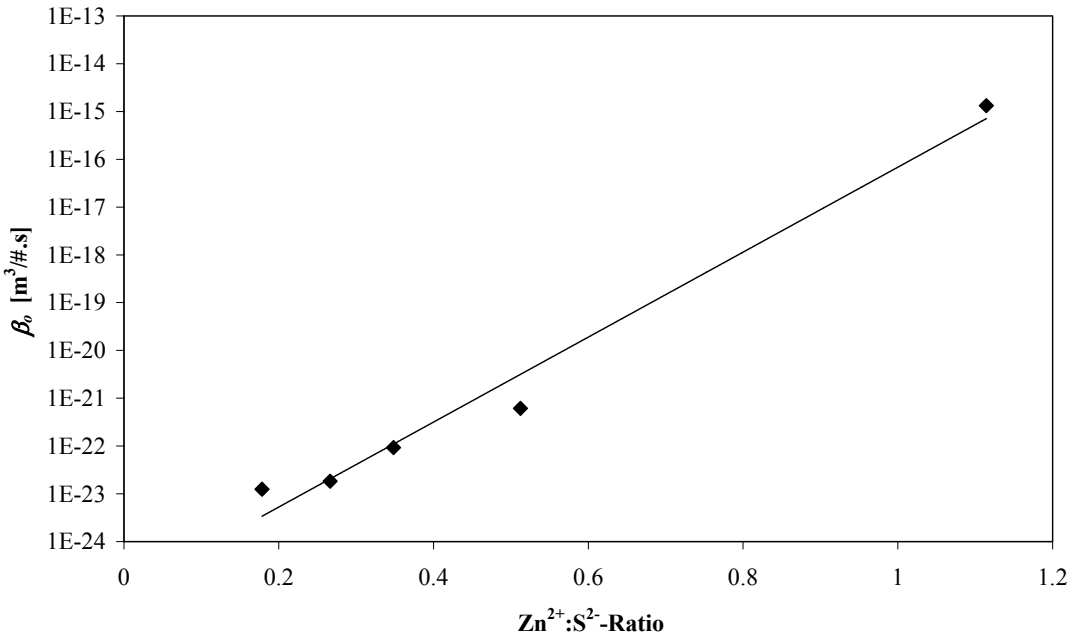

Figure 14: *Effect of molar feed ratio on agglomeration kernel. RPM = 720, pH = 5.6, residence time = 157 s, $[Zn^{2+}]_{inlet}$ = 2.6~14.3 mol/m^3, $[S^{2-}]_{inlet}$= 3 ~ 15 mol/m^3*

Figures 15, 16 and 17 show the effects of pH on volume average growth rate, primary nucleation rate and agglomeration kernel respectively. The pH was adjusted by adding sulfuric acid to the Zn^{2+} feed stream. In all experiments 50~90% conversion of Zn^{2+} was observed. Increasing the pH up to a value of about 5 increases the volume average growth rate and agglomeration kernel whereas it decreases the primary nucleation rate. One can thus conclude that a pH-value of around 5 is optimum when large crystals are to be produced. This can be due to the relation between crystal growth and the electrical charge at the crystal surface, which seems to reverse at a pH value of about 5 (the so-called iso-electric point).

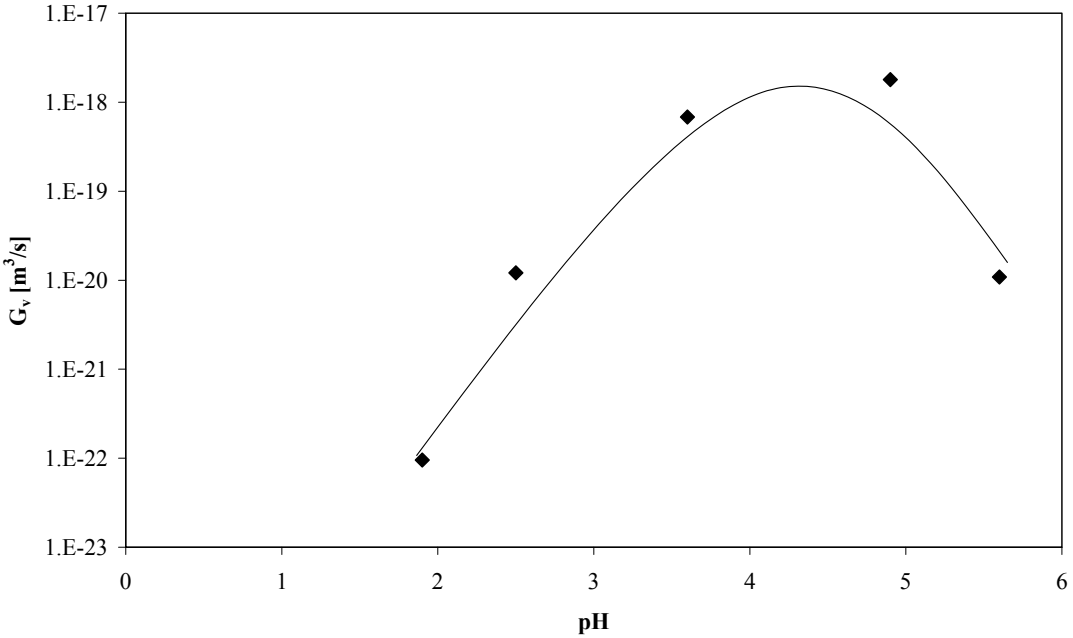

Figure 15: *Effect of pH on volume average growth rate. Molar feed ratio Zn^{2+}:S^{2-} = 1:1, RPM = 720, $[Zn^{2+}]_{inlet}=[S^{2-}]_{inlet}$= 8.9 mol/$m^3$, residence time = 157 s*

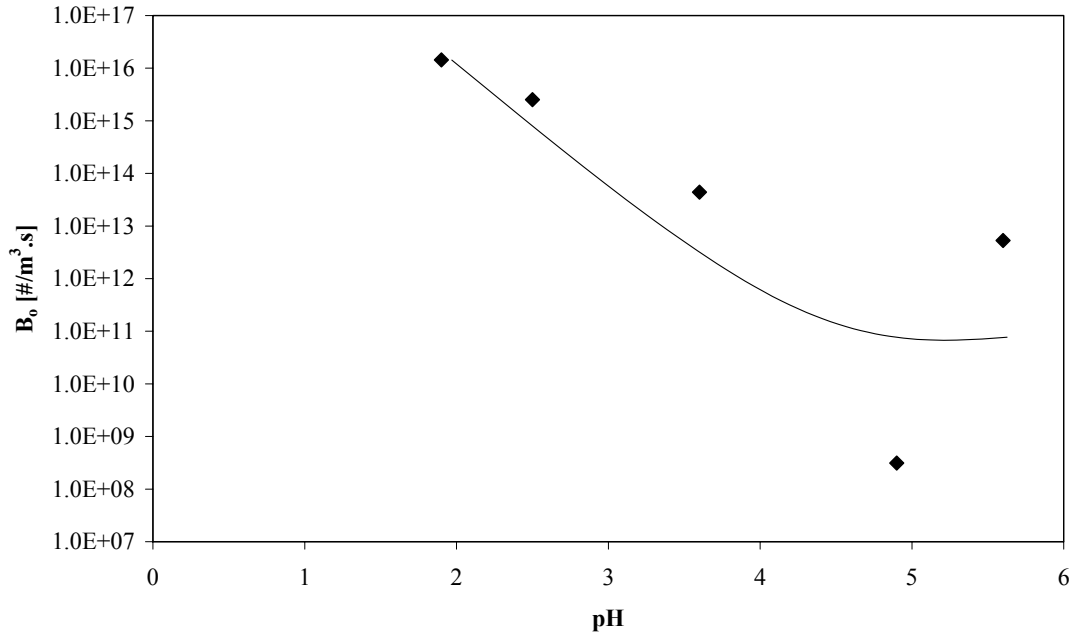

Figure 16: *Effect of pH primary nucleation rate. Molar feed ratio Zn^{2+}:S^{2-} = 1:1, RPM = 720, $[Zn^{2+}]_{inlet}=[S^{2-}]_{inlet}$= 8.9 mol/$m^3$, residence time = 157 s*

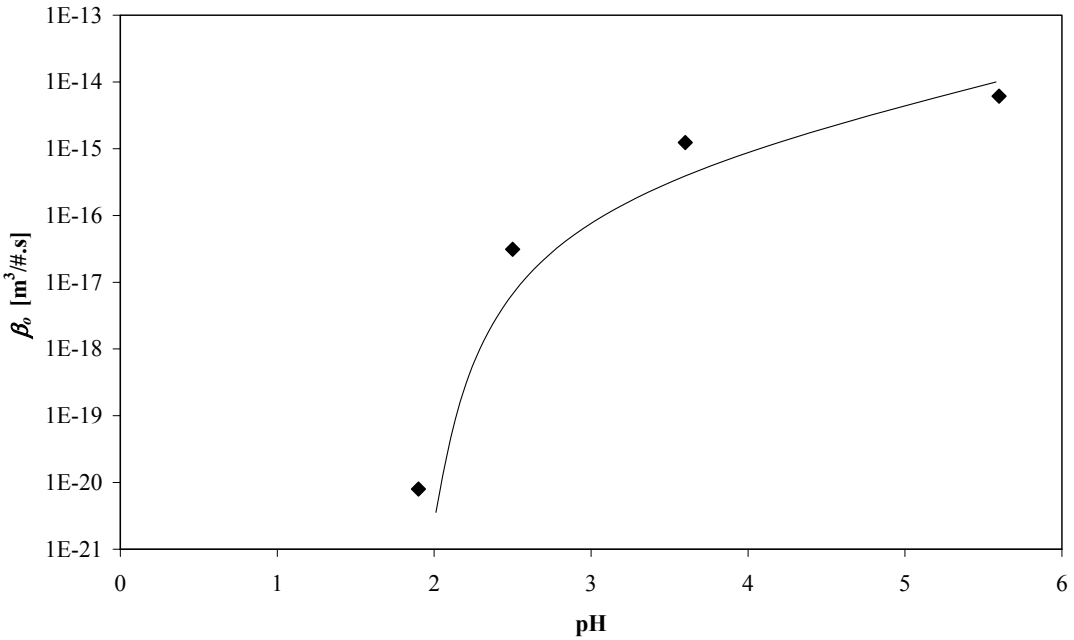

Figure 17: *Effect of pH on agglomeration kernel. molar feed ratio Zn^{2+}:S^{2-} = 1:1, RPM = 720, $[Zn^{2+}]_{inlet}=[S^{2-}]_{inlet}$= 8.9 mol/m^3, residence time = 157 s*

Figures 18 and 19 show the effect of injection point positioning on the average volume growth rate and primary nucleation rate respectively. Four cases were tested see Figure 18. The lowest G_v-value was obtained for position 1 while the highest value was achieved at position 4. On the other hand the primary nucleation rate was found to be the highest at position 1 and lowest at position 2. When the injection points are placed adjacent to eachother, local supersaturation is higher which encourages primary nucleation and reduces the volume average growth rate. At positions 2 and 3 reactants are more diluted before they meet eachother and therefore react at lower supersaturation which is advantageous for crystal growth.

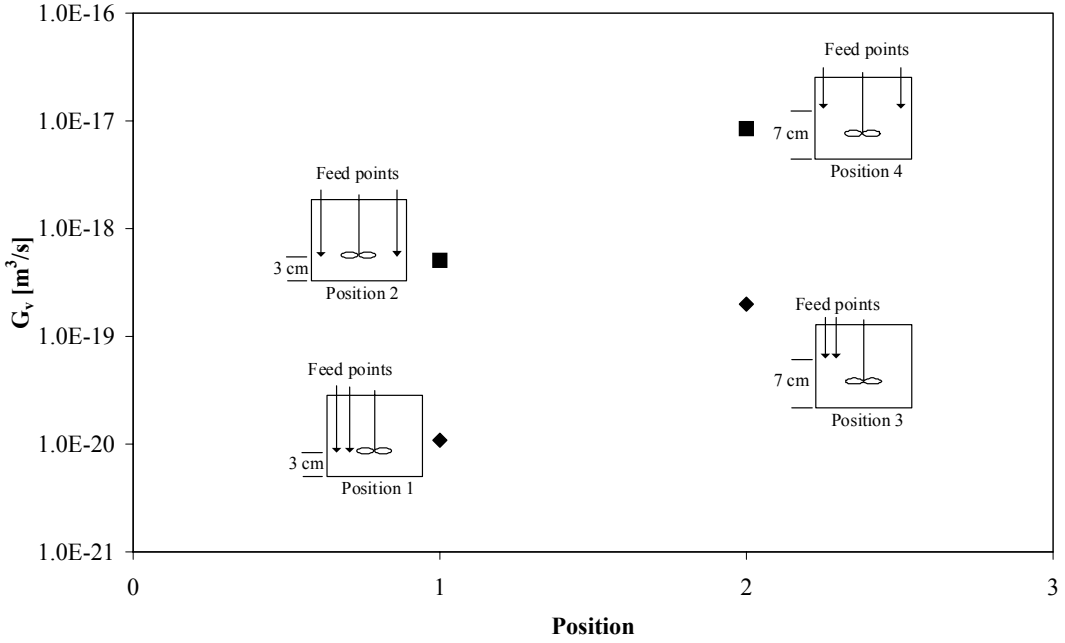

Figure 18: *Effect of feeds positions on volume average growth rate. Molar feed ratio Zn^{2+}:S^{2-} = 1:1, RPM = 720, $[Zn^{2+}]_{inlet}=[S^{2-}]_{inlet}$= 8.9 mol/m^3 ,residence time 157 s, pH = 5.6*

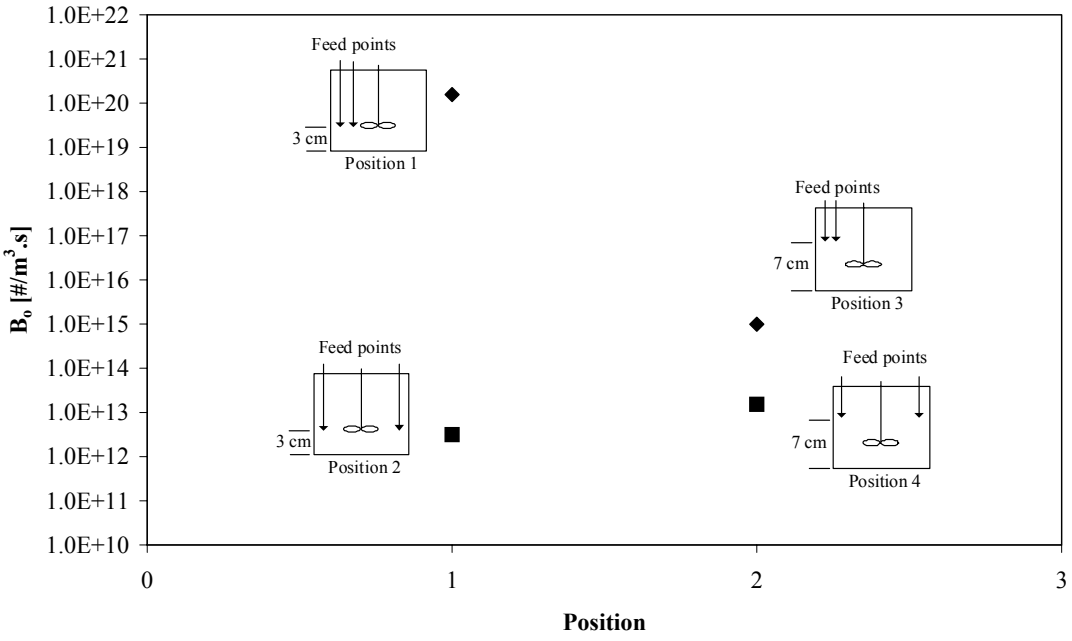

Figure 19: *Effect of feeds positions on primary nucleation rate. Molar feed ratio Zn^{2+}:S^{2-} = 1:1, RPM = 720, $[Zn^{2+}]_{inlet}=[S^{2-}]_{inlet}$= 8.9 mol/m^3, residence time 157 s, pH = 5.6*

3.8 Conclusions

The size distribution of particles produced in a crystallizer depends on the kinetics of nucleation and crystal growth. In a precipitation process where solids are formed with an extremely low solubility it is also strongly influenced by agglomeration. This work was concerned with the characterization of crystallization kinetics (primary nucleation, crystal growth and agglomeration) of ZnS using an MSMPR crystallizer. Crystallization kinetics of ZnS were found to depend on supersaturation, stirrer speed, pH, molar feed ratio and residence time (see Table 1). An increase in supersaturation leads to an increase in volume average crystal growth rate, agglomeration kernel and primary nucleation rate. However, one should bear in mind that these results were influenced by unknown mixing phenomena as has been demonstrated by varying stirrer speed and feed injection point positioning. Using the obtained kinetic data for design or scale up purposes can therefore be dangerous. In a future paper we will present an alternative method to measure intrinsic crystallization kinetics in the absence of unknown hydrodynamic phenomena. The results could be used though for similar reactor types than the one applied in this work.

Table 1: *ZnS crystallization kinetic.*

Growth	$G_v = 9.77x10^{-23}(S-1)^{0.47}$
Primary nucleation	$B_o = 1.66x10^{-18} G_v^{-1.76} \varphi_T^{1.6}$
Agglomeration kernel	$\beta_o = 2.27x10^{-44} B_o^{0.3} G_v^{-1.47}$

Acknowledgment

This project was supported with a grant of the Dutch Programme EET (Economy, Ecology, Technology) a joint initiative of the Ministries of Economic Affairs, Education, Culture and Sciences, and of Housing, Spatial Planning and Environment. This program is coordinated by the EET Program Office, a partnership of Senter and Novem.

List of symbols

a_T	Specific surface area of the produced particles [m^2/m^3]
B	Secondary nucleation rate [$\#/m^3.m^3.s$]
B_o	Primary nucleation rate [$\#/m^3.s$]
c*	Equilibrium molar concentration [mol/m^3]
c_c	Crystal molar density [mol/m^3]
D	Death rate [$\#/m^3.m^3.s$]
D_{AB}	Diffusion coefficient of A in B [m^2/s]

d_s	Sauter average particle size [m]
f	Correction factor between 0.9 and 0.5 in eqn 3 [-]
g	Supersaturation exponent in the growth rate correlation [-]
G_L	Linear average crystal growth rate [m/s]
G_v	Volume average crystal growth rate [m^3/s]
h	Exponent of growth rate in the agglomeration kernel correlation [-]
i	Exponent of growth rate in the primary nucleation correlation [-]
j	Exponent of solid holdup in the primary nucleation correlation [-]
k_β	Rate coefficient for agglomeration kernel [m^3/#.s]
k_g	Growth rate constant [m/s]
k_n	Nucleation rate constant [#/m^3.s]
K_R	Relative nucleation rate constant [#/m^3.s]
k_{sp}	Solubility constant [mol^2/m^6]
L_{50}	Average particle size [m]
n	Crystal volume population density [#/m^3.m^3]
N_A	Avocado number [#/mol]
n_b	Supersaturation exponent in the primary nucleation rate correlation [-]
p	Exponent of nucleation rate in agglomeration correlation [-]
q	Exponent of mean residence time in agglomeration correlation [-]
S	Relative supersaturation [-]
t	Time [s]
V	Volume of reactor [m^3]
v	Volume [m^3]
v_p	Volume of particle [m^3]
$\dot{V}$	Volumetric flowrate [m^3/s]

Greek

σ	Absolute relative supersaturation [-]
φ_T	Solid holdup [kg/m^3]
β	Agglomeration kernel in volume coordinates [m^3/#.s]
β_o	Size independent agglomeration kernel in volume coordinate [m^3/#.s]
μ_j	Moment of j
τ	Residence time [s]
ρ_s	Density of solids [mol/m^3]
κ	Constant in equation (17) [m]
ν	Stoichiometric ratio [-]

References:

1. Herman J.M. Kramer, Sean K. Bermingham and Gerda M. van Rosmalen. "Design of industrial crystallisers for a given product quality". Journal of crystal growth, Vol. 198/199, pp 729-737, 1999.
2. Jones A.G, Hostomsky J and Shun Wachi."Modelling and analysis of particle formation during agglomeration crystal precipitation processes". Chem. Eng. Comm. Vol. 146, pp 105-130 1996.
3. Jones A.G. Falope G. O. and R. Zauner, "On modelling continuous agglomerative crystal precipitation via Monte Carlo simulation". Chem. Eng. Sci. Vol. 56, pp 2567-2574, 2001.
4. Hatakka H, Oinas P. Reunanen J. and Palosaari S. "The effect of supersaturation on agglomeration". Chem. Eng. Comm. Vol. 146, pp 76-78 1996.
5. Narayan S. Tavare and Anand V. Patwardhan. "Agglomeration in continuous MSMPR crystallizer". AIChE J. Vol. 38, No.3, pp 377-384, 1992.
6. Alan G. Jones, Jiri Hostomsky and Shun Wachi. "Modelling and analysis of particle formation during agglomerative crystal precipitation processes". Chem. Eng. Comm. Vol.146, pp 105-130, 1996.
7. Zuoliang SHA and Seppo Palosaari, "A model of crystallization in an imperfect suspension crystallizer. Acta Polytech". Scand, Chem Technol. Ser 244, pp 79-81,1997
8. Ingo H. Leubner. "A new crystal nucleation theory for continuous precipitation of silver halides". J. Imaging Sci & Tec. Vol. 42, no. 4, pp 355-364, 1998.
9. Alan G. Jones and Rudolf Zauner, "Determination of nucleation, growth, agglomeration and disruption kinetics from experimental precipitation data: the calcium oxalate system". Chem. Eng. Sci. Vol. 55, pp 4219-4232, 2000.
10. Al-Tarazi Mousa, A. Bert M. Heesink, Mohammed O.J. Azzam, Salah Abu Yahya and Geert F. Versteeg. "Crystallization kinetics of CuS precipitation; an experimental study using the MSMPR Method". Submitted to Separation Science and Technology, 2004.
11. Mersmann A. Crystallization technology handbook. New York, (1995).
12. Mullin J. W. Crystallization, third edition, plant tree, London-UK, (1992).
13. Mersmann A. "Calculation of interfacial tension". J. of crystal growth, Vol. 102,841-847, 1990

14. Hounslow M. J, A.S. Bramley, R. Newman, W.R. Paterson and C. Pogessi. “The role of solution composition on aggregation during precipitation”, Trans IchemE, Vol. 75, Part A, pp119-124, 1997.

15. Bramley A.S, M.J. Hounslow and R. L. Ryall. Aggregation during precipitation from solution: a method for extracting rates from experimental data, Journal of Colloid Science, vol. 183, pp 155-165, 1996

Chapter 4

New method for the Determination of Precipitation Kinetics Using Laminar Jet Reactor

Abstract

In this paper a new experimental method for determining the kinetics of fast precipitation reactions is introduced. Use is made of a laminar jet reactor which is also frequently applied to determine the kinetics of homogeneous gas-liquid reactions. The liquid containing one or more of the precipitating reactants passes a gas filled reactor as a stagnant jet in which no mixing occurs. The remaining reactant needed for precipitation is supplied in gaseous form and causes the precipitation reaction to occur while it is diffusing into the jet. Hydrodynamics as well as transport phenomena are precisely defined for this system, whereas agglomeration can be minimized by adjustment of the concentration of the solute supplied by the gas. The kinetics of the crystallization steps (nucleation, growth and aggregation) can be determined by analyzing the size distribution of the particles present in the effluent of the laminar jet reactor. This new method is experimentally demonstrated for the precipitation of CuS using H_2S gas. The obtained data were successfully used to simulate a packed bed absorber in which H_2S is absorbed by a $CuSO_4$-solution.

4.1 Introduction

In a precipitation process, two or more reactants form a solid product [1]. In many cases, the solubility of this product is very low. So when the reactants are brought together a high degree of supersaturation occurs which leads to the nucleation of new crystals and subsequent crystal growth. These processes proceed simultaneously in a given system. Secondary processes such as agglomeration and Ostwald ripening may also occur. All processes together determine ultimate product properties such as particle size distribution.

In almost all industrial cases precipitation is followed by a separation process that prefers coarse over fine particles. In most crystallizers it is therefore desired to produce coarse particles of narrow size distribution. Although precipitation is a common operation in chemical industry, it remains very difficult to predict the size distribution of the produced particles. Particle size is a complex function of nucleation rate, crystal growth and agglomeration of the crystals [2]. Knowledge of intrinsic precipitation kinetics is of crucial importance for the design and control of a precipitator. Such kinetic data have been measured for better soluble solids such as calcium carbonate, silver nitrate and calcium oxalate using the conventional Mixed Suspension Mixed Product Removal (MSMPR) method, using a more or less ideally stirred vessel. For determining the crystallization kinetics of very fast precipitating solids, the MSMPR method is less suited since (local) precipitation rates may be much faster than (local) mixing rates. The precise hydrodynamics inside the crystallizer should be known then, but this is hardly the case with the MSMPR method. Nevertheless, because of lack of alternative methods, many researchers have applied the MSMPR-method to measure precipitation kinetics of sparingly soluble solids (e.g. [3-8]).

In gas-liquid precipitation reactions, a gaseous reactant A is contacted with a liquid solution of reactant B. Gas A is absorbed, dissociates and reacts with B ions to produce AB product. When the concentration of the produced AB exceeds the solubility concentration, supersaturation occurs and nuclei are formed which start to grow to form bigger crystals. When the concentration of the crystals increases, the chances of forming agglomerates or aggregates become higher. When two or more crystals meet they may aggregate and grow further as one crystal or agglomerate. These steps are illustrated by Figure 1.

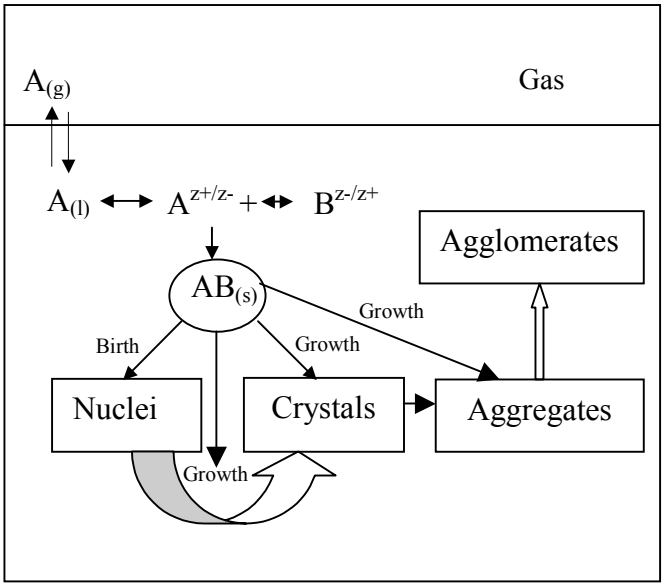

Figure 1: *The process of gas-liquid precipitation*

4.2 Previous Work

Tavare and Patwardhan (1992) studied the agglomeration of copper sulfate pentahydrate, nickel ammonium sulfate, potassium sulfate and soy protein in a continuous MSMPR crystalliser [8]. They determined the rates of nucleation, growth and agglomeration for these precipitates.

Jones et al (1996) developed a model describing particle formation during an agglomerative precipitation process [9]. In their work, processes that determine the formation of both primary particles and crystal agglomerates respectively are briefly reviewed together with simulation techniques that predict primary and secondary particle size distributions.

Zuoliang and Palosaari (1997) developed a model to determine the rates of nucleation and crystal growth from the particle size distribution obtained in a non-ideal MSMPR crystallizer [10]. Their model takes effects of mixing intensity and product removal location into account.

Hounslow et al (1997) investigated the role of solution composition in aggregation during precipitation [11]. In their work, experimental data of calcium oxalate monohydrate precipitation was used to show how the aggregation rate depends on solution composition. A discretized population balance method was used to extract growth and aggregation rates from experimental particle size distributions collected at regular time intervals. They found the measured growth rate to be second order in the relative supersaturation, regardless of the solution composition, that is the calcium to oxalate ion ratio. Furtheron, they demonstrated that the rate of aggregation exhibits a more complex

dependency on solution composition than the growth rate. In their work they presented a new model based on the diffusion of solute ions to a cementing site, which, despite a number of simplifying assumptions, was able to explain the experimentally observed aggregation rate.

Leubner (1998) has developed a new crystal nucleation theory for the continuous precipitation of silver halides [12]. His model was based on a dynamic balance between growth and nucleation. The model is applicable for non-seeded systems with homogeneous nucleation and diffusion controlled growth. It can predict the particle size distribution on basis of average crystal size, residence time, solubility, feed concentrations and temperature. Also the model can predict the maximum growth rate, the ratio of nucleation rate to growth rate, the ratio of average to critical crystal size and the size of nasent nuclei. The experimental results show good agreement with model predictions.

Jones and Zauner (2000) studied the precipitation kinetics of calcium oxalate using the MSMPR method [13]. They operated their reactor at 37^{o}C at various residence times, feed concentrations, stirrer speeds and feed points. A procedure to determine the kinetic parameters for nucleation, growth, agglomeration and disruption from the size distribution of the produced particles was introduced by them. They concluded that crystal growth occurs through a surface-integration controlled mechanism with a second order dependency of the growth rate on the absolute supersaturation. The nucleation rate was found to depend on power input and feed point position, and therefore was controlled by the rate of mixing. Agglomeration rates exhibited a maximum with increasing power input through the stirrer.

Jones et al (2001) developed a model of agglomerative precipitation based on Monte Carlo simulation techniques [14]. The processes of nucleation, crystal growth and agglomeration are first simulated to obtain the particle size distribution (PSD) obtained in a continuous MSMPR unit. An extension is then introduced to account for particle disruption by considering two size reduction mechanisms- one of particle splitting into two parts of equal volume, and the other taking micro attrition into account. A comparison was made with experimental data for both calcium oxalate and calcium carbonate precipitation showing reasonable agreement.

The determination of precipitation kinetics using the MSMPR method can be risky, especially with sparingly soluble material due to the extremely high degrees of supersaturation existing in such systems. In such cases local mixing may become the rate determining step rather than the intrinsic kinetics. A more precise method is therefore needed to determine the precipitation kinetics of sparingly soluble material.

4.3 Present Work

In this work a new method to determine the precipitation kinetics of solids with an extremely low solubility is presented. This method makes use of a laminar jet reactor [15]. In a laminar jet reactor a gas is contacted with a stagnant liquid beam of known dimensions. The rate of absorption of the gas into the liquid can be easily modeled by Higbie's penetration model for gas-liquid absorption [16]. Making use of this mass transfer model, supersaturation can be calculated as a function of penetration depth while assuming kinetic expressions for nucleation and growth rates. By tuning these expressions, the predicted size distribution of the particles can be fitted to the measured size distribution, and thus kinetic data can be obtained. Contrary to the MSMPR reactor in a laminar jet no mixing due to convection takes place. Diffusion is the only transport mechanism and contrary to the transport mechanisms inside a conventional MSMPR reactor its behavior is precisely known.

Before going into more detail about the new method, the theory of crystallization and the MSMPR-method for measuring crystallization kinetics are discussed.

4.4 Theory of Crystallization

To predict crystallizer performance, three conservation laws need to be taken into account, namely mass balances, energy balances and population balances. The mass balances yield the concentrations of the reactants as a function of place whereas the energy balance can be used to derive the temperature at each location. Isothermal conditions were assumed and therefore energy balances are not needed. Population balances are needed to determine the size distribution of the produced crystals. To be able to use a population balance, nucleation, growth, aggregation and agglomeration must be quantified [17]. The crystal population balance is illustrated in Figure 2.

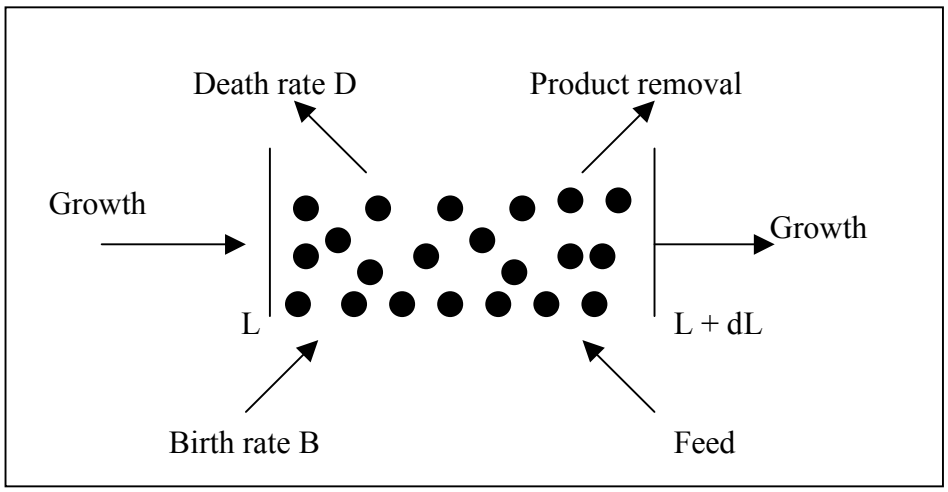

Figure 2: *Change in the number of crystals per unit of volume in the crystal size range of L and L+dL*

The general expression of the population balance for a crystallizer having volume V is given by [17]:

$$\frac{\partial n}{\partial t} + \frac{\partial (G_L n)}{\partial L} + n\frac{\partial V}{V \partial t} + D(L) - B(L) + \sum_k \frac{\dot{V}_k \cdot n_k}{V} = 0 \qquad (1)$$

Where n is the number of particles per unit volume in the crystal size interval [L, L+dL] ($n = \frac{dN_T}{dL}$ (#/m^4)) and G_L represents the linear growth rate of the crystals (m/s). The parameters D(L) and B(L) respectively represent the death and birth rates due to agglomeration, attrition or breakage of the crystals. Finally, the term ($\sum_k \dot{V}_k n_k / V$) gives the sum of particles entering and leaving the crystallizer by convection. The above equation is difficult to solve since B(L) and D(L) can not be formulated in a general way. These two terms depend on crystallizer geometry and operation conditions (hydrodynamics) which are very difficult to characterize. The processes of nucleation and growth interact in a crystallizer, and both affect the obtained particle size distribution (PSD) of the product [18].

The moments of the number density distribution can be used to calculate important parameters such as total number of crystals, surface area and crystal volume; each per suspension volume unit. The total number of particles (N_T) can be calculated by the following formula:

$$N_T = \int_0^\infty n dL \qquad \left[\frac{particles}{m^3_{suspension}}\right] \qquad (2)$$

The surface area (a_T) by:

$$a_T = \beta \int_0^\infty L^2 n \, dL \qquad \left[\frac{m^2_{crystals}}{m^3_{suspension}}\right] \qquad (3)$$

(where β is the surface shape factor; for a sphere β = π)

The volumetric solids hold up (φ_T) can be obtained from:

$$\varphi_T = \alpha \int_0^\infty L^3 \, n \, dL \qquad \left[\frac{m^3_{crystals}}{m^3_{suspension}}\right] \qquad (4)$$

(where α is the volume shape factor; for a sphere α = π/6)

The rates of nucleation, crystal growth, aggregation and agglomeration are functions of supersaturation, which is the driving force for these processes. Mostly relative supersaturation is used in expressions that describe these functions:

$$S = \sqrt{\frac{A.B}{k_{sp}}} \tag{5}$$

The growth rate can often be written in terms of relative supersaturation using a conventional power law [17, 18]:

$$G_L = k_g \left[S - 1\right]^g \tag{6a}$$

It can either be controlled by transport of ions through the solution to the surface of the crystal (caused by convection and diffusion), by surface integration, or by a combination of these two. For sparingly soluble salts the growth rate is normally surface reaction controlled. Three different mechanisms are proposed, i.e. i) ion transport (g =1 in eqn 6a), ii) surface spiral growth (g=2 in eqn 6a) and iii) surface polynucleation (eqn 6b).

$$G_L = k_g S^{7/6} \left[S - 1\right]^{2/3} (\ln S)^{1/6} \exp(-k_{sp} / (\ln S)) \tag{6b}$$

The primary nucleation rate B_o (#/m^3.s), which is the rate at which new nuclei are formed, can be calculated from [17]:

$$B_0 = \frac{dN_0}{dt} = \frac{dN_0}{dL}\frac{dL}{dt} \tag{7}$$

The primary nucleation rate can be derived from the difference between the free enthalpies of the crystal and the solution. A detail derivation leads to the following expression [17]:

$$\frac{B_o}{D_{AB}(N_A c_c)^{5/3}} = 0.965 \left(\frac{c^*}{c_c}\right)^{7/3} S^{7/3} \sqrt{f \ln \frac{c_c}{c^*}} \exp\left[-1.19 f \left(\ln \frac{c_c}{c^*}\right)^3 \left(\frac{1}{\nu \ln S}\right)^2\right] \tag{8a}$$

This formula is based on several assumptions. In some cases, especially at high relative supersaturation a deviation of 200% can exist [19]. In order to establish a more stable numerical routine in case of modeling, a simple power law formula is proposed [3, 8, 17, 20]:

$$B_o = n_o G_L \tag{8b}$$

with

$$n_o = k_n [S-1]^n \tag{8c}$$

During precipitation the formed crystals have the tendency to cluster forming aggregates held together by physical bonds such as van der Waals forces and agglomerates held together by chemical bonds through joint crystal growth of clustered aggregates or particles. Inter-particle collisions may result in permanent attachment if the particles are small enough for the van der Waals forces to compensate gravitational and kinetic forces, a condition generally obeyed by particles smaller than 1 micron. Unlike nucleation and growth, aggregation and agglomeration do not occur in all crystallization process. Whether or not crystals will cluster depends on their physicochemical properties, the concentration of these crystals and on hydrodynamic conditions. Three types of clustering can be distinguished [17]:

1. If the cohesion forces are weak, clustering is referred to as flocculation.
2. If supersaturation is high enough to cause bridging between the particles through crystal growth, the process is called agglomeration.
3. For intermediary processes it is defined as aggregation.

Key parameters that affect agglomeration are:

1. Hydrodynamic conditions (mixing, local turbulence, etc.)
2. Nature of the solvent (viscosity, density, etc.)
3. Size and morphology of the crystals, which may have a strong influence on collision behavior. In case of small particles, agglomeration will become more important.
4. Population density or concentration of the crystals.
5. Supersaturation and related growth rate, which affect the formation of stable agglomerates.
6. Cohesion forces between the solvent, impurities and crystals.

Agglomeration during crystallization has been poorly studied because it is very difficult to measure the number and size of the monocrystals inside a particle (agglomerate).

4.5 MSMPR Method for Measuring Crystallization Kinetics

Kinetic data needed for crystallizer design purposes can in many cases be measured in a laboratory scale Mixed-Suspension, Mixed-Product Removal (MSMPR) crystallizer. Figure 3 shows a possible setup of an MSMPR crystallizer.

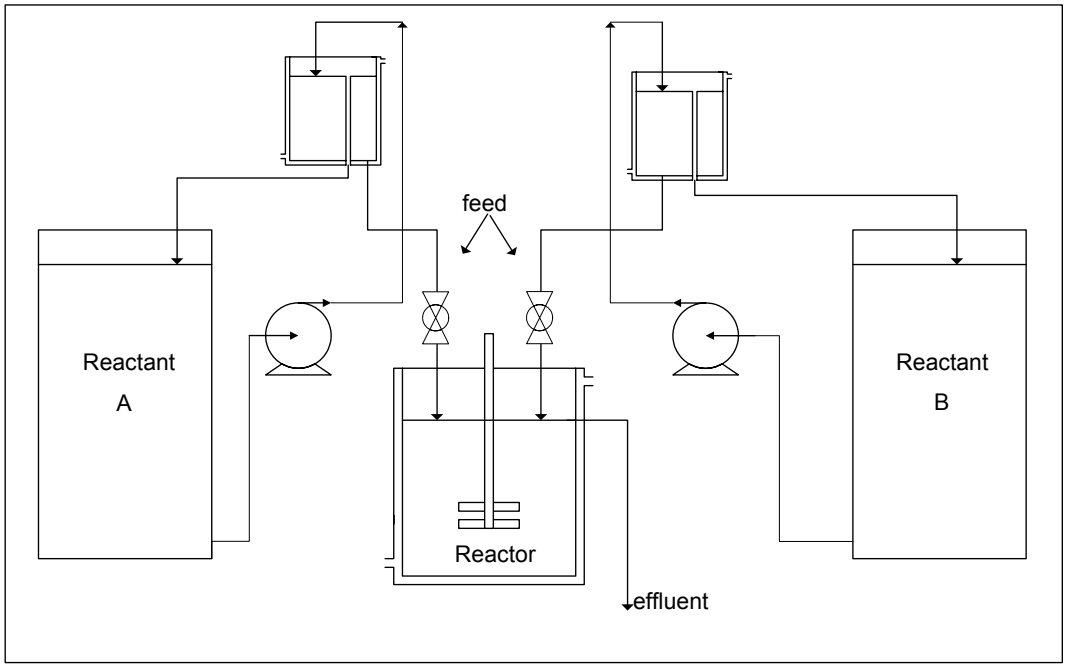

Figure 3: *Possible setup of an MSMPR crystallizer [6].*

The MSMPR method is based on some assumptions. It is assumed that all crystals have the same shape, that no attrition occurs, that the reaction volume is constant, that no crystals are present in the feed, that the crystals do not redissolve and, finally, that steady state operation is established and that the reactor content is ideally mixed. In that case the population balance [equation (1)] can be rewritten as:

$$\frac{\partial(G_L n)}{\partial L} + n\frac{\dot{V}}{V} = 0 \tag{9}$$

If the particles stay relatively small linear growth can be regarded to be independent of particle size [17]. Furthermore, the residence time of such small particles will be equal to that of the liquid. Therefore the above equation can be rewritten as:

$$G_L \frac{\partial n}{\partial L} + \frac{n}{\tau} = 0 \tag{10}$$

This greatly simplified relationship only applies to MSMPR crystallizers and only then when the above mentioned assumptions are valid. Equation (10) can be integrated using the boundary condition of $n=n_o$ at crystal size $L=L_o$:

$$n = n_o \exp\left(-\frac{L}{G_L \tau}\right) \tag{11}$$

Making use of equations (2, 3, 4, 5 and 11), the following moment equations are obtained:

$$N_T = n_o G_L \tau \tag{12}$$

$$a_T = 2\beta n_o \left(G_L \tau\right)^3 \tag{13}$$

$$\varphi_T = 6\alpha\ n_o \left(G_L \tau\right)^4 \tag{14}$$

$$B_0 = n_0 G_L \tag{15}$$

In an MSMPR experiment reactants A and B are continuously added to the reactor, mostly in an equimolar ratio. When steady state operation is reached (typically after 10 residence times) a sample of the effluent is taken for analysis. The sample is analyzed (e.g by using Laser Doppler Diffraction) to determine the average particle size (L_{50}), surface area of the particles (a_T), solids hold up (φ_T) and the particle number density as a function of particle size. On the basis of these measurements nucleation and growth rates can be calculated at a certain supersaturation. By performing experiments at different feed concentrations, a set of nucleation and growth rates is obtained that corresponds with a set of supersaturations. Using equations (6a) and (8c), logarithmic plots can be produced that yield the values of g, k_g, n and k_n.

In the case of a sparingly soluble solid AB, A and B will react so fast that it is not possible to keep the reactor content ideally mixed. The conditions (i.e. supersaturation) at which precipitation takes place will therefore vary and will not be precisely known. In such systems the rate of precipitation will be a function of local hydrodynamics rather than of kinetics. To determine the kinetics of fast precipitation reactions more precisely, a new method is introduced.

4.6.1 A New Method To Determine Precipitation Kinetics: The Laminar Jet Reactor

A laminar jet reactor is commonly used to measure the kinetics of fast gas-liquid reactions [15]. Figure 4 shows schematically this model reactor. The stagnant nature of a laminar jet justifies the use of the penetration theory to describe the process of gas-liquid mass transfer accompanied by chemical reaction.

A laminar jet reactor offers the following features that make it quite appropriate for measuring precipitation kinetics:

1. A well defined contact area between gas and liquid.
2. The locally generated supersaturation is much lower than in a MSMPR-reactor resulting in less solids hold-up and thus less aggregation and agglomeration.

3. The transfer of gas into the liquid can be described and estimated very accurately with Higbie's penetration model for gas-liquid absorption.
4. Well defined hydrodynamics (precise contact time, diffusion only).
5. Accurate measurement of the flux, enabling the precise calculation of the precipitate production.

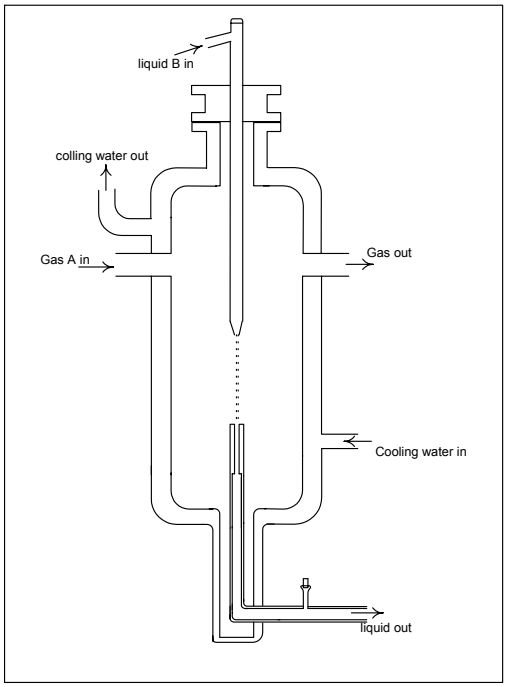

Figure 4: *Laminar jet reactor*

In this work it is therefore proposed to use the laminar jet reactor to determine the kinetics of very fast gas-liquid precipitation reactions. The precipitation of CuS from dissolved H_2S-gas and dissolved copper ions is used as an example to demonstrate this new method. A gas containing H_2S is contacted with a laminar water jet containing Cu^{2+} ions. After being absorbed, H_2S dissolves, dissociates and reacts as S^{2-} with Cu^{2+} to produce solid CuS (see Figure 5).

The chemistry of the mixed ions system ($CuSO_4$ is assumed as liquid feed) can be described by the following reactions:

$$H_2S_{(g)} \rightarrow H_2S_{(l)} \quad \text{(A)}$$

$$H_2S_{(l)} \longleftrightarrow HS^- + H^+ \quad \text{(B)}$$

$$HS^- \longleftrightarrow S^{2-} + H^+ \quad \text{(C)}$$

$$Cu^{2+} + S^{2-} \longrightarrow CuS \quad \text{(D)}$$

$$H^{+} + OH^{-} \longleftrightarrow H_2O \quad \text{(E)}$$

$$HSO_4^{-} \longleftrightarrow SO_4^{2-} + H^{+} \quad \text{(F)}$$

The reversible reactions are assumed to be at equilibrium.

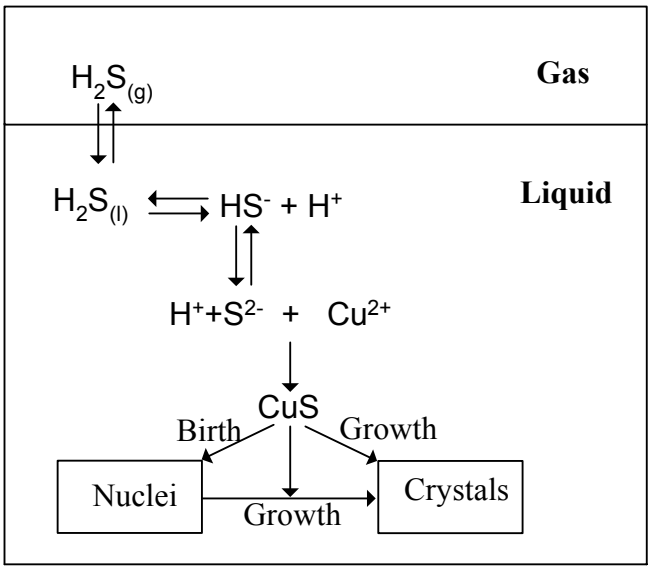

Figure 5: *Schematic diagram for the precipitation of CuS from gaseous H_2S*

The concentration profiles of the different species present in the jet can be calculated by making use of Higbie's penetration model for gas-liquid absorption [16]:

$$\frac{\partial c_i}{\partial t} = \frac{D_i}{r}\frac{\partial}{\partial r}\left(r\frac{\partial c_i}{\partial r}\right) + \frac{z_i D_i}{r}\frac{F}{RT}\frac{\partial}{\partial r}\left(r\nabla\phi\, c_i\right) - R_i \quad (16)$$

where R_i represents the consumption rate of component i. The electrostatic potential gradient ($\nabla\phi$) can be calculated by the use of the Nernst-Einstein [21] equation assuming dynamic electroneutrality:

$$\nabla\phi(r,t) = -\frac{RT}{F}\frac{\sum_{i=1}^{NC} z_i D_i \frac{\partial c_i}{\partial r}}{\sum_{i=1}^{NC} z_i^2 D_i c_i} \quad (17)$$

Assuming no that agglomeration or attrition (death and secondary nucleation) occurs, crystal properties can be calculated from the population balance (in moments notation) as follows [22]:

$$\frac{\partial \mu_k}{\partial t} = \frac{D_p}{r}\frac{\partial}{\partial r}\left(r\frac{\partial \mu_k}{\partial r}\right) + kG\mu_{k-1} + 0^j.B^0 \qquad k = 0,1,2,3,\ldots,m \tag{18}$$

The consumption rates of metal ions and sulfide ions can be calculated (assuming instantaneous precipitation) from:

$$R_{Cu^{2+},S^{2-}} = \alpha\rho B_0 L_o^3 + \beta\rho\mu_2(r)\,G_L \tag{19}$$

4.6.2 Derivation of Kinetic Data from Laminar Jet Experiments

A typical laminar jet reactor experiment to determine the kinetics of CuS precipitation involves the measurement/adjustment of H_2S flux, contact time ($k_{m,L}$), pH, Cu^{2+} concentration and particle size distribution of the produced solids. An experiment is carried out at fixed values of the gas inlet concentration, Cu^{2+} inlet concentration, temperature and pressure. The gas in the laminar jet is assumed to be ideally mixed. Making use of experimental results, equations (5, 6a, 8b, 8c, 16, 17, 18 and 19) and assuming simple stoichiometric kinetics for reactions (A, B, C, D, E and F) the laminar jet can precisely be modeled. The calculated results are then compared with the experimental ones. Using the following error objective function and Newton's method for multi-dimensional optimization the best fit kinetic data was obtained.

$$\begin{aligned} error = {} & (J_{H_2S}\big|_{model} - J_{H_2S}\big|_{experiment})^2 + (Cu^{2+}_{outlet}\big|_{model} - Cu^{2+}_{outlet}\big|_{experiment})^2 \\ & + 100\sum_{k=0}^{3}(\mu_k\big|_{model} - \mu_k\big|_{experiment})^2 + (pH_{outlet}\big|_{model} - pH_{outlet}\big|_{experiment})^2 \end{aligned} \tag{20}$$

The moment terms are some what arbitrarily multiplied by a weight factor of 100 to make these more effective in the objective function. The derivative of the objective function with respect to the optimized parameters (k_g, g, k_n, n) was evaluated numerically. To carry out these calculations, values of the kinetic parameters have to be given. The kinetics of the dissociation reactions (B, C, D, E and F) have to be inserted as well. These were taken from literature [23, 24 and 25]. The simulation starts with guess values for the coefficients in equations (6a) and (8c) and uses the experimentally applied values of $k_{m,L}$ ($= 2\sqrt{D_{H_2S}/\pi\tau}$), pressure, temperature, H_2S inlet concentration, Cu^{2+} inlet concentration and inlet pH to calculate the Cu^{2+} outlet concentration, pH, moments 0,1,2,3 of the measured PSD, and finally the measured H_2S flux. Using the objective function (equation

20) and Newton's optimization method, the model calculates the search direction, the step values and then a new set of values for the kinetic parameters. The simulation keeps iterating until the error is minimized. Several initial guesses are inserted to make sure that the output of the simulation represents a global minimum and not a local one. Figure 6 illustrates the applied routine.

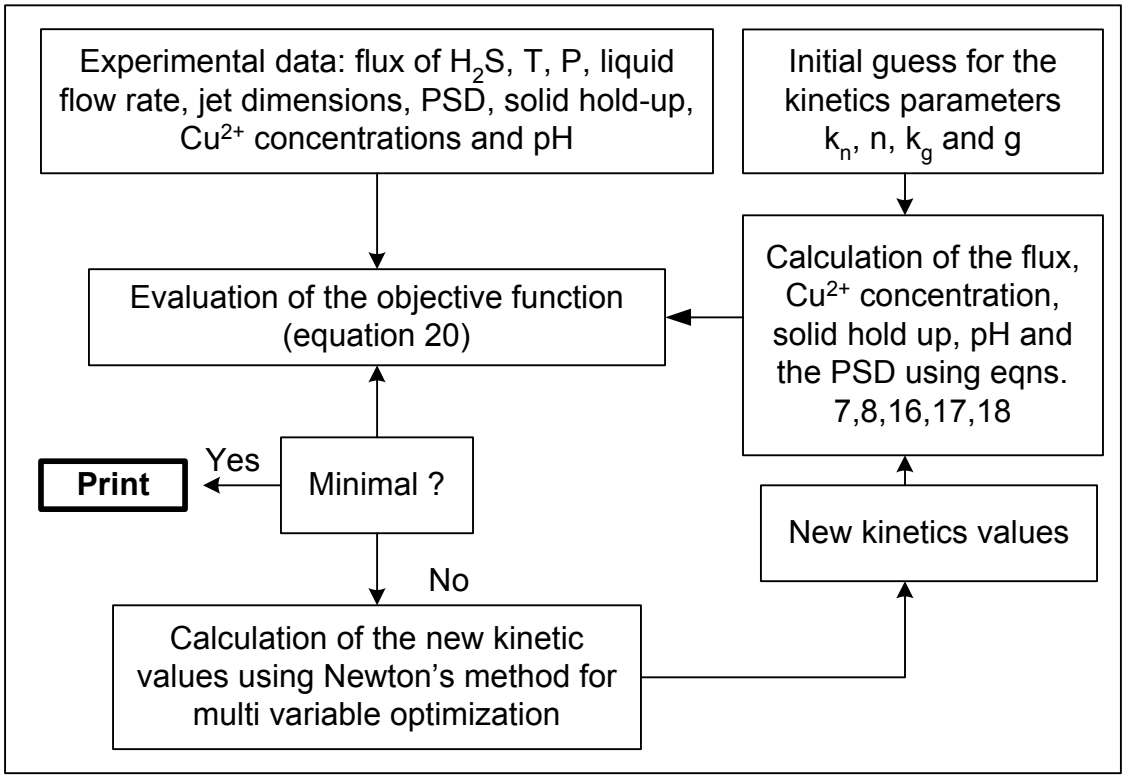

Figure 6: *Algorithm for the calculation of precipitation kinetics from laminar jet experiments.*

4.6.3 Experimental

A laminar jet reactor was used to study the kinetics of CuS precipitation. The contact time between the H_2S containing gas and the Cu^{2+} containing jet was kept short (~0.018 to 0.05 sec). A scheme of the experimental setup used is presented in Figure 7. The laminar jet reactor consists of a double walled glass vessel of 500 ml internal volume. The liquid enters the reactor via a glass tube, which ends in a tapered nozzle with a diameter of 1.1 mm and a length of 8 mm. The liquid leaves the nozzle as a jet which is exposed to the gas and then caught by a receiver (1.3 mm in diameter) from where it leaves the reactor. The receiver is attached to a moving table that can be positioned with a precision of 0.05 mm in a plane perpendicular to the inlet nozzle. The moving table allows to align the jet nozzle to the receiver to avoid spilling of liquid. The length of the jet can be adjusted by moving the inlet tube vertically (between 4 and 8 cm). Jet height and diameter are measured by means of a cathetometer. The composition and mass flowrate of the entering

gas is controlled and measured by means of mass flow meters (Brooks, model 5851). The setup is equipped with two mass flow controllers for the gas inlet mixture, each having a capacity of 150ml/min. These are used to startup each experiment in order to flush the lines and the gas chamber with the desired gas mixture quickly. After 20 min of flushing, a switch is made to two other mass flow controllers with a lower capacity (20ml/min) to ensure more accurate flow measurement. The H_2S gas is supplied from a cylinder containing H_2S of 0.996 purity. The liquid flowrate is controlled by means of a frequency controlled gear pump. A data logging system was used to monitor the temperatures of the gas and liquid streams, pressure, gas mass flow rates, the pH and concentrations of S^{2-} and Cu^{2+} in the liquid effluent. The particle size distribution of the produced solids is measured within 10 minutes after sampling by Dynamic Light Scattering (DLS). In order to prevent agglomeration of particles, a small amount of soap (Triton X100, 0.1 ml of X100/1000 ml of sample) was added to the sample directly after sampling. Some samples were also studied under TEM and SEM at room temperature.

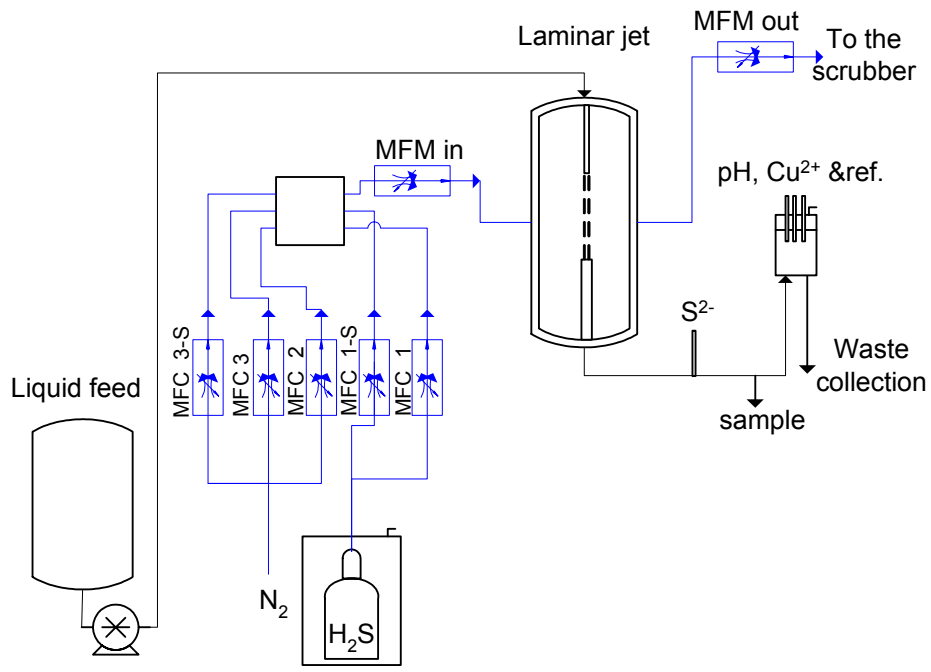

Figure 7: *Laminar jet experimental setup.*

To determine the crystallization kinetics of CuS, several experiments using different Cu^{2+} concentrations, H_2S concentrations and mass transfer coefficient ($k_{m,L}$) values were carried out. The mass transfer coefficient (i.e. contact time) was adjusted by changing liquid flowrate and/or jet height. Before starting the experiments, the laminar jet was calibrated by measuring the diffusion coefficients of CO_2 and H_2S in pure water. These diffusion coefficients of CO_2 and H_2S were determined within an accuracy of 95% corresponded to literature data.

4.7.1 Results and Discussion

Figure 8 shows the average size of the precipitated CuS particles as a function of H_2S-outlet concentration at different $k_{m,L}$-values. Increasing the H_2S concentration not necessarily results in a decrease of the average particle size as to be expected on basis of theory which predicts that smaller average particle sizes are obtained at higher supersaturation due to increase in the nucleation rate [12]. This behavior was noticed at all applied $k_{m,L}$ values. This can be due to the surface activity of CuS. The existence of particles near the gas-liquid interface can either increase or decrease the liquid side mass transfer. An increase can be caused by the so called shuttle mechanism [15] where particles act as H_2S/S^{2-}-carriers where as a decrease can be caused by blocking of the free surface area. An increase in mass transfer will result in higher supersaturation inside the jet and therefore in more nucleation and smaller particles. A decrease in mass transfer will have the opposite effects. The actual effect will probably depend on the solid hold-up. Although the largest particles were found at the lowest $k_{m,L}$ value, decreasing the $k_{m,L}$ value not necessarily yields an increase in particle size as can be seen by comparing the results obtained at $k_{m,L}$ values of 3.72×10^{-4} and 3.3×10^{-4} m/s.

Comparing the experimentally obtained fluxes with those calculated from theory shows that both no chemical enhancement and no significant gas phase resistance existed within the tested range respectively.

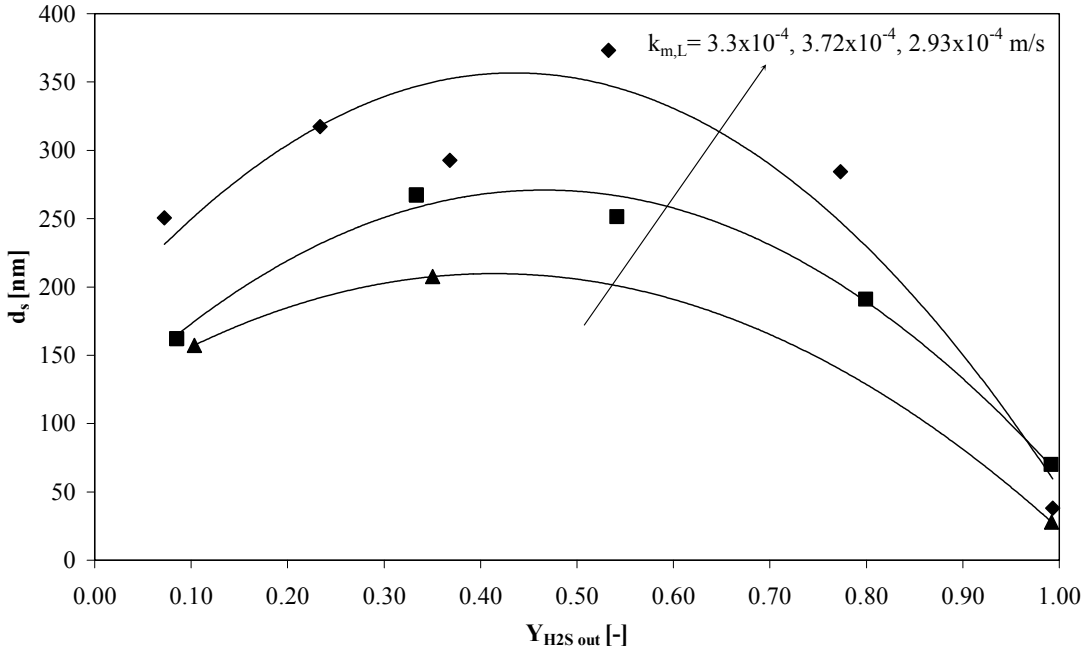

Figure 8: *Effect of the H_2S concentration on the average particle size at different liquid side mass transfer coefficient values; Liquid flowrate= 0.24 ml/s, P = 1.025 bar, T = 21.6 °C, inlet copper concentration = 183ppm.*

The effect of copper concentration on the average particle size at different $k_{m,L}$-values is shown in Figure 9. Increasing the copper concentration from 100 to 250 ppm results in an significant increase in average particle size, while increasing the mass transfer coefficient only has a minor effect. When increasing the copper concentration, the solids hold up near the interface will also increase resulting in more growth and less nucleation. An increase in solids hold-up will also enhance the agglomeration of particles which can be seen in Figures 12 and 13 to be discussed further on.

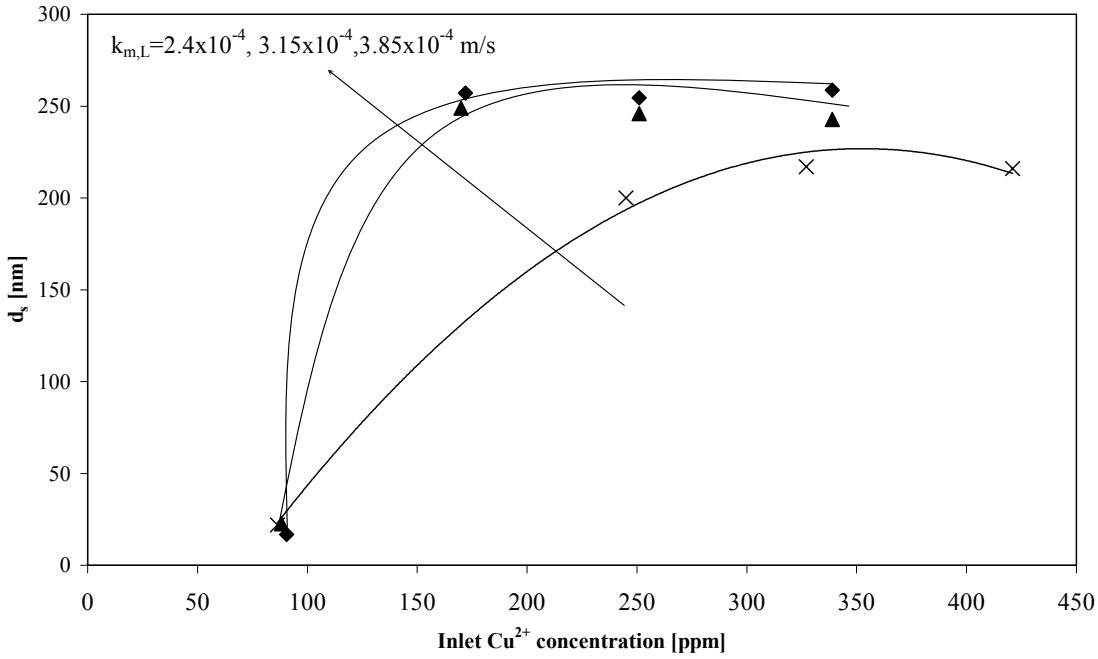

Figure 9: *Effect of inlet copper concentration on average particle size at different $k_{m,L}$-values. Liquid flowrate= 0.24 ml/s, P= 1.025 bar, T = 21.6 ^{o}C, inlet H_2S gas concentration= 99.6 vol%.*

Figures 10 and 11 show the effects of copper concentration and $k_{m,L}$-value on the flux of H_2S into the jet. Increasing the copper concentration results in a slight increase in H_2S flux. This indicates that the reaction of Cu^{2+} with S^{2-} is fast. However not much enhancement is observed due to the very low metal concentrations applied [26]. The infinite enhancement factor [$E_{a,\infty}$ see equation (21)] is not much higher than 1 indicating that enhancement indeed will be small.

$$E_{a,\infty} = 1 + \frac{c^{bulk}_{Cu^{2+}}}{c^{i}_{H_2S}} \left(\frac{D_{Cu^{2+}}}{D_{H_2S}} \right)^{0.5} \qquad (21)$$

Increasing the $k_{m,L}$ value will increase the H_2S gas flux as to be expected. In Figure 11 the absorption of H_2S by a jet of pure water was also plotted as a function of $k_{m,L}$. The line

shows that for low $k_{m,L}$ values the fluxes measured during reactive experiments are somewhat higher than the flux in water alone. At high $k_{m,L}$ values the situation is reversed, supporting the hypothesis that a solid layer near the interface is formed that reduces the rate of the mass transfer into the jet via the addition of extra resistance layer.

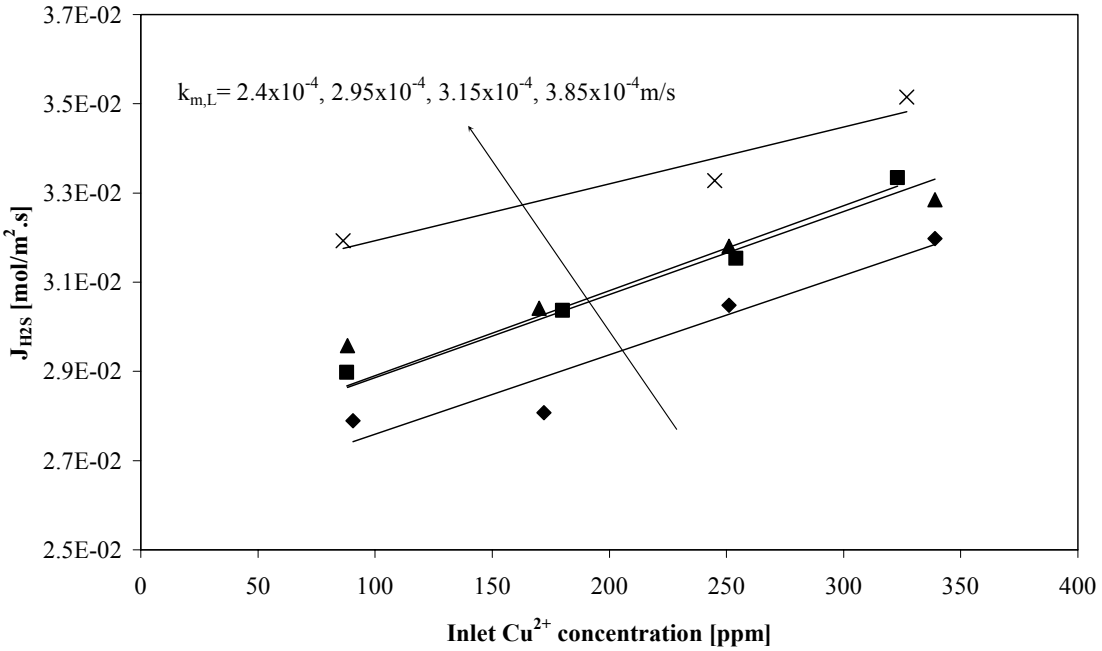

Figure 10: *Effect of copper concentration on H_2S flux at different $k_{m,L}$-values. Liquid flowrate = 0.24 ml/s, P = 1.025 bar, T = 21.6 ^oC, inlet H_2S gas concentration = 99.6 vol%.*

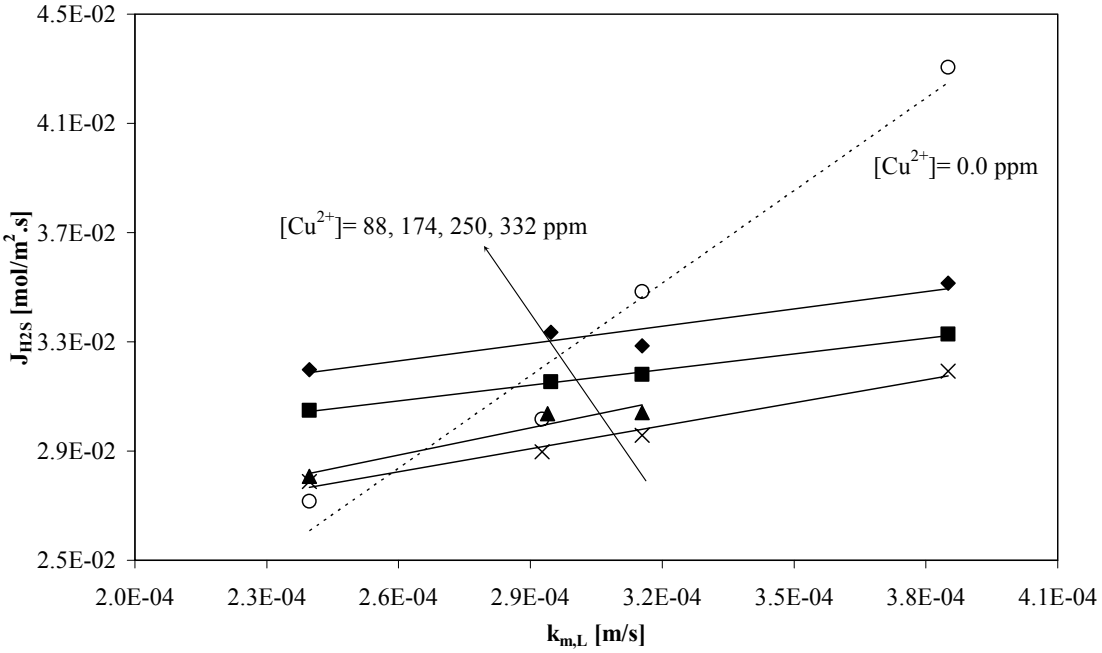

Figure 11: *Effect of $k_{m,L}$ on H_2S flux at different copper concentrations. Liquid flowrate = 0.24 ml/s, P = 1.025 bar, T = 21.6 ^oC, , inlet H_2S gas concentration = 99.6 vol%.*

Figure 12 shows a typical particle size distribution as measured by DLS. Figure 13 shows a SEM picture of the same sample. It is clear from both figures that particles have agglomerated. Agglomeration is most likely to happen after the sample has been taken because the contact time in the laminar jet is much smaller than the lag time between sampling and analysis.

In order to prove that the new technique can be applied the particle size distribution was analyzed of a single sample using SEM and TEM photos. The average crystal size was obtained by dividing aggregates and agglomerates into single crystals. The results of that analysis together with the experimental conditions as well as the outcome of the simulation routine are presented in Table 1.

Table 1: *Crystallization kinetics of CuS for the experiment described in figures 12 and 13.*

Simulation Input	
T	21.1^{o}C
P	1.025 bar
D_s	20 nm
L_{crit}	3.4 nm
H_2S Flux	2.75x10^{-2} mol/m^2.s
$K_{m,L}$	2.4x10^{-3} m/s
Gas concentration	0.996
Inlet Cu^{2+} concentration	80 ppm
Outlet Cu^{2+} concentration	0 ppm
Inlet pH ,measured	5.5
Outlet pH, measured	2.9
Simulation results	
k_g	1.72x10^{-28} m/s
g	2
k_n	1.954x10^{-34} #/m^3.s
n	6.25

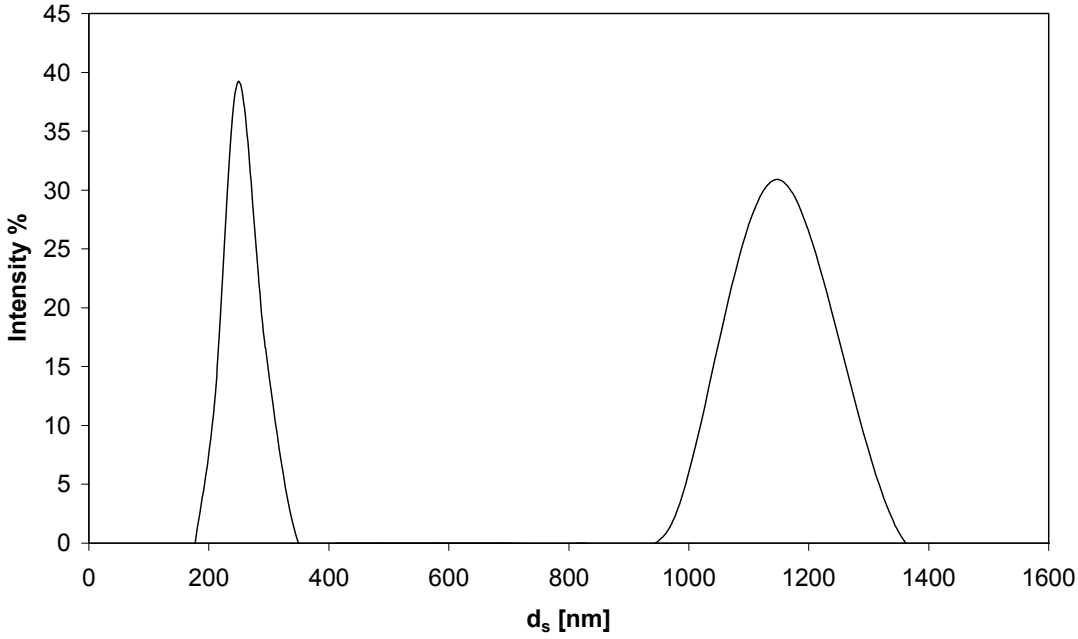

Figure 12: *Intensity % of light in DLS vs. particle size. The agglomeration of produced CuS particles is clearly demonstrated by the second peak. Liquid flowrate = 0.24 ml/s, P = 1.025 bar, T = 21.6 ^oC, outlet pH = 2.6, Cu^{2+} conversion = 100%, inlet H_2S gas concentration 99.6 vol%, inlet copper concentration=340 ppm, $k_{m,L}$= 2.4x10^{-4}, diameter of the jet = 1.1 mm, height of the jet = 54.7 mm.*

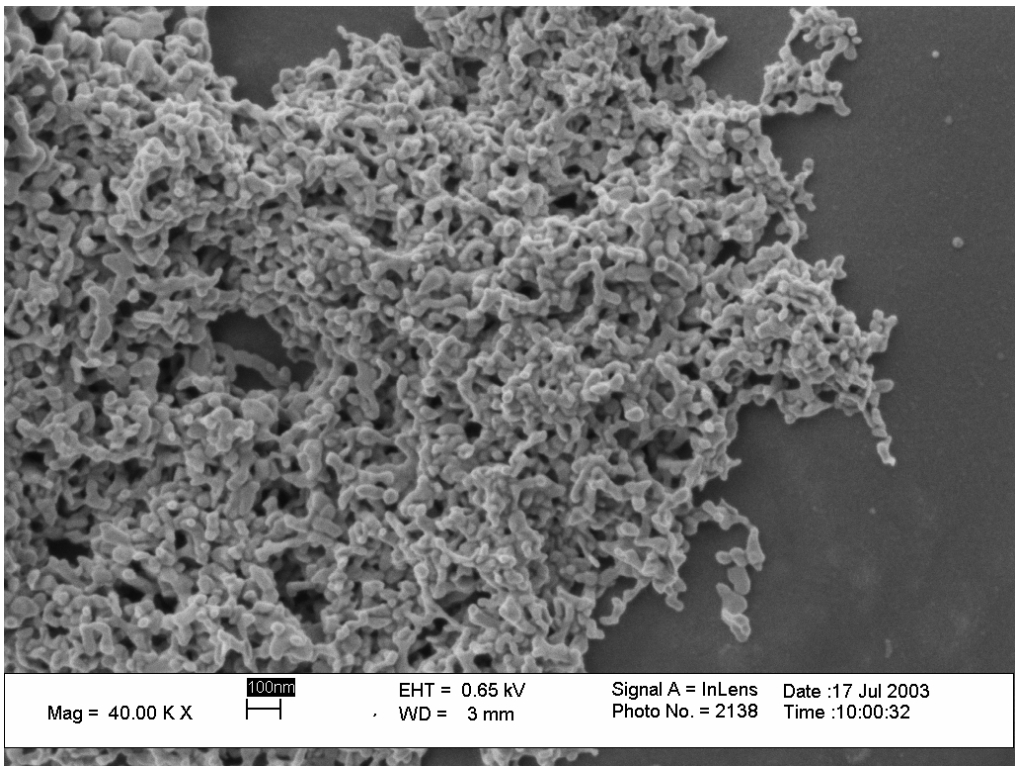

Figure 13: *SEM photo showing agglomeration of primary particles. Liquid flowrate 0.24 ml/s, P = 1.025 bar, T = 21.6 ^oC, outlet pH= 2.6, Cu^{2+} conversion = 100%, inlet H_2S gas concentration 99.6 vol%, inlet copper concentration = 340 ppm, $k_{m,L}$ = 2.4x10^{-4} m/s, diameter of the jet = 1.1 mm, height of the jet =54.7 mm*

4.7.2 Simulation of a Packed Column Precipitator

In order to verify the laminar jet method, the kinetic data obtained through this method were used to simulate a counter current packed bed gas-liquid precipitator in which H_2S is removed from a gas stream using a $CuSO_4$-solution. The specifications of the column and the streams, as applied by Ter Maat et al. [27], are given in Table 2. This scrubber has been in operation for a few months at the premises food company positioned at the gas outlet of an anaerobic digester Relevant mass transfer data were calculated from well established relations reported in literature and are also included in that Table.

The column was simulated by assuming plug flow behavior of both gas and liquid. Higbie's penetration model was applied to describe the transfer of H_2S from gas to liquid. See Al Tarazi et al. [28]. Furthermore, it is assumed that the incoming solution does not contain any CuS crystals. The liquid is assumed to trickle down as thin films (with an indefinite depth). After each 5 centimeters, gas and liquid are assumed to be ideally mixed again.

Besides the kinetic data obtained in this work while applying the laminar jet method, for the sake of comparison also the data earlier obtained by us with the MSMPR method [7] were inserted in the model. Figure 14 shows the calculated H_2S profiles in the gas phase for both sets of kinetic data. The actual experimental profile has not been measured however, only inlet and outlet concentrations were measured. At a height of 0.8 m the outlet concentration of the column was 0.01 vol% H_2S. With the MSMPR-data the model predicts that a height of 5.5 m is required whereas a height of 1.4 m is predicted when the laminar jet data are applied. It is clear that in the column simulations the data derived from the laminar jet coincides considerably better with the experimental column behavior compared to those obtained with the MSMPR method.

The differences between the simulation and the experimental performance of the packed column seems rather high (about 40%), however, it should be noted that the values used for specifically $k_{m,L}$, $k_{m,g}$ and a differ substantially depending on the literature source used.

Table 2: *In- and output of simulation using both Laminar jet and MSMPR kinetic data sets.*

	Unit	***Actual***	***Laminar jet***	***MSMPR***
Specifications				
Diameter	m	0.15	0.15	0.15
Height packing	m	0.8	1.4	5.5
Temperature	°C	12 ºC	12 ºC	12 ºC
Pressure	Pa	10^5	10^5	10^5
Packing type	-	Pall rings	Pall rings	Pall rings
Packing diameter	m	16×10^{-3}	16×10^{-3}	16×10^{-3}
Specific surface area	$m^2\ m^{-3}$	340	340	340
Liquid flow rate	$kg\ s^{-1}$	0.039	0.039	0.039
Gas flow rate	$m^3\ s^{-1}$	8.3×10^{-4}	8.3×10^{-4}	8.3×10^{-4}
Inlet H_2S concentration	Vol%	0.12	0.12	0.12
Outlet H_2S concentration	Vol%	0.01	0.01	0.01
Applied mass transfer data				
$k_{m,L}$ [29]	$m\ s^{-1}$	1.1×10^{-4}	1.1×10^{-4}	1.1×10^{-4}
a_w [29]	$m^2\ m^{-3}$	46	46	46
$k_{m,G}$ [29]	$m\ s^{-1}$	2.0×10^{-3}	2.0×10^{-3}	2.0×10^{-3}
k_La [29]	s^{-1}	5.3×10^{-3}	5.3×10^{-3}	5.3×10^{-3}
k_Ga [29]	s^{-1}	9.0×10^{-2}	9.0×10^{-2}	9.0×10^{-2}
Kinetics parameters				
k_g	m/s or m^3/s*	-	1.72×10^{-28}	3.87×10^{-36} [6]*
g	-	-	2	1 [6]*
k_n	$\#/m^3.s$	-	1.954×10^{-34}	4.36×10^{18} [6]*
n	-	-	6.25	-0.26 [6] *

*Calculated using volume coordinates population balance

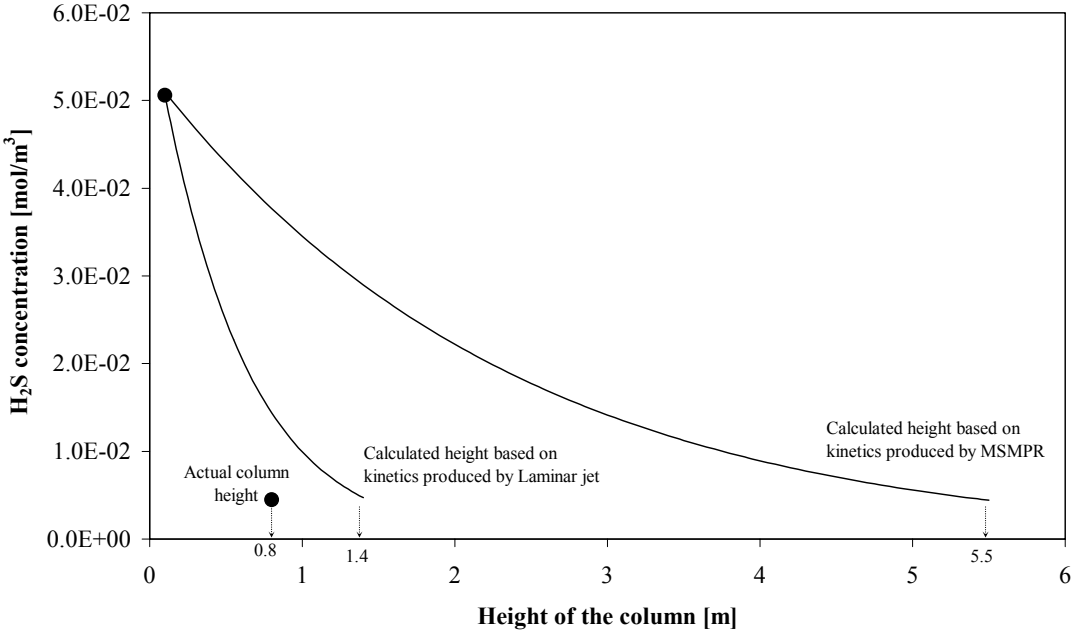

Figure 14: *Calculated H_2S concentration profiles.*

4.8 Conclusions

A new method has been introduced for measuring the kinetics of fast precipitation reactions. This method makes use of a so-called laminar jet reactor which is also applied for measuring the kinetics of gas-solid reactions. When compared to the traditional MSMPR method, the laminar jet method offers the following advantages:

1. It works at low supersaturation; instead of direct addition in ionic form, the precipitating agent is slowly added by diffusion;
2. Due to this slow addition, the solids hold-up can be kept minimal, resulting in less aggregation and agglomeration and more accurate determination of nucleation and crystal growth kinetics;
3. While making use of Higbie's penetration theory, the supersaturation inside the jet can be precisely calculated as a function of place;
4. No mixer is involved and the hydrodynamic conditions are precisely known (stagnant).

The new method was demonstrated for the precipitation of CuS by contacting a jet of a $CuSO_4$-solution with H_2S gas. The obtained data were successfully used to predict the performance of a gas scrubber in which gaseous H_2S is removed by a $CuSO_4$-solution. This was not possible when applying kinetic data earlier obtained with the MSMPR-method.

The Laminar jet method does not necessarily replace the MSMPR method but can add information, especially with regard to primary nucleation and crystal growth. This information added to that from MSMPR measurements offers the possibility to discriminate between the different mechanisms in crystallization.

Acknowledgment

This project was supported with a grant of the Dutch Program EET (Economy, Ecology, Technology), a joint initiative of the Ministries of Economic Affairs, Education, Culture and Sciences, and of Housing, Spatial Planning and Environment. This program is coordinated by the EET Program Office, a partnership of Senter and Novem. The authors wish to thank Benno Kaken and Wim Leppink for their technical support. We also thank Hans Kuipers and Martin van Sint Annaland for their help in solving the numerical difficulties.

List of symbols

a_T	Surface area of crystals [m^2_c/m^3_s]
a_w	Specific interfacial area [m^2/m^3]
B	Secondary birth rate [$\#/m^4.s$]
B_o	Nucleation rate [$\#/m^3.s$]
c^*	Equilibrium concentration [$mole/m^3$]
c_c	Molar crystal density [$mole/m^3$]
D	Death rate due to attraction [$\#/m^4.s$]
D_{AB}	Diffusion coefficient of AB from the solution to the surface of the crystals [m/s]
D_i	Diffusion coefficient of component *i* [m^2/s]
D_p	Diffusion coefficient of particles [m^2/s]
d_s	Sauter diameter [m]
F	Faraday constant [c/mole]
f	Correction factor that account the wetting surface of the foreign particles [-]
G_L	Linear growth rate [m/s]
g	Exponent of growth rate [-]
(g)	Gas
i	At interface
k_g	Growth rate constant [m/s]
k_Ga	Volumetric gas mass transfer coefficient [1/s]
$k_{g,L}$	Liquid side mass transfer coefficient [m/s]
$k_{m,L}$	Gas side mass transfer coefficient [m/s]
k_La	Volumetric liquid mass transfer coefficient [1/s]
k_n	Nucleation rate constant [$\#/m^4$]
k_{sp}	Solubility product constant [mol^2/m^6]
L	Particle diameter [m]
L_0	Effective nuclei diameter [m]
(l)	Liquid (subscript)
J_{H2S}	H_2S flux [$mole/m^2s$]
n	Number of particles per unit volume in the crystal size interval ΔL [$\#/m^4$]
n	Exponent of nucleation [-]
N_A	Avogadro number [#/mole]
n_o	Nucleation particle density [$\#/m^4$]
N_T	Total number of particles [#]
P	Pressure [bar]
p	Particle (subscript)
R_i	Rate of consumption of i [mole/s]
r	Distance in the radial direction from the center of the jet [m]

S	Relative supersaturation [-]
R	Reversible gas constant [J/mole.K]
T	Temperature [K]
t	Time [s]
V	Volume [m^3]
$\dot{V}$	Flow rate [m^3/s]
x	Place in package [m]
Y_{H2S}	Volume fraction of H_2S in gas [-]
z	Valence of ions[-]
Greek	
α	Volume to length shape factor [-]
β	Surface to length shape factor [-]
ρ	Crystal density [$mole/m^3$]
μ_k	Moment of k
ν	Stoichiometric reaction ratio [-]
τ	Residence time [s]
φ_T	Solid hold up [m^3_c/m^3_s]
$\nabla\phi$	Electrostatic potential gradient [C/m]
#	number

References:

1. Mersmann, Alfons, Martin Angerhöfer, Jürgen franke. " Controlled precipitation", Chem. Eng. Technol. Vol.17, pp1-9, 1994
2. Mersmann A. "Batch precipitation of barium carbonate". Che. Eng. Sci. Vol. 48, No.17, pp 3083-3088, 1993
3. Rodgers A. and T. Bertherton. "crystallization of calcium oxalate in minimally diluted urine", Journal of Crystal growth, Vol. 192, pp 448-455, 1998.
4. Palosaari S, Z. L. Sha, H. Hatakka and M. Louhi-kultanen. "Crystallization kinetics of potassium sulfate in an MSMPR stirred crystallizer", Journal of Crystal growth, Vol. 166, pp 1105-1110, 1996.
5. Graber T. A, M. E. Taboada, O. Rocha. "Decahydrated sodium sulphate crystallization kinetics and scale-up study in MSMPR crystallizers", Anales de Quimica, Vol. 92, pp 219-222, 1996.
6. Al-Tarazi Mousa, A. Bert M. Heesink, Mohammed O.J. Azzam, Salah Abu Yahya and Geert F. Versteeg. "Crystallization kinetics of CuS precipitation; an

experimental study using the MSMPR Method". Submitted to Separation Science and Technology, 2004.

7. Al-Tarazi Mousa, A. Bert M. Heesink, Mohammed O.J. Azzam, Salah Abu Yahya and Geert F. Versteeg. "Crystallization kinetics of ZnS precipitation; an experimental study using the MSMPR Method". Submitted to Crystal research and Technology, 2004.
8. Narayan S. Tavare and Anand V. Patwardhan. "Agglomeration in continuous MSMPR crystallizer". AIChE J. No.3, Vol. 38, pp 377-384, 1992.
9. Alan G. Jones, Jiri Hostomsky and Shun Wachi. "Modelling and analysis of particle formation during agglomerative crystal precipitation processes". Chem. Eng. Comm. Vol. 146, pp 105-130, 1996.
10. Zuoliang SHA and Seppo Palosaari," a model of crystallization in an imperfect suspension crystallzer. Acta Polytech". Scand, Chem Technol. Ser 244, pp79-81, 1997.
11. Hounslow M. J, A.S. Bramley, R. Newman, W.R. Paterson and C. Pogessi. "The role of solution composition on aggregation during precipitation", Trans IchemE, Vol. 75, Part A, pp119-124, 1997.
12. Ingo H. Leubner." A new crystal nucleation theory for continuous precipitation of silver halides". J. Imaging Sci & Tec. Vol. 42 no. 4, pp 355-364, 1998.
13. Alan G. Jones and Rudolf Zauner. " Determination of nucleation, growth, agglomeration and disruption kinetics from experimental precipitation data: the calcium oxalate system", Chemical Engineering Science, Vol. 55, pp 4219-4232, 2000.
14. Jones A.G. Falope G. O. and R. Zauner, "On modelling continuous agglomerative crystal precipitation via Monte Carlo simulation". Che. Eng. Sci. Vol. 56, pp 2567-2574, 2001.
15. Westerterp K. R. W.P.M. Swaaij and A.A.C.M. Beenackers. Chemical reactor design and operation. John Wiley & Sons, New York, (1987).
16. R.D. Vas Bhat, W.P.M. van Swaaij, J.A.M. Kuipers and G.F. Versteeg: "Mass transfer with complex chemical reaction in gas-liquid systems-I. Consecutive reversible reactions with equal diffusivities", Chem. Eng. Sci. Vol. 54, no. 1, pp. 121-137,1999.
17. Mersmann A. Crystallization technology handbook. New York, (1995).
18. Mullin J. W. Crystallization, third edition, plant tree, London-UK, (1992).

19. Mersmann A. ”Calculation of interfacial Tensions”, J. of crystal growth, Vol. 102, pp 841-847, 1990.

20. Jones A. G., J. Mydlarz. “Crystallization and agglomeration kinetics during the batch drowing-out precipitation of potash alum with aqueous acetone” Powder Technology, Vol. 65, pp197-194, 1991.

21. Horvath A.L. Handbook of Aqueous electrolytes solution physical properties, estimation and correlation methods, John Wiley & Sons, New York (1985).

22. Randolph, A.D. and Larson, M.A. Theory of Particulate Processes, 2nd edn, Academic Press, New York (1988).

23. Dean, John A. Lange’s Handbook of Chemistry, Fourteenth edition, McGraw-Hill, New York (1992).

24. Horvath A.L. Handbook of Aqueous electrolytes solution physical properties, estimation and correlation methods, John Wiley & Sons, New York (1985).

25. David R. Lide. Handbook of chemistry and physics, 75th edition, CRC, London (1994).

26. Versteeg, G.F, J. A. M. Kuipers, F.P. H. Beckum and W. P. M. Van Swaaij. Mass Transfer with Complex Reversible Chemical Reactions-I. Single Reversible Chemical Reaction. Chem. Eng. Sci. Vol. 44, No. 10, pp 2295-2310, 1989.

27. Ter Maat H. J.A. Hogendoorn and G.F. Versteeg. “The removal of hydrogen sulfide from gas streams using an aqueous metal sulfate absorbent - Part I: The absorption of hydrogen sulfide in metal sulfate solutions” submitted to Journal of Separation Technology

28. Mousa Al-Tarazi, Bert Heesink, Geert Versteeg. “ The precipitation of water dissolved heavy metals using gaseous hydrogen sulfide: mathematical modeling”, Chemical Engineering Science, Vol. 59 no. 3, pp 567-579, 2004.

29. Onda K., Hiroshi Takeuchi and Yoshio Okumoto. “Mass transfer coefficients between gas and liquid phases in packed columns”. J. chem.. Eng. of Jap. Vol 1, no. 1, pp 56-62, 1968.

Chapter 5

Precipitation of CuS and ZnS in Bubble Column Reactor

Abstract

This work presents an experimental study into the precipitation of CuS and ZnS in a semi-batch wise operated bubble column. First the applied bubble column was characterized with respect to mass transfer phenomena. The influences of ionic strength and superficial gas velocity on volumetric mass transfer coefficient and gas hold-up respectively were determined using both CO_2 and H_2S gas. Increasing the ionic strength was found to increase the gas hold up and volumetric mass transfer coefficient. Although the gas hold-up with H_2S was found to be higher than with CO_2 at the same ionic strength and superficial gas velocity, the measured volumetric mass transfer coefficient was for CO_2 absorption. In the second part of the study the influences of the H_2S gas concentration, initial metal concentration and gas pressure on the precipitation of ZnS and CuS were investigated. An increase in the H_2S concentration, initial Zn ions concentration or pressure yields a decrease in the average size of produced ZnS particles. No significant effects could be observed when producing CuS particles. This was probably due to the surface activity of such particles, causing them to cluster and form agglomerates. The results are useful for scale up and design of similar type of precipitator.

5.1 Introduction

Bubble columns are widely used in industry as gas-liquid (-solid) contactors because of their simple construction and operation [1]. Bubble columns are not only applied for biotechnological or environmental purposes but also for conventional chemical reactions as in the methanol synthesis. The bubble column in its simplest form does not contain sensitive mechanical devices such as stirrers and can be build in various dimensions (see Figure1).

A bubble column consists of a vertical cylinder containing liquid and gas dispersed as bubbles in it. The bubbles either are homogeneous in size (at relatively low superficial gas velocities) or are heterogeneous in size (at high superficial velocities), larger bubbles rise faster than smaller ones [2]. The heterogeneous regime is characterized by intense liquid circulation, turbulence and large eddies which are non-stationary with respect to time and space.

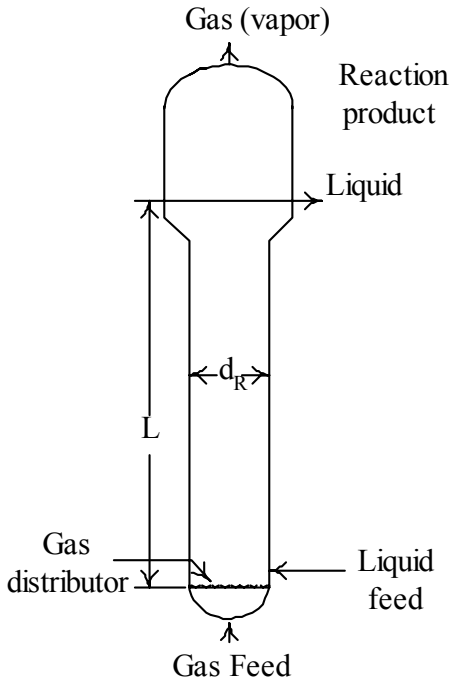

Figure 1: *Simple bubble column*

For the design of a bubble column, knowledge of various design parameters such as mass transfer coefficients, gas hold up, residence time distribution, rate of mixing and pressure drop is crucial. The prevailing procedures to quantify these parameters are largely empirical and in most cases experimental work is needed. A more fundamental approach is possible through the understanding of macro and micro flow patterns [3]. Much progress has been achieved but a general model which is able to simulate all interactions simultaneously is still out of sight.

Besides a gas and a liquid phase, a solid phase is added or formed inside the bubble column in some industrial applications such as the production of (in)organic salts, fine chemicals and biotechnological materials [4]. The design of a bubble column in which solids are formed is rather complex as many phenomena interact: multiphase flow dynamics, mass transfer, chemical reactions, as well as nucleation and growth of crystals. The ultimate challenge is to predict and control the physical properties of produced solids such as their mean particle size. Although precipitation is a common operation in chemical industry, it remains very difficult to predict the size distribution of the produced particles. Particle size is a complex function of nucleation rate, crystal growth and agglomeration of the crystals [5]. Therefore determination of the influence of different process conditions on the behavior of a bubble column as well as product quality is of crucial importance for the design and control of a bubble column precipitator.

In gas-liquid precipitation reactions, a gaseous reactant A is contacted with a liquid solution of reactant B [6]. Gas A is absorbed into the solution, dissociates and reacts instantaneously with B ions to produce AB clusters. When the concentration of the produced clusters exceeds the solubility concentration supersaturation occurs. Due to the generated supersaturation, nuclei are formed which start to grow to form crystals. When the concentration of the crystals increases, the chances for forming agglomerates or aggregates become higher. If two or more crystals meet they may aggregate and grow further as one crystal. All steps are illustrated on Figure 2.

Heavy metal ions such as copper and zinc that are present in the wastewater of a zinc factory can be precipitated as copper sulfide and zinc sulfide when contacted with hydrogen sulfide (H_2S) [7,8]. In this work the precipitation of copper and zinc sulfide in a bubble column reactor is studied.

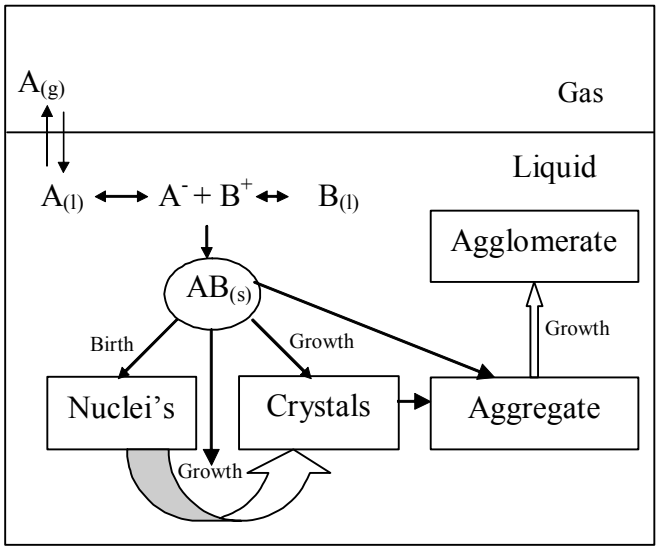

Figure 2: *Schematic diagram of a gas-liquid precipitation reaction*

5.2 Previous Work

Marraucci (1969) developed a theory that describes the effect of the electrolyte concentration on bubble coalescence [9]. According to Marraucci, salts inhibit bubble coalescence by retarding the thinning of the intervening liquid film between bubble pairs. Moreover, it was concluded that increasing the salt concentration increases the film surface tension, which develops an opposite force to the direction of the flow at the gas-liquid boundary. As a result of that, the thinning time during bubble coalescence increases. At sufficiently high salt concentrations, this force even immobilizes the gas-liquid interface.

Alvarez-Cuena and Nerenberg (1981) used the Plug Flow Module (PFM) to study mass transfer inside a bubble column and to predict concentration profiles [10]. They aimed to show the significance of the volumetric mass transfer coefficient when using the plug flow model for design purposes. An analysis of the PFM was made by comparing experimental and calculated concentration profiles over the entire column. Relative deviation, as high as 68% were observed in the grid region. They concluded that the PFM can not describe mass transfer in bubble columns.

Shum Wach and Jones (1990) studied the characteristics of gas-liquid heterogeneous precipitation systems by measuring particle size distributions under various operating conditions and mass transfer resistances [11]. They used a mixed-suspension, mixed-product removal reactor (MSMPR) in their experiments. They found that the mass transfer resistance affects the average particle size. Larger particles were formed under conditions of high mass transfer into a large liquid volume (high Hinterland ratio), while small particles were produced at low mass transfer coefficients.

Tustsumi et al. (1991) studied the role of bubble wakes in the formation of calcium carbonate particles in a semi-batch bubble column reactor [12]. They found that secondary nucleation occurred in the wake region and explained this by the attrition of crystals caused by vortical motion. They also found that during the early stages of reaction a significant change in the size distribution of agglomerates occurs in the wake.

Jones et al. (1992) studied the effect of liquid mixing on the average particle size of calcium carbonate particles in a small flat-interface gas-liquid reaction cell [13]. It was found that crystal size increases with increasing agitation rate due to its effect on gas-liquid mass transfer.

Deckwer and Schumpe (1993) presented a review of the correlations available for the estimation of gas holdup, mass transfer and mixing coefficients [14]. According to them the uncertainties and errors in the bubble column design arise partly from over simplification in the applied models.

Hostomsky and Jones (1995) used the penetration model to describe mass transfer and crystal precipitation near the gas-liquid interface and to predict the effect of liquid agitation on the mean particle size of precipitates while using thermodynamic and kinetic data from literature [15]. It was found that at decreasing mass transfer rate, the nucleation rate increases in the region close to the interface. Nucleation rate, particle number density and the mean particle size were found to be maximal at a certain distance from the gas-liquid interface.

Eigenberger and Bauer (1999) have developed a concept for iterative multi-scale modelling and simulation of gas/liquid bubble column reactors with and without liquid recycle [3]. Their concept includes mass transfer accompanied by chemical reaction as well as detailed (unsteady state) hydrodynamics. They used a one-dimensional model to describe mass transfer and reaction rate and coupled that with a hydrodynamic model to predict bubble size and bubble size distribution.

Teixeira et al. (2000) studied the effect of orifice diameter in the distributor plate, airflow rate, solid loading and solid density on hydrodynamics (gas holdup, circulation time and liquid velocity) of a three-phase external-loop airlift reactor [7]. They observed that the gas distributor has a small effect on gas holdup, circulation time and downcomer liquid velocity. However, airflow rate, solid loading and solid density appeared to have significant effects.

Jones and Rigopoulos (2001) presented a dynamic model of a bubble column reactor with particle formation, using a hybrid CFD-reaction engineering approach [4]. They employed CFD for estimating the hydrodynamics based on the two-phase Eulerian-Eulerian method. They made use of the penetration theory as well as the population balance to predict average particle size. They applied the model on the precipitation of $CaCO_3$ via CO_2 absorption into a $Ca(OH)_2$ solution in a draft tube bubble column and obtained insight into phenomena underlying crystal size evolution.

Joshi (2001) presented a paper that reviews the modelling efforts on bubble column flow patterns of the last 30 years [2]. According to his review developments mainly were on three fronts, (i) formation of interface forces (ii) closure problem for the eddy viscosity and (iii) modelling of the Reynolds averaging procedure.

Kluytmans et al. (2001) studied the effects of electrolyte and particle concentrations on the gas holdup in a slurry bubble column for both the homogenous and the heterogeneous flow regime [16]. They determined bubble behaviour in a 2D slurry column by video recording. They also measured gas holdup. They found out that adding electrolyte or solid carbon particles leads to a considerable increase in gas holdup until a critical concentration is reached. Afterwards no further effects were found. According to their

results the conditions for transition from the homogenous to the heterogeneous regime were not influenced by the concentration of the electrolyte or the solid particles.

Bouaifl Mounir et al. (2001) studied gas holdup, mass transfer, interfacial area, bubble size and bubble distribution in bubble columns as well as vessels equipped with various dual impellers [17]. They studied the effects of gas flow rate, sparger type and column diameter in bubble column. They compared their results with similar results reported in literature.

5.3 Present Work

The present work focuses on the precipitation of water dissolved heavy metals (copper or zinc) by contacting them with hydrogen sulfide gas in a bubble column contactor. Volumetric mass transfer and gas hold-up were studied using both CO_2 and H_2S gas. The effects of ionic strength and superficial velocity on mass transfer and gas hold-up were investigated as well as the effects of copper/zinc concentration, superficial gas velocity and H_2S concentrations on the size distribution of the produced metal sulfide particles.

5.4 Experimental

The applied experimental setup is illustrated in Figure 3. The bubble column reactor was a double walled glass vessel having a length of 60 cm and an internal diameter of 7.5 cm. A cooler was placed at the top of the column to condense any evaporated water. The temperature of the gas feed (N_2/H_2S or N_2/CO_2) and the column was controlled by means of a thermostat bath. All experiments were carried out at 20^oC. The flowrate and composition of the gas were controlled with the help of electronic mass flow controllers (MFC). The flowrate of the effluent gas was measured by using an electronic mass flow meter (MFM). The column was operated under semi-batch conditions, implying a continuous gas flow through a single batch of liquid (demi-water or a solution of $CuSO_4$ or $ZnSO_4$ in demi water). The effluent was sent to a scrubber to remove any non-absorbed H_2S. Temperature, pressure, pH, metal concentration (in the case of copper), sulfide concentration and inlet/outlet gas flowrates were registered every second by a PC. Samples were taken during and after each precipitation experiment for the determination of particle size distribution and metal concentration. Just after sampling, the samples were stripped with N_2 to remove any dissolved H_2S. Particle size was measured by X-ray diffraction (0.1μm - 704μm, Microtrac X-100) or Dynamics Light Scattering DLS (1nm - 5000nm, Zeita-sizer 5000) depending on the size of the produced particles. After a sample was taken from the reactor, a small amount of Triton X-100 was added to prevent particle agglomeration and to fixate the size distribution of the produced particles (0.1 ml of X-100/1000 ml of sample).

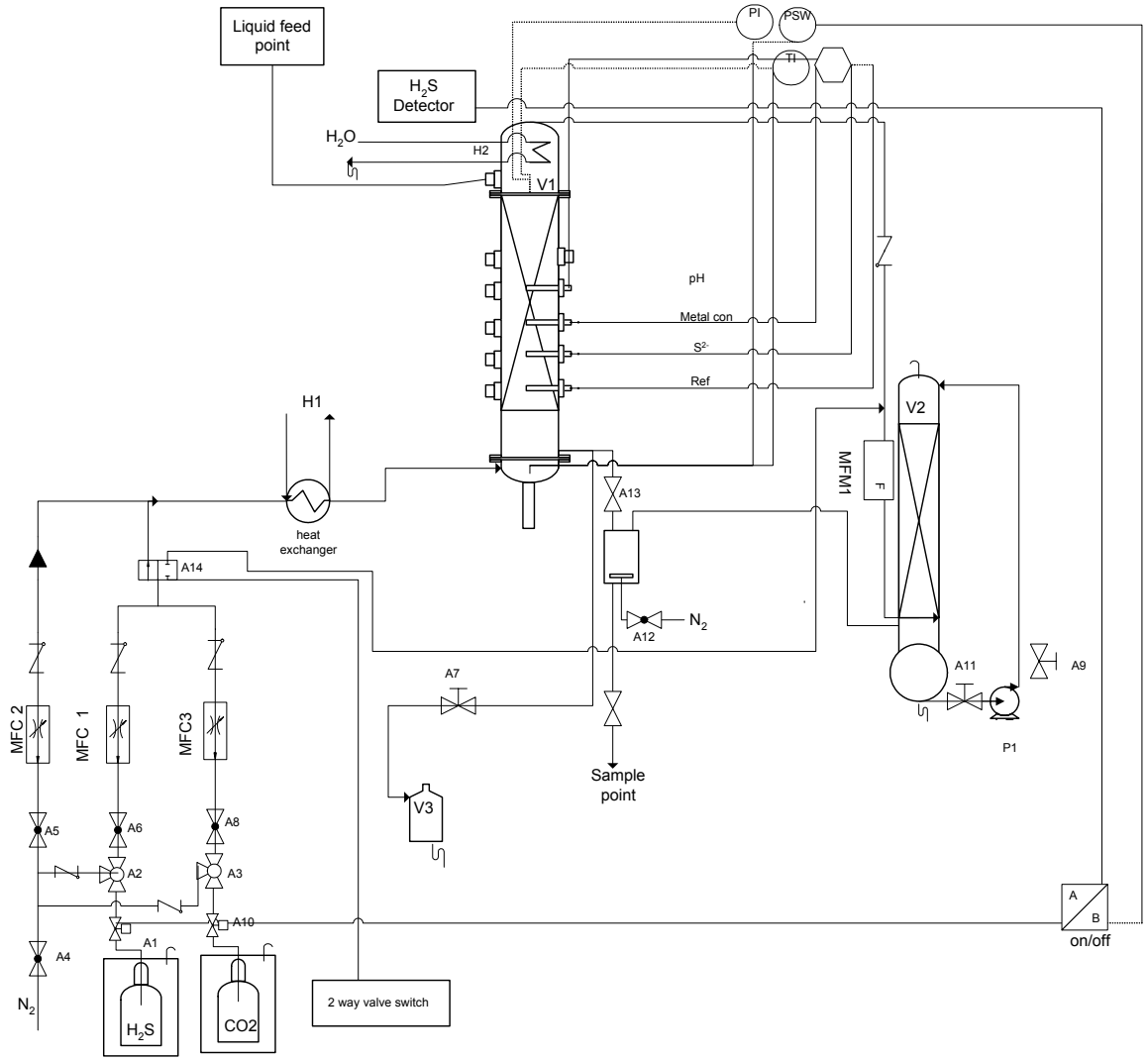

Figure 3: *Experimental setup for the precipitation of heavy metals from wastewater.*

This work is divided into two parts, namely (i) a study of bubble column hydrodynamics and (ii) precipitation of zinc and copper sulfide in that same bubble column. All experiments were carried out in the homogeneous bubble regime. The fist part involves the determination of the gas hold-up and the volumetric mass transfer coefficient (k_La) while using pure CO_2 and H_2S gas. The effects of superficial gas velocity as well as ionic strength of the solution were investigated. The volumetric mass transfer coefficient (k_La) was determined by monitoring the concentration of CO_2 or H_2S in the solution as a function of time after starting gas supply (see equations 1 a- c). Concentrations of CO_2 or H_2S were determined from the mass balance over the gas phase. Gas hold-up was calculated from experimentally observed values of the liquid height and the height of the gas-liquid dispersion (see equation 2).

$$\frac{dc_A^b}{dt} = k_L a(c_A^i - c_A^b)\text{, where A is } CO_2 \text{ or } H_2S \qquad (1a)$$

$$c_A^b = \frac{\dot{m}_{in} - \dot{m}_{out}}{V_L} \tag{1b}$$

$$\ln\left(\frac{c_A^i - c_A^o}{c_A^i - c_A^b}\right) = k_L a\, t \tag{1c}$$

$$\varepsilon_G = \frac{V_d - V_L}{V_d} \tag{2}$$

The experimentally obtained values of k_La and ε_G were fitted as a function of superficial velocity using simple power law relationships:

$$k_L a = b u_t^{0.8} \tag{3a}$$

$$\varepsilon_G = c u_t^{0.9} \tag{3b}$$

In the second part of the study (precipitation), the bubble column was operated in semi-batch mode whereas a mixture of H_2S and N_2 was used to precipitate the Cu^{+2} or Zn^{+2} ions present in the solution. The ionic strength of the solution was kept constant by adding excess KCl salt. In these experiments, the flowrates of influent and effluent as well as temperature, pressure and pH were monitored versus time. At the end of each experiment a sample was taken and analyzed by X-ray (0.45-3000μm) or DLS (1-5000 nm) to measure the particle size distribution of the formed solids. The metal concentration was measured at the beginning and at the end of each experiment using an atomic absorption spectrometer (AAS). The effects of initial metal concentration, inlet H_2S concentration and pressure on the average H_2S flux, metal conversion and average particle size were investigated. The average H_2S flux was calculated using the mass balance on the gas side (see equation 4). The specific area of the bubble column was estimated using equation (5) [20].

$$J_{H_2S} = \frac{\dot{m}_{in} - \dot{m}_{out}}{a V_L}(1 - \varepsilon_G) \tag{4}$$

$$a = 3.32\left(u_t \rho_L g\left(1 - \varepsilon_G\right)\right)^{0.69} \tag{5}$$

5.5 Results and Discussion

The effects of superficial velocity and ionic strength on gas hold-up (ε_G) and the volumetric mass transfer coefficient (k_La) when using CO_2 is shown in Figures 4 and 5. In the Figures, the points represent the experimental values while the lines represent the fits

according to eqns (3a-b) while the exponent (n) was fixed at 0.9 for ε_G and at 0.8 for k_La. Only the pre-exponential values of b and c were calculated to get the best fit. The best fit values of b were found to vary from 0.05 to 0.08 whereas those of c varied from 0.029 to 0.037. As to be expected, increasing the superficial gas velocity increases both ε_G and k_La as it increases the bubble population density [1, 18]. It is known from literature that increasing the superficial velocity further, will result in bubble coalescence and finally to a constant gas holdup [17]. On the other hand, upon increasing the superficial velocity the mass transfer coefficient k_L will continuously increase due to the formation of bigger bubbles that have a higher rise velocity [1, 2, 6, 20]. However, an increase in average bubble size will correspond with a decrease in interfacial area [20]. However, the overall effect of raising the gas velocity on volumetric mass transfer coefficient was always positive.

Increasing the ionic strength increases the values of ε_G and k_La. This can be due to an increase in surface tension [19], which stabilizes the bubbles and decreases bubble coalescence [9].

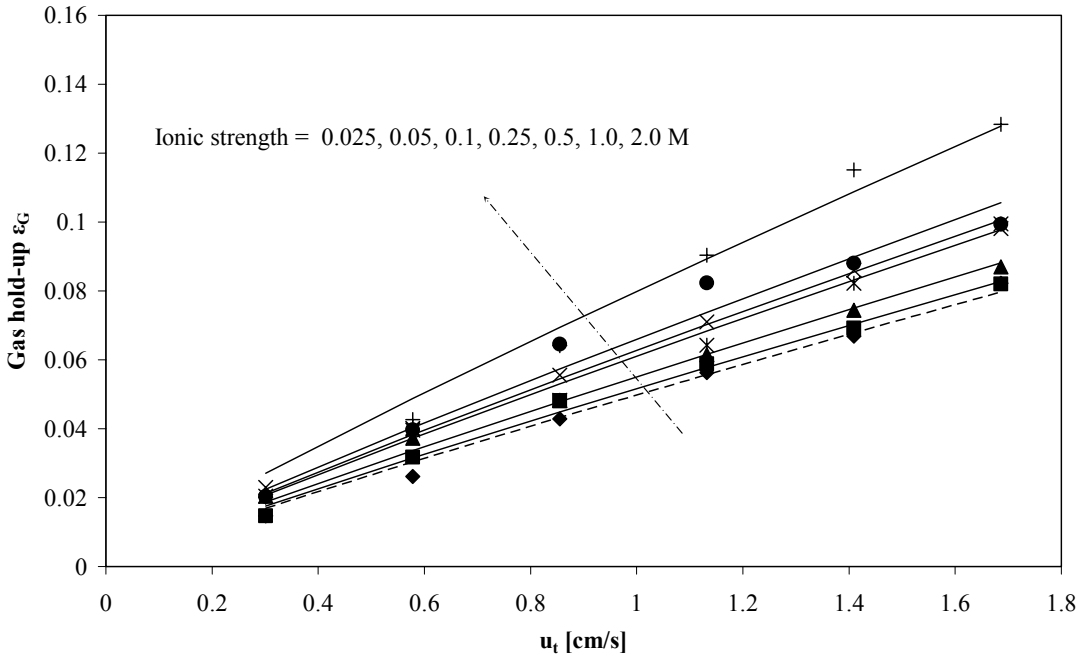

Figure 4: *Effects of superficial gas velocity and ionic strength on gas hold-up (ε_G). T = 20^{o}C, V_L= 2 L, P = 1.01 bar, gas = CO_2*

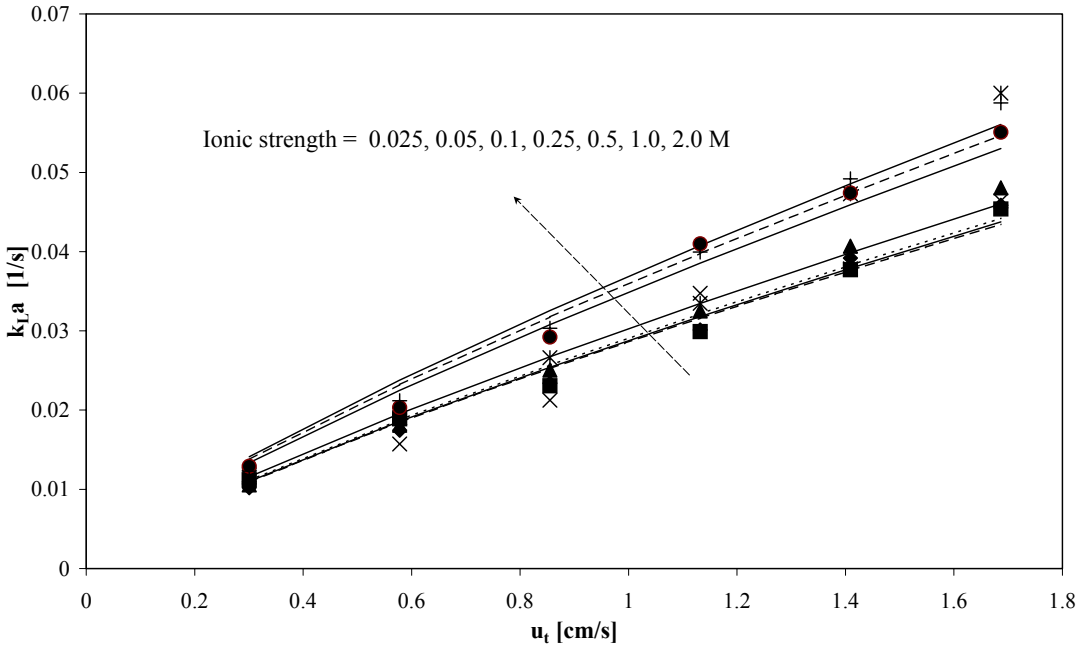

Figure 5: *Effects of superficial gas velocity and ionic strength on the volumetric mass transfer coefficient (k_La). T = 20°C, V_L= 2L, P = 1.01 bar, gas = CO_2*

Figures 6, 7 and 8 show the effects of superficial velocity and ionic strength on gas holdup and volumetric mass transfer coefficient when using H_2S. In general the same trends were found as with the CO_2 experiments. However, gas holdup values were higher for H_2S than for CO_2 (see Figures 9 and 11). This can be due to a difference between the surface tensions of the water-CO_2 and water-H_2S. On the other hand the measured k_La values for H_2S were lower than for CO_2 (see Figures 10 and 12). This is mainly due to the formation of smaller bubbles when H_2S is used (observed experimentally) that rise slower. In general the values of k_La and ε_G increased with ionic strength and superficial gas velocity in a power law manner. The most significant influence was observed at low ionic strengths and low superficial velocities.

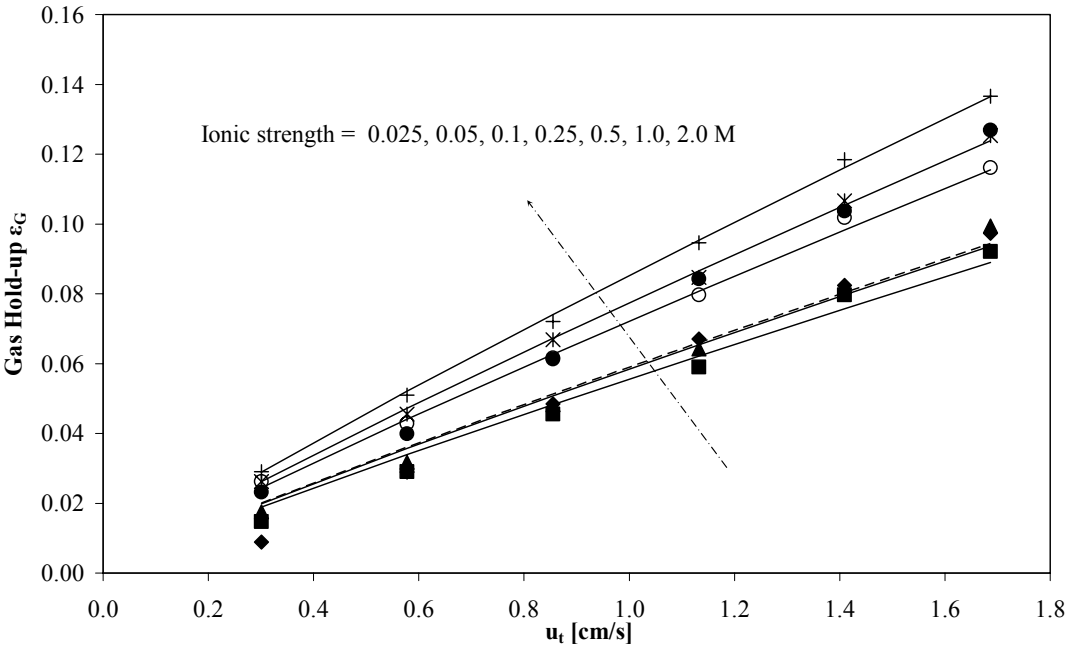

Figure 6: *Effects of superficial gas velocity and ionic strength on gas hold-up (ε_G). T = 20°C, V_L = 2 L, P = 1.01 bar, gas = H_2S*

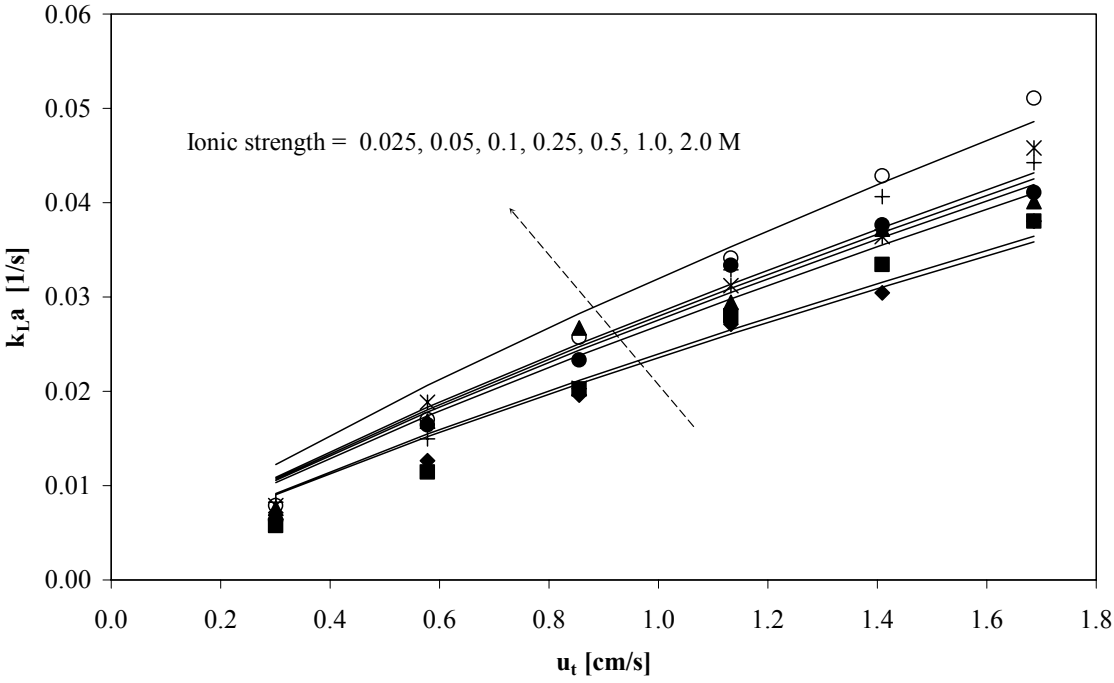

Figure 7: *Effects of superficial gas velocity and ionic strength on the volumetric mass transfer coefficient (k_La). T = 20°C, V_L= 2 L, P = 1.01 bar, gas = H_2S*

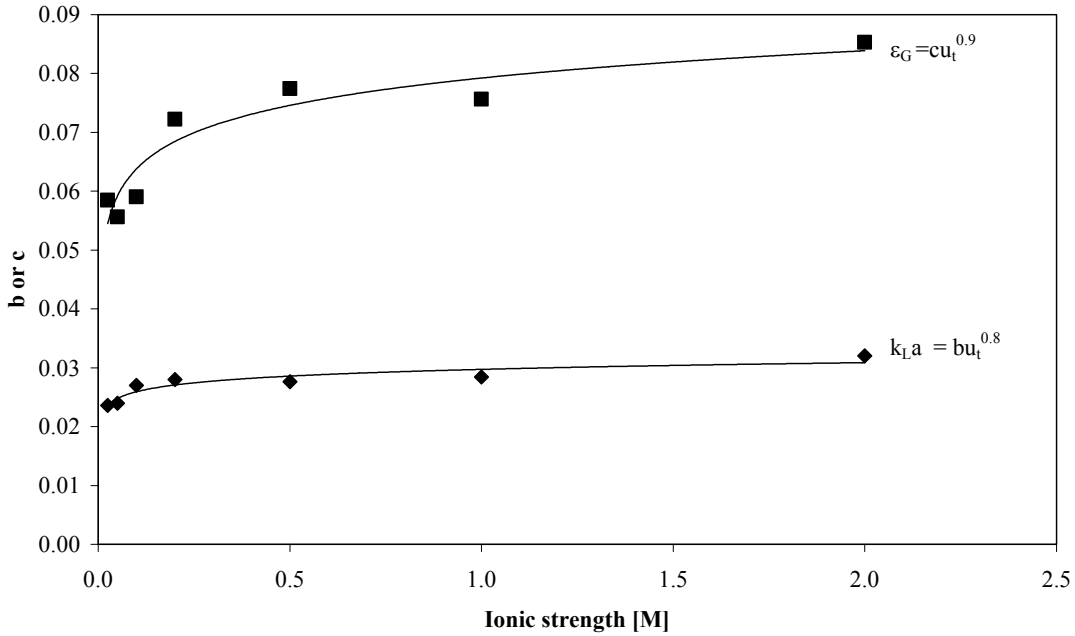

Figure 8: *Effects of ionic strength on the fitting parameter b or c for both volumetric mass transfer coefficient (k_La) and gas hold-up (ε_G). T = 20 ^oC, V_L = 2 L, P = 1.01 bar, gas = H_2S*

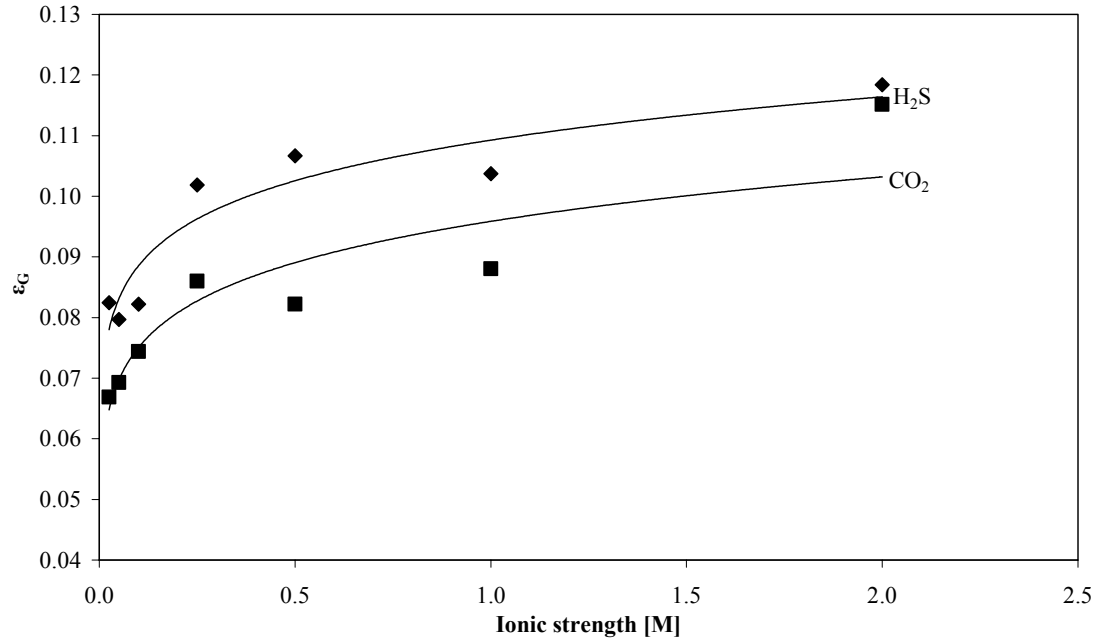

Figure 9: *Effects of ionic strength on gas hold-up (ε_G) for both CO_2 and H_2S gas. T = 20 ^oC, V_L = 2 L, P = 1.01 bar, u_t = 1.41 cm/s*

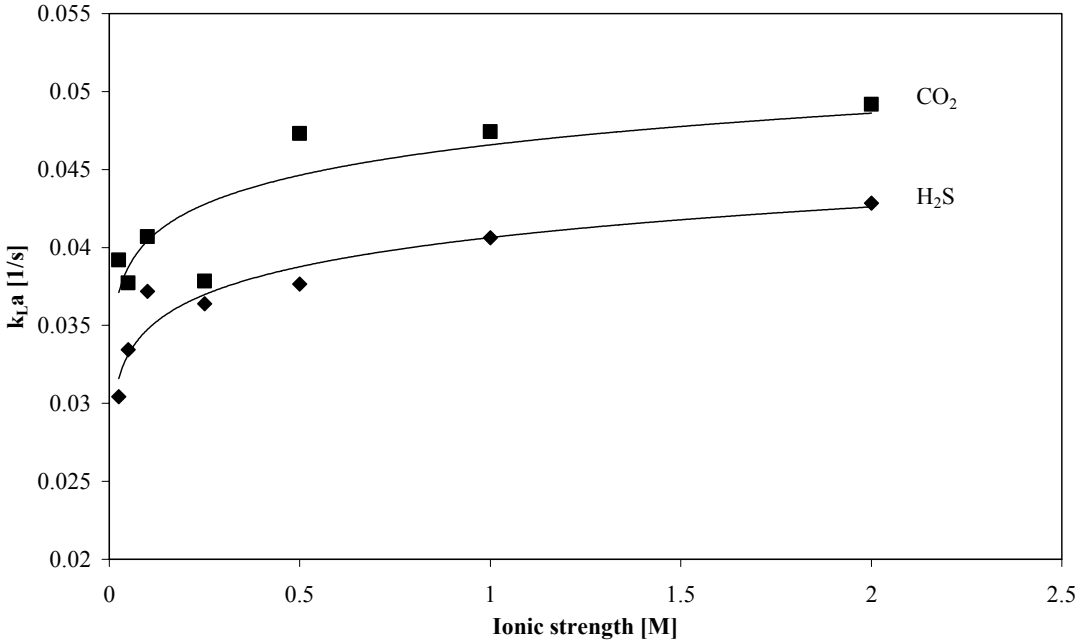

Figure 10: *Effects of ionic strength on the volumetric mass transfer coefficient (k_La) for both CO_2 and H_2S gas. T = 20 ^oC, V_L = 2 L, P = 1.01 bar, u_t = 1.41cm/s*

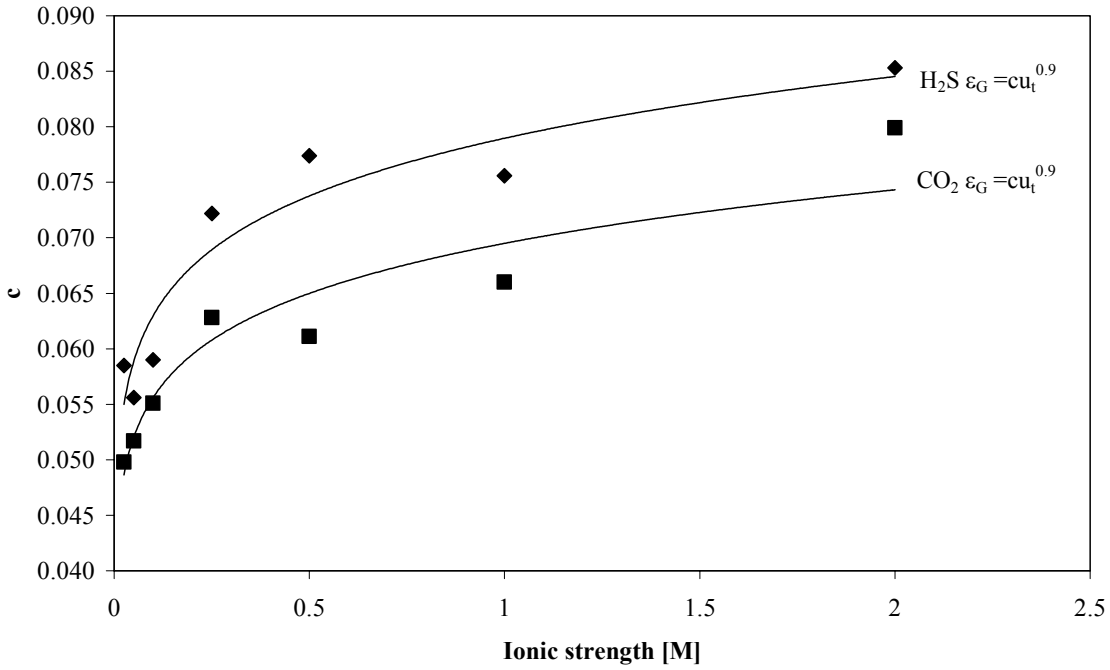

Figure 11: *Effects of ionic strength on the fitting parameter c of gas hold-up (ε_G) for both CO_2 and H_2S gas. T = 20 ^oC, V_L = 2 L, P = 1.01 bar, u_t = 1.41cm/s*

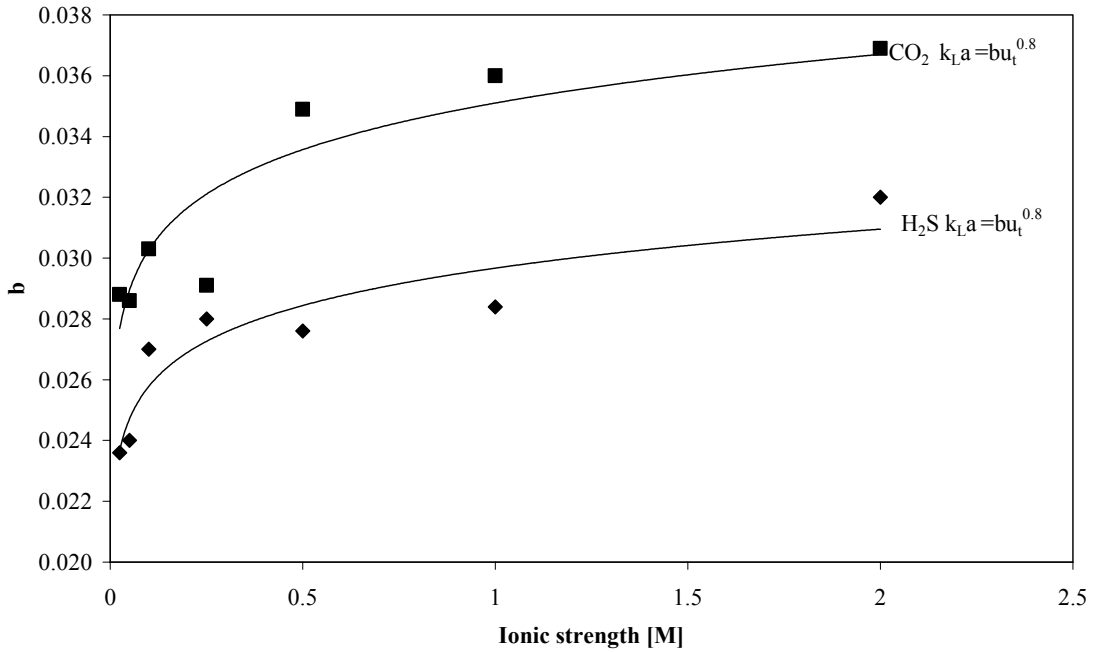

Figure 12: *Effect of ionic strength on the fitting parameter b for the volumetric mass transfer coefficient (k_La) for both CO_2 and H_2S gas. $T = 20\ ^oC$, $V_L = 2$ L, $P = 1.01$ bar, $u_t = 1.41$cm/s*

Figure 13 shows the effects of H_2S inlet concentration and initial zinc ions concentration on the average H_2S flux. The first parts of the curve represent the displacement of nitrogen that already exists in the gas cap of the bubble column as well as the reaction with metal ions (if present). After most metal ions have been consumed and the nitrogen is displaced, the H_2S concentration in the liquid starts to increase. Due to this increase in H_2S concentration the overall driving force starts to decrease and consequently the H_2S flux starts to decrease as well. When comparing the natural absorption curve (without metal ions) with reaction curves three important differences can be noticed namely (i) it takes more time for a reactive system to build-up H_2S in the liquid, (ii) small chemical enhancement of mass transfer due to the fast precipitation reaction, and (iii) still some enhancement occurs even after the reaction has been completed. Chemical enhancement increases with the concentration of zinc ions as to be expected [21]. Chemical enhancement is due to the fact that the reaction between S^{2-} and Zn^{2+} is instantaneous. The infinite enhancement factor can be calculated from:

$$E_{A,\infty} \cong 1 + \frac{D_{Zn^{2+}} \bar{c}_{Zn^{2+}}}{\nu_{Zn^{2+}} D_{H_2S} c^i_{H_2S}} \left(\frac{D_{H_2S}}{D_{Zn^{2+}}} \right)^{0.5} \tag{6}$$

The obtained values are only slightly higher than unity which is in agreement with the small enhancement that is initially observed.

Figure 14 shows the effect of the H_2S inlet concentration on the average particle size of the produced ZnS at different initial zinc ions averages particle as (local) supersaturation will increase and hence the rate of nucleation. Increasing the zinc ions concentration has a similar effect. See Figures 15 and 16. These figures show the effects of initial zinc ions concentration on the average H_2S flux and the average size of the produced particles. In general, increasing the initial metal concentration corresponds with an increase in H_2S flux and a decrease of the average size of the produced solids. An increase of the metal concentration will lead to steeper concentration profiles near the interface, and therefore higher H_2S fluxes [21]. Good agreement was found between the measured enhancement factor and the calculated values assuming instantaneous reaction (equation 6). Also the gas holdup was observed to increase with increasing initial zinc concentration. This can be due to the fact that solids attach to the bubbles thereby stabilizing the bubbles and decreasing bubble coalescence. On the other hand attached solids cause the bubbles to slow-down and reduce the available gas-liquid interface. Finally, the solids can act as transport accelerators by adsorbing H_2S at the interface and carrying it to the liquid bulk. The net effect of all phenomena together apparently was positive as enhancement was experimentally observed.

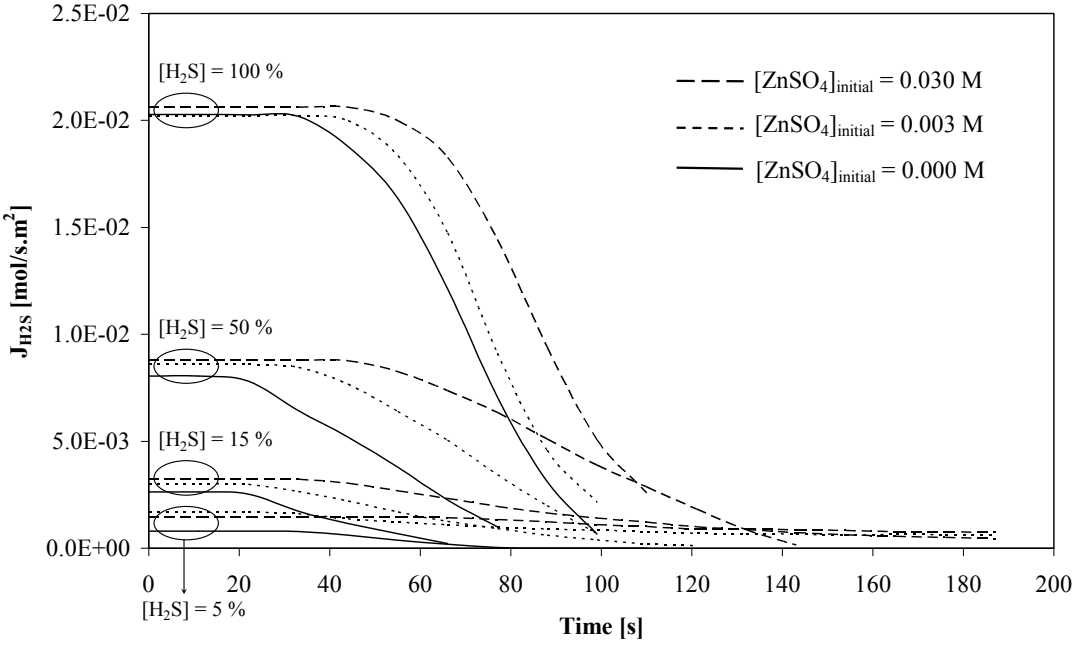

Figure 13: *Effect of initial zinc ions concentration and H_2S inlet concentration on average H_2S flux. T = 20°C, V_L = 1.5 L, P = 1.27 bar, u_t = 2.15 cm/s, specific area (a) = 89.56 m^2/m^3, k_La = 0.0524 s^{-1}, ionic strength = 1 M*

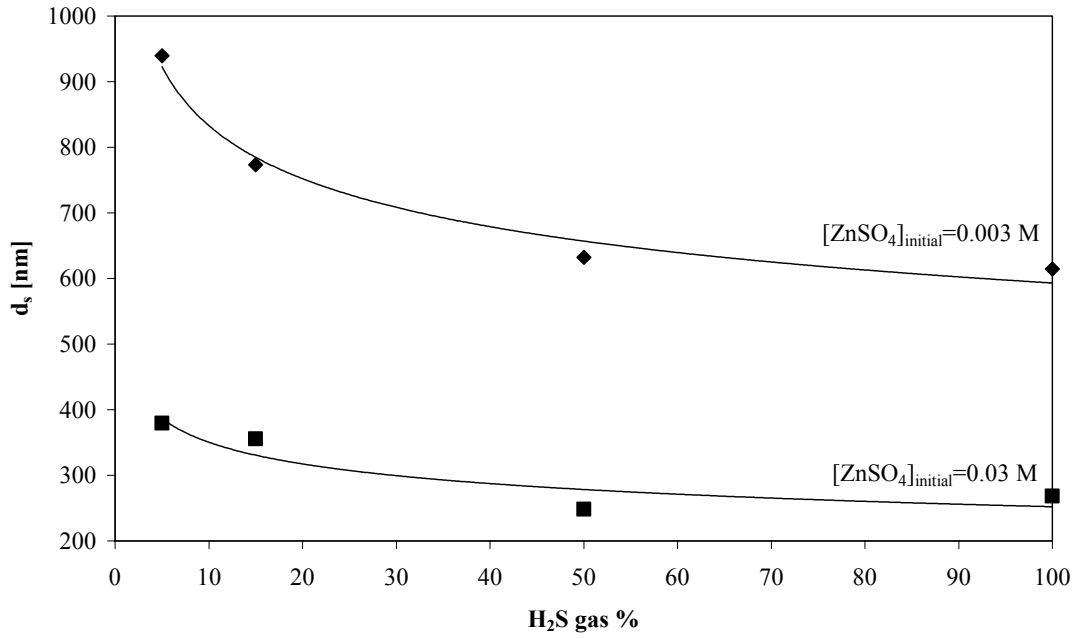

Figure 14: *Effect of inlet H_2S concentration on the average particle size of the produced solids. T = 20 ^oC, V_L = 1.5 L, P = 1.27 bar, u_t = 2.15 cm/s, specific area (a) = 89.56 m^2/m^3, k_La = 0.0524 s^{-1}, ionic strength = 1 M*

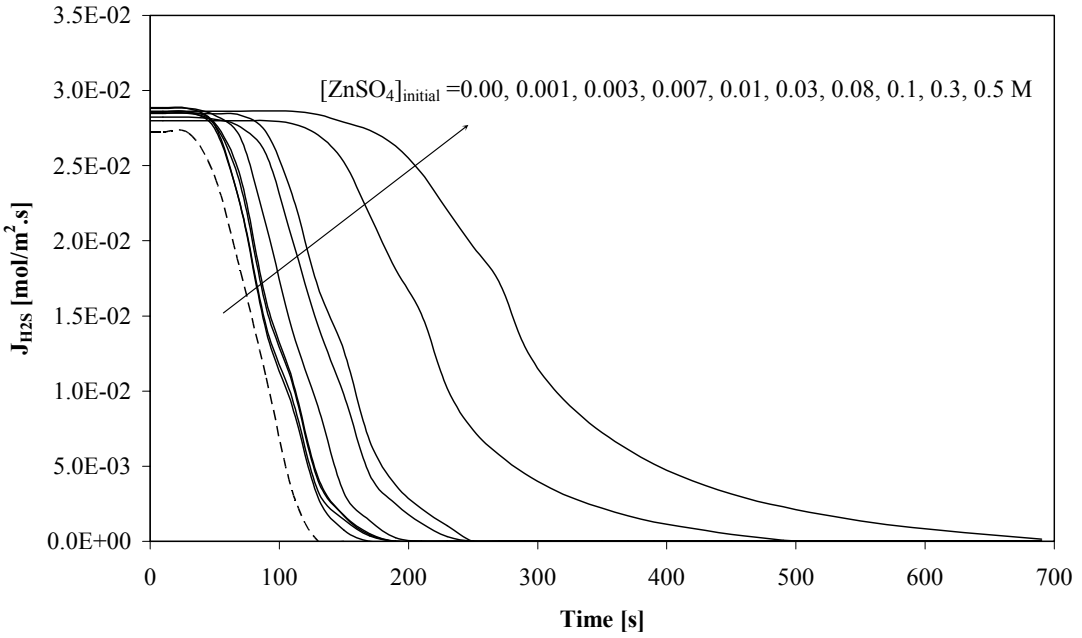

Figure 15: *Effect of initial $ZnSO_4$ concentration on the H_2S flux. T = 20 ^oC, V_L = 1.5 L, P = 1.36 bar, u_t = 1.41cm/s, specific area (a) = 69.79 m^2/m^3, k_La = 0.0406 s^{-1}, ionic strength = 1 M, H_2S inlet concentration = 100%, X=50~60%..*

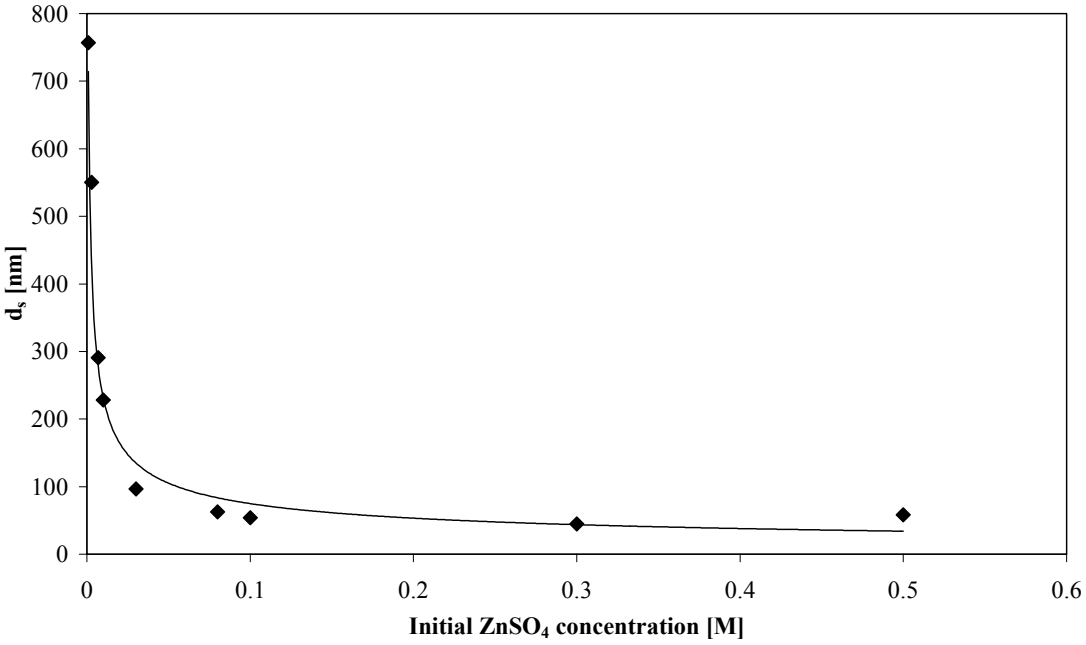

Figure 16: *Effect of the initial $ZnSO_4$ concentration on the average particle size. T = 20 °C, V_L = 1.5 L, P = 1.36 bar, u_t = 1.41 cm/s, specific area (a) = 69.79 m^2/m^3, k_La = 0.0406 s^{-1}, ionic strength = 1 M, H_2S inlet concentration = 100%, X = 50~60%*

The effect of gas pressure on the average particle size is shown in Figure 17. Increasing the bubble column pressure by 0.3 bar leads to a decrease of the average particle size of about 25%. Increasing the system pressure corresponds with an increase in gas concentration, and consequently with a higher H_2S concentration on the liquid side. This increase in H_2S concentration increases the supersaturation and thus the nucleation rate and the growth rate of the crystals. However, a higher supersaturation is more favorable for primary nucleation than for crystal growth and consequently more particles of smaller size are produced.

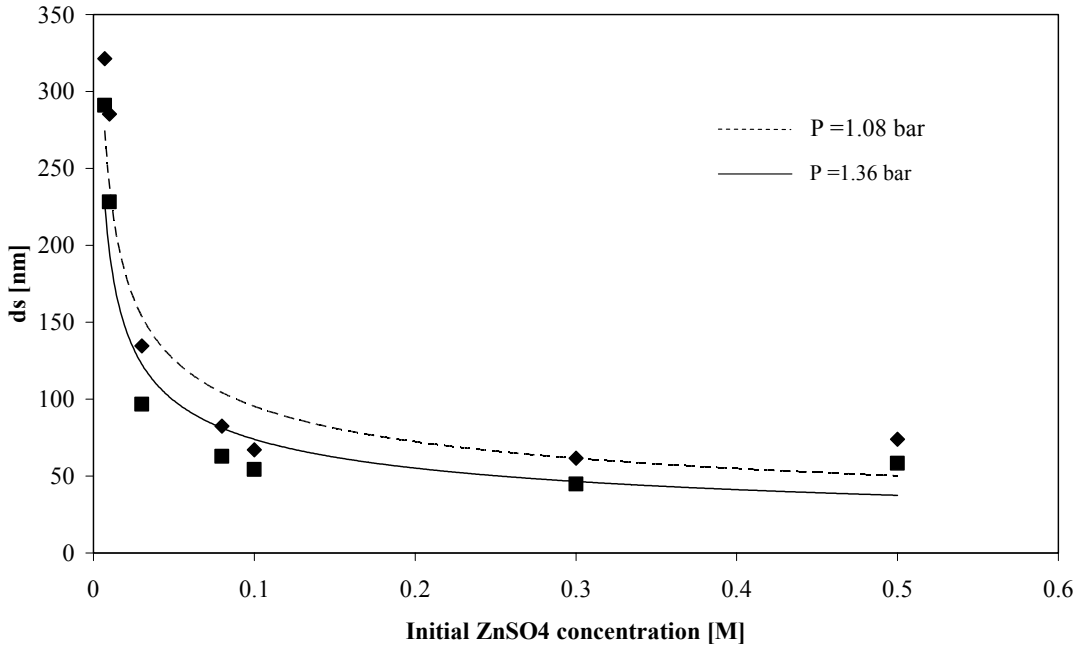

Figure 17: *Effects of bubble column pressure and initial $ZnSO_4$ concentration on the average particle size. T = 20 °C, V_L = 1.5L, u_t = 1.41cm/s, specific area (a) = 69.79 m^2/m^3, k_La = 0.0406 s^{-1}, ionic strength = 1 M, H_2S inlet concentration = 100%, X = 50~60%.*

Precipitation experiments were carried out with copper ions as well. Figures 18 and 19 show the effects of the copper ions concentration on the average H_2S flux and the average size of the produced CuS particles. A slight increase in average H_2S flux was observed when increasing the initial copper ions concentration. As the applied concentrations were quite low, hardly any enhancement in H_2S flux was observed (see equation 6). The average size of the produced particles also hardly varied with the concentration of copper ions. Based on the difference in the solubility products of ZnS and CuS (CuS being much less soluble) much smaller particles were expected when using copper instead of zinc. However, copper sulfide particles were found to be surface active and to cluster at the gas liquid interface, resulting in the formation of agglomerates. These agglomerates make it very difficult to see any effect of copper concentration on the average particle size. It must be noted that the agglomerate sizes of CuS are in the order of 10-15 μm while the ZnS particles were about 0.5 μm max.

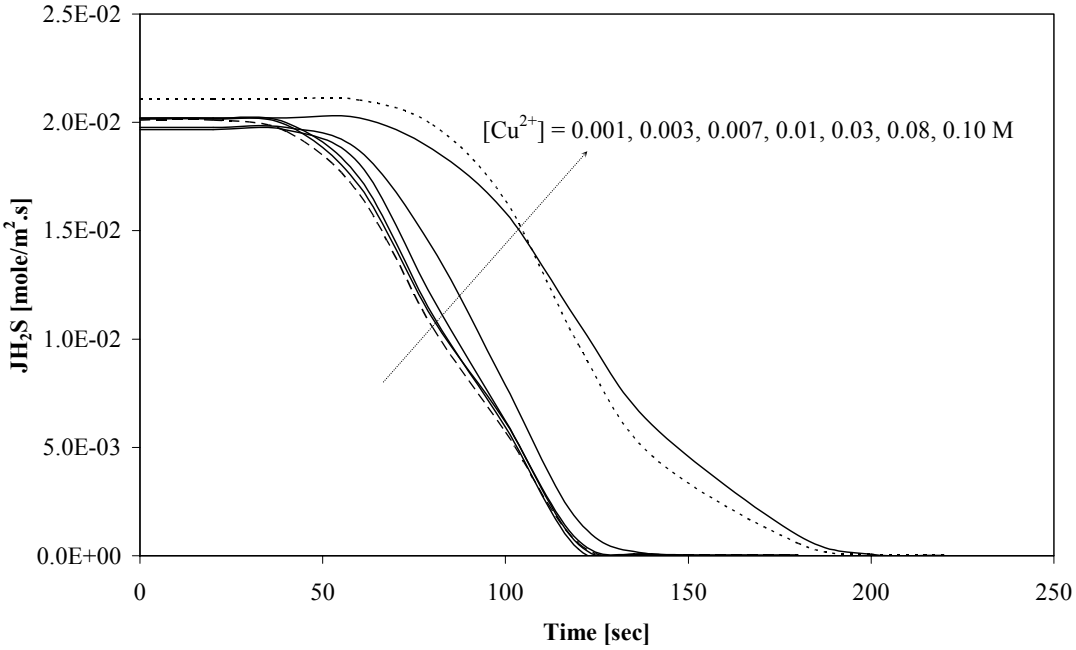

Figure 18: *Effect of copper ions concentration on the average flux of H_2S. T = 20 ^oC, V_L = 1.5 L, P = 1.01 bar, u_t = 1.41 cm/s, H_2S gas concentration = 100%.*

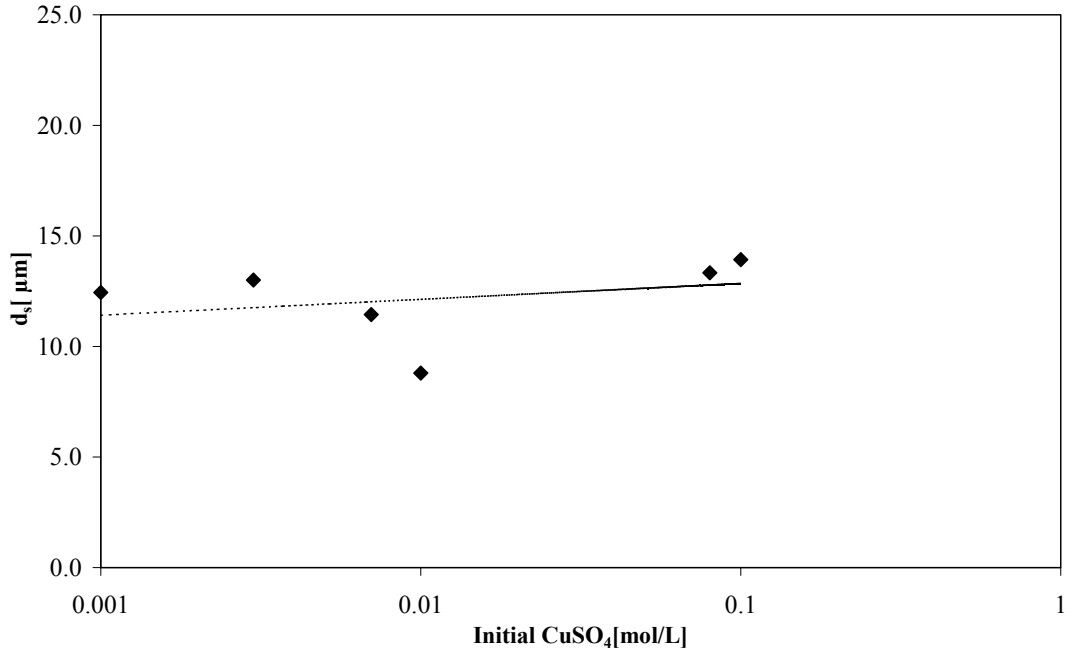

Figure 19: *Effect of initial copper ions concentration on the Sauter diameter of the produced particles. T = 20 ^oC, V_L = 1.5 L, P = 1.01 bar, u_t = 1.41cm/s, H_2S gas concentration = 100%*

5.6 Conclusions

The precipitation of CuS and ZnS by contacting an aqueous solution of $CuSO_4$ or $ZnSO_4$ with H_2S gas in a bubble column reactor was studied. First the hydrodynamic behavior of

the bubble column reactor was characterized using both CO_2 and H_2S gas. Then precipitation experiments were carried out. All experiments were performed in the homogeneous regime. Gas hold-up as well as volumetric mass transfer were found to increase with superficial gas velocity in a power law manner, the exponent being 0.9 for gas hold-up and 0.8 for volumetric mass transfer. The highest gas hold-up values were obtained when using H_2S gas, whereas volumetric mass transfer was highest when CO_2 was used. The addition of electrolytes led to an increase in the value of the pre-exponential factor. The presence of ZnS or CuS particles caused enhancement of the H_2S absorption rate, especially at high initial copper- or zinc sulfate concentrations.

Furthermore it was found that smaller ZnS-particles are produced when the H_2S concentration of the gas and/or the $ZnSO_4$ of the solution is increased. No significant effects were observed with copper due to severe agglomeration of the surface active CuS particles.

Acknowledgment

This project was supported with a grant of the Dutch Program EET (Economy, Ecology, Technology), a joint initiative of the Ministries of Economic Affairs, Education, Culture and Sciences, and of Housing, Spatial Planning and Environment. This program is coordinated by the EET Program Office, a partnership of Senter and Novem. The authors wish to thank Benno Kaken for his effort in building the experimental setup.

List of symbols

a	Bubble column specific area [m^2/m^3]
b	Pre-exponent
c_A^b	Bulk concentration of component A in the bubble column [mol/m^3]
c_A^o	Initial concentration of component A in the bubble column [mol/m^3]
$c_{H_2S}^i$	Interfacial concentration of H_2S [mol/m^3]
$\overline{c}_{Zn^{2+}}$	Bulk concentration of Zinc ions [mol/m^3]
D_{col}	Diameter of bubble column [cm]
D_{H_2S}	Diffusion coefficient for H_2S [m^2/s]
$D_{Zn^{2+}}$	Diffusion coefficient for zinc ions [m^2/s]
E_a	Enhancement factor [-]
$E_{A,\infty}$	Infinite enhancement factor [-]
J_{H2S}	H_2S flux [$mol/m^2.s$]
g	Gravitational acceleration [m^2/s]
[H_2S]	H_2S concentration [vol%]
k_La	Volumetric mass transfer coefficient [1/s]

$\dot{m}_{in}$	Inlet mass flow [mol/s]
$\dot{m}_{out}$	Outlet mass flow [mol/s]
n	Exponent
P	Pressure [bar]
V_d	Dispersed volume [m^3]
V_L	Volume of the liquid in the bubble column [l]
u_t	Superficial velocity [m/s]
T	Temperature [^oC]
t	Time [s]
X	Conversion of metal into metal sulfides [%]
Greek	
ρ_L	Liquid density [kg/m^3]
ε_G	Gas holdup [-]
$\nu_{Zn^{2+}}$	Reaction stoichiometric [-]

References:

1. Deckwer W D. Bubble column reactors, John Wiley & sons LTd, England, (1992).
2. JoshiJ.B. Computational flow modeling and design of bubble column reactors, Che. Eng. Sci. Vol. 56, pp 5893-5933, 2001.
3. Eigenberger G. and M. Bauer. A concept for multi-scale modeling of bubble columns and loop reactors. Che. Eng. Sci. Vol. 54, pp 5109-5117,1999.
4. Jones Alan G. and Stelios Rigopoulos. Dynamic modeling of bubble column for particle formation via a gas-liquid reaction. Che. Eng. Sci. Vol. 56, pp 6177-6184, 2001.
5. Mersmann A. “Batch precipitation of barium carbonate”. Che. Eng. Sci. Vol. 48, No.17, pp 3083-3088, 1993.
6. Mousa Al-Tarazi, Bert Heesink, Geert Versteeg ” New method for the Determination of Precipitation Kinetics”, The fourth Jordanian International Chemical Engineering conference, 22-24 Sep. 2002, Amman, Jordan.
7. Teixeira Jose A, Carla Freitas, Maria Fialova and Jindrich Zahradnik. Hydrodynamics of three-phase external-loop airlift bioreactor. Che. Eng. Sci. Vol. 55, pp 4961-4972, 2000
8. Paques, www.paques.nl
9. Marracci G. A Theory of Coalescence. Che. Eng.. Sci. Vol. 24, pp 975-987, 1969.

10. Alvarez-cuena M. and M. A. Nerenberg. The plug flow model for mass transfer in three phase fluidized beds and bubble columns. Can. J. Che. Eng. Vol. 59, pp 739-745, 1981.

11. Wach S and A. G. Jones. Mass transfer with chemical reaction and precipitation. Che. Eng. Sci. Vol. 40, pp1027-1033, 1990.

12. Tsutsumi A. Jenn-Yeu Nieh and Liang-Shih Fan. Role of the bubble wake in fine particle production of calcium carbonate in bubble column system", Ind. Eng. Chem. Vol. 30, pp 2328-2333, 1991.

13. Jones A. J. J. Hostomsky and Z. Li. On the effect of liquid mixing rate on primary crystal size during the gas-liquid precipitation of calcium carbonate", Che. Eng. Sci. Vol. 47, (13/14), pp 3817-3824, 1992.

14. Deckwer W.D. and A. Schumple. Improved tools for bubble column reactor design and scale-up. Che. Eng. Sci. Vol. 48, No. 5, pp 889-911, 1993

15. Hostomsky J. A. G. Jones. A penetration model of the gas-liquid reactive precipitation of calcium carbonate crystals. Trans IChemE. Vol. 73, Part A, pp 241-245, 1995.

16. Jeroen H.J. Kluytmans, Berend G.M. van Wachem, Ben F.M. kuster and Jaap C. Schouten. Gas Holdup in a slurry bbble column: influence of electrolyte and carbon particles. Ind. Eng. Chem. Res. Vol. 40, pp 5326-5333, 2001.

17. Mounir Bouaifl, Gilles Hebrard, Dominique Bastoul, Michel Roustan. A comparative study of gas holdup, bubble size, interfacial area and mass transfer coefficients in stirred gas- liquid reactors and bubble columns. Che. Eng. and Proc. Vol. 40, pp 97-111, 2001.

18. Koide K. Design Parameters of Bubble Column Reactors With and Without Solid Suspensions. J. Che. Eng. Japan, Vol. 29 (5), 1996.

19. Christenson H. K. and V. Yaminsky. Solute effects on bubble coalescence. J. phys. Chem. Vol. 99, p 10420, 1995.

20. Trambouze P., H. Van Laneghem and J.P. Wauquier. Chemical reactors design/engineering/operation, Paris, technip, (1988).

21. Versteeg, G.F, J. A. M. Kuipers, F.P. H. Beckum and W. P. M. Van Swaaij. Mass Transfer with Complex Reversible Chemical Reactions-I. Single Reversible Chemical Reaction. Chem. Engg. Sci. Vol. 44, No. 10, pp 2295-2310, 1989.

Chapter 6

Effects of Reactor Type and Mass Transfer on the Morphology of CuS and ZnS Crystals

Abstract

For the precipitation of CuS and ZnS, the effects of the reactor/precipitator type, mass transfer and process conditions on crystal morphology were studied. Either H_2S gas or a S^{2-} solution were applied. Three different types of reactors have been tested, namely a laminar jet, a bubble column and an MSMPR reactor. The choice of reactor type as well as mass transfer and metal concentration all have a considerable influence on the morphology of the produced crystals. A well mixed bubble column with H_2S containing gas as feed yields the coarsest crystals. Use is then made of the surface active properties of CuS-particles, which induce agglomeration at the gas-liquid interface, where as the low metal concentrations inside the reactor also contribute to the formation of coarser particles (especially for ZnS).

6.1 Introduction

Many specialty chemicals are manufactured in crystalline form through precipitation processes. The majority of such industrial processes involve simultaneous chemical reaction and crystallization or precipitation. A variety of gas-liquid and liquid-liquid processes can result in the production of different crystalline products, but studies on the interactions between process conditions and reactor layout on the one hand and crystal morphology on the other are scarce in literature. In precipitation the generation of supersaturation conditions with respect to the desired crystallizing product results as a consequence of chemical reaction. Reaction kinetics should therefore be known to characterize the performance of a reactive crystallizer. In many occasions, solution chemistry may be equally complex, and simplification may be necessary to describe the physicochemical processes in a system. In simple cases, reaction kinetics may be assumed to be first order with respect to each of the reactants and both solubility and solvent capacity may be regarded constant throughout a crystallizer. In many other cases, however, more complex physicochemistry is needed to describe the process adequately. In any case, a good understanding of the interaction between the different processes that are involved is needed to identify the improvements that may be achieved in crystal quality and the cost effectiveness of crystal production.

In recent years, more studies on reactive crystallization have been reported in literature, but not many on precipitation accompanied by a gas-liquid reaction, although this is frequently encountered in chemical industry. These three phase systems have a complex nature and not much is known about the interactions between process conditions and crystal quality [1].

The objectives of a crystallization process are to meet product specifications: (a) a narrow crystal size distribution, (b) maximum crystal purity, (c) a high yield and (d) acceptable crystal morphology. Depending on product applications, one of these can be more critical than the others. The optimum conditions to obtain crystals that meet such specifications are often determined in an empirical way, either by controlled growth through proper adjustment of supersaturation or by addition of certain habit modifiers. It is extremely difficult to predict crystal properties like lattice, morphology, hardness, strength, ductility, etc. on the basis of a fundamental approach. Parameters that are important are [2]:

1. Properties of the solution (density, viscosity, supersaturation, ionic strength, pH, etc.);
2. Operation mode and conditions (pressure, temperature, specific power input, residence time distribution, feed ratio of reactants, feed point location(s), etc.).

The best combination of these parameters should be determined in practice or on lab-scale. The intrinsic processes that determine the shape of crystals are:

1. The different growth rates of the different crystal faces;
2. Possible blockage of growth of certain faces due to the adsorption of impurities/additives;
3. Agglomeration of crystals;
4. Abrasion and attrition of crystals or agglomerates;
5. Breakage of crystals.

In most cases crystal morphology and crystal purity are interrelated. For some applications, e.g. in optics or medical ones crystal morphology is of utmost important. But morphology can also be important from a more fundamental viewpoint as it can give indications with regard to growth mechanism (surface integration, spiral growth), crystal purity and the rate determining step in gas-liquid precipitation.

6.2 Previous Work

Chen et al. (1997) studied the polymorphism of calcium carbonate crystals by introducing CO_2 gas through a gas sparger or a double-tube gas injection nozzle into a pH-stat crystallizer containing calcium chloride solution [3]. They investigated the effects of several variables such as supersaturation and pH. They found that at ambient temperature either calcite or vaterite is the major product, depending on the applied conditions. They also studied the growth kinetics of calcite crystals using the same experimental setup. They found that the growth rates of calcite seeds increased with increasing supersaturation and crystal size. They concluded that the morphology and growth rate of calcium carbonate are controllable in a gas-liquid-solid reactive crystallizer, using a pH-stat operation mode.

Bredol and Merikhi (1998) investigated the morphology of ZnS particles used in cathode-ray tube luminescent materials [4]. They studied the effect of different preparation methods (homogeneous precipitation and precipitation in the liquid crystal phase) and the introduction of ZnS seeds on morphology. They used powders produced by different processes to prepare luminescent materials in a standard manner. Their results show the effects of raw ZnS powder properties (including morphology) on the performance of annealed phosphor powders.

Yukiya et al. (1999) studied the relationship between the morphology of alumina hydroxide particles and the concentrations of the precipitating species [5]. They developed a model which is based on minimization of the Gibbs energy regarding temperature, solvent effects and ion–ion interactions. They calculated the solvent effect by use of the Born equation. The effect of ion–ion interaction was calculated by the extended Debye-Huckel equation. They found that particle morphology is mainly

determined by selective adsorption of positive charged $Al(OH)^{2+}$ ions on the negatively charged faces of the AlOOH crystals.

Wang et al. (2000) investigated the morphology of calcium carbonate particles produced by CO_2-$Ca(OH)_2$ precipitation in a Couette-Taylor reactor [6]. They found that particle morphology is dominated by the excess concentration of reactants in the solution. They found that the largest mean particle size and the most cube-like particle shape are obtained at the stoichiometric reaction conditions. As stoichiometry starts to deviate from unity, particle morphology shifts to a spindle-like shape and the mean particle size decreases. They predicted these effects by making use of the Bliznakov equation which is based on mono-layer adsorption.

Chen et al. (2001) used a double-jet feed, semi-batch crystallization system to explore nucleation kinetics, growth kinetics and morphology of barium carbonate crystals [7]. They determined nucleation and growth rates by the initial rate method. Their results show that heterogeneous nucleation is dominant in primary nucleation, the effect of specific power input on the rate of nucleation being significant. They also found that pH and initial concentration affect the morphology of the produced barium carbonate crystals. They produced crystals that are floc-like, candy-like, olivary-like and needle-like at different operating conditions. At moderate to high supersaturation floc-like precipitates are dominant in the pH range of 9.0–10.0. At low to moderate supersaturation, candy-like and olivary-like crystals become the major products. At low supersaturation and low pH values olivary-like and needle-like crystals are formed.

Sung et al. (2003) investigated the effects of Taylor vortices on the mean size, size distribution, and morphology of calcium carbonate crystals formed by the reaction of CO_2 and aqueous calcium hydroxide in a Couette–Taylor reactor [8]. They measured the mass transfer coefficient of CO_2 into pure water at various rotating speeds of the inner cylinders in the Couette–Taylor reactor. They observed that calcium carbonate crystals changed in morphology (polymorphs of rhombohedral-, spindle or needle-shaped) by changing the reactant concentrations, flow rate and/or rotating speed of the inner cylinder. They introduced a dimensionless parameter representing the operating conditions, to demonstrate that the morphology of the calcium carbonate crystals can be predicted from operating conditions. They concluded that the mean crystal size (predominantly controlled by agglomeration) is mostly influenced by the fluid dynamic conditions, which are related to the rotating speed of the inner cylinder and the reactor geometry.

6.3 Present Work

This work is part of a large study into the precipitation of heavy metal ions (mainly Cu^{2+} and Zn^{2+}) present in wastewater from the Pasminco zinc factory in Budel the Netherlands.

Use is made of the Paques Thiopaq® process, which involves biological reduction of sulfate, which is also present in the wastewater, towards sulfide. The sulfide subsequently reacts with the metal ions to form metal sulfides that can be removed by use of a settler or a centrifuge. To enable sufficient removal of the metal sulfides, coarse particles are to be produced (>10 μm). In this work it is examined how reactor layout and process conditions affect the size of the produced particles

Besides direct precipitation where sulfide ions are formed in the metal ions containing water, one might also consider a different process layout in which biological sulfate reduction reaction and metal sulfide precipitation are carried out in different reactors. The sulfide ions formed in the biological reduction reactor are in that case stripped off as H_2S gas and is then led to the precipitator, which is placed in front of the reduction reactor. See Figure 1.

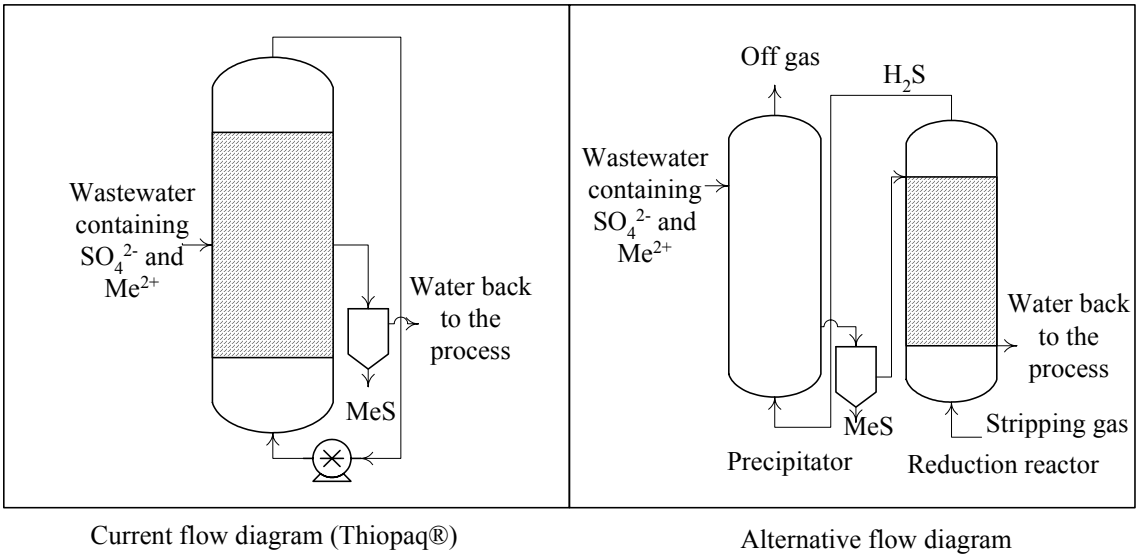

Figure 1: Possible *process flow diagrams.*

One may expect that particle morphology will become different when applying this process instead of the standard Thiopaq® process. Therefore, in this work the effects of reactor type, reactor configuration process conditions and liquid side mass transfer on the crystal morphology of CuS and ZnS were investigated. An MSMPR reactor, a bubble column and a laminar jet reactor were used to study these effects.

6.4 Experimental

An MSMPR reactor, a bubble column and a laminar jet reactor were used to study the effects of reactor layout and operating conditions on the morphology of the produced solids. Figure 2 shows a schematic diagram for the used experimental setups. In the MSMPR reactor the Cu^{2+} (or Zn^{2+}) and S^{2-} were introduced in aqueous solutions. In the

bubble column and the laminar jet reactor, an aqueous solution that contains the Cu^{2+} or Zn^{2+} ions was contacted with H_2S gas. Detailed descriptions of the applied experimental setups and the experimental procedures can be found in [9], [10] and [11]. Table 1 shows the main characteristics of each reactor.

Table 1: *Main characteristics of the applied experimental setups.*

Characteristics	**Bubble column**	**Laminar jet**	**MSMPR**
Phases	Gas-liquid	Gas-Liquid	Liquid-Liquid
Crystal residence time	20-50 s	0.03-0.07 s	150-300 s
Tested Me^{2+} concentrations	2000-6000 ppm	200- 600 ppm	2000- 4000 ppm
Liquid volume	1500 ml	0.04 ml	1000 ml
Mixing Gas: **Liquid:**	plug flow, well mixed	Well mixed No mixing	Well mixed No gas
Flow	Batch liquid, Continuous gas	Continuous gas, Continuous liquid	Continuous liquid
Key variables	Superficial gas velocity	Liquid flow rate	Mixer speed

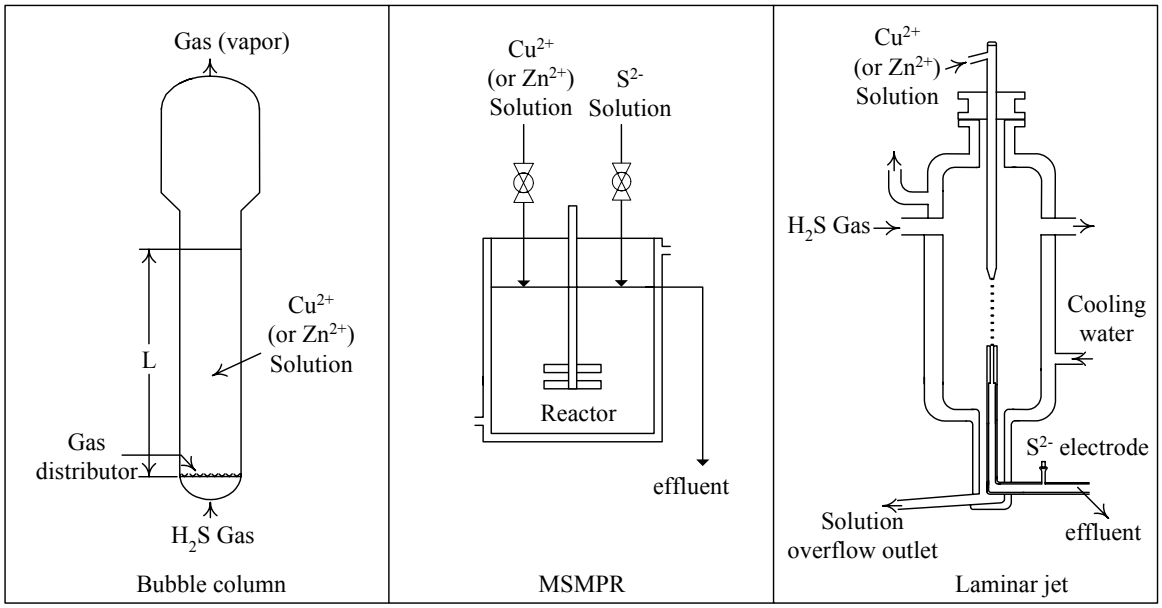

Figure 2: *Schematic diagrams of the applied experimental setups.*

Scanning Electron Microscope (SEM) and Transmission Electron Microscope (TEM) were used to investigate the morphology of the produced solids.

6.5 Results and Discussion

To demonstrate the effects of reactor geometry and operating conditions on crystal morphology, several experiments in different types of reactors have been carried out. Typical results are shown by Figures 3 to 8.

Figure 3 shows the influence of the liquid side mass transfer coefficient on the morphology of CuS crystals produced in the laminar jet reactor. In this reactor agglomeration can be minimized possible influences of mechanical mixing devices and shear flow can be avoided. Decreasing the liquid side mass transfer coefficient by 38% already leads to a dramatic change in morphology as can be seen in Figure 3. Particles produced at $k_L=3.85x10^{-4}$ m/s (A) seem to be flat plates while the particles produced at $k_L=2.4x10^{-4}$ m/s (B) are spherical. In case A the amount of absorbed H_2S is higher, which may reduce the local pH. It is known [3] that the pH is of utmost importance in this respect. Another explanation may be that in case A mass transfer was not fully rate determining while it was in case B. In literature several studies have been reported that demonstrate the influence of mass transfer on crystal morphology [6, 8].

Figures 4 and 5 show the effect of Zn^{2+} concentration on the size and morphology of ZnS crystals, also produced in the laminar jet reactor. As it can be seen, increasing the metal concentration in this case only has a small influence on crystal size and crystal morphology. The ZnS crystals seem spherical in all cases. This can be due to the domination of nucleation at the tested conditions since the contact time between liquid and gas was very short (0.03 sec). The size of the primary crystals, which can only be determined by the applied TEM method, is much smaller than the size of the aggregates observed when applying analysis methods such as X-ray diffraction or dynamic light scattering DLS. For example the average particle size measured by DLS of the sample presented in Figure 4 was 500 nm. Comparing the morphology of the produced ZnS with that of the CuS particles (Figure 3) one observes large differences: The CuS crystals can be plates-like for while spheres are observed for ZnS. Also the sizes of the CuS clusters are much bigger indicating their tendency to agglomerate.

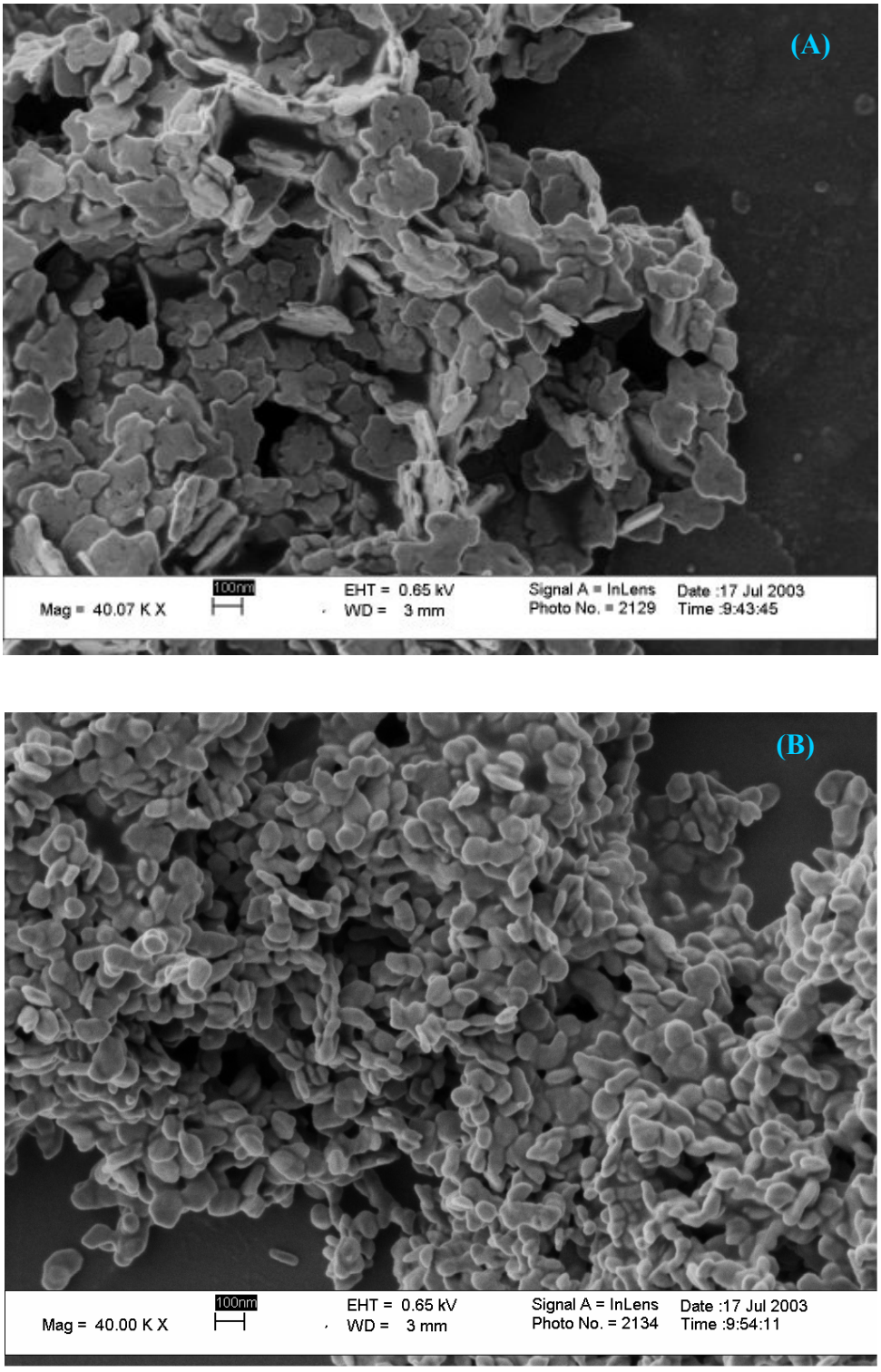

Figure 3: *Effect of liquid side mass transfer coefficient (k_L) on the morphology of CuS particles produced in a laminar jet reactor according to SEM. Liquid flowrate 0.24 ml/s, P = 1.025 bar, T = 21.6 °C, inlet H_2S gas concentration = 99.6 vol%, $[Cu^{2+}]_{feed}$ = 100 ppm, (A) $k_L = 3.85x10^{-4}$ m/s, (B) $k_L = 2.4x10^{-4}$ m/s.*

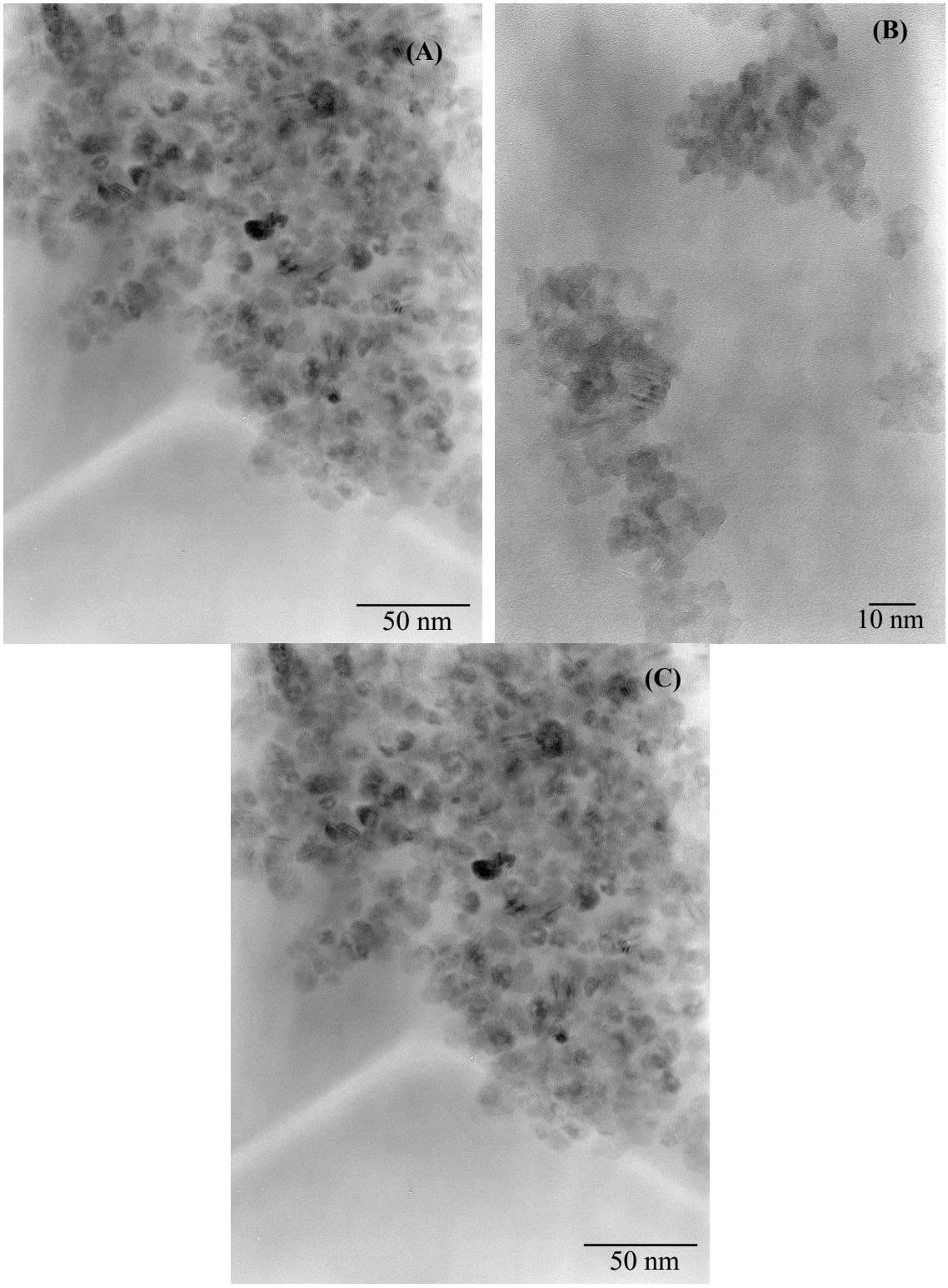

Figure 4: *Effect of Zn^{2+} concentration on the morphology of ZnS particles produced in the laminar jet reactor according TEM. Liquid flowrate 0.24 ml/s, P = 1.025 bar, T = 21.6 ^{o}C, inlet H_2S gas concentration = 99.6 vol% , $k_L = 3.94x10^{-4}$, $[Zn^{2+}]_{feed}$ = (A) 97.3 ppm, (B) 253 ppm, (C) 666 ppm.*

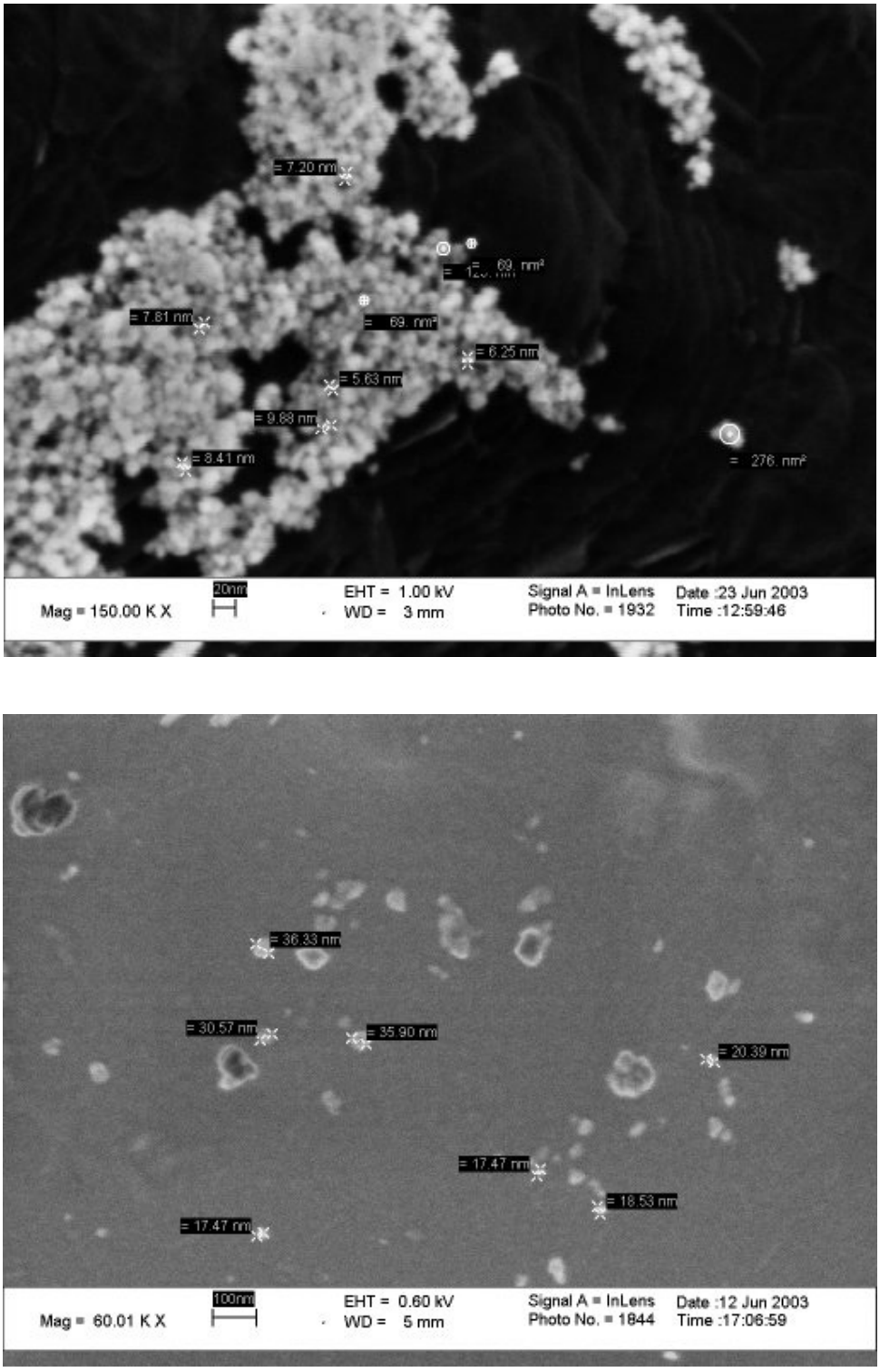

Figure 5: *SEM pictures of ZnS particles produced in the laminar jet reactor. Liquid flowrate 0.24 ml/s, P = 1.025 bar, T = 21.6 ^{o}C, inlet H_2S gas concentration = 99.6 vol% , $k_L = 3.85x10^{-4}$ m/s, $[Zn^{2+}]_{feed}$ = 253 ppm.*

Figure 6 shows the effect of initial Zn^{2+} concentration on the crystal morphology of ZnS when a bubble column is used as precipitator. Increasing the initial concentration of Zn^{2+}

by 25% resulted in a decrease in particle size of more than 50% while crystal morphology was hardly affected. The particles obtained in both cases have a plate-like shape. Figure 6 also shows that increasing the concentration yields a broader particle size distribution. When comparing the size of the particles produced in the bubble column with the ones produced in the laminar jet reactor one can conclude that the particles from the bubble column are much larger than those from the laminar jet whereas morphology has changed from sphere like to plate like. This can be due to the much higher zinc concentrations which reduces the local pH of the produced solution and may enhance agglomeration in the bubble column [3].

Figure 7 shows the effect of initial Cu^{2+} concentration on the morphology of CuS particles produced in the bubble column precipitator. The opposite effect was observed as with zinc: increasing the initial concentration of Cu^{2+} by 25% corresponded to a 300% increase in particle size. Crystal morphology also changed, i.e. from cube like to sphere like. Particles produced at the high initial copper concentration are bigger and have a more defined cubic shape. Experimentally it was noticed that CuS particles, due to their surface active nature, tend to attach to the rising bubbles. Increasing the initial Cu^{2+} concentration leads to higher initial nucleation rates. The produced nuclei tend to block the interfacial surface area as they remain at the interface, which leads to enhancement of crystal growth, lower nucleation rates and ultimately larger particles. When comparing the particles from the bubble column with those from the laminar jet reactor, many differences are observed. First of all the particles from the bubble column are much larger. Particles could have different morphology and can be spheres cubes or slides depending on the operating conditions in the applied precipitators.

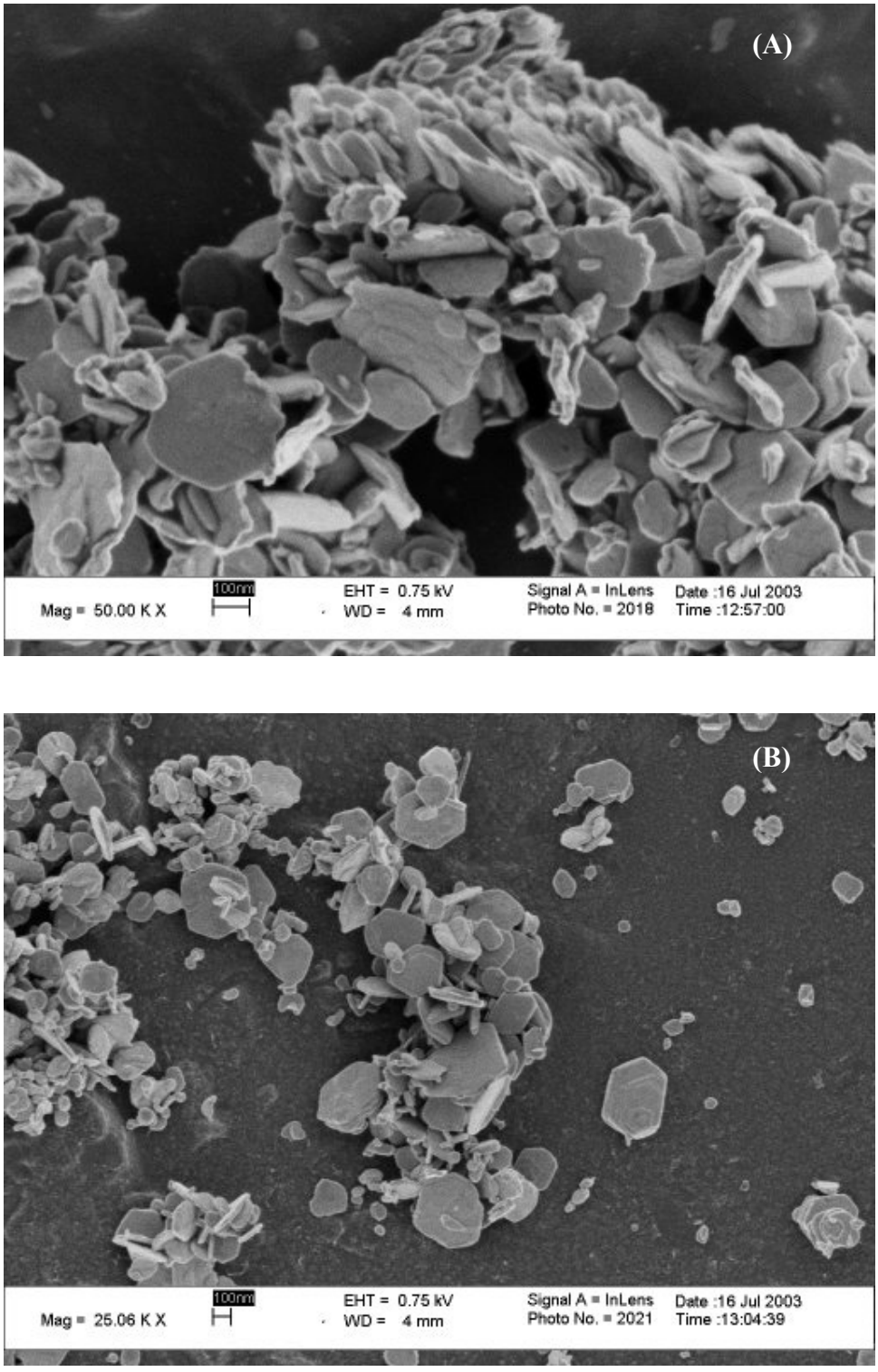

Figure 6: *Effect of initial Zn^{2+} concentration on the morphology of ZnS particles produced in a bubble column reactor according SEM. P = 1.125 bar, T = 21.6 ^{o}C, inlet H_2S gas concentration = 99.6 vol% , k_La = 0.0406 1/s, $[Cu^{2+}]_{initial}$ = (A) 5084 ppm and (B) 6355 ppm.*

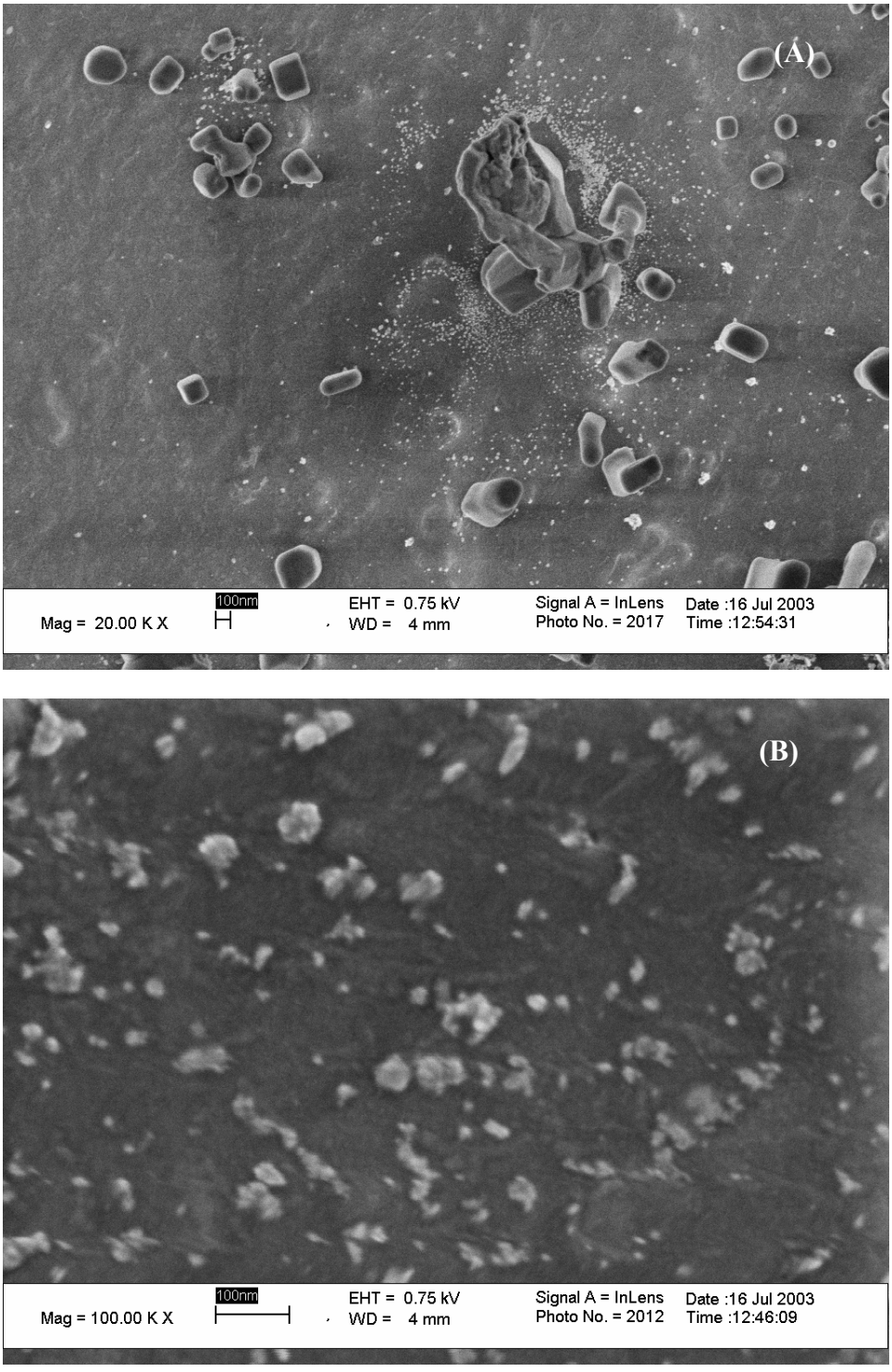

Figure 7: *Effect of initial Cu^{2+} concentration on the morphology of CuS particles produced in the bubble column reactor according SEM. P = 1.125 bar, T = 21.6 ^{o}C, inlet H_2S gas concentration = 99.6 vol% , k_La =0.0406 1/s, $[Cu^{2+}]_{initial}$ = (A) 6538 ppm (B) 5230 ppm.*

Finally, ZnS was produced in an MSMPR crystallizer. Figure 8 shows SEM and TEM pictures of the produced particles. In this experiment S^{2-} and Zn^{2+} ions were introduced in dissolved form. As can be seen the produced crystals are spherical. In general the size of

the produced particles was much smaller than that of the particles produced in the laminar jet and bubble column reactors. This can be due to the high local supersaturation values near the feeding points which enhance nucleation resulting in the production of many small particles.

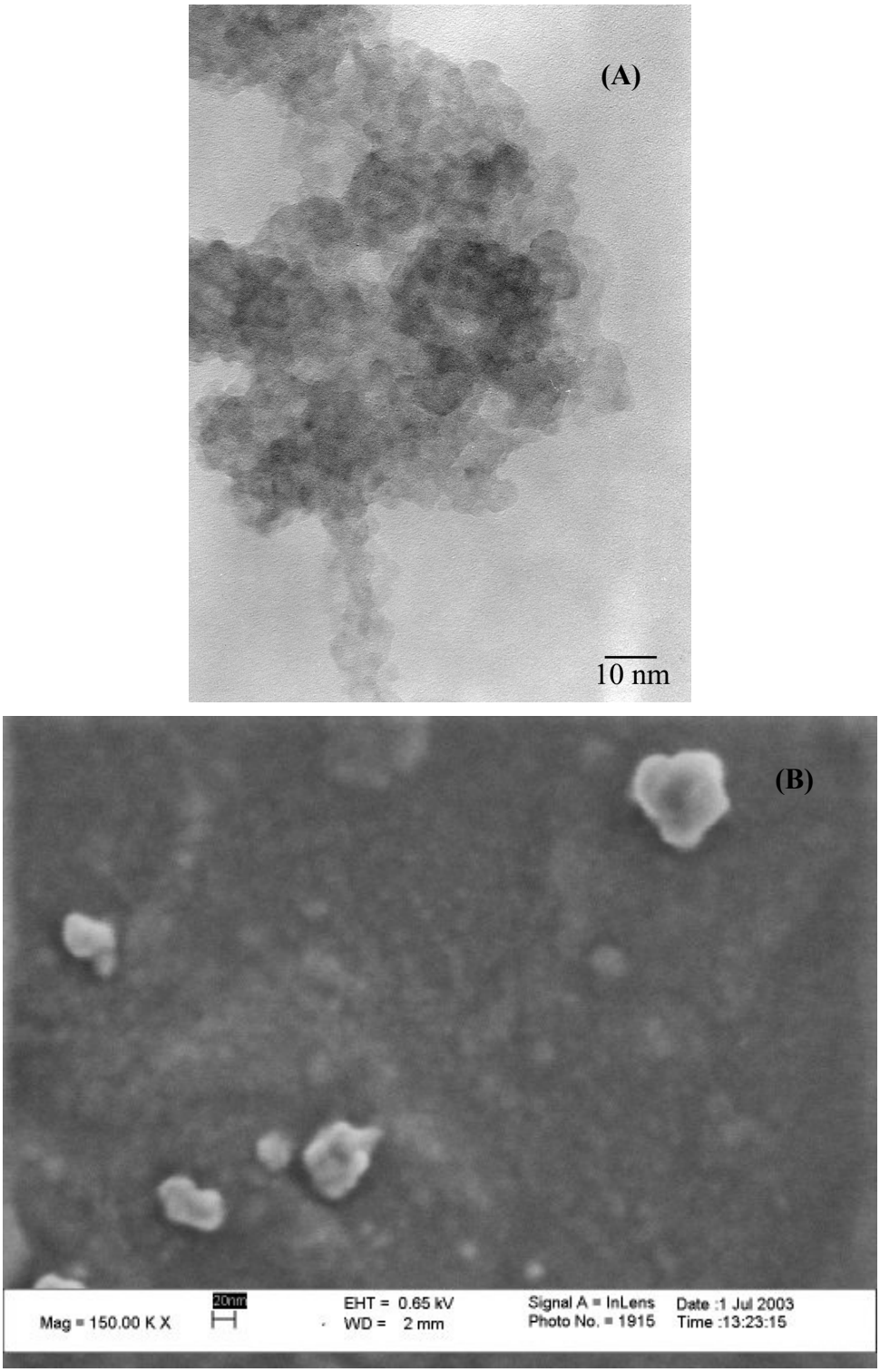

Figure 8: *Crystal morphology of ZnS particles produced in an MSMPR reactor. RPM = 710, molar feed ratio Zn^{2+}:S^{2-} = 1:1, pH = 5.9, residence time = 157 s, A: TEM, B: SEM.*

6.6 Conclusions

Control of crystal morphology is difficult as it highly depends on reactor type and process conditions. Local supersaturation, residence time of the crystals, hydrodynamics, contacting mode and surface active properties of the crystals, all play an important role with regard to the final size and shape of the produced crystals. A small change in one of these parameters may result in large differences in crystal morphology.

When designing a CuS precipitator, use should be made of the surface active properties of CuS in order to make use of agglomeration yielding coarser particles. Therefore a gas-liquid reactor is to be preferred over a single liquid phase reactor as applied in the Thiopaq® process. As for ZnS precipitation, particle size appears to be independent of reactor type, though it is strongly influenced by the concentration of Zn^{2+} ions, lower concentrations resulting in coarser particles and in a narrower particle size distribution. A reactor with a well mixed liquid phase will therefore yield the coarsest ZnS particles. A bubble column therefore is also suitable to produce coarse ZnS particles.

Acknowledgment

This project was supported with a grant of the Dutch Program EET (Economy, Ecology, Technology) a joint initiative of the Ministries of Economic Affairs, Education, Culture and Sciences, and of Housing, Spatial Planning and Environment. This program is coordinated by the EET Program Office, a partnership of Senter and Novem.

References

1. Narayan S. Tavare. Batch Crystallizers, Reviews in chemical engineering, vol. 7, no. 3-4, pp 213-351, 1991.
2. Mersmann A. Crystallzation Technology Handbook. Marcel Dekker Inc. New Yourk, (1995).
3. Pao-Chi Chen, Clifford Y. Tai and K.C. Lee. ‘ Morphology and growth rate of calcium carbonate crystals in a gas-Liquid-solid reactive crystallizer’. Chemical engineering science, vol. 52, no. 21/22, pp 4171-4177, 1997
4. M. Bredol, J. Merikhi. ZnS precipitation: morphology control, Journal of Materials Science, vol. 33, pp 471–476, 1998.
5. Yukiya Hakuta, Tadafumi Adschiri, Hideyuki Hirakoso and Kunio Arai.’ Chemical equilibria and particle morphology of boehmite (AlOOH) in sub and supercritical water’. Fluid Phase Equilibria, vol. 158-160, pp 733-742, 1999.

6. Wang Mo Jung, Sung Hoon Kang, Woo-Sik Kim and Chang Kyun Choi.' Particle morphology of calcium carbonate precipitated by Gas-liquid reaction in a Couette-Taylor reactor'. Chemical Engineering Science, vol. 55, pp 733-747, 2000.
7. Pao-Chi Chen, G.Y. Cheng, M.H. Kou and P.Y. Shia, P.O. Chung.' Nucleation and morphology of barium carbonate crystals in a semi-batch crystallizer'. Journal of Crystal Growth, vol. 226, pp 458–472, 2001.
8. Sung Hoon Kang, Sang Goo Lee, Wang Mo Jung, Min Chan Kim, Woo-Sik Kim, Chang Kyun Choi, Robert S. Feigelson. Effect of Taylor vortices on calcium carbonate crystallization by gas–liquid reaction. Journal of Crystal Growth, vol. 254, pp 196–205, 2003.
9. Al-Tarazi Mousa, B. Heesink, M. Azzam, S. Abu Yahya and G. Versteeg. Crystallization kinetics of CuS using MSMPR. Submitted to Separation Science and Technology.
10. Al-Tarazi Mousa, B. Heesink, M. Azzam, K. Azzam and G. Versteeg. Precipitation of ZnS in bubble column reactor. Submitted to AICHE.
11. Al-Tarazi Mousa, B. Heesink and G. Versteeg. New method for the determination of precipitation kinetics using a laminar jet reactor. Submitted to Journal of Chemical Engineering Science

Summary

Precipitation of solids promoted by gas-liquid reactions is applied in many industrial processes such as the production of ammonium phosphate, ammonium sulphate, barium carbonate, calcium carbonate, calcium fluoride, gypsum (calcium sulphate), goethite, sodium bicarbonate, strontium carbonate and terephthalic acid. In addition gas-liquid precipitation can be applied in gas cleaning, heavy metal removal and in biotechnology. Despite the importance of this subject no extensive studies have yet been conducted until recently.

Heavy metals wastewater streams are found in many segments of the process industry; for example zinc factories produce wastewater containing diluted sulphuric acid contaminated with heavy metals. Due to the increase in the awareness and understanding of the impact of heavy metals on the environment and human health, in many countries landfill is only allowed in special depots while landfill taxes are increasing. A new process to remove heavy metals from industrial wastewater has been developed by Paques (www.paques.com). The process makes use of a bio-reactor in which sulfate is reduced to sulfide. The sulfide from the bio-reactor is then mixed with the heavy metal ions containing stream resulting in the precipitation of the metal ions as metal sulfides. The sulfide can either be supplied as dissolved ions or as H_2S-gas obtained by stripping the contents of the bio-reactor. The metal sulfides can be removed by making use of liquid-solid separators such as a settler. Although this process has been implemented on a large scale the influence of different parameters on the performance of this process is not fully understood. It is for example not fully known what to do to produce coarse easily to separate metal sulfide particles.

The main objective of this study is to gain fundamental insight in the Paques process that can help in the improvement of existing and the design of new plants. The emphasis of this study was on the use of H_2S-gas rather than sulfide solutions to treat the heavy metal containing wastewater. When using gaseous hydrogen sulfide in the precipitation step of the Paques process both mass transfer and precipitation are simultaneously occurring phenomena that will interact with each other in a complex way. It is perhaps no wonder that operation of such precipitation processes has sometimes been called an art rather than a science, but to do so today would be to ignore the tremendous advances that have been made over the past decades in both the theory and practice of the subject.

In Chapter 1 a mathematical model has been developed that describes the precipitation of metal sulfides in an aqueous solution that contains two different heavy metals and is contacted with H_2S-gas. The aqueous solution is assumed to consist of a well-mixed bulk and an interfacial region that is contacted with hydrogen sulfide gas. The model makes

use of Higbie's penetration model to calculate the transfer rate of gaseous hydrogen sulfide through the gas-liquid interface. The conditions that have been used in the simulations resemble those of industrial wastewater from a zinc factory. The model predicts the rate of H_2S absorption, the size distribution of the metal sulfide crystals and the selectivity of precipitation.

Higher precipitation rates are predicted at higher pH-values and higher H_2S concentrations. In all cases considered, the rate of precipitation is fully controlled by mass transfer of H_2S, higher H_2S concentrations and higher specific surface areas yielding higher precipitation rates. The size of the obtained crystals is predicted to increase with H_2S concentration, but to decrease with specific surface area and liquid side mass transfer. These results illustrate the importance of reactor selection and operating conditions on the process of gas-liquid precipitation.

Kinetic data of metal sulfide precipitation reactions are needed to come to optimal designs of industrial precipitators. However, published data are scarce and frequently unreliable. Different investigators may report rates that differ by an order of magnitude. In Chapters 2 and 3, the precipitation kinetics of copper sulphide and zinc sulphide were studied using a lab scale mixed-suspension-mixed-product removal (MSMPR) precipitation reactor. Measurements were done at different feed concentrations, molar ratios, stirrer speeds, pH-values and residence times. Primary nucleation and volume average crystal growth rates as well as agglomeration kernel were determined. Relationships were found between the rates of the different crystallization steps on the one hand and supersaturation, stirrer speeds, pH-values and Cu^{2+}-(or Zn^{2+}-) to S^{2-}-ratio on the other. For CuS precipitation, larger crystals will be obtained at high supersaturation, moderate stirrer speeds, small residence times, a pH-value of around 5 and high Cu^{2+} to S^{2-} ratios. Using the same feed concentrations, stirrer speeds and molar feed ratios higher growth rates were observed for ZnS precipitation. In general ZnS particles were much coarser than CuS particles. One should realize though that the applied MSMPR method is not the most optimal technique for examining fast precipitation reactions. The crystallization rate may be much higher than (local) mixing rates making it impossible to measure the intrinsic kinetics of the different crystallization steps.

A new experimental method for determining the intrinsic kinetics of fast precipitation reactions is introduced in Chapter 4. Use is made of a laminar jet reactor that has also frequently been applied to determine the kinetics of homogeneous gas-liquid reactions. The liquid containing one or more of the precipitating reactants (here heavy metal ions) passes a gas filled reactor as a stagnant jet in which no mixing occurs. The remaining reactant needed for precipitation is supplied in gaseous form and causes the precipitation reaction to occur while it is diffusing into the jet. Hydrodynamics as well as transport phenomena are precisely defined for this system, whereas agglomeration can be

minimized by adjustment of the concentration of the solute supplied by the liquid. The kinetics of primary nucleation and crystal growth can be determined by analyzing the size distribution of the particles present in the effluent of the laminar jet reactor. The new method was experimentally demonstrated for the precipitation of CuS using H_2S gas. The obtained data were successfully used to simulate an industrial packed bed absorber in which H_2S is absorbed by a $CuSO_4$-solution.

In order to validate the simulation results obtained in Chapter 1, an experimental study into the precipitation of CuS and ZnS in a semi-batch wise operated bubble column was carried out (Chapter 5). First the applied bubble column was characterized with respect to gas-liquid mass transfer. The influences of ionic strength and superficial gas velocity on volumetric mass transfer and gas hold-up were determined using both CO_2 and H_2S gas. Increasing the ionic strength was found to increase both volumetric mass transfer and gas hold up in a power law manner. Although the gas hold-up with H_2S was found to be higher than with CO_2 at the same ionic strength and superficial gas velocity, volumetric mass transfer was faster when applying CO_2. The influences of H_2S concentration, initial metal concentration and gas pressure on the precipitation of ZnS and CuS were also investigated. An increase in H_2S concentration, initial Zn^{2+} concentration and/or gas pressure was found to yield a decrease in the average size of produced ZnS particles. No significant effects could be observed for CuS precipitation due to its surface-active nature, which causes it to agglomerate at the gas-liquid interface.

Crystal properties such as particle size distribution and particle morphology strongly affect the performance of units placed after the crystallizer (filters, settlers, dryers, caking machines, etc.). For the precipitation of CuS and ZnS, the effects of reactor/precipitator type and process conditions on crystal morphology were therefore studied in Chapter 6. Either H_2S gas or a sulfide containing solution was applied. Three different types of reactors were tested, namely a laminar jet reactor, a bubble column and an MSMPR reactor. Reactor type, mass transfer rate and metal concentration were shown to have a considerable influence on the morphology of the produced crystals.

Precipitation reaction control is difficult and highly depends on the reactor geometry and process conditions. A better insight was gained by applying modeling and new characterization techniques such as laminar jet. The results will help in the design and scale-up of metal sulfide precipitators.

This project was supported with a grant of the Dutch Program EET (Economy, Ecology, Technology) a joint initiative of the Ministries of Economic Affairs, Education, Culture and Sciences, and of Housing, Spatial Planning and Environment. This program is coordinated by the EET Program Office, a partnership of Senter and Novem.

Samenvatting

Bij vele industriële productieprocessen treedt tijdens gas-vloeistof reacties gelijktijdige neerslagvorming van het gewenste product op. Voorbeelden hiervan zijn de productie van ammoniumfosfaat, ammoniumsulfaat, bariumcarbonaat, calciumfluoride, calciumsulfaat, natriumbicarbonaat, strontiumcarbonaat en tereftaalzuur. Hiernaast kunnen gas-vloeistof neerslagreacties worden toegepast bij het zuiveren van (af)gassen, het verwijderen van zware metalen uit waterige stromen en in de biotechnologie. Ondanks het belang van dit onderwerp zijn er tot voor kort geen uitgebreide studies naar uitgevoerd.

Afvalwaterstromen verontreinigd met zware metalen komen in vele segmenten van de procesindustrie voor. Als voorbeeld kan de productie van zink worden genoemd, waar afvalwaterstromen zowel zwavelzuur als zware metalen bevatten. Door een toename van de kennis omtrent de gevaren van zware metalen voor mens en milieu is het storten van afvalstromen die zware metalen bevatten alleen nog mogelijk in speciale depots en tegen steeds maar toenemende kosten. Een nieuw proces om zware metalen efficiënt uit industrieel afvalwater te verwijderen en in geconcentreerde vorm te verkrijgen is ontwikkeld door Paques (www.paques.com). Dit Paques proces maakt gebruik van een bio-reactor waarin in een waterige fase sulfaat gereduceerd wordt tot sulfide. De sulfide bevattende waterige stroom afkomstig uit de bioreactor kan vervolgens direct worden toegevoegd aan de afvalwaterstroom die de zware metalen bevat. Doordat metaalsulfiden in zijn algemeenheid slecht oplosbaar in water zijn, leidt deze toevoeging tot de neerslagvorming van metaalsulfiden. Het gevormde metaalsulfide kan vervolgens eenvoudig worden afgescheiden door gebruik te maken van vloeistof-vast scheidingsprocessen zoals bijvoorbeeld een settler. Als alternatief van het hierboven beschreven proces kan de sulfide bevattende waterstroom met een inert gas worden worden gestript waardoor de uittredende gasstroom het sulfide in de vorm van H_2S bevat. In plaats van de complete waterige sulfidestroom, hoeft nu alleen de H_2S bevattende gasstroom in contact te worden gebracht met de te behandelen afvalwaterstroom. Alhoewel dit proces op grote schaal wordt toegepast, is de invloed van de verschillende procesparameters niet goed duidelijk. Zo is het bijvoorbeeld niet bekend hoe groffe, gemakkelijk te scheiden metaalsulfide deeltjes moeten worden geproduceerd.

Het voornaamste doel van deze studie is een fundamenteel inzicht te krijgen in het Paques proces om daarmee zowel bestaande als nieuwe processen te kunnen optimaliseren en ontwerpen. Deze studie concentreert zich op de verwijdering van de zware metalen uit afvalwaterstromen middels het gebruik van H_2S bevattende gasstromen waardoor er sprake is van een gas-vloeistof proces met gelijktijdige neerslagvorming. Tijdens dit proces vindt er een complexe interactie tussen stofoverdracht en precipitatie plaats. Het is

dan ook niet verwonderlijk dat het bedrijven van soortgelijke processen in het verleden ook wel een ‘kunst’ werd genoemd in plaats van een ‘kunde’. Gezien de grote vooruitgang die de afgelopen jaren op dit onderzoeksgebied -zowel theoretisch als experimenteel- heeft plaatsgevonden moet men nu echter van een volwaardige wetenschap spreken.

In Hoofdstuk 1 staat een wiskundig model beschreven dat de neerslagvorming van metaalsulfiden beschrijft indien een waterige oplossing met daarin twee verschillende zware metalen in contact wordt gebracht met gasvormig H_2S. In het model is aangenomen dat de waterige fase ideaal gemengd is. Het model maakt gebruik van Higbie’s penetratiemodel om de stofoverdrachtssnelheid van H_2S vanuit de gasfase naar de vloeistoffase te kunnen berekenen. In de met het model uitgevoerde simulaties zijn de condities gebruikt zoals die in het afvalwater van een zinkfabriek kunnen worden aangetroffen. Het model voorspelt niet alleen de absorptiesnelheid van H_2S maar tevens de deeltjesgrootteverdeling en de selectiviteit van de neerslagreactie ten opzichte van beide metaalionen. Bij een toename van de H_2S concentratie en de pH neemt de snelheid waarmee de neerslag gevormd wordt toe. In alle uitgevoerde simulaties blijkt de snelheid waarmee de neerslag gevormd wordt volledig gecontroleerd te worden door de absorptiesnelheid van H_2S: hogere H_2S concentraties en een groter uitwisselend gas-vloeistof contactoppervlak hadden een hogere precipitatiesnelheid tot gevolg. De simulatieresultaten duiden aan dat de grootte van de gevormde metaalsulfide kristallen toeneemt met de H_2S concentratie maar afneemt met een toename van het gas-vloeistof contactoppervlak en de stofoverdrachtscoëfficiënt aan de vloeistofzijde.

De intrinsieke kinetiek van de precipitatie van metaalsulfiden is nodig om tot een optimaal ontwerp van industriële metaalsulfide kristallisatoren te komen. Helaas blijken deze kinetiekdata in de literatuur slechts beperkt beschikbaar te zijn. Daarnaast is de betrouwbaarheid van de gerapporteerde data in veel gevallen ook nog eens twijfelachtig aangezien verschillende bronnen voor identieke systemen kinetiekdata geven die een orde grootte kunnen verschillen. De precipitatiekinetiek van kopersulfide en zinksulfide is onderzocht door gebruik te maken van een zogenaamde MSMPR (mixed-suspension-mixed-product removal) precipitatie reactor. De experimentele resultaten van deze studie staan beschreven in Hoofdstuk 2 en 3. Er zijn metingen uitgevoerd bij verschillende voedingsconcentraties, voedingsratios, roersnelheden, pH-waarden en verblijftijden. De resultaten zijn gebruikt om de primaire nucleatiesnelheid, de volume gemiddelde kristalgroeisnelheid en de agglomeratiesnelheidsconstante te bepalen. De relatie tussen de snelheid van de verschillende kristallisatiestappen aan de ene kant en de oververzadiging, roersnelheid, pH en de concentratieratio tussen Cu^{2+} (of Zn^{2+}) ten opzichte van S^{2-} aan de andere kant is vastgesteld. In het geval van de precipitatie van CuS worden er groffe kristallen verkregen in geval van een hoge mate van oververzadiging van de voeding,

hoge ratio van Cu^{2+} t.o.v. S^{2-}, gematigde roersnelheden, korte verblijftijden en een pH van ongeveer 5. De bruikbaarheid van de MSMPR reactor voor het bepalen van de precipitatiekinetiek van snelle precipitatiereacties is echter beperkt. De reden hiervan is dat de (lokale) mengsnelheid van de reactanten tijdens de experimenten veel lager kan zijn dan de eigenlijke kristallisatiesnelheid, waardoor het bepalen van de intrinsieke precipitatiekinetiek van snelle reacties met deze techniek niet mogelijk is.

Voor het bepalen van de intrinsieke kinetiek van snelle neerslagreacties is een nieuwe methode ontwikkeld die beschreven staat in Hoofdstuk 4. De methode is gebaseerd op het gebruik van een laminaire jet reactor die vaak gebruikt wordt voor het bepalen van de kinetiek van homogene gas-vloeistof reacties. Bij de experimenten werd een waterige oplossing -met daarin aanwezig de zware metaalionen- als een vloeistofstraal (jet) door de reactor geleid waarin gasvormig H_2S aanwezig was. De vloeistofstraal was zodanig dat daarin geen radiële convectieve menging optrad, en deze dus opgevat kon worden als 'stagnant'. Gedurende het verblijf van de jet in de reactor staat deze aan de buitenkant in contact met H_2S dat de straal in diffundeert en bij contact met de metaalionen een neerslagreactie tot gevolg heeft. Bij gebruik van de laminaire jet reactor zijn de hydrodynamica en stofoverdrachtscoëfficiënten exact bekend, en kan de agglomoratie geminimaliseerd worden door de concentratie H_2S aan te passen. Onder deze omstandigheden kan niet alleen de kinetiek van de primaire nucleatie worden vastgesteld maar tevens kan de kristalgroeisnelheid bepaald worden aan de hand van de deeltjesgrootteverdeling in het effluent van de reactor. Er zijn experimenten uitgevoerd voor de vaststelling van de precipitatiekinetiek van CuS. Deze kinetiek is vervolgens toegepast in een simulatiemodel van een continu bedreven gepakt bed reactor waarin de H_2S absorptie in een $CuSO_4$ oplossing plaatsvindt.

Om de in Hoofdstuk 1 verkregen simulatieresulaten te verifiëren is een experimentele studie in een semi-batch bedreven bellenkolom uitgevoerd (batch m.b.t. vloeistoffase, continu m.b.t. gasfase). In een eerste fase van dit in Hoofdstuk 5 beschreven onderzoek is de bellenkolom gekarakteriseerd. Bij deze karakterisering is de invloed van de ionsterkte van de gebruikte vloeistof en de invloed van de superficiële gassnelheid op zowel de stofoverdracht als de gas hold-up experimenteel bepaald. Alhoewel de gas hold-up bij gebruik van H_2S hoger was dan bij gebruik van CO_2 bleek de volumetrische stofoverdrachtssnelheid bij gebruik van CO_2 hoger. De invloed van de H_2S concentratie, initiële metaalion concentratie en gasdruk op het precipitatiegedrag van ZnS en CuS zijn bestudeerd. Een toename van de H_2S concentratie, initiële Zn^{2+} concentratie en/of gasdruk leverde een afname van de gemiddelde deeltjesgrootte van het ZnS neerslag op. Bij gebruik van een waterige Cu^{2+} oplossing (en dus bij vorming van CuS) kon geen eenduidige invloed van de verschillende procesparameters worden vastgesteld door

agglomoratie van CuS kristallen aan het gas-vloeistof grensvlak die veroorzaaakt werd door de oppervlakte-actieve eigenschappen van CuS.

Kristaleigenschappen als deeltjesgrootte(verdeling) en deeltjes morfologie hebben een grote invloed op het functioneren van apparaten die na de kristallisator volgen (filters, settlers, drogers, etc.). Voor de precipitatie van ZnS en CuS is daarom de invloed van het type reactor/kristallisator en de procescondities op de kristalmorfologie bestudeerd (zie Hoofdstuk 6). In de in Hoofdstuk 6 beschreven studie is als sulfide bron zowel gebruik gemaakt van H_2S gas alsook een waterige sulfide oplossing. Drie verschillende types reactoren zijn getest: een laminaire jet reactor, een bellenkolom en een MSMPR reactor. Zowel het reactortype, de stofoverdrachtssnelheid als de metaalion concentratie bleken allen een aanzienlijke invloed op de morfologie van de gevormde kristallen te hebben. Het bleek dat bij gebruik van een goed gemengde bellenkolom die doorstroomd wordt met gasvormig H_2S (dat dient als sulfide bron) een grof neerslag wordt verkregen dat eenvoudig kan worden afgescheiden.

Het in dit proefschrift beschreven onderzoek heeft laten zien dat snelheid en morfologie van neerslagvorming die bij gas-vloeistof reacties optreedt in sterke mate afhangt van de reactor geometrie en procescondities. Door het gebruik van toegesneden mathematische modellen en nieuwe karakteriseringstechnieken (zoals de laminaire jet reactor) is een goed indruk van de precipitatiekinetiek van een aantal metaalsulfiden verkregen. De in dit proefschrift verkregen inzichten, kinetiekdata en mathematische modellen kunnen gebruikt worden voor het opschalen en ontwerpen van metaalsulifde kristallisatoren.

Dit onderzoek is financieel ondersteund door het EET programma (Economie, Ecologie, Technologie), een gezamenlijk initiatief van de minsteries van Economische Zaken, OCW en VROM.

Acknowledgement

Carrying out this work would not be possible without the help of many. I gratefully acknowledge all who gave me support and contributed to my Ph.D-program and the quality of my life during my stay in the Netherlands of the past four years.

I am especially grateful to my promotor Geert Versteeg for hosting me in his group as a Ph.D-student. His supervision and continuous support stimulated tremendously in my research work. Through rewarding discussions with him, I have gained much more knowledge. His kind help in all aspects has made the past years an ever-good memory in my life. I also deeply thank my mentor Bert Heesink who guided me through the field of reactor design. His constant guidance and encouragement as well as many opportunities he gave me to practice have stimulated many of my interests and enabled me to gain more experience in research. I have learned quite a lot from his extensive knowledge in chemical engineering and many brilliant and creative ideas.

I am very grateful to Hans Kuipers for helping me in solving the numerical difficulties in my modeling work. Thanks also to Martin van Sint Annaland for helping me in Delphi programming.

I am indebted to Naif Darwish from Jordan University of Science and Technology who took the initiative to transfer Jordanian students all the way from Jordan to the Netherlands. Many thanks to you Naïf for all your efforts. I would like to express my thanks also to Mohammad Osama Azzam who supported this study by sending two of his best master students to carry out of the experimental work of my Ph.D-project.

Next, I would like to express my sincere thanks to the many representatives of Paques, Pasminco. Especially to Jacco Huisman, Roy Van Lier, Wiel Vermeulen and Renate Ruitenberg. The brain storming sessions with you during the project meetings were very useful.

Carrying out all the experimental work would not have been possible without the help of graduate students. My first student was Jeroen Stuurwold who worked on the laminar jet reactor. Khalid Al-Azzam and Salah Abu Yahya came over come from Jordan to do the experimental part of their master studies with me. Salah examined the crystallization kinetics of ZnS and CuS using the multi-suspension-multi-product-removal reactor. Khalid studied the precipitation of CuS and ZnS in the bubble column reactor. Many thanks to all of them.

I am sincerely grateful to the University of Twente who offered me all study material, lecturers and facilities needed for my Ph.D-work. In particular I would like to express my great thanks to Irene Gootjes who answered all my questions (even the silly ones) and

helped me in arranging the visas for my family needed to attend my graduation ceremony. I also enjoyed chatting with her on various cultural topics. I am also grateful to Nicole Haitjema who welcomed me when I arrived in the Netherlands and helped me in arranging my stay in the Netherlands. I thank Britta Olbertz for all her help as well.

The experimental setups for this Ph.D project were built by highly skilled technicians. I am in debt to Wim Leppink who built the laminar jet reactor setup. Benno Knaken who built the bubble column setup. His brilliant ideas turned my imagination into reality "ik ben jou dankbaar Benno". I am also thankful to Henk Jan Moed who built the MSMPR setup. Thanks also go to Robert Meijer for his support regarding instrumentation and computer maters, Wim lengton, Adri Hovestad and Annemarie Mantanano-Christenhusz helped me in the analysis part and the glass blowers who helps in built the glass parts of the experimental setups.

Taking up my study after a few years of working experience was not too easy for me also because of the totally different environment and culture that I encountered. But with the help of my colleagues it was possible. Thanks to you Toine for all the interesting discussions, to Vishwas for standing me as annoying officemate, to Senthil for the nice chats during the coffee breaks and finally to my wonderful new colleagues Jens, Peter, Zeljko and Pranay. I wish you all lots of success in your futures. Thanks also to all TwAIOs and AIOs from the Vlugter Lab for the "gezelligheid".

During my Ph.D study, I had to teach Chemical Reaction Engineering for undergraduate students. Many thanks to Herman Bruns who helped me to translate all the Dutch assignments into English. Bedankt Herman for your help.

Many new friendships were born during my stay in Twente Aljbour, Ayser, Abu Zahra, Adballah, Al-Haddad, Fahuim, Halabi, Jad Allah, Khalid, Mohammad, Mohannad, Mommo, Mustafa, Mutasim, Nidal, Racan, Sagheer,Tareq Yahya, Kapil, Jens, Salim, Senthil and Vishwas thank you all.

Most of all, I should thank my family: my loving soul mate, my wife ShanShan, for giving me the most patient and loving support and encouragement; my parents, for their ever-lasting support and understanding during my studies in the Netherlands; my brothers and sisters: Mefleh, Faleh, Mohammad, Samer, Nihad, Hala, Safa and Wesal for their continuous support at distance.

Finally I would like to say that it is impossible to mention everyone who helped me in my new life in the Netherlands. Many thanks to all of you and my apologies to those I may have forgotten.

Yours Mousa

Résumé

Mousa Al-Tarazi was born on August 21st, 1972 in Irbid, Jordan. In 1990, he started his B.Sc. study in Chemical Engineering at the Jordan University of Science and Technology (JUST) in the same city of Irbid. During his bachelor study he worked as a trainee process engineer at the Jordan Petroleum Refining Company and for TU-Dresden in Germany as a trainee researcher. In Sep 1994 he obtained his Bachelors in Chemical Engineering.

In 1995, he joined the Master program on Chemical Engineering at JUST. He worked on a dissertation entitled "Destruction of Halide Organic Compounds using Electrolysis" under the guidance of Dr. M.O. Azzam. During his master study he worked at JUST as a teaching and research assistant.

After graduating in 1997, he joined the company AT International in Dubai-UAE as a consultant engineer. He advised to oil & gas companies, and producers of polyester resin, detergents and paints regarding production processes and industrial wastewater treatment water treatment. In 1999 he joined Jordan Petroleum Refining Company as a process engineer for the naphtha-hydrotreatment and topping units. At the end of 1999 he got an offer from the Al-Balqa University in Amman-Jordan. He joined that university as a lecturer to teach fluid dynamics and unit operations courses.

In February 2000, Al-Tarazi started the PhD-project described in this thesis for the Development and Design of Industrial Processes (OOIP) group within the Faculty of Science and Technology of the University of Twente the Netherlands. From April 2004 on, he will be working as a post-doc with Prof.dr.ir Hans Kuipers of the group Fundamentals of Chemical Reaction Engineering (FAP) group of the same faculty. The project is entitled "the flow of granular solids material in pipes and open channels".